CALT-68-1855
DOE RESEARCH AND
DEVELOPMENT REPORT

Inclusive Weak Decays of Charmed Mesons

Thesis by

Christopher Gerald Matthews

In Partial Fulfillment of the Requirements

for the Degree of

Doctor of Philosophy

California Institute of Technology

Pasadena, California

1993

(Defended December 7, 1992)

© 1993
Christopher Gerald Matthews
All Rights Reserved

Abstract

Inclusive analyses provide a different insight into our understanding of weak decay physics. In this thesis, I experimentally determine inclusive decay properties of charmed D mesons. I also use exclusive decay predictions from a variety of theoretical models to make predictions about inclusive properties. Both experimental and theoretical realms benefit from the new techniques presented in this thesis.

Inclusive properties derived are the multiplicity distributions, average multiplicities and inclusive branching ratios of charged particles, charged and neutral kaons, and charged pions. The center-of-mass momentum spectra of charged and neutral kaons are also obtained. Additionally, in the theoretical realm only, the inclusive properties of neutral pions, and the center-of-mass momentum spectra of charged and neutral pions are determined.

The experimental analysis, which uses data from the Mark III experiment at the Stanford Linear Accelerator Center, employs an unfold technique utilizing fold matrices to obtain the charged particle and kaon properties. A new, enhanced unfold technique involving fold tensors obtains the first-ever results for the inclusive charged pion properties. The average strange quark contents and the average charged lepton multiplicities of the D^+, D^0, and D_s^+ are also presented.

In the theoretical analysis, the exclusive decay mode predictions from the factorization model of Bauer, Stech and Wirbel; the quark diagram scheme of Chau and Cheng; and the QCD sum rules model of Blok and Shifman are processed to determine inclusive properties. It is hoped that an examination of a model's inclusive predictions will lead to a better understanding of the model. I also derive inclusive predictions from the D meson exclusive branching ratios compiled by the Particle Data Group.

Acknowledgments

This thesis owes it existence to my advisor, David Hitlin. His patience, encouragement and support kept me going through some difficult stages. I appreciated the independence he allowed me throughout the entire process.

Allen Mincer and Dave Coward helped initiate my experimental analysis. Frank Porter, Bill Wisniewski, Gerald Eigen, and more recently, Jon Urheim and James Oyang lent me their ears and their experience when I needed to discuss my latest ideas and problems with someone.

My fellow graduate students, Ernest Prabhakar, Michael Kelsey and Lawrence Jones were another source of several animated and spirited discussions. They also proofread early copies of this thesis.

Gregory Dubois, my longtime officemate, friend, and fellow graduate student, shared with me so many things — his love and knowledge of physics, his dedication to perfection, his tool-building fervor, and his encouragement and support. I hope that I was able to reciprocate.

My parents, family, friends and fellow folkdancers reminded me what life is about outside of school.

Nothing compares, however, to the support, sacrifices and gifts of love from my wife, friend, and companion, Diana. Her tangible and pragmatic contributions — typing many of the more complex tables and proofreading and editing — saved me many weeks of work and produced a much more readable thesis. But it was her intangible and spiritual contributions that most strongly affected my life during this long and arduous process and gave me the courage to finally finish.

Contents

Acknowledgments iii

Abstract iv

List of Figures ix

List of Tables xii

PART I INTRODUCTION

Chapter 1 Introduction 2

1.1 Charmed Mesons 2

1.2 Weak Decays 2

1.3 Inclusive Decay Properties 11

PART II EXPERIMENTAL RESULTS

Chapter 2 The Mark III Detector 16

2.1 A Brief History 16

2.2 The Drift Chamber 18

2.3 The Time-of-Flight (TOF) System 21

2.4 Shower Counters 22

2.5 Muon System 23

Chapter 3 The D Data Sets 25

3.1 The D^0 and D^+ Data Sets 25

3.2 The D_s^+ Data Set 32

Chapter 4 Experimental Technique 37

4.1 Introduction 37

4.2 The Fold Matrix 38

4.3 Analytic Unfold 41

4.4 Unfold using Maximum Likelihood 42

4.5 The Fold Tensor 45

4.6 The [$\pi^{\pm}$, $X^{\pm}$] Topology Unfold 54

4.7 Particle Class Definitions 55

4.8 Determining the Initial Background 57

4.9 Estimating Systematic Errors 58

4.10 Kaon Momentum Spectra 59

Chapter 5 Experimental Results 61

5.1 D^+ Inclusive Multiplicity Distributions 61

5.2 D^+ Inclusive Momenta Spectra 69

5.3 D^0 Inclusive Multiplicity Distributions 71

5.4 D^0 Inclusive Momenta Spectra 76

5.5 D_s^+ Inclusive Multiplicity Distributions 79

5.6 D_s^+ Inclusive Momenta Spectra 83

5.7 Tables of Fold Matrices/Tensors 85

5.8 Tables of Observed Multiplicity Distributions 96

PART III THEORETICAL PREDICTIONS

Chapter 6 Inclusive Predictions from Theoretical Models 106

6.1 Introduction 106

6.2 Normalization Schemes 107

6.3 Analytic Calculation of Inclusive Properties 107

6.4 Monte Carlo Calculation of Inclusive Properties 112

Chapter 7 The Factorization Model of Bauer, Stech, and Wirbel 113

7.1 Introduction 113

7.2 Calculating Amplitudes — A General Description 114

7.3 The $\overline{K}\pi$ System 115

7.4 The $\overline{K}a_1$ System 119

7.5 Semileptonic Decays 122

7.6 Isospin Decomposition 123

7.7 Solving for the Parameters a_1 and a_2 127

7.8 Several Hadronic Predictions 129

7.9 Exclusive Mode Predictions 131

7.10 Inclusive Predictions 136

7.11 Enhancements and Conclusions 151

Chapter 8 The Quark Diagram Scheme of Chau and Cheng 155

8.1 Diagrams and Parameters 155

8.2 Octet-Singlet Mixing 157

8.3 Solving for the CC Model Parameters 158

8.4 Exclusive Mode Predictions 162

8.5 Inclusive Predictions 168

8.6 Conclusions 173

Chapter 9 The QCD Sum Rules Model of Blok and Shifman 175

9.1 Introduction 175

9.2 Exclusive Modes 177

9.3 Inclusive Predictions 180

9.4 Conclusions 184

Chapter 10 The Particle Data Group Model 186

10.1 Introduction 186

10.2 Exclusive Modes 186

10.3 Inclusive Predictions 191

10.4 Conclusions and Enhancements 200

PART IV CONCLUSIONS

Chapter 11 Conclusions 204

11.1 Comparisons 204

11.2 Conclusions 205

PART V APPENDICES

Appendix A PREDICT User's Guide 211

A.1 Inclusive Analysis with PREDICT 211

A.2 Syntax 212

A.3 Hierarchy of Options and Parameters 215

A.4 Defining Defaults via GLOBALV 220

A.5 Output 221

A.6 Questions? 223

Appendix B Calculation of the Semileptonic Decay Width $D \to \overline{K}\ell^+\nu$ using the BSW Model 224

Appendix C Decomposition with the Wigner-Eckart Theorem 230

Bibliography 232

List of Figures

1.1 Quark generations 3

1.2 Leptonic decay of the D^+ at a) the low energy hadron level and b) the quark level 4

1.3 Semileptonic decay of a D meson 6

1.4 Spectator diagram 7

1.5 One loop gluon corrections 8

1.6 a) Annihilation and b) W-exchange diagrams at the quark level 11

2.1 Mark III detector (axial view) 17

2.2 Mark III detector (transverse view) 17

2.3 Inner trigger chamber 19

2.4 Main outer drift chamber (transverse view) 19

2.5 Particle identification using the time-of-flight system 22

2.6 Barrel shower counter 23

2.7 Endcap shower counter 24

3.1 Mass-energy correlation of the D^+ 27

3.2 Mass-energy correlation of the D^0 28

3.3 Beam-constrained mass histograms for the D^+ decay modes 29

3.4 Beam-constrained mass histograms for the D^0 decay modes 30

3.5 Invariant mass histograms for the D_s^+ decay modes 31

3.6 Invariant mass of K^+K^- 34

3.7 Invariant mass of $K^\pm\pi^\mp$ after the $P(\chi^2)$ and $|\cos\theta_\pi|$ cuts 34

3.8 Invariant mass of $\pi^+\pi^-$ using different cuts 35

4.1 Kaon momenta efficiency correction functions 60

5.1 Background fits for various charged particle multiplicities for the D^+ . . 64

5.2 Log likelihood function for the charged multiplicity unfold of the D^+ . . 66

5.3 D^+ inclusive center-of-mass momentum spectra 70

5.4 Background fits for various charged particle multiplicities for the D^0 . . 72

5.5 D^0 inclusive center-of-mass momentum spectra 77

5.6 D^0 inclusive K^- center-of-mass momentum spectrum with fits 78

5.7 Background fits for various charged particle multiplicities for the D_s^+ . . 81

5.8 D_s^+ inclusive center-of-mass momentum spectra 84

6.1 An example decay chain showing final states of $\overline{K}^{*0}\rho^+$ 110

7.1 Contour plot of the χ^2 function showing 1σ and 2σ contours of a_1 and a_2 128

7.2 Comparison between BSW model predictions and Mark III experimental results 131

7.3 D^+ average charge multiplicity as a function of a_1 and a_2 in the BSW model 137

7.4 D^0 average charge multiplicity as a function of a_1 and a_2 in the BSW model 138

7.5 D_s^+ average charge multiplicity as a function of a_1 and a_2 in the BSW model 138

7.6 BSW: D^+ center-of-mass momentum spectra (letters indicating structure are explained in the text) 146

7.7 BSW: D^0 center-of-mass momentum spectra (letters indicating structure are explained in the text) 147

7.8 BSW: D_s^+ center-of-mass momentum spectra (letters indicating structure are explained in the text) 148

7.9 Efficiency-corrected BSW D^+ center-of-mass momentum spectra after reconstruction and processing 149

7.10 Efficiency-corrected BSW D^0 center-of-mass momentum spectra after reconstruction and processing 150

8.1 Chau and Cheng's quark diagrams and associated parameters 155

8.2 Hairpin diagrams 156

9.1 QCD sum rules: factorizable diagrams (a) annihilation (b,c) spectator; where a wavy line represents a meson current, a double line represents a charm quark, and a single line represents a light quark 176

10.1 PDG: D^+ center-of-mass momentum spectra (letters indicating structure are explained in the text) 197

10.2 PDG: D^0 center-of-mass momentum spectra (letters indicating structure are explained in the text) 198

10.3 PDG: D_s^+ center-of-mass momentum spectra (letters indicating structure are explained in the text) 199

List of Tables

1.1 Summary of charmed meson properties 2

1.2 Estimates of leptonic partial widths and branching ratios for $f_D = f_{D_s} = 200$ MeV 6

2.1 Data collection history of D mesons at Mark III 18

3.1 D^+, D^0 and D_s^+ tagging modes and counts 26

3.2 Mass-energy correlations for the D^+ and D^0 26

5.1 Table identifiers for the D^+ results 61

5.2 D^+ unfolded charged particle multiplicity distribution and average . . . 63

5.3 D^+ unfolded kaon multiplicity distribution and average 65

5.4 D^+ unfolded pion multiplicity distribution and average 67

5.5 Table identifiers for the D^0 results 71

5.6 D^0 unfolded charged particle multiplicity distribution and average 73

5.7 D^0 unfolded kaon multiplicity distribution and average 74

5.8 D^0 unfolded pion multiplicity distribution and average 75

5.9 Table identifiers for the D_s^+ results 79

5.10 D_s^+ unfolded charged particle multiplicity distribution and average . . . 80

5.11 D_s^+ unfolded kaon multiplicity distribution and average 82

5.12 D_s^+ unfolded pion multiplicity distribution and average 83

5.13 D^+ charged particle ($P^\pm$) fold matrix 85

5.14 D^+ like-sign kaon (K^+) fold matrix 85

5.15 D^+ unlike-sign kaon (K^-) fold matrix 85

5.16 D^+ charged kaon fold ($K^\pm$) matrix 86

5.17 D^+ neutral kaon (K_S) fold matrix 86

5.18 D^+ unlike-sign pion (π^-) fold matrix 86

5.19 D^+ like-sign pion (π^+) fold tensor 87

5.20 D^+ charged pion ($\pi^\pm$) fold tensor 88

5.21 D^0 charged particle ($P^{\pm}$) fold matrix 89
5.22 D^0 like-sign kaon (K^+) fold matrix 89
5.23 D^0 unlike-sign kaon (K^-) fold matrix 89
5.24 D^0 charged kaon fold ($K^{\pm}$) matrix 90
5.25 D^0 neutral kaon (K_S) fold matrix 90
5.26 D^0 unlike-sign pion (π^-) fold matrix 90
5.27 D^0 like-sign pion (π^+) fold tensor 91
5.28 D^0 charged pion ($\pi^{\pm}$) fold tensor 92
5.29 D_s^+ charged particle ($P^{\pm}$) fold matrix 93
5.30 D_s^+ like-sign kaon (K^+) fold matrix 93
5.31 D_s^+ unlike-sign kaon (K^-) fold matrix 93
5.32 D_s^+ charged kaon fold ($K^{\pm}$) matrix 94
5.33 D_s^+ neutral kaon (K_S) fold matrix 94
5.34 D_s^+ unlike-sign pion (π^-) fold matrix 94
5.35 D_s^+ like-sign pion (π^+) fold tensor 95
5.36 D_s^+ charged pion ($\pi^{\pm}$) fold tensor 96
5.37 D^+ observed charged particle ($P^{\pm}$) multiplicities 96
5.38 D^+ observed like-sign kaon (K^+) multiplicities 97
5.39 D^+ observed unlike-sign kaon (K^-) multiplicities 97
5.40 D^+ observed charged kaon ($K^{\pm}$) multiplicities 97
5.41 D^+ observed neutral kaon (K_S) multiplicities 97
5.42 D^+ observed like-sign pion (π^+) multiplicities 98
5.43 D^+ observed unlike-sign pion (π^-) multiplicities 98
5.44 D^+ observed charged pion ($\pi^{\pm}$) multiplicities 99
5.45 D^0 observed charged particle ($P^{\pm}$) multiplicities 100
5.46 D^0 observed like-sign kaon (K^+) multiplicities 100
5.47 D^0 observed unlike-sign kaon (K^-) multiplicities 100

5.48 D^0 observed charged kaon ($K^{\pm}$) multiplicities 100

5.49 D^0 observed neutral kaon (K_S) multiplicities 100

5.50 D^0 observed unlike-sign pion (π^-) multiplicities 101

5.51 D^0 observed like-sign pion (π^+) multiplicities 101

5.52 D^0 observed charged pion ($\pi^{\pm}$) multiplicities 102

5.53 D_s^+ observed charged particle ($P^{\pm}$) multiplicities 102

5.54 D_s^+ observed like-sign kaon (K^+) multiplicities 103

5.55 D_s^+ observed unlike-sign kaon (K^-) multiplicities 103

5.56 D_s^+ observed charged kaon ($K^{\pm}$) multiplicities 103

5.57 D_s^+ observed neutral kaon (K_S) multiplicities 103

5.58 D_s^+ observed unlike-sign pion (π^-) multiplicities 103

5.59 D_s^+ observed like-sign pion (π^+) multiplicities 104

5.60 D_s^+ observed charged pion ($\pi^{\pm}$) multiplicities 104

6.1 Branching ratios used to decay secondary particles ($\pi^{\pm}$, $K^{\pm}$, and K_L are considered "stable") 109

7.1 Values used in the calculations 116

7.2 Overlap factors (form factors at $q^2 = 0$) 116

7.3 Pole masses used in the calculations 117

7.4 Cabibbo-Kobayashi-Maskawa matrix elements 117

7.5 Partial width predictions for $D \to \overline{K}\pi$ 119

7.6 Partial width predictions for $D \to \overline{K}a_1$ 122

7.7 BSW semileptonic partial widths 123

7.8 Semileptonic partial widths for $D \to \overline{K}\ell^+\nu$ decays 123

7.9 Correlation coefficients from the $\overline{K}\pi$ isospin decomposition 126

7.10 Comparison of $D \to \overline{K}\pi$ isospin decompositions. 127

7.11 Solution to a_1 and a_2 from $D \to \overline{K}\pi$ isospin analysis. 128

7.12 Comparison between BSW model predictions and Mark III experimental results using a_1 = 1.13 and a_2 = –0.47 130
7.13 BSW: D^+ exclusive decay modes 132
7.14 BSW: D^0 exclusive decay modes 133
7.15 BSW: D_s^+ exclusive decay modes 135
7.16 BSW: inclusive charged particle multiplicity distribution and average . 137
7.17 BSW: D^+ inclusive kaon multiplicity distribution and average 139
7.18 BSW: D^+ inclusive pion multiplicity distribution and average 139
7.19 BSW: D^0 inclusive kaon multiplicity distribution and average 140
7.20 BSW: D^0 inclusive pion multiplicity distribution and average 140
7.21 BSW: D_s^+ inclusive kaon multiplicity distribution and average 141
7.22 BSW: D_s^+ inclusive pion multiplicity distribution and average 141
7.23 Comparison between BSW predictions and experimental results . . . 152
7.24 BSW+: additional D^+ exclusive decay modes 153
7.25 BSW+: additional D^0 exclusive decay modes 154
8.1 CC: $D^+ \rightarrow$ PP exclusive decay modes 163
8.2 CC: $D^+ \rightarrow$ VP exclusive decay modes 163
8.3 CC: $D^0 \rightarrow$ PP exclusive decay modes 164
8.4 CC: $D^0 \rightarrow$ VP exclusive decay modes 165
8.5 CC: $D_s^+ \rightarrow$ PP exclusive decay modes 167
8.6 CC: $D_s^+ \rightarrow$ VP exclusive decay modes 168
8.7 CC: inclusive charged particle multiplicity distribution and average . . 169
8.8 CC: D^+ inclusive kaon multiplicity distribution and average 170
8.9 CC: D^+ inclusive pion multiplicity distribution and average 170
8.10 CC: D^0 inclusive kaon multiplicity distribution and average 171
8.11 CC: D^0 inclusive pion multiplicity distribution and average 171
8.12 CC: D_s^+ inclusive kaon multiplicity distribution and average 172

8.13 CC: D_s^+ inclusive pion multiplicity distribution and average 172
8.14 Comparison between CC predictions and experimental results 174
9.1 BS: D^+ exclusive decay modes 178
9.2 BS: D^0 exclusive decay modes 179
9.3 BS: D_s^+ exclusive decay modes 180
9.4 BS: inclusive charged particle multiplicity distribution and average . . 181
9.5 BS: D^+ inclusive kaon multiplicity distribution and average 182
9.6 BS: D^+ inclusive pion multiplicity distribution and average 182
9.7 BS: D^0 inclusive kaon multiplicity distribution and average 183
9.8 BS: D^0 inclusive pion multiplicity distribution and average 183
9.9 BS: D_s^+ inclusive kaon multiplicity distribution and average 184
9.10 BS: D_s^+ inclusive pion multiplicity distribution and average 184
9.11 Comparison between BS predictions and experimental results 185
10.1 PDG: D^+ exclusive decay modes 187
10.2 PDG: D^0 exclusive decay modes 188
10.3 PDG: D_s^+ exclusive decay modes 190
10.4 PDG: inclusive charged particle multiplicity distribution and average . 191
10.5 PDG: D^+ inclusive kaon multiplicity distribution and average 192
10.6 PDG: D^+ inclusive pion multiplicity distribution and average 192
10.7 PDG: D^0 inclusive kaon multiplicity distribution and average 193
10.8 PDG: D^0 inclusive pion multiplicity distribution and average 193
10.9 PDG: D_s^+ inclusive kaon multiplicity distribution and average 194
10.10 PDG: D_s^+ inclusive pion multiplicity distribution and average 194
10.11 Comparison between PDG predictions and experimental results . . . 201
10.12 PDG+: postulated additional D^+ exclusive decay modes 201
10.13 PDG+: postulated additional D^0 exclusive decay modes 202
11.1 Comparison of inclusive charged particle properties 207

11.2 Comparison of inclusive kaon properties 208

11.3 Comparison of inclusive pion properties 209

B.1 Semileptonic partial widths for $D \to \overline{K}\ell^+\nu$ decays 229

PART I
INTRODUCTION

"Let's start at the very beginning.

It's a very good place to start.

When you read you begin with a-b-c.

When you sing you begin with do-re-mi."

Rodgers and Hammerstein

The Sound of Music

Chapter 1 Introduction

Section 1.1 Charmed Mesons

Glashow, Iliopoulos and Maiani first predicted the charm quark in 1970 to explain the lack of strangeness-changing neutral currents.[1] The discovery of the J/ψ in 1974 verified their prediction.[2, 3] The J/ψ is a bound state of a charm quark and an anticharm antiquark ($c\bar{c}$) with zero net charm. The first charmed mesons,* the D^0 and D^+, were discovered in 1976.[4, 5]

The lightest charmed mesons are the D^0, D^+, and D_s^+ with masses 1864.5 MeV, 1869.3 MeV, and 1968.8 MeV respectively.[6] They are bound states of a charm quark and a light antiquark — the D^0 is the $c\bar{u}$ state, the D^+ is the $c\bar{d}$ state, and the D_s^+ is the $c\bar{s}$ state. All three mesons are pseudoscalars with $J^P = 0^-$. Table 1.1 summarizes the properties of these charmed mesons.

Charmed mesons decay via a weak decay of the constituent c quark. Weak decays are discussed in the next section.

Table 1.1 Summary of charmed meson properties[6]

Particle	Quark Content	Isospin $\lvert I, I_3\rangle$	Mass (MeV)	Lifetime (10^{-13} s)	Anti-Particle
D^0	$c\bar{u}$	$\lvert\frac{1}{2}\,\frac{-1}{2}\rangle$	1864.5 ± 0.5	4.20 ± 0.08	$\overline{D}^0$
D^+	$c\bar{d}$	$\lvert\frac{1}{2}\,\frac{1}{2}\rangle$	1869.3 ± 0.5	10.66 ± 0.23	D^-
D_s^+	$c\bar{s}$	$\lvert 0\,0\rangle$	1968.8 ± 0.7	$4.50^{+0.30}_{-0.26}$	D_s^-

Section 1.2 Weak Decays

The Quark Mixing Matrix

Each of the three generations of quarks is arranged as a left-handed doublet and two right-handed singlets (Figure 1.1). The primed quarks are orthogonal combinations of

* Throughout this thesis, I adopt the convention that reference to a charmed meson also implies reference to its charge conjugate. Also, the generic term "D meson" refers to the D^+, D^0, and D_s^+ mesons.

$$\begin{pmatrix} u \\ d' \end{pmatrix}_L \qquad \begin{pmatrix} c \\ s' \end{pmatrix}_L \qquad \begin{pmatrix} t \\ b' \end{pmatrix}_L$$

$$u_R, d_R \qquad c_R, s_R \qquad t_R, b_R$$

Figure 1.1 Quark generations

the mass eigenstates and are mixed according to a mixing matrix:[7]

$$\begin{pmatrix} d' \\ s' \\ b' \end{pmatrix} = \mathbf{V} \begin{pmatrix} d \\ s \\ b \end{pmatrix} = \begin{pmatrix} V_{ud} & V_{us} & V_{ub} \\ V_{cd} & V_{cs} & V_{cb} \\ V_{td} & V_{ts} & V_{tb} \end{pmatrix} \begin{pmatrix} d \\ s \\ b \end{pmatrix}$$

where $\mathbf{V}$ is the 3×3 unitary matrix known as the Cabibbo-Kobayashi-Maskawa (CKM) matrix. The CKM matrix has many possible parametrizations. A common parametrization of this matrix is:

$$\mathbf{V} = \begin{pmatrix} V_{ud} & V_{us} & V_{ub} \\ V_{cd} & V_{cs} & V_{cb} \\ V_{td} & V_{ts} & V_{tb} \end{pmatrix} = \begin{pmatrix} c_1 & s_1c_3 & s_1s_3 \\ -s_1c_2 & c_1c_2c_3 - s_2s_3e^{i\delta} & c_1c_2s_3 + s_2c_3e^{i\delta} \\ -s_1s_2 & c_1s_2c_3 + c_2s_3e^{i\delta} & c_1s_2s_3 - c_2c_3e^{i\delta} \end{pmatrix}$$

where the $c_i = \cos\theta_i$ and $s_i = \sin\theta_i$. The θ_i are quark mixing angles and the phase δ parameterizes CP violation.

Since the values of θ_2 and θ_3 are small, and since the t and b quarks play a negligible role in charmed meson decay, the CKM matrix can be expressed in a reduced form using a single parameter. The quark mixing becomes:

$$\begin{pmatrix} d' \\ s' \end{pmatrix} = \begin{pmatrix} \cos\theta & \sin\theta \\ -\sin\theta & \cos\theta \end{pmatrix} \begin{pmatrix} d \\ s \end{pmatrix}$$

where θ is called the Cabibbo angle. Both forms of the mixing matrix are used throughout this thesis depending upon the nature of the calculation.

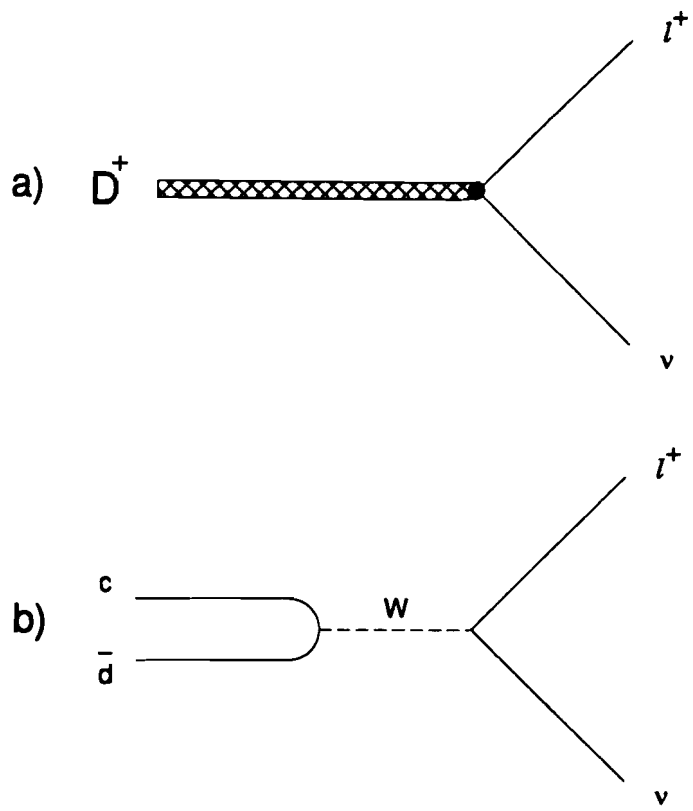

Figure 1.2 Leptonic decay of the D^+ at a) the low energy hadron level and b) the quark level

Leptonic Decays

The D^+ leptonic decay width is fairly straightforward to calculate. To first order, the amplitude for the decay $D^+ \to \ell^+\nu$ (see Figure 1.2a) is:

$$A(D^+ \to \ell^+\nu) = \frac{G_F}{\sqrt{2}} V_{cd}\left(i f_D p_\sigma^D\right)\bar{u}(\nu_\ell)\gamma^\sigma(1-\gamma^5)v(\ell^+)$$

where f_D is the D^+ decay constant. Squaring and summing over spin states we get:

$$\begin{aligned}
|A|^2 &= \sum \frac{G_F^2 f_D^2 V_{cd}^2}{2}[\bar{u}\,\not{p}\,(1-\gamma_5)v]^*[\bar{u}\,\not{p}\,(1-\gamma_5)v] \\
&= \sum \frac{G_F^2 f_D^2 V_{cd}^2}{2}\left[v(1+\gamma^5)\,\not{p}\,\bar{u}\right]\left[\bar{u}\,\not{p}\,(1-\gamma^5)v\right] \\
&= \frac{G_F^2 f_D^2 V_{cd}^2}{2}\mathrm{Tr}\left[(1+\gamma^5)\,\not{p}\not{p}_\nu\not{p}\,(1-\gamma^5)(\not{p}_\ell + m_\ell)\right] \\
&= \frac{G_F^2 f_D^2 V_{cd}^2}{2} 8(2(p_\ell\cdot p_D)(p_\nu\cdot p_D) - (p_\ell\cdot p_\nu)(p_D\cdot p_D)) \\
&= 4G_F^2 f_D^2 V_{cd}^2(2E_\ell m_D E_\nu m_D - (E_\ell E_\nu + p^2)m_D^2) \\
&= 4G_F^2 f_D^2 V_{cd}^2 m_D^2(E_\ell E_\nu - p^2)\,.
\end{aligned}$$

In the D^+ rest frame, the lepton and neutrino are produced back-to-back with equal momenta p. For a two-body decay with the parent at rest, this momentum is:

$$p(M \to m_1 m_2) = \left(M^2 - (m_1 + m_2)^2\right)^{1/2} \left(M^2 - (m_1 - m_2)^2\right)^{1/2} / (2M) .$$

In this case, $m_\nu = 0$, so:

$$p = \frac{m_D}{2}\left(1 - \frac{m_\ell^2}{m_D^2}\right) .$$

Also, $E_\nu = p$ and E_ℓ is:

$$\begin{aligned} E_\ell &= \left(m_\ell^2 + p^2\right)^{1/2} \\ &= \left(m_\ell^2 + \frac{m_D^2}{4}\left(1 - \frac{2m_\ell^2}{m_D^2} + \frac{m_\ell^4}{m_D^4}\right)\right)^{1/2} \\ &= \frac{m_D}{2}\left(1 + \frac{m_\ell^2}{m_D^2}\right) . \end{aligned}$$

Therefore,

$$E_\nu E_\ell - p^2 = \frac{m_\ell^2}{2}\left(1 - \frac{m_\ell^2}{m_D^2}\right) .$$

Thus, the amplitude squared becomes:

$$|A|^2 = 4G_F^2 f_D^2 V_{cd}^2 m_D^2 \left[\frac{m_\ell^2}{2}\left(1 - \frac{m_\ell^2}{m_D^2}\right)\right] .$$

The two-body decay partial width is given by:

$$\begin{aligned} \Gamma &= \frac{1}{8\pi}|A|^2 \frac{p}{m_D^2} \\ &= \frac{1}{8\pi}\left(2G_F^2 f_D^2 V_{cd}^2 m_D^2 m_\ell^2 \left(1 - \frac{m_\ell^2}{m_D^2}\right)\right) \frac{\frac{m_D}{2}\left(1 - \frac{m_\ell^2}{m_D^2}\right)}{m_D^2} \\ &= \frac{G_F^2}{8\pi} V_{cd}^2 f_D^2 m_D m_\ell^2 \left(1 - \frac{m_\ell^2}{m_D^2}\right)^2 . \end{aligned}$$

Thus, the width of leptonic D^+ decay is:

$$\Gamma(D^+ \to \ell^+ \nu) = \frac{G_F^2}{8\pi} V_{cd}^2 f_D^2 m_D m_\ell^2 \left(1 - \frac{m_\ell^2}{m_D^2}\right)^2 .$$

The decay constant f_D has not yet been experimentally measured. Theoretical predictions based on lattice calculations estimate $f_D \approx 200$ MeV and $f_{D_s} \approx 230$ MeV.[8]

Experimentally an upper bound of 290 MeV exists.[9] Table 1.2 lists predictions for D^+ and D_s^+ leptonic decays using $f_D = f_{D_s} = 200$ MeV, $V_{cd} = 0.2$ and $V_{cs} = 0.975$.

Table 1.2 Estimates of leptonic partial widths and branching ratios for $f_D = f_{D_s} = 200$ MeV

	D^+		D_s^+	
	Γ (GeV)	BR (%)	Γ (GeV)	BR (%)
e	4.22×10^{-21}	6.8×10^{-7}	1.06×10^{-19}	7.2×10^{-6}
μ	1.79×10^{-16}	0.029	4.50×10^{-15}	0.30
τ	4.09×10^{-16}	0.066	4.13×10^{-14}	2.8

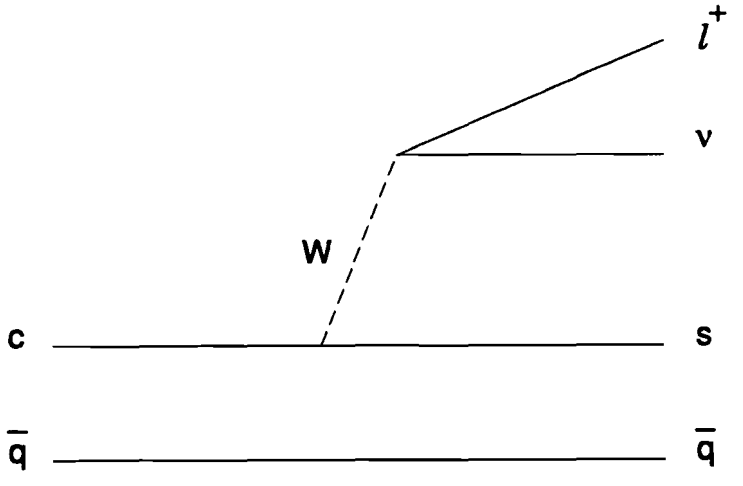

Figure 1.3 Semileptonic decay of a D meson

Semileptonic Decays

Semileptonic decays of charmed mesons proceed primarily through the weak decay of the c quark into a lepton pair (Figure 1.3). This type of diagram is called a spectator diagram because the non-charmed quark of the charm meson (indicated by " $\bar{q}$ " in Figure 1.3) plays no active role. The rate for this semileptonic decay can be approximated

by scaling from the muon decay rate $\Gamma(\mu^+ \to e^+\overline{\nu}_e\nu_\mu) = G_F^2 m_\mu^5/192\pi^3$:

$$\begin{aligned}
\Gamma(c \to se^+\nu_e) &= |V_{cs}|^2 \frac{G_F^2 m_c^5}{192\pi^3} F\left[\frac{m_s}{m_c}\right] \\
&= |V_{cs}|^2 \times F\left[\frac{m_s}{m_c}\right] \times \left(\frac{m_c}{m_\mu}\right)^5 \times \frac{1}{\tau(\mu^+ \to e^+\nu_e\bar{\nu}_\mu)} \\
&= (.975)^2 \times 0.87 \times (1.5/.105)^5 \times \frac{1}{2.2 \times 10^{-6}\ s} \\
&= 22.4 \times 10^{10}\ s^{-1} \\
&= 1.47 \times 10^{-13}\ \text{GeV}
\end{aligned}$$

using $m_c = 1.5$ GeV and $m_s = .2$ GeV. A phase-space factor, the function $F[x] = 1 - 8x^2 + x^6 - x^8 - 24x^4 \ln x$, accounts for the non-zero masses of the quarks.[10]

Another approach to calculate semileptonic decay widths is the factorization technique. Chapter 7 describes this approach as used by Bauer, Stech and Wirbel.

Hadronic Decays

The spectator diagram serves as a starting point in the consideration of purely hadronic decays of charmed mesons.

The lowest order effective Hamiltonian for a hadronic weak decay of a charmed meson, corresponding to the spectator diagram (Figure 1.4) is:

$$H_W^0 = \frac{G_F}{\sqrt{2}}\left(\bar{s}'\gamma_\mu(1-\gamma_5)c\right) \times \left(\bar{u}\gamma^\mu(1-\gamma_5)d'\right).$$

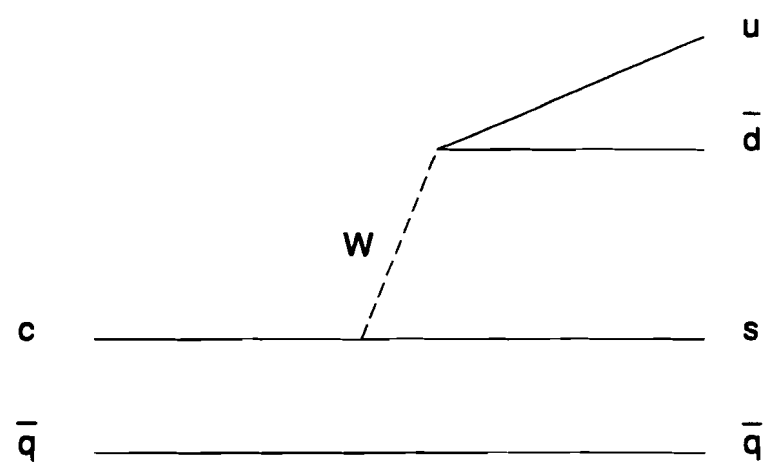

Figure 1.4 Spectator diagram

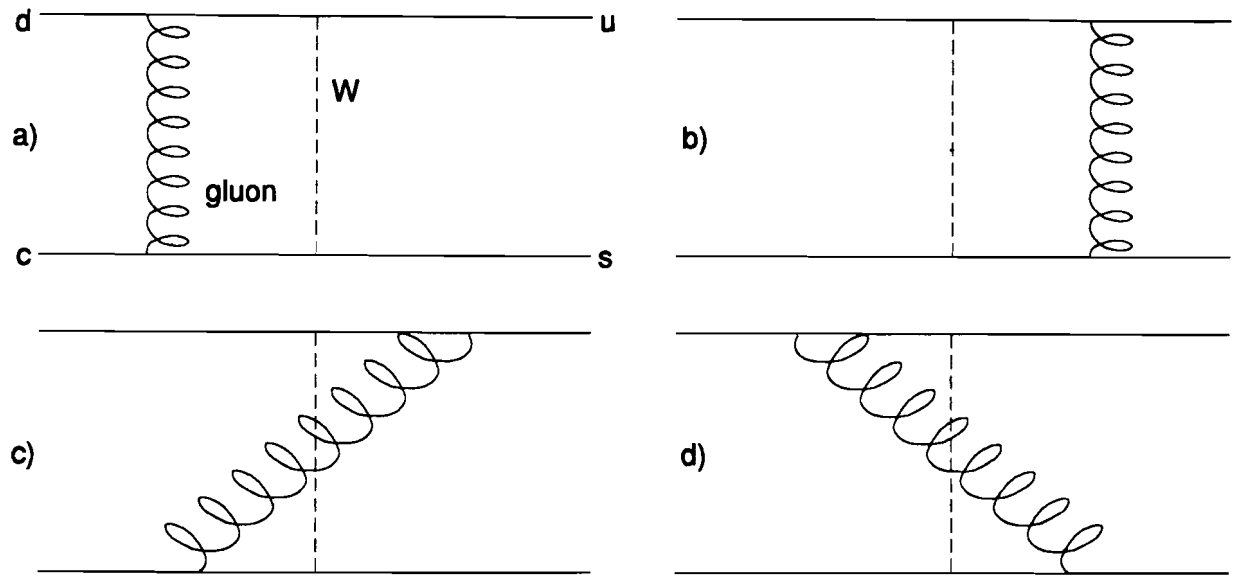

Figure 1.5 One loop gluon corrections

Expanding the primed forms by using the CKM matrix:

$$d' = V_{ud}d + V_{us}s$$

$$s' = V_{cd}d + V_{cs}s$$

and keeping only the Cabibbo-favored terms V_{ud} and V_{cs}, yields:

$$H_W^0 = \frac{G_F}{\sqrt{2}} V_{cs} V_{ud} \bar{s}\gamma_\mu(1-\gamma_5)c\bar{u}\gamma^\mu(1-\gamma_5)d\,.$$

However, the strong interaction effects of QCD modify this Hamiltonian. In particular, single hard gluon exchanges between the quarks, represented by the four gluon exchange diagrams (Figure 1.5), contribute to this modification. The first-order correction to the Hamiltonian is:

$$H_W^{(1)} = -\frac{G_F}{\sqrt{2}}\frac{3\alpha_s}{8\pi}\ln\left(\frac{M_W^2}{\mu^2}\right) V_{cs}V_{ud}\bar{s}\gamma_\mu(1-\gamma_5)\lambda_a c\bar{u}\gamma^\mu(1-\gamma_5)\lambda^a d$$

where α_S is the strong coupling constant. Color currents, λ_a, have been introduced into this first-order correction, which otherwise has the same chiral and flavor structure as the zeroth order. Using the Fierz transformation:

$$[\gamma_\mu(1-\gamma_5)]_{\alpha\beta}[\gamma^\mu(1-\gamma_5)]_{\delta\epsilon} = -[\gamma_\mu(1-\gamma_5)]_{\alpha\epsilon}[\gamma^\mu(1-\gamma_5)]_{\delta\beta}$$

and the color algebra relation:

$$(\lambda_a)_{ij}(\lambda^a)_{kl} = -\tfrac{2}{3}\delta_{ij}\delta_{kl} + 2\delta_{il}\delta_{kj}$$

we can write the Hamiltonian in terms of color-singlet transitions only:

$$H_W^{(1)} = \frac{G_F}{\sqrt{2}} V_{cs} V_{ud} \left[\frac{\alpha_s}{4\pi} \ln\left(\frac{M_W^2}{\mu^2}\right) (\bar{s}c)_L (\bar{u}d)_L - \frac{3\alpha_s}{4\pi} \ln\left(\frac{M_W^2}{\mu^2}\right) (\bar{s}d)_L (\bar{u}c)_L \right]$$

using the notation $(\bar{s}c)_L \equiv \sum_{i=1}^{3} \bar{s}_i \gamma^\mu (1-\gamma_5) c_i$ (summation over color indices). The hard gluon exchanges have the property of inducing effective neutral currents and renormalizing the strength of the charged currents. The Hamiltonian is now:

$$\begin{aligned} H_W &= H_W^0 + H_W^{(1)} \\ &= \frac{G_F}{\sqrt{2}} V_{cs} V_{ud} \left[\left(1 + \frac{\alpha_s}{4\pi} \ln\left(\frac{M_W^2}{\mu^2}\right)\right) (\bar{s}c)_L (\bar{u}d)_L - \frac{3\alpha_s}{4\pi} \ln\left(\frac{M_W^2}{\mu^2}\right) (\bar{s}d)_L (\bar{u}c)_L \right] . \end{aligned}$$

This can be rewritten in terms of the symmetric and antisymmetric operators:

$$O_\pm = \tfrac{1}{2}[(\bar{s}c)_L (\bar{u}d)_L \pm (\bar{s}d)_L (\bar{u}c)_L] .$$

The zeroth order Hamiltonian then becomes:

$$H_W^0 = \frac{G_F}{\sqrt{2}} V_{cs} V_{ud} (O_+ + O_-) .$$

Defining:

$$\begin{aligned} c_+^{(1)} &= 1 - \frac{\alpha_s}{2\pi} \ln\left(\frac{M_W^2}{\mu^2}\right) \\ c_-^{(1)} &= 1 + \frac{\alpha_s}{\pi} \ln\left(\frac{M_W^2}{\mu^2}\right) \end{aligned}$$

the first-order corrected Hamiltonian becomes:

$$H_W^{(1)} = \frac{G_F}{\sqrt{2}} V_{cs} V_{ud} \left(c_+^{(1)} O_+ + c_-^{(1)} O_- \right) .$$

The form of this equation is, in fact, valid to all orders of perturbation theory. From renormalization group techniques,[10, 11] the constants have the values:

$$c_\pm = \left[\frac{\alpha_S(M_W^2)}{\alpha_S(\mu^2)} \right]^{\gamma_\pm}$$

where the $\gamma_\pm$ are the anomalous dimensions with:

$$\gamma_+ = \frac{6}{33 - 2n_f} = -\frac{\gamma_-}{2}.$$

This Hamiltonian, which is based solely on the spectator diagram and ignores the contribution of the spectator quark, produces the same predictions for all three varieties of D mesons, a fact that is not borne out by experiment. However, annihilation and W-exchange diagrams (see Figure 1.6) which do involve the non-charmed quark will further affect the Hamiltonian and should produce results which depend upon the variety of auxiliary quark. Since these effects are difficult to calculate, a number of phenomenological and theoretical approaches have evolved in an attempt to explain and/or model weak decays of heavy quarks.

Literature abounds with regard to hadronic decays. Most of these papers can be grouped together into several approaches — three of which are described in this thesis.

The factorization approach, a vacuum insertion method, is represented in this thesis by the work of Bauer, Stech and Wirbel[12] and is described in Chapter 7.

The quark diagram scheme is a "model-independent" approach used by Chau and Cheng[13] to explain some of the relationships among various exclusive decay rates and is presented in Chapter 8.

Blok and Shifman's[14–17] perspicacious employment of QCD sum rules to explain weak decays is described in Chapter 9.

Excellent review articles exist which compare and contrast these and other theoretical models.[18, 19, 20]

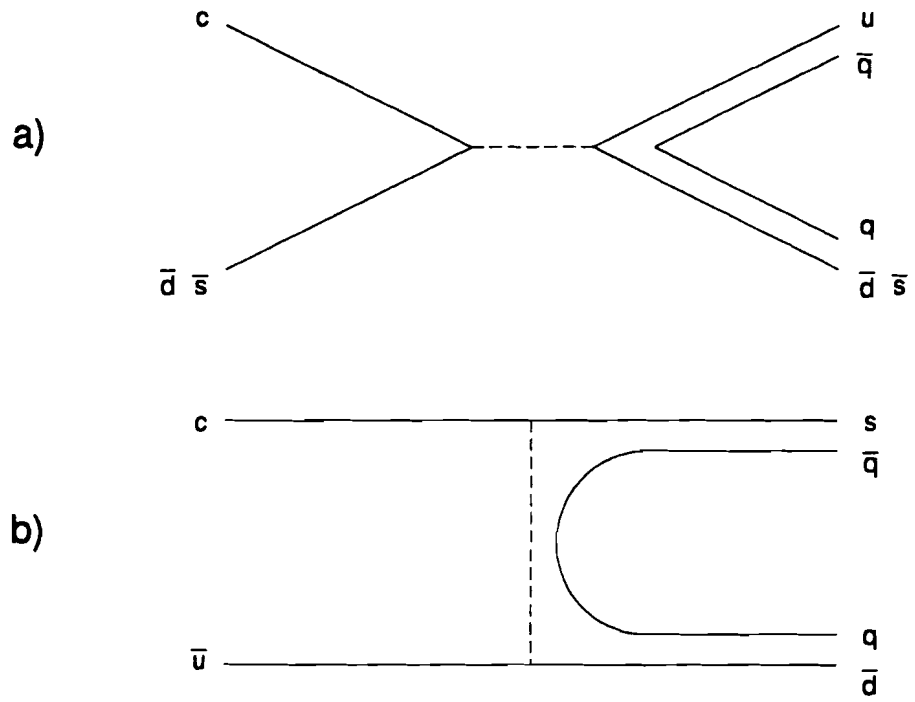

Figure 1.6 a) Annihilation and b) W-exchange diagrams at the quark level

Section 1.3 Inclusive Decay Properties

An exclusive decay property, such as an exclusive branching ratio, is one that depends upon a single decay mode, exclusive of all others. In contrast, an inclusive decay property is one that includes the effects from all decay modes.

The main objective of this thesis is to experimentally determine inclusive properties of D mesons. Another objective is to use exclusive predictions from a variety of theoretical models to make predictions of inclusive properties. It is hoped that an examination of a model's inclusive predictions will lead to a better understanding of the model and possibly to a better determination of the model's parameters.

Charged Particle Multiplicity Distribution

One of the properties which can be determined in an inclusive analysis is the multiplicity distribution of charged particles. Due to conservation of charge, the charge of a decaying D meson will equal the net charge of its decay products. However, the number of decay products will vary from event to event. The distribution of the number

of charged decay products is an inclusive property: the branching ratio for a D meson decaying to n charged particles or $B(D \rightarrow nP^{\pm}X^0)$ where $n = 0, 1, 2, \ldots$ and $P^{\pm}$ represents a charged particle (also known as a *prong*) and X^0 represents zero or more neutral particles.

Another inclusive property, which can be calculated from the charged particle multiplicity distribution, is the average charged particle multiplicity:

$$\langle n_{\rm ch} \rangle = \sum_{n=0}^{\infty} n \times B(D \rightarrow nP^{\pm}X^0) .$$

Kaon Properties

The inclusive properties of charged and neutral kaons are also of interest. For example, a Cabibbo-favored spectator decay of the D^+ or D^0 typically has one s quark in the final state, whereas a D_s^+ decay typically has two s quarks. Thus one expects that the average kaon multiplicity, $\langle n_K \rangle$, for a D_s^+ to be twice as large as for a D^+ or D^0. Annihilation diagrams, however, may alter this simple picture.

The inclusive kaon properties calculated in this analysis are:

- the charged kaon multiplicity distribution. Charged kaons can be divided into *like-sign* kaons (the charge of the kaon matches the *charm* of the D) and *unlike-sign* kaons (the charge of the kaon is opposite the charm of the D).* Throughout this work, whenever inclusive properties are listed, the symbol K^+ will designate a like-sign kaon and the symbol K^- will designate an unlike-sign kaon. There are three charged kaon multiplicity distributions:

  1. $B(D \rightarrow nK^+X)$ where X represents zero or more particles which are not K^+ but can include K^-;
  2. $B(D \rightarrow nK^-X)$ where X represents zero or more particles which are not K^- but can include K^+;

* An equivalent definition for a like-sign kaon is it has the same sign *strangeness* as the charm of the D meson.

3. $B(D \rightarrow nK^{\pm}X)$ where X represents zero or more particles which are neither K^+ nor K^- but can include anything else.

- the neutral kaon multiplicity distribution. Neutral kaons can be described either as a system of K^0 and $\overline{K}^0$ or as a system of K_S and K_L. Theoretical models use the K^0 and $\overline{K}^0$ system, as these are states of definite strangeness, whereas experimentally one measures the K_S and K_L properties. The multiplicity distribution of $K^0 \vee \overline{K}^0$ does not equal the distribution of $K_S \vee K_L$ due to the additional source of K_S and K_L from $\phi(1020)$ decays. The difference is small. There are four neutral kaon multiplicity distributions examined in this thesis:

  1. $B(D \rightarrow nK^0X)$ where X represents zero or more particles which are not K^0 but can include $\overline{K}^0$;
  2. $B\left(D \rightarrow n\overline{K}^0X\right)$ where X represents zero or more particles which are not $\overline{K}^0$ but can include K^0;
  3. $B\left(D \rightarrow n\left(K^0 \vee \overline{K}^0\right)X\right)$ where X represents zero or more particles which are neither K^0 nor $\overline{K}^0$ but can include anything else;
  4. $B(D \rightarrow nK_SX)$ where X represents zero or more particles which are not K_S but can include anything else.

- the inclusive kaon branching ratios, e.g., the fraction of events with at least one K^+ in the final state, $B(D \rightarrow K^+X)$. This is the inclusive property typically reported in the literature.
- the average multiplicity for the K^+, K^-, $K^{\pm}$, K^0, $\overline{K}^0$, and K_S as well as the average multiplicity of any neutral kaon (i.e., $K^0 \vee \overline{K}^0$).
- the momentum spectra for the K^+, K^-, and K_S.

Pion Properties

The inclusive pion properties calculated in this analysis are:

- ☐ the charged pion multiplicity distribution $B(D \to n\pi^{\pm}X)$, where X represents zero or more particles which are not charged pions. As with the kaon case, charged pions can be divided into like-sign and unlike-sign pions. A like-sign pion has the same charge as the charm of its parent D meson. An unlike-sign pion has a charge opposite in sign from the charm of its parent D meson. The charged pion multiplicity distribution separates into:

  1. $B(D \to n\pi^{+}X)$ where X represents zero or more particles which are not π^{+} but can include π^{-};
  2. $B(D \to n\pi^{-}X)$ where X represents zero or more particles which are not π^{-} but can include π^{+};
  3. $B(D \to n\pi^{\pm}X)$ where X represents zero or more particles which are neither π^{+} nor π^{-} but can include anything else.

- ☐ the neutral pion multiplicity distribution $B(D \to n\pi^{0}X)$ where X represents zero or more particles which are not neutral pions.
- ☐ the inclusive branching ratios for π^{+}, π^{-}, $\pi^{\pm}$, and π^{0}, i.e., the fraction of events with at least one pion in the final state $B(D \to \pi X)$.
- ☐ the average multiplicity for π^{+}, π^{-}, $\pi^{\pm}$, and π^{0}.
- ☐ the momentum spectra for the π^{+}, π^{-} and π^{0}.

PART II
EXPERIMENTAL RESULTS

"It is a capital mistake to theorize before one has data."

Sir Arthur Conan Doyle

A Scandal in Bohemia

Chapter 2 The Mark III Detector

Section 2.1 A Brief History

The Mark III spectrometer, used to collect data for this analysis, has served the high energy physics community rather well. Designed in 1978 and installed in the west pit of SPEAR at SLAC in 1981, the detector gathered worthwhile data annually through the end of 1988, and was officially decommissioned in 1990.

Four predominant center-of-mass energy regions have been the focus of intensive study. Physics of the J/ψ and $\psi(3685)$ has occupied about half of the running time of the detector. Charmed meson physics has occupied the other half of the detector's span (see Table 2.1) with D^+ and D^0 mesons originating from decays of the $\psi(3770)$, and the creation of charmed-strange mesons occurring at $\sqrt{s} = 4.14$ GeV — an energy chosen because $D_s^{\pm} D_s^{*\mp}$ production is believed to be maximal with respect to $D_s^+ D_s^-$ production and $D_s^* \overline{D_s}^*$ production.[21]

The Mark III physics program required a detector with the following features:[22]

- large solid angle to identify leptons and hadrons,
- good low-energy photon efficiency to reconstruct π^0 and η mesons,
- minimal amount of material to minimize multiple Coulomb scattering, nuclear interactions, and photon conversions,
- good K/π/e separation at momenta less than 1 GeV by TOF measurement, and additional separation by dE/dx measurement at low momenta, and
- low cost.

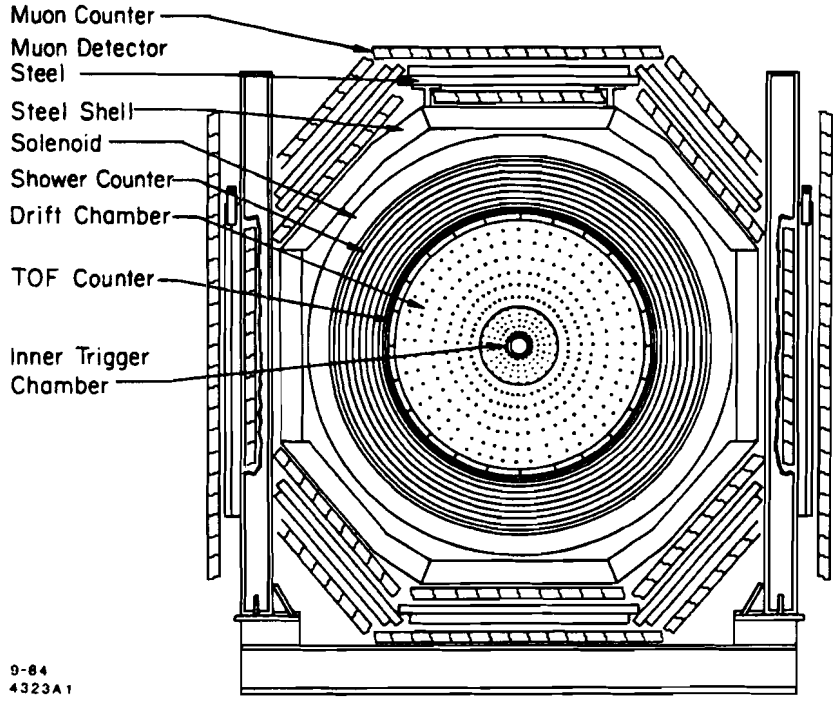

Figure 2.1 Mark III detector (axial view)

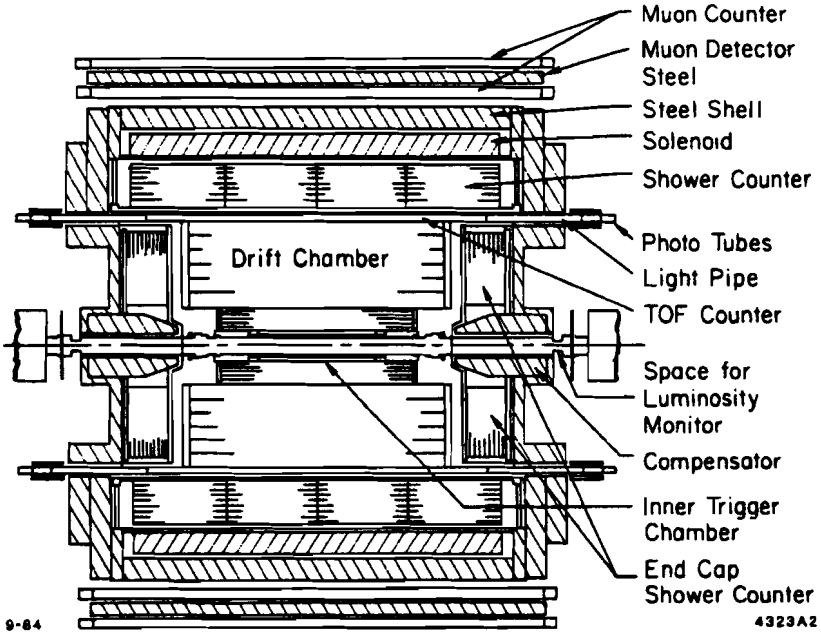

Figure 2.2 Mark III detector (transverse view)

Table 2.1 Data collection history of D mesons at Mark III

Date		Run	Energy	Integrated
Run Start	Run End	Numbers	(GeV)	Luminosity
11/82	12/82	1047 - 1312	3.772	1.51 pb^{-1}
3/83	5/83	1644 - 2085	3.770	3.89 pb^{-1}
1/84	3/84	2219 - 2982	3.766	4.16 pb^{-1}
12/85	2/86	4094 - 4741	4.14	6.30 pb^{-1}

Many papers and theses have described the detector and its components (see References 22–26 for a representative sample). Therefore, only a brief overview of the detector will be presented here. Figures 2.1 and 2.2 present a schematic of the Mark III detector.

Section 2.2 The Drift Chamber

Measuring the positions and momenta of charged particles is the primary purpose of the drift chamber. Providing event triggering information is an important secondary purpose.

The overall momentum resolution of the drift chamber is:

$$\left(\frac{\sigma_p}{p}\right)^2 = (0.015)^2 + \left(0.015\frac{p}{\mathrm{GeV}}\right)^2 .$$

The first term is the error resulting from multiple Coulomb scattering and the second term is the error in the measurement of track sagitta.

Two main elements comprise the drift chamber — the inner trigger chamber (called layer 1), which is situated around the beam pipe, and the main outer drift chamber (layers 2–8), which surrounds the inner trigger chamber.

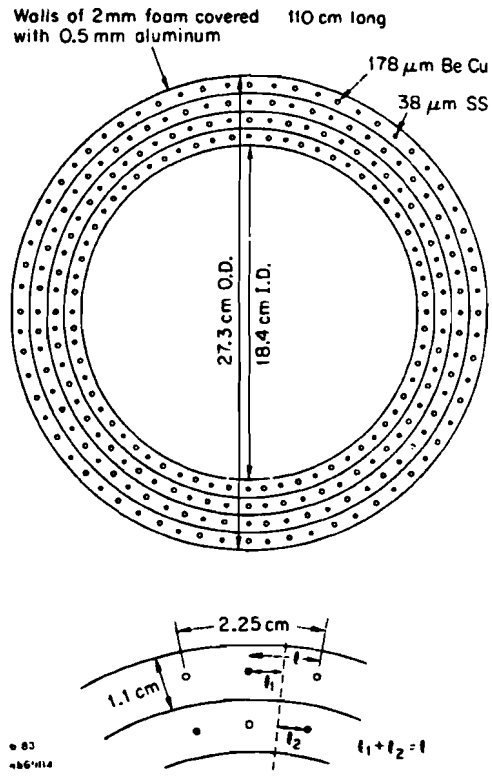

Figure 2.3 Inner trigger chamber

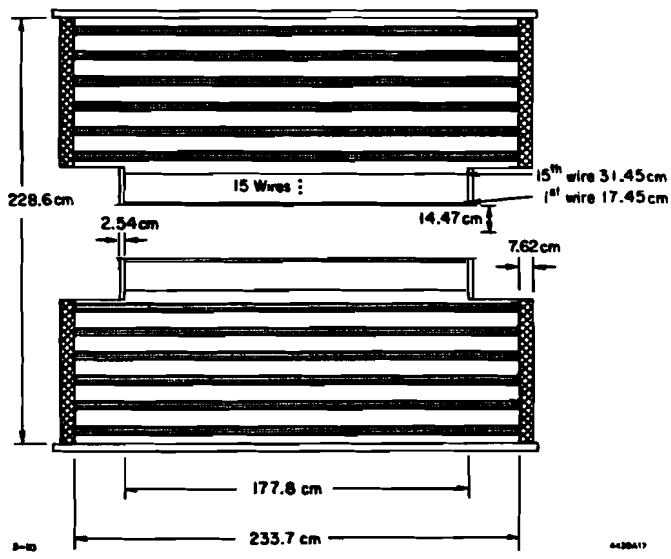

Figure 2.4 Main outer drift chamber (transverse view)

Inner Trigger Chamber

The inner trigger chamber (Figure 2.3) was designed in order to reduce the trigger rate due to cosmic rays and beam gas events and to furnish points near the interaction region for tracking. An important consideration in its design was the minimization of multiple scattering by introducing a minimal amount of material into the detector.

This chamber covers a solid angle of 98% of 4π sr, has a length of 110 cm, an inner radius of 9.2 cm, and an outer radius of 13.65 cm. It consists of four layers of concentric cylinders. The cylinders are separated by 2 mm of foam covered with 0.5 mm of aluminized mylar, thus providing negligible mass in order to reduce scattering of low momentum particles.

Each cylindrical layer consists of a "plane" of 32 cells. Cells are formed by alternating 178 μm thick Be Cu guard wires (at –200 V) with 33 μm stainless steel sense wires (at about 2100 V). Adjacent layers are offset by 1/2 cell.

A gas mixture of 70% Ar and 30% C_2H_6 filled the inner chamber and provided the environment for charged particles to deposit ionized tracks.

The inner trigger chamber was not operational during the D_s run at $\sqrt{s} = 4.14$ GeV. In 1988, a new vertex chamber replaced the inoperative inner trigger chamber.[27]

Main Drift Chamber

The main drift chamber has a 2.29 meter outer diameter, a 2.34 meter length, and consists of seven cylindrically nested regions (layers 2–8). Each region consists of N$\times$16 cells (where N = layer number).

The innermost region (layer 2) is 1.83 m long and consists of 32 axial cells. Each cell is composed of 12 radially positioned tungsten sense wires and 3 guard wires (located at both ends and the middle of the cell). Drift time and charge deposition are measured (dE/dx). A wire stagger of ± 150 μm helps resolve left/right ambiguity as does comparing the χ^2 from fits using left side or right side track hypotheses.

The outer regions (layers 3 through 8) are 2.39 m long. Each cell in these regions consist of three sense wires surrounded by two guard wires at the top and bottom of the cell and bounded on the side with five field wires. Only drift time is measured. Left/right ambiguity is resolved by staggering the sense wires by ±400 μm.

Layers 4 and 6 (stereo layers) help provide a track's z information due to their being twisted, in opposite directions, from axial alignment by 7.7° for layer 4 and –9.0° for layer 6.

The main drift chamber gas is an 89:10:1 mixture of Ar, CO_2, and methane.

Additional information on the main drift chamber can be found in Reference 28.

Section 2.3 The Time-of-Flight (TOF) System

The time-of-flight (TOF) system measures a track's travel time from the interaction point to the TOF system. This time combined with the momentum and position information from the drift chamber yields the velocity and mass of the track.

The time resolution of the time-of-flight system is approximately 200 ps. This provides a 3σ K/π separation up to 0.8 GeV (see Figure 2.5).

The TOF system consists of 48 scintillation counters made of Nuclear Enterprises Pilot F scintillator. Each scintillator has a 5 cm thickness, a 3.2 m length and a slight trapezoidal cross section with an average width of 15.6 cm. The counters are arranged in a cylindrical geometry at a distance of 1.2 m from the interaction region and they cover a solid angle of 80% of 4π sr.

Light pipes direct the scintillation light from each scintillator to Amperex XP2020 photomultiplier tubes. Both ends of the scintillator are read out and a determination of the track's position in z can be made by comparing the times from each end.

See Reference 29 for more information on the TOF system.

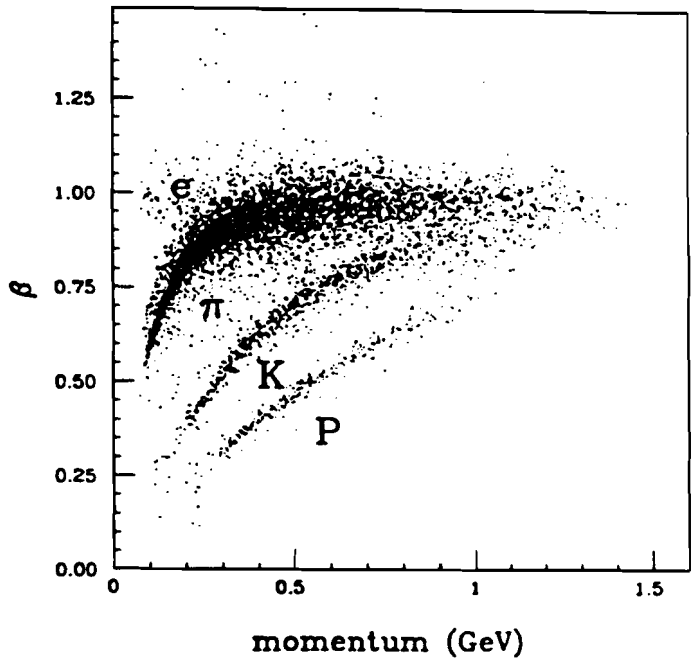

Figure 2.5 Particle identification using the time-of-flight system

Section 2.4 Shower Counters

Detecting photons, especially low-energy photons, is the primary purpose of the shower counter. To accomplish this, the shower counter is situated inside the solenoid coil so that the amount of material between the interaction region and the shower counter is minimized.

The shower counter actually consists of three components. The first component is a cylindrically shaped structure, called the barrel counter (Figure 2.6), which surrounds the TOF system, and covers a solid angle of 80% of 4π. It has a length of 3.85 m and an inner diameter of 2.52 m. The other two components are the endcap shower counters which are located at each end of the detector and extend solid angle coverage to 95% of 4π.

Each component of the shower counter consists of 24 layers of proportional tubes. Adjacent layers are separated by a 0.5 radiation length of lead-antimony alloy. A 47 μm stainless steel sense wire is used to read out both ends of the proportional tube, which is filled with a gas mixture of 80% argon and 20% methane. The location of the shower

in the tube is computed by charge division. The first six layers of proportional tubes are read out individually while the remaining 18 layers are read out as six groups of three.

The shower counter system has an overall energy resolution of:

$$\frac{\sigma_E}{E} = \frac{0.17}{\sqrt{E/\mathrm{GeV}}}$$

and spatial resolutions of $\sigma_z = 2.7$ cm and $\sigma_\phi = 7$ mr.

Additional information about the barrel shower counters can be found in Reference 30. Additional information about the endcap shower counters can be found in Reference 31.

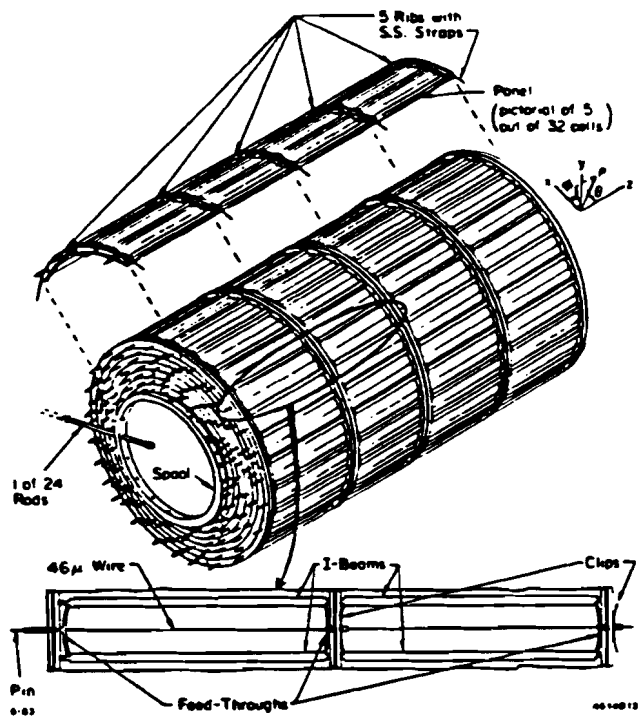

Figure 2.6 Barrel shower counter

Section 2.5 Muon System

Situated outside the shower counter, the solenoid coil, and 20 cm of flux return steel lies the muon system consisting of two octagonal layers of proportional tubes separated by 13 cm of steel. The muon system aids in the identification of muons since only minimum ionizing particles tend to reach the system.

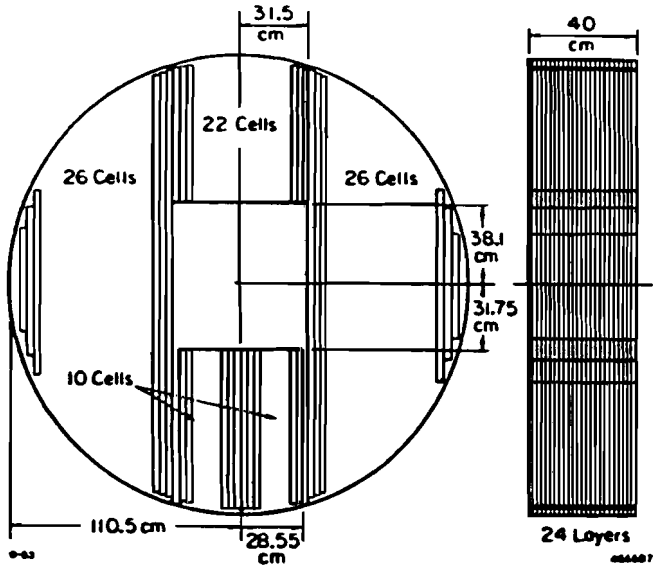

Figure 2.7 Endcap shower counter

Muon detection threshold is at 0.550 GeV. The detection efficiency is very good (greater than 95%) for muons with momenta greater than 0.7 GeV.

Additional information about the muon system can be found in Reference 32.

Chapter 3 The D Data Sets

Section 3.1 The D^0 and D^+ Data Sets

The D^0 and D^+ data were collected in three sets (see Table 2.1) using the reaction $e^+e^- \rightarrow \psi(3770) \rightarrow D\overline{D}$ at a nominal center-of-mass energy of 3.77 GeV. The raw data were reconstructed to yield tracking information with associated position, momentum and energy information. From the reconstructed data, a search was made for D meson decays. All events containing such decays were logged to separate data tapes.

Tagging

The process of identifying tracks originating from a D meson decay is known as tagging. This analysis uses tags from three D^+ decay modes and three D^0 decay modes (see Table 3.1). (D_s^+ tagging is described in the next section.) Decay modes involving π^0 mesons were not used, since they had a substantially higher background. The tagged data set used in this analysis is the same "official" Mark III D^+ and D^0 tagged data set used in many other Mark III analyses. For more information on the tagging process of the D^+ and D^0, see References 24 and 33.

The kinematics of an event, along with the finite resolution of the detector, sometimes make it possible for two or more tags within a single event to share one or more tracks. This ambiguity, which is more prevalent in events with a large number of tracks, must be resolved by a process known as weeding before further analysis can occur.

Weeding

Weeding resolves any conflicts between "overlapping" tags (i.e., tags which share common tracks or have the same charm) in a reconstructed tagged event. When two tags overlap, the tag with the best (i.e., smallest) "measure" is kept and the other is discarded.

Table 3.1 D^+, D^0 and D_s^+ tagging modes and counts

Mode	Number of Tags			
	Total	Weeded	Weeded	Fitted BG
D^+ Mass Regions:	1.8 - 1.9 GeV		1.8621 - 1.8763 GeV	
$D^+ \rightarrow \overline{K}^0\pi^+$	357	353	219	25.2
$\rightarrow K^-\pi^+\pi^+$	2878	2789	1729	255.1
$\rightarrow \overline{K}^0\pi^+\pi^+\pi^-$	1821	1435	473	166.2
Total:		4577	2421	477.6
D^0 Mass Regions:	1.8 - 1.9 GeV		1.8560 - 1.8730 GeV	
$D^0 \rightarrow K^-\pi^+$	1625	1619	1207	131.5
$\rightarrow \overline{K}^0\pi^+\pi^-$	1398	1300	581	218.2
$\rightarrow K^-\pi^+\pi^+\pi^-$	5825	4661	2216	761.0
Total:		7580	4004	1143.2
D_s Mass Regions:	1.65 - 2.05 GeV		1.9416 - 2.0016 GeV	
$D_s^+ \rightarrow \phi\pi^+$	45	43	22	3.8
$\rightarrow \overline{K}^{*0}K^+$	126	120	35	12.5
$\rightarrow \overline{K}^0K^+$	97	97	31	6.2
Total:		260	88	27.9

Table 3.2 Mass-energy correlations for the D^+ and D^0

Property	D^+	D^0
$\overline{m}$	1.8693 GeV	1.8646 GeV
σ_m	0.0036 GeV	0.0029 GeV
$\overline{E}$	1.884 GeV	1.883 GeV
σ_E	0.021 GeV	0.022 GeV
θ	2.5°	1.6°
$\rho_{m.E}$	-24%	-21%
Mass Fit Range	1.860 - 1.880 GeV	1.858 - 1.872 GeV
Number of Tags	2690	3937

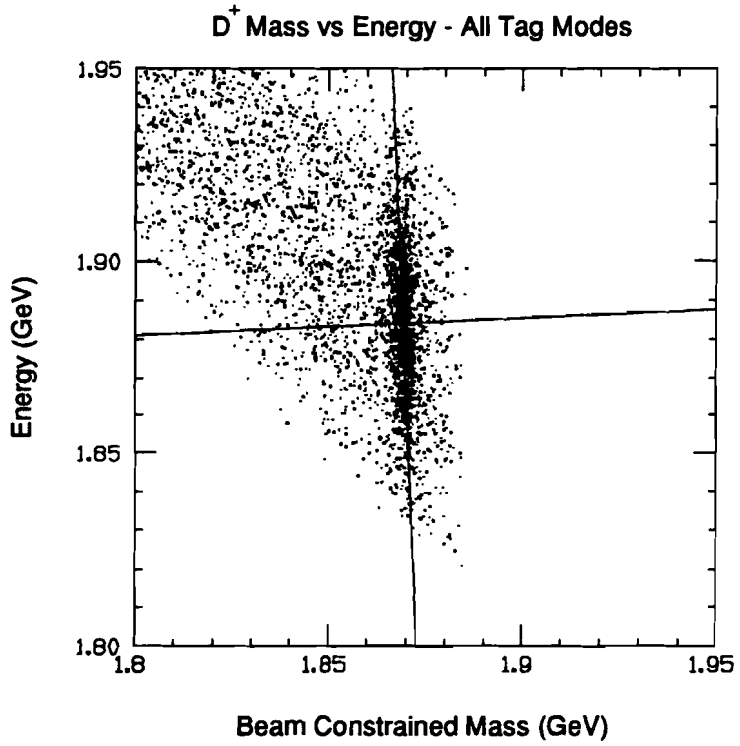

Figure 3.1 Mass-energy correlation of the D^+

This measure depends upon two variables:

1. The mass of the D tag. For D^+ and D^0 tags, the beam-constrained mass, $m_{BC} = \sqrt{E_{\text{beam}}^2 - (\sum \vec{p}_i)^2}$, is used instead of the invariant mass, $m_{\text{inv}} = \sqrt{(\sum E_i)^2 - (\sum \vec{p}_i)^2}$, due to its superior resolution, which arises from the smaller uncertainty in the beam energy versus track energy.
2. The energy of the D tag. It is defined as $E = \sum \sqrt{(p_i^2 + m_i^2)}$, where the m_i are the mass hypotheses of the tag's tracks.

A small correlation exists between these two variables (see Table 3.2 and Figures 3.1 and 3.2) in the mass-energy plane. This leads to defining the measure of a tag as:

$$R^2 = \left| \begin{pmatrix} \cos\theta & \sin\theta \\ -\sin\theta & \cos\theta \end{pmatrix} \begin{pmatrix} (m - \overline{m})/\sigma_m \\ (E - \overline{E})/\sigma_E \end{pmatrix} \right|^2$$

where:

- θ is the angle of rotation of the mass-energy ellipse,

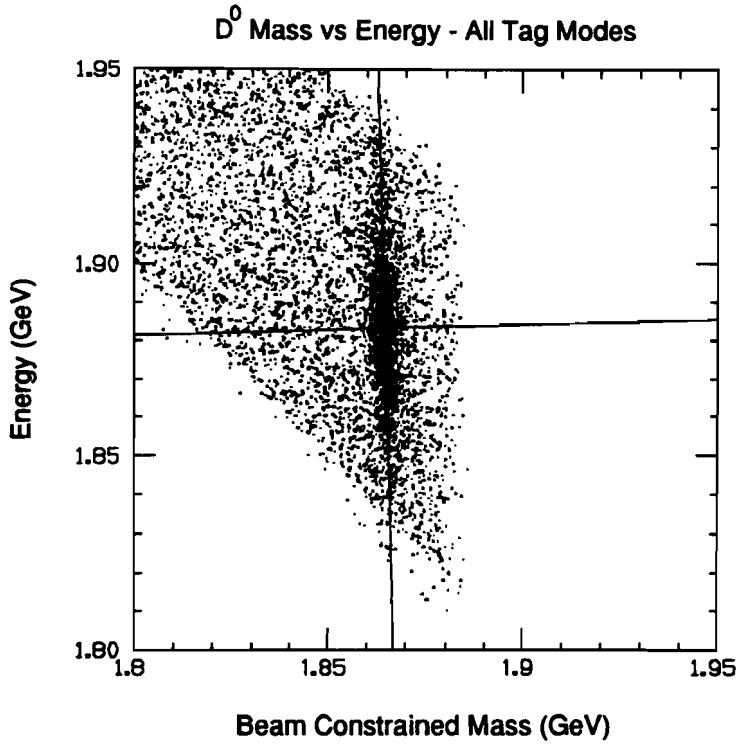

Figure 3.2 Mass-energy correlation of the D^0

- m is the beam-constrained mass of the tag, $\overline{m}$ is the mean mass of all the tags, σ_m is the standard deviation of the mass of all the tags,
- E is the energy of the tag, $\overline{E}$ is the mean energy of all the tags, and σ_E is the standard deviation of the energy of all the tags.

A plot of the beam-constrained mass of the non-overlapping tags in the region 1.8 to 1.9 GeV with the fitted background curve overlaid is shown in Figures 3.3 and 3.4. The signal region is eight bins wide centered on the signal peak. Table 3.1 lists the following information:

a. the total number of tags found in the region plotted in Figures 3.3 and 3.4;

b. the number of non-overlapping, unique (i.e., weeded) tags found in this region;

c. the size of the signal region;

d. the total number of weeded tags in the signal region;

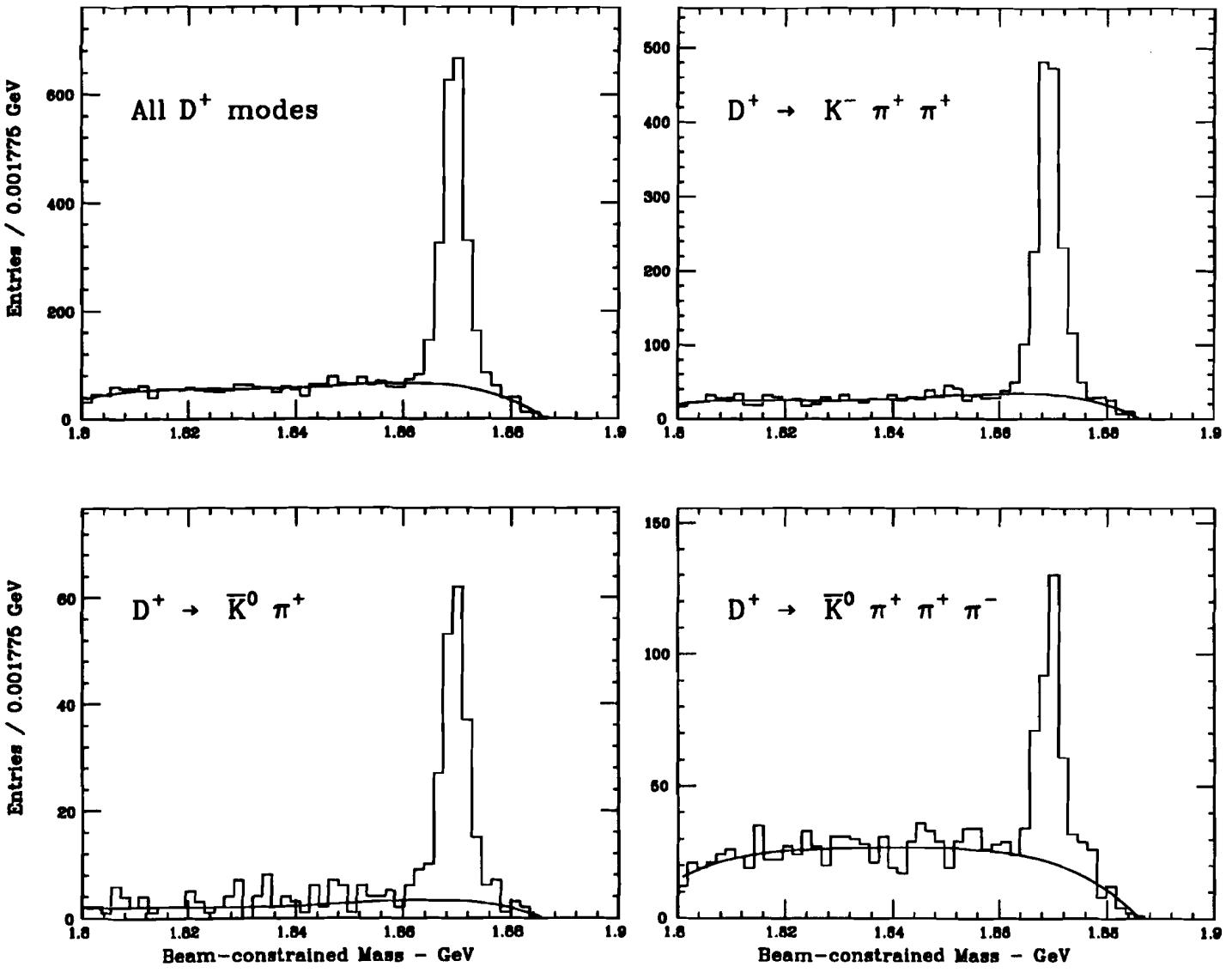

Figure 3.3 Beam-constrained mass histograms for the D^+ decay modes

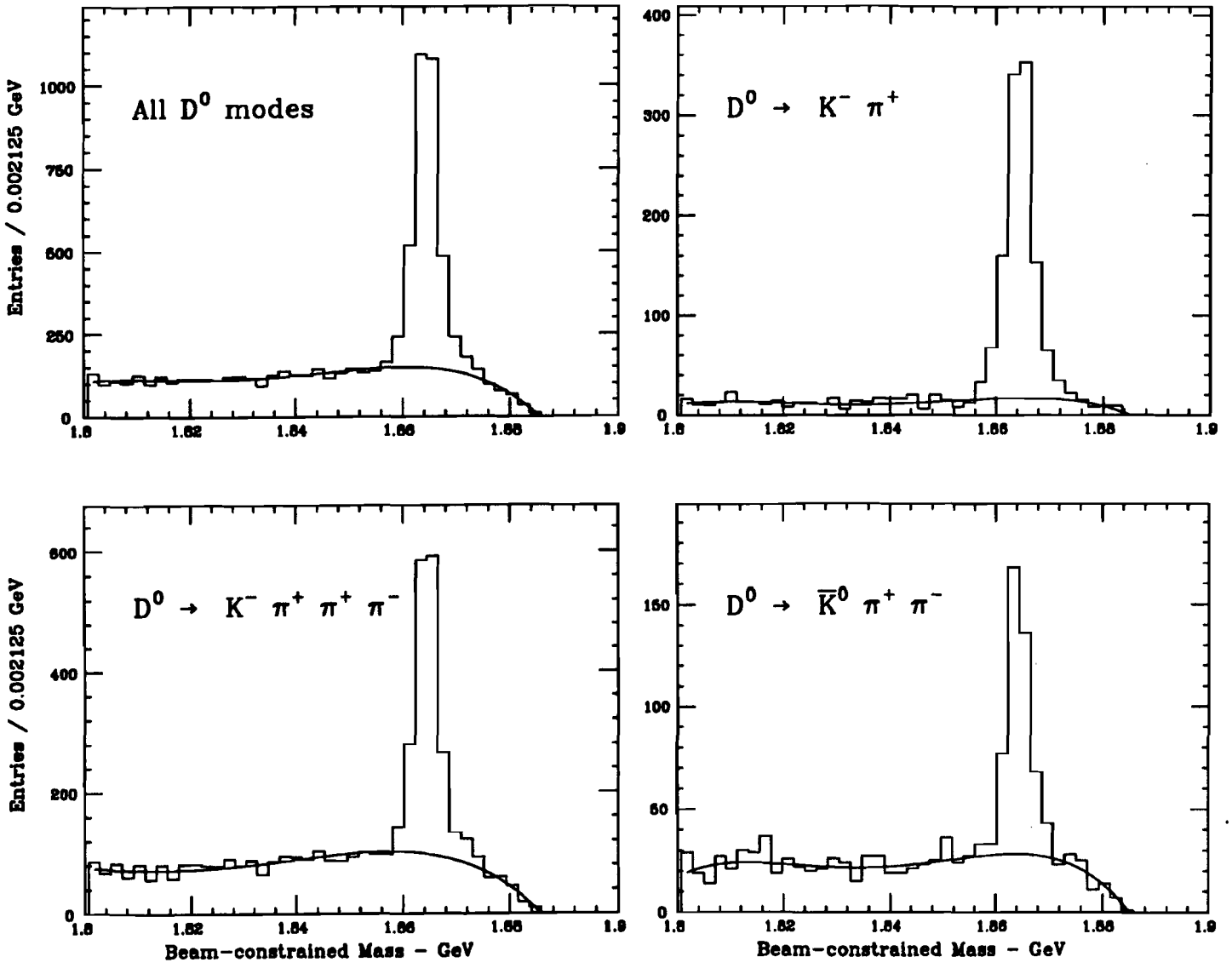

Figure 3.4 Beam-constrained mass histograms for the D^0 decay modes

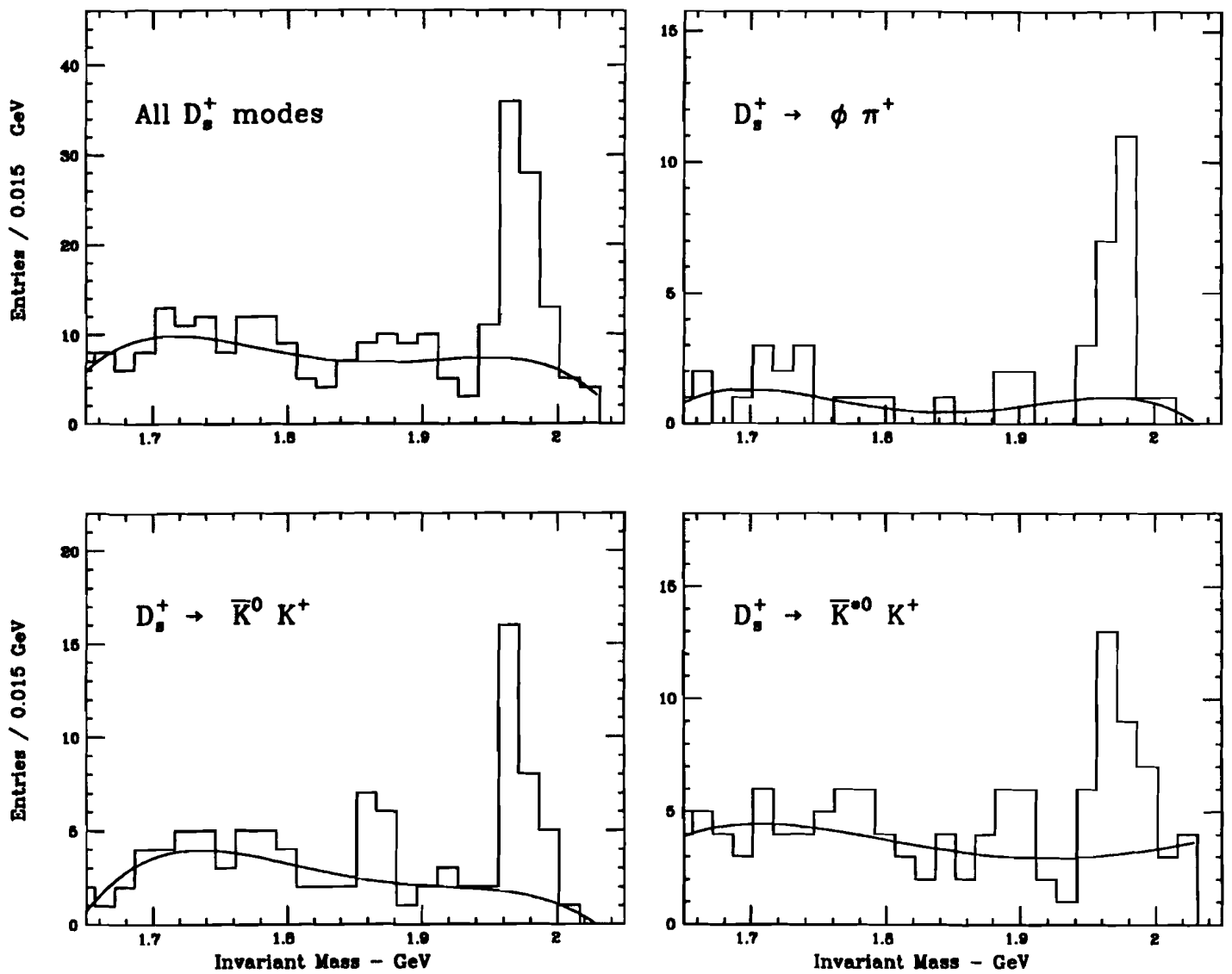

Figure 3.5 Invariant mass histograms for the D_s^+ decay modes

e. the estimated number of background tags in the signal region. This background is determined by fitting all non-zero bins outside of the signal region to a quartic polynomial and determining the area under the curve within the signal region.

Section 3.2 The D_s^+ Data Set

The D_s^+ data were collected in the fall of 1986 at a center-of-mass energy of 4.14 GeV. The reaction $e^+e^- \rightarrow D_s^+D_s^-$ and the reaction $e^+e^- \rightarrow D_s^\pm D_s^{*\mp}$, where the D_s^* meson decays to a D_s meson and a photon, are both possible at this energy.

Three decay modes of the D_s^+ comprise the tag sample (see Table 3.1). Figure 3.5 shows the invariant mass plots with fitted background curves for these modes. The tagging process described below is consistent with other Mark III D_s^+ tagged analyses.[34, 35]

The tagging process differs from the procedure used in forming D^+ and D^0 tags in that it involves a fitting procedure. Because of this, the weeding procedure also differs, since a tag's mass and energy are no longer independent quantities. Only the *invariant* mass of the tag is used in the weeding of overlapping tags.

Particle Identification

In forming a candidate D_s^+ tag, only charged kaon tracks or charged pion tracks are of interest.

Kaon and pion candidate tracks must both:

1. originate within 2 cm radially of the beam axis;
2. have a minimum transverse momentum of 65 MeV;
3. make a sufficiently large angle with the beam axis ($|\cos\theta| \leq 0.85$);
4. be sufficiently well-defined in z to satisfy a helix fit;
5. satisfy a beam-constrained fit to originate within the beam spot with $P(\chi^2) \geq 10^{-4}$;
6. have a good, clean TOF measurement.

A track must meet two additional requirements to be considered a kaon:

$$\frac{|t - t_K|}{\sigma_K} < \frac{|t - t_\pi|}{\sigma_\pi} \qquad \text{and} \qquad \frac{|t - t_K|}{\sigma_K} < 5$$

where:

- t is the measured TOF,
- t_K and t_π are the kaon and pion TOF hypotheses, and
- σ_K and σ_π are the kaon and pion TOF resolutions.

Tracks which do not meet these additional criteria are treated as pions.

The $D_s^+ \to \phi\pi^+$ Decay Mode

A kinematic fitter aids in the tagging of the decay sequence $D_s^+ \to \phi\pi^+ \to K^+K^-\pi^+$ by performing a 1–C (one constraint) kinematic fit on every $K^+K^-\pi^\pm$ combination using the hypothesis $e^+e^- \to K^+K^-\pi^\pm D_s^{*\mp}$. The $D_s^{*\mp}$ is considered to be "missing" with its mass constrained to equal 2.1093 GeV. Only candidates with $P(\chi^2) > 1\%$ for the fit are kept.

To select tags containing a $\phi(1020)$, a cut of $m_{K^+K^-} \in (1.00, 1.04)$ GeV on the fitted K^+K^- mass is imposed (see Figure 3.6). The final invariant mass spectrum is shown in Figure 3.5.

The $D_s^+ \to \overline{K}^{*0}K^+$ Decay Mode

The decay sequence $D_s^+ \to \overline{K}^{*0}K^+ \to K^-\pi^+K^+$ is found by performing a 1–C fit on every $K^+K^-\pi^\pm$ combination using the hypothesis $e^+e^- \to K^+K^-\pi^\pm D_s^{*\mp}$. As before, the $D_s^{*\mp}$ is considered to be "missing" with its mass constrained to equal 2.1093 GeV. Only candidates with $P(\chi^2) > 10\%$ for the fit are kept.

Additional background is rejected by requiring that the angle θ_π of the π^+ in the $\overline{K}^{*0}$ helicity frame satisfy $|\cos\theta_\pi| > 0.3$, since it has a $\cos^2\theta_\pi$ distribution.

Tags with a $\overline{K}^{*0}$ present are selected by cutting on the $K^\pm\pi^\mp$ mass with $m_{K^\pm\pi^\mp} \in$ (0.857, 0.933) GeV (see Figure 3.7). The final invariant mass spectrum is shown in Figure 3.5.

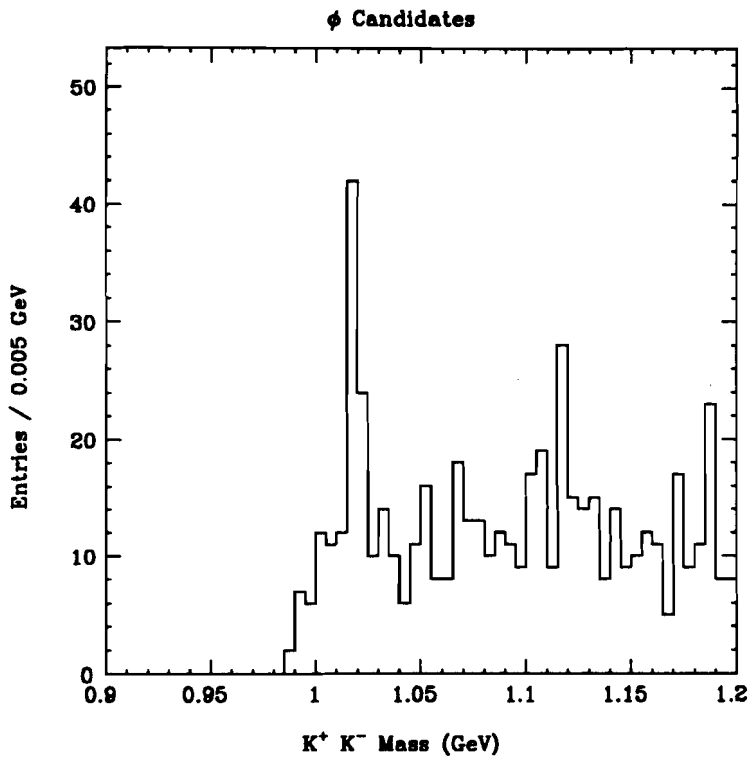

Figure 3.6 Invariant mass of K^+K^-

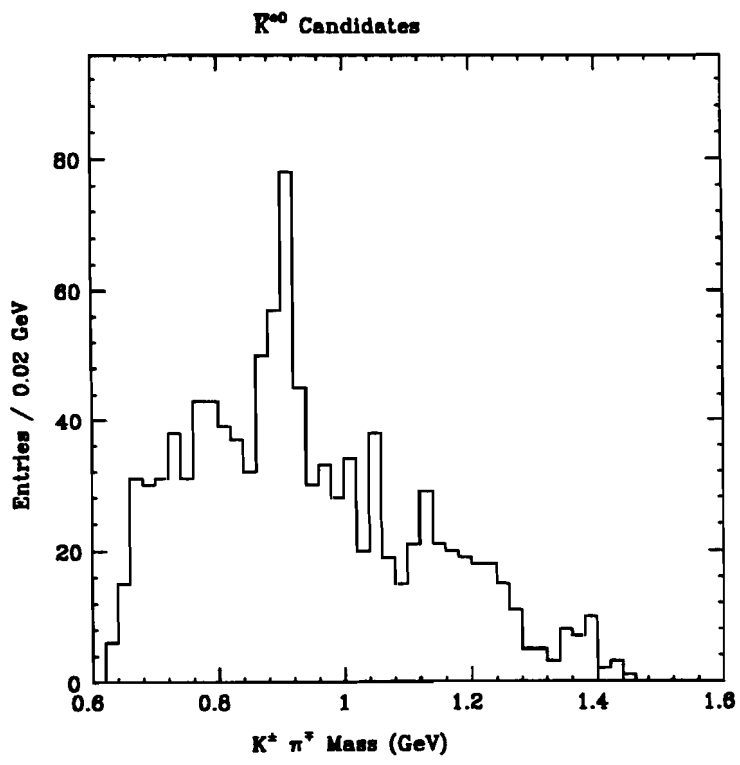

Figure 3.7 Invariant mass of $K^{\pm}\pi^{\mp}$ after the $P(\chi^2)$ and $|\cos\theta_\pi|$ cuts

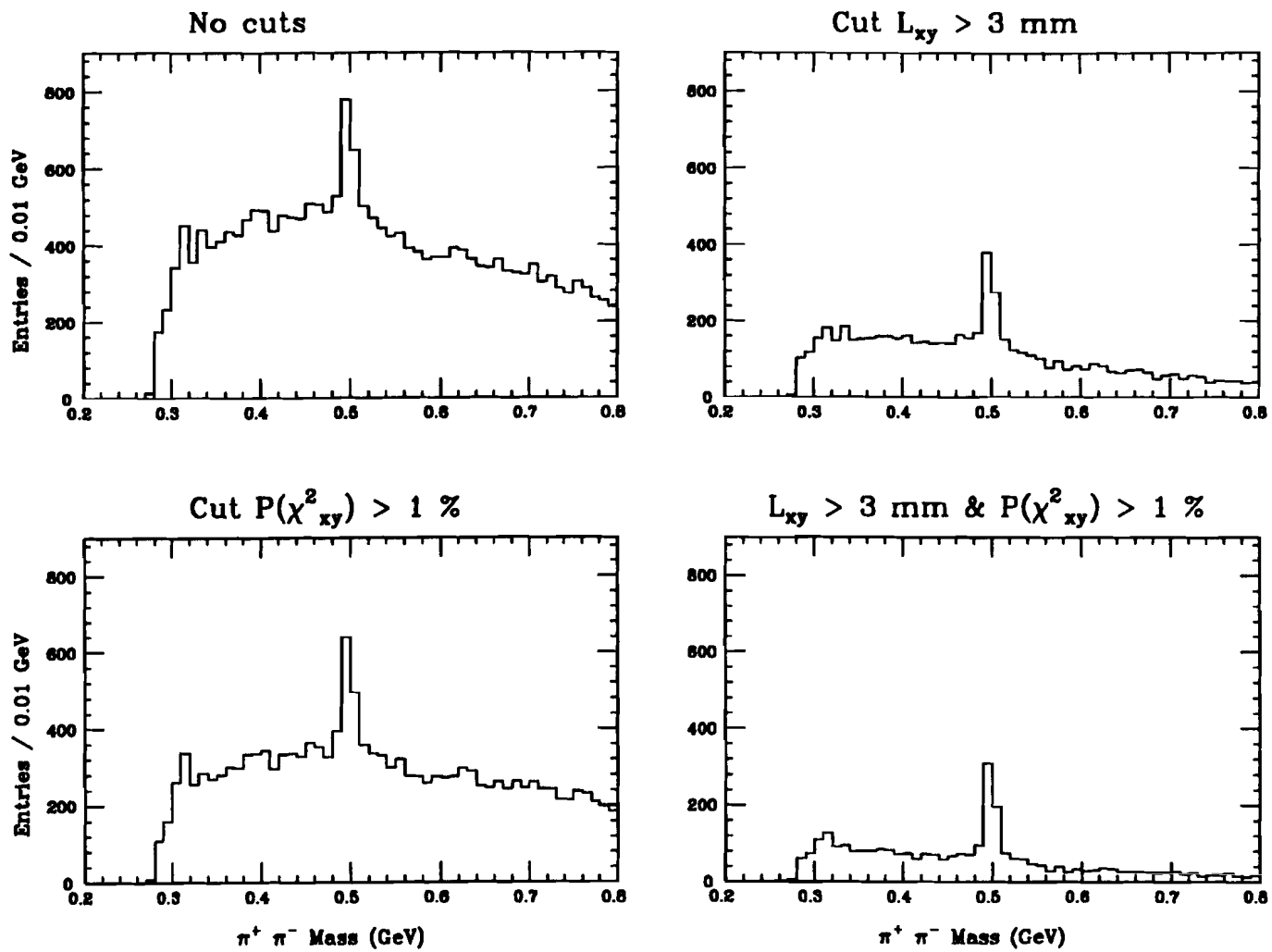

Figure 3.8 Invariant mass of $\pi^+\pi^-$ using different cuts

The $D_s^+ \rightarrow \overline{K}^0 K^+$ Decay Mode

The decay sequence $D_s^+ \rightarrow \overline{K}^0 K^+ \rightarrow \pi^+\pi^- K^+$ is found by performing a 2–C fit on most $\pi^+\pi^- K^\pm$ combinations to the hypothesis $e^+e^- \rightarrow K_S K^\pm D_s^{*\mp}$, constraining the pion pair to originate from a K_S decay. The $D_s^{*\mp}$ is considered to be "missing" with its mass constrained to equal 2.1093 GeV. Only candidates with a $P(\chi^2) \geq 1\%$ from the fit are kept.

$\overline{K}^0$ decays are found through the process $K_S \rightarrow \pi^+\pi^-$. All pairs of oppositely charged tracks are considered $\pi^+\pi^-$ candidates to the K_S fitter, KLAMS.[36] KLAMS uses the dE/dx-corrected track parameters and calculates the crossing points of the track circles projected in the (x,y) plane. The best crossing point is chosen, the track parameters are "swum" to the point, and the $\pi^+\pi^-$ 4–momentum is calculated.

Each K_S candidate must:

1. have its momentum align with the line from the crossing point to the interaction point with a $P(\chi^2) \geq 1\%$, and
2. have a decay length greater than 3 mm.

These additional constraints greatly improve the signal-to-background ratio (see Figure 3.8). K_S candidates are then passed to the kinematic fitter where the constraint that the $\pi^+\pi^-$ mass equal the nominal mass of the K_S is imposed. The final $\pi^+\pi^- K^\pm$ invariant mass spectrum is shown in Figure 3.5.

Chapter 4 Experimental Technique

Section 4.1 Introduction

The main objective of this thesis is to experimentally determine inclusive properties of D mesons. A complete list of inclusive properties presented in this analysis can be found in Section 1.3.*

Since D mesons are produced in pairs ($e^+e^- \rightarrow D\overline{D}$), inclusive properties are studied by examining the tracks recoiling from a tagged D (or $\overline{D}$) decay. A recoil track is defined as a track that does not comprise the tag or any decay product of the tag. Each recoil track is considered for membership in every class of particle studied inclusively. Qualifying members (i.e., those that pass the particle identification cuts) are called candidates. The term "n-candidate event" is defined as an event with n candidates of a particular class recoiling against the tag. For example, an event with three kaons in the recoil is a 3–kaon event. Charged particles are termed prongs: an event with five charged particles is a 5–prong event.

The determination of inclusive properties would be relatively simple if it only involved counting n-candidates. The major difficulties in an inclusive analysis are correcting for track loss due to the inefficiencies of the detector and correcting for impure candidate samples due to the misidentification of non-candidates as candidates.

Previous experimental analyses[37, 35] have determined inclusive charged particle properties by a technique which utilizes a "fold" matrix to compensate for track loss inefficiencies. In the following sections, I present the "fold" matrix technique which I developed for my charged particle analysis and my extension of the technique to kaon analyses; followed by a generalization of the fold matrix concept — the fold tensor — which compensates for particle misidentification.

* The inclusive properties of neutral pions are not experimentally determined in this thesis. Also, the K_S is the only neutral kaon studied experimentally.

Section 4.2 The Fold Matrix

The number of recoiling charged particles, henceforth called recoil prongs, can be miscounted for several reasons. The detector lacks a full 4π coverage: recoil prongs can exit the detector through its cracks or down the beam pipe without being observed. In addition, the particle identification cuts used to define a charged particle will unavoidably reject some good tracks. For example, an angle cut will discard all tracks near the detector's axis.

Monte Carlo studies can be used to estimate these effects on the ability to count recoil prongs. The result can be expressed in the form of an efficiency matrix or "fold" matrix, which takes the generated physics and "folds" it into what is observed. The number of events detected with i recoiling charged particles (called an i-prong event), represented by N_i, is a linear summation of all the events generated from D meson decays with j recoiling charged particles, G_j, folded by the probability of observing a j-prong event as an i-prong event; plus the number of background events, B_i, which do not originate from the D meson decays:

$$N_i = \sum_{j=0}^{\infty} P_{j\to i} G_j + B_i \,.$$

This process can be expressed as the vector equation:

$$\mathbf{N} = F\mathbf{G} + \mathbf{B}$$

where each element of the fold matrix $F_{ij} = P_{j\to i}$ represents the probability that a generated j-prong event will be observed as an i-prong event.

This vector equation can be divided on both sides by the total number of detected tags, $N_T = G_T + B_T$. Using a circumflex symbol to denote a normalized vector, the vector equation becomes:

$$\hat{N} = f_S F \hat{G} + f_B \hat{B}$$

where:

$\hat{N}_i = N_i/N_T$ is the fraction of detected events with i recoil prongs,

$\hat{G}_j = G_j/G_T$ is the fraction of generated events with j recoil prongs,

$\hat{B}_i = B_i/B_T$ is the fraction of i-prong background events,

$f_S = G_T/N_T$ is the fraction of events originating from D meson decays, and

$f_B = B_T/N_T$ is the fraction of events originating from non-D meson decays.

Note that $f_S + f_B = 1$.

For the case of charged multiplicity fold matrices, we can take advantage of the conservation of charge (a D^0 decay does not generate odd-prong events and a D^+ or D_s^+ does not generate even-prong events) to separate the fold matrix into two — even-prong matrices and odd-prong matrices. Every second column of these fold matrices is identically zero. To facilitate notation, these zero columns, and the corresponding zeroes in the vector $\hat{G}$, are collapsed. At Mark III energies, detected charged particle multiplicities larger than seven or eight rarely occur, so these higher multiplicity elements are also dropped from the vectors. This yields charged particle fold matrices with dimensions of 7×4 or 8×4 typically.

Fold Matrix Approximation

To a first approximation, the fold matrix measures detector efficiency. The fold matrix can be parameterized by a single parameter ϵ, which is the efficiency of single charged particle detection. Each element of the fold matrix would be:

$$F_{ij} = P_{j\to i} = \binom{j}{i}\epsilon^i(1-\epsilon)^{j-i}$$

where:

i is the number of detected prongs,

j is the number of generated prongs, and

$\binom{j}{i}$ is the combinatorial term.

For example, a first estimate to the charged particle detection efficiency is $\epsilon = 0.85$, since the definition of a charged particle includes a cut of $|\cos\theta| \leq 0.85$. A 6×3 charged particle fold matrix for the D^+ would thus look like:

$$\begin{pmatrix} 1-\epsilon & (1-\epsilon)^3 & (1-\epsilon)^5 \\ \epsilon & 3\epsilon(1-\epsilon)^2 & 5\epsilon(1-\epsilon)^4 \\ 0 & 3\epsilon^2(1-\epsilon) & 10\epsilon^2(1-\epsilon)^3 \\ 0 & \epsilon^3 & 10\epsilon^3(1-\epsilon)^2 \\ 0 & 0 & 5\epsilon^4(1-\epsilon) \\ 0 & 0 & \epsilon^5 \end{pmatrix} = \begin{pmatrix} .150 & .003 & .000 \\ .850 & .057 & .002 \\ 0 & .325 & .024 \\ 0 & .614 & .138 \\ 0 & 0 & .392 \\ 0 & 0 & .444 \end{pmatrix}.$$

However, this approach is too simplified, since many other processes contribute to the efficiency matrix. A better approach is to determine the fold matrix via Monte Carlo simulation.

Fold Matrix Determination

To determine a fold matrix, a Monte Carlo sample of events is generated, reconstructed, tagged, and weeded.* Each event then goes through the following steps:

1. Matching. Each remaining weeded tag (there may be two) is compared to the generated Monte Carlo tags for that event. Those that match are marked for inclusion in the fold matrix. Matching requires that:

   a. the decay mode of the reconstructed tag is the same as the generated tag's decay mode,

   b. the tracks making up the reconstructed tag are the same tracks making up the generated tag, and

   c. the charm of the reconstructed tag is the same as the charm of the generated tag.†

---

* The tagging and weeding procedures are briefly described in Section 3.1.

† This condition is relaxed for the decay mode $D^0 \to \overline{K}^0\pi^+\pi^-$ since it is impossible to determine the charm of the D^0.

2. Counting. The number of recoil j-prongs generated and the number of recoil i-prongs detected are determined. The corresponding element, (i,j), in a matrix is incremented by one.
3. Normalizing. When all the tagged events have been processed, each *column* of the matrix is normalized to one. This column-normalized matrix is the fold matrix.

Extension to Other Particle Species

A fold matrix can also be used to analyze classes of particles other than the "charged particle" class. Each class of particle, such as K^+, K^-, $K^\pm$, or K_S, will have its own fold matrix. The term "i-prong", which refers to charged particles, gives way to the term "i-candidate", which refers to the number of recoiling tracks belonging to the candidate's species. In the instances where confusion may arise, a superscript on the fold matrix, detected vector or generated vector elements will indicate the particle class (e.g., $F_{ij}^{(P^\pm)}$ versus $F_{ij}^{(K^+)}$, where the $P^\pm$ indicates a charged particle).

The fold matrix technique fails, however, when misidentification of non-candidate species' tracks as candidate particles causes significant contamination of the candidate sample. This is the case, for example, with the π^+ and $\pi^\pm$ classes of particles, which have a large contamination due to lepton misidentification. Even so, an extension of the fold matrix — the fold tensor — can resolve this difficulty. The fold tensor technique is described in Section 4.5.

Section 4.3 Analytic Unfold

The equation $\hat{N} = f_S F \hat{G} + f_B \hat{B}$ can be solved for $\hat{G}$ by a least squares technique. The solution is analytically expressed as:

$$\hat{G} = \left(F^t F\right)^{-1} F^t \left(\hat{N} - f_B \hat{B}\right) \frac{1}{f_S}$$

where F^t is the transpose of the fold matrix F. This technique, however, has two deficiencies.

First, it requires that the background vector elements, $\hat{B}_i$, be predetermined and fixed parameters. A better technique would be one for which background fractions could be made free parameters and solved simultaneously with the $\hat{G}$. The least squares technique is unable to handle this requirement in a natural way.

Second, the solution will not always normalize to one. The least squares technique returns the best solution in $\hat{G}$ space without the constraint that the elements of $\hat{G}$ must sum to one. This solution is unphysical.

Section 4.4 Unfold using Maximum Likelihood

A better technique, where the solution can be constrained to a unit normalization and the background events can be fit, is the method of maximum likelihood.

The likelihood function for any multiplicity distribution is a multinomial probability distribution:

$$\mathcal{L} = \left(\prod_{i=0}^{n} (P_i)^{N_i} \right) \frac{N_T!}{\prod_i (N_i!)}$$

where:

P_i is the probability of observing an i-candidate,

N_i is the total number of observed i-candidate events,

$N_T = \sum_i N_i$ is the total number of events,

n is the maximum candidate number,* and

$N_T! / \prod_i (N_i!)$ is the combinatorial term.

Taking the natural logarithm of the likelihood function gives us the log likelihood:

$$\log \mathcal{L} = \left(\sum_{i=0}^{n} N_i \times \log (P_i) \right) + \log (N_T!) - \sum_{i=0}^{n} \log (N_i!) .$$

The terms $\log (N_T!)$ and $\sum_i \log (N_i!)$ are constants and can be discarded, since they do not contribute to finding the location of the maximum. The log likelihood function thus

* Although in principle there can exist events with a large i-candidate count, in practice one imposes a cutoff at some number designated here as n.

becomes:

$$\log \mathcal{L} = \sum_{i=0}^{n} N_i \times \log(P_i).$$

It is this function which is to be maximized.

The i-candidate probability, P_i, consists of a signal part and a background part:

$$P_i = f_S \left(\sum_j F_{ij} \hat{G}_j \right) + f_B \hat{B}_i$$

where:

- $\sum_j F_{ij} \hat{G}_j$ is the fraction of signal i-candidates,
- $\hat{B}_i = B_i / B_T$ is the fraction of background i-candidates with B_i being the fitted number of background events within the signal region and $B_T = \sum_i B_i$ being the total number of background events,
- $f_S = G_T / N_T$ is the global fraction of signal events, and
- $f_B = B_T / N_T$ is the global background fraction, with $f_S + f_B = 1$.

Background Fitting

An added benefit to using a maximum likelihood method is that the background can be fit. Unfortunately, the background cannot be a completely free parameter since there are not enough constraints to give an unambiguous solution.

If an independent estimate of the background can be obtained, however, then one may impose additional constraints by requiring that the fitted number of background events be approximately equal to the observed number of background events. This produces additional terms in the likelihood function:

$$\prod_{i=0}^{n} P_B(B_i, B_i^0).$$

The form of the background distribution is difficult to determine a priori. For this analysis a Gaussian distribution is used:

$$P_B(x_i, \mu_i, \sigma_i) = \frac{1}{\sigma_i \sqrt{2\pi}} e^{\frac{-(x_i - \mu_i)^2}{2\sigma_i^2}}$$

where:

$x_i = B_i$ is the fitted number of background events,

$\mu_i = B_i^0$ is the observed number of background events, and

$\sigma_i = \sigma_{B_i^0}$ is the standard deviation of the observed number of background events.

Other possible distributions are the Poisson distribution:

$$P_B(x_i, \mu_i) = \frac{\mu_i^{x_i}}{x_i!} e^{-\mu_i}$$

and a "constant" distribution:

$$P_B(x_i, \mu_i) = \delta(x_i - \mu_i)$$

that fixes the fitted number of background events to equal the observed number of background events. These two distributions are used when estimating the size of the systematic error of the unfold results.

Log Likelihood Function

The complete expression for the log likelihood function becomes:

$$\log \mathcal{L} = \sum_{i=0}^{n} N_i \times \log \left(\left(1 - \frac{B_T}{N_T}\right) \sum_j F_{ij} \hat{G}_j \; + \; \frac{B_i}{N_T} \right) + \log \left(P_B(B_i, B_i^0) \right).$$

Maximizing the Log Likelihood Function

The general-purpose minimization program MINUIT[38] is used to maximize the log likelihood expression,* yielding the optimal values of the $\hat{G}_j$ and the B_i.

In order to build in the constraints $\sum \hat{G}_i = 1$ and $0 \leq \hat{G}_i \leq 1$ while maintaining a smooth likelihood function (discontinuities can cause problems when using minimization algorithms), a change of variables is required. The variables, $\hat{G}_i$, become functions of new variables:

$$\hat{G}_i = \frac{x_i^2}{\sum_j x_j^2}$$

* Instead of finding the maximum of the log likelihood, one finds the minimum of the negative log likelihood.

and the new variables, x_i, are used by MINUIT with no bounds. This fulfills the requirement that $\hat{G}$ is normalized and each component has a value between 0 and 1. However, the constraint $\sum \hat{G}_i = 1$ degenerates the problem by one independent variable. This is implemented by constraining one of the x_i to be constant. The result depends neither upon which x_i is chosen to be constant nor upon the value of that constant.

When calculating the error matrix of the $\hat{G}$ elements from the x_i, the standard transformation formula is used:

$$\sigma^2_{\hat{G}_a\hat{G}_b} = \sum_j \sum_k \sigma^2_{x_j x_k} \left(\frac{\partial \hat{G}_a}{\partial x_j}\right)\left(\frac{\partial \hat{G}_b}{\partial x_k}\right)$$

$$\frac{\partial \hat{G}_a}{\partial x_a} = \frac{2x_a\left(1-\hat{G}_a\right)}{\sum_k x_k^2}$$

$$\frac{\partial \hat{G}_a}{\partial x_j} = \frac{-2x_j\hat{G}_a}{\sum_k x_k^2} \qquad a \neq j\,.$$

Section 4.5 The Fold Tensor

One of the problems with the fold matrix approach, especially when used with a particular particle species (as opposed to generic charged particles), is that misidentification of non-candidate species as candidate particles will cause the unfold process to fail. The unfold formalism, as presented so far, is not designed to compensate for misidentification contamination. A new formalism is required.

The new formalism which I have developed utilizes a fold tensor, which is a generalization of the fold matrix concept. A fold tensor must be used when there is significant misidentification among particle species. The vector equation $\mathbf{N} = F\mathbf{G} + \mathbf{B}$ (i.e., $N_i = \Sigma F_{ij} G_j + B_i$) generalizes to the tensor equation $\mathsf{N} = \mathsf{F}\mathsf{G} + \mathsf{B}$.

Topology

With a tensor formalism, two or more classes of species are analyzed simultaneously. The ordering of the species has a one-to-one correspondence with the indices of the various tensors. This ordering is called a "topology". A rank R topology, $[p, q, r, ...]$, is an ordered R-tuple representation of particle species $p, q, r, ...$ When referring to the indices of a tensor, an $(ijk...)$ topology implicitly refers to the topology $[p, q, r, ...]$ and is an event with i particles of species type p, j particles of type q, k of type r, etc. The species involved are usually clear from the context of the problem, but explicit superscripts will be used whenever confusion may occur. The mathematics remains the same, however.

In a rank 4 $\left[e^{\pm}, \mu^{\pm}, \pi^{\pm}, K^{\pm}\right]$ topology, for example, a (1031) topological event indicates an event containing one electron, no muons, three charged pions and one charged kaon. G_{1031} is the number of generated events with a (1031) topology.

Each element of N in the tensor equation $\mathsf{N} = \mathsf{F}\mathsf{G} + \mathsf{B}$ can be represented as a linear summation of the tensors G and B. The expression for a fourth rank topology is:

$$N_{abcd} = \sum_{i=0}^{n_1} \sum_{j=0}^{n_2} \sum_{k=0}^{n_3} \sum_{l=0}^{n_4} F_{abcdlkji} G_{ijkl} + B_{abcd}$$

where:

- N_{abcd} is the number of events detected with topology $(abcd)$,
- $F_{abcdlkji} = P_{ijkl \to abcd}$ is the probability of observing an event with a $(abcd)$ topology when an event with a $(ijkl)$ topology is generated,
- G_{ijkl} is the number of events generated with topology $(ijkl)$,
- n_1, n_2, n_3, and n_4 are the upper limit cutoffs for the indices i, j, k, and l, and
- B_{abcd} is the number of background events (from non-D tags) with topology $(abcd)$.

The fold tensor notation $F_{abcdlkji}$ has a somewhat non-obvious meaning. Thus, the equivalent notation $P_{ijkl \to abcd}$ will henceforth be used.

The tensor rank of the fold tensor is a function of the topology. The topology chosen will depend upon the problem being analyzed. A general case example is the topology $[e^+, e^-, \mu^+, \mu^-, \pi^+, \pi^-, \pi^0, K^+, K^-, K_S^0, K_L^0, \gamma]$, which yields rank 12 N, G, and B tensors and a rank 24 fold tensor, F. Fortunately, under certain circumstances the fold tensor equation simplifies. The topology can even reduce to a single particle class topology, in which case the fold tensor reduces to the case of the fold matrix. However, this requires that the particle identification for that particle class be sufficiently good so that no impurities enter the sample. This requirement will be demonstrated later in this chapter.

Fold Tensor Parametrization

As the fold matrix (a rank 1 topology) can be parametrized by a single parameter, the fold tensor for a rank R topology, $[p, q, r, ...]$, can be parametrized by R^2 parameters.

In the general case of $P_{ijk...\rightarrow abc...}$, I will denote the generated topology indices as $(ijk...)$, the detected topology indices as $(abc...)$, and the corresponding parameters as $p_n, q_n, r_n, ...$, where $n = 0, 1, ..., R$.

Recall, for a rank 1 topology:

$$P_{i\rightarrow a} = \binom{i}{a}(p_1)^a(p_0)^{i-a}$$

where:

p_1 is the probability of detecting the track from a particle p as a particle p,

$p_0 = 1 - p_1$ is the probability of not detecting the track at all, and

$\binom{i}{a}$ is the number of ways of choosing the a detected particles from the i generated particles.

For a rank 2 topology:

$$P_{ij\to ab} = \sum_{i_2=0}^{i}\sum_{j_2=0}^{j}\binom{i}{i_2}\binom{i-i_2}{a-j_2}(p_2)^{i_2}(p_1)^{a-j_2}(p_0)^{[(i-i_2)-(a-j_2)]}$$
$$\times\binom{j}{j_2}\binom{j-j_2}{b-i_2}(q_2)^{j_2}(q_1)^{b-i_2}(q_0)^{[(j-j_2)-(b-i_2)]}$$

where:

p_1 is the probability of identifying a particle p track as a particle p,

p_2 is the probability of identifying a p track as the particle q, and

$p_0 = 1 - p_1 - p_2$ is the probability of not detecting the particle p track at all.

Similarly,

q_1 is the probability of identifying a particle q track as a particle q,

q_2 is the probability of identifying a q track as a particle p, and

$q_0 = 1 - q_1 - q_2$ is the probability of not detecting the particle q track at all.

In addition,

i_2 and j_2 are indices indicating the number of misidentified p and q particles,
$\binom{i}{i_2}$ and $\binom{j}{j_2}$ are the number of combinations of misidentified p and q particles,
$\binom{i-i_2}{a-j_2}$ and $\binom{j-j_2}{b-i_2}$ are the number of combinations of non-misidentified, detected p and q particles.

In this form, $0^0 \equiv 1$ and $\binom{n}{m} \equiv 0$ if $n < 0$ or $m < 0$.

For a rank 3 topology (p, q, r), the fold tensor elements are:

$$P_{ijk\to abc} = \sum_{i_2=0}^{i}\sum_{i_3=0}^{i}\sum_{j_2=0}^{j}\sum_{j_3=0}^{j}\sum_{k_2=0}^{k}\sum_{k_3=0}^{k}$$
$$\times\binom{i}{i_2}\binom{i-i_2}{i_3}\binom{i-i_2-i_3}{a-k_2-j_3}(p_2)^{i_2}(p_3)^{i_3}(p_1)^{a-k_2-j_3}(p_0)^{[(i-i_2-i_3)-(a-k_2-j_3)]}$$
$$\times\binom{j}{j_2}\binom{j-j_2}{j_3}\binom{j-j_2-j_3}{b-i_2-k_3}(q_2)^{j_2}(q_3)^{j_3}(q_1)^{b-i_2-k_3}(q_0)^{[(j-j_2-j_3)-(b-i_2-k_3)]}$$
$$\times\binom{k}{k_2}\binom{k-k_2}{k_3}\binom{k-k_2-k_3}{c-j_2-i_3}(r_2)^{k_2}(r_3)^{k_3}(r_1)^{c-j_2-i_3}(r_0)^{[(k-k_2-k_3)-(c-j_2-i_3)]}$$

where:

p_1 is the probability of identifying a particle p track as a particle p,

p_2 is the probability of identifying a p track as a particle q,

p_3 is the probability of identifying a p track as a particle r, and

$p_0 = 1 - p_1 - p_2 - p_3$ is the probability of not detecting the particle p track at all.

Similarly,

q_1 is the probability of identifying a particle q track as a particle q,

q_2 is the probability of identifying a q track as a particle r,

q_3 is the probability of identifying a q track as a particle p, and

$q_0 = 1 - q_1 - q_2 - q_3$ is the probability of not detecting the q track at all.

In addition,

r_1 is the probability of identifying a particle r track as a particle r,

r_2 is the probability of identifying an r track as a p,

r_3 is the probability of identifying an r track as a q, and

$r_0 = 1 - r_1 - r_2 - r_3$ is the probability of not detecting the particle r track at all.

As we go to higher tensor ranks, the number of summation signs increases as $R \times (R-1)$. Each of the R particles in the topology has $R-1$ summations associated with it. Each summation represents the number of particles misidentified as one of the other types.

Tensor Dimensions

Any given topology has a cutoff in the upper limit of a particular index. For example, in a $[e^{\pm}, \mu^{\pm}, \pi^{\pm}, K^{\pm}]$ topology, one might not expect more than three electrons or one muon or eight pions or three kaons. Since tensor indices are zero based in this formalism, the tensor G_{ijkl} has a dimension of 4×2×9×4.

Defining n_i as the cutoff associated with the ith particle in the topology, the maximum number of particles possible for a given topology is $n = \sum_{i=1}^{R} n_i$, where R is the rank of the topology. In the above example, $n_1 = 3$, $n_2 = 1$, $n_3 = 8$, $n_4 = 2$, and $n = 3 + 1 + 8 + 3 = 15$ particles possible in the final state.

The number of particles possible in the final state, n, is important for determining the dimensions of the tensor N_{abcd}. To allow for the possible case of all n particles becoming misidentified into one category, one could dimension N as $(n+1)\times(n+1)\times(n+1)\times\ldots$ for a total of $(n+1)^R$ "slots". Many of these "slots" will equal zero.

In making the assumption that particles can only be identified correctly, misidentified or lost (i.e., particles are not created from "nothing"), a reasonable condition on the fold tensor is:*

$$P_{ijkl\rightarrow abcd} = 0 \qquad \forall \quad (i+j+k+l) < (a+b+c+d)\,.$$

This statement reduces the maximum number of non-zero slots to $(n+R)!/(n!R!)$.

Matrix Equivalent Form

One can express the tensor equations involved in a vector form for ease of visualization and without loss of generality. The N tensor is expressed as an $n_N \times 1$ column vector, where $n_N = (n+R)!/(n!R!)$. The G tensor is expressed as an $n_G \times 1$ column vector where $n_G = (n_1+1)\times(n_2+1)\times(n_3+1)\times\ldots$. The fold tensor is expressed as an $n_N \times n_G$ matrix. There is no "natural" correspondence between a tensor's elements and the elements of the new column vector.

The matrix equivalent form is possible because the indices of the fold tensor do not mix. In other words, the form $N_{abcd} = P_{ijkl\rightarrow abcd}G_{ijkl}$ is similar to the matrix equation $N_A = P_{I\rightarrow A}G_I$, but now we generalize with $A = (abcd)$ and $I = (ijkl)$.

---

* This condition is not enforced when calculating the fold tensor from a Monte Carlo analysis, but is listed to reduce the number of equations involved in studying the behavior of fold tensors.

Separating the Fold Tensor

Under what conditions can we reduce the two particle topology [$K^{\pm}$, $X^{\pm}$] to the single rank topology [$K^{\pm}$]? In the rank 2 topology, the first index refers to the number of charged kaons ($K^{\pm}$) and the second index refers to the number of other charged particles ($X^{\pm}$). For illustrative purposes, let us assume that the maximum number of kaons will be two and the maximum number of other particles will be one so that the dimension of the G tensor is 3×2.

The fold tensor equation is:

$$N_{ab} = \sum_{i=0}^{2} \sum_{j=0}^{1} P_{ij \to ab} G_{ij} + B_{ab} \, .$$

Using the parametrization for a rank 2 topology (see page 48), the parameters are now defined as:

p_1 is the probability of identifying a single kaon track as a kaon,

p_2 is the probability of misidentifying a kaon track as something else,

$p_0 = 1 - p_1 - p_2$ is the probability of not detecting a kaon track,

and

q_1 is the probability of identifying a non-kaon track as a non-kaon,

q_2 is the probability of misidentifying a non-kaon track as a kaon,

$q_0 = 1 - q_1 - q_2$ is the probability of not detecting a non-kaon track.

We can write the fold tensor equation into a matrix equivalent form (absorbing the

background term by defining $D_{ab} = N_{ab} - B_{ab}$) as:

$$\begin{pmatrix} D_{00} \\ D_{01} \\ D_{02} \\ D_{03} \\ D_{10} \\ D_{11} \\ D_{12} \\ D_{20} \\ D_{21} \\ D_{30} \end{pmatrix} = \begin{pmatrix} P_{00\to00} & P_{01\to00} & P_{10\to00} & P_{11\to00} & P_{20\to00} & P_{21\to00} \\ 0 & P_{01\to01} & P_{10\to01} & P_{11\to01} & P_{20\to01} & P_{21\to01} \\ 0 & 0 & 0 & P_{11\to02} & P_{20\to02} & P_{21\to02} \\ 0 & 0 & 0 & 0 & 0 & P_{21\to03} \\ 0 & P_{01\to10} & P_{10\to10} & P_{11\to10} & P_{20\to10} & P_{21\to10} \\ 0 & 0 & 0 & P_{11\to11} & P_{20\to11} & P_{21\to11} \\ 0 & 0 & 0 & 0 & 0 & P_{21\to12} \\ 0 & 0 & 0 & P_{11\to20} & P_{20\to20} & P_{21\to20} \\ 0 & 0 & 0 & 0 & 0 & P_{21\to21} \\ 0 & 0 & 0 & 0 & 0 & P_{21\to30} \end{pmatrix} \begin{pmatrix} G_{00} \\ G_{01} \\ G_{10} \\ G_{11} \\ G_{20} \\ G_{21} \end{pmatrix}.$$

In this form, the matrix is column-normalized. The elements of the fold tensor in this parametrization are:

$$P_{00\to00} = 1 \qquad P_{01\to00} = q_0 \qquad P_{10\to00} = p_0$$

$$P_{01\to01} = q_1 \qquad P_{10\to01} = p_2$$

$$P_{01\to10} = q_2 \qquad P_{10\to10} = p_1$$

$$P_{11\to00} = p_0 q_0 \qquad P_{20\to00} = p_0^2$$

$$P_{11\to01} = p_2 q_0 + p_0 q_1 \qquad P_{20\to01} = 2p_0 p_2$$

$$P_{11\to02} = p_2 q_1 \qquad P_{20\to02} = p_2^2$$

$$P_{11\to10} = p_1 q_0 + p_0 q_2 \qquad P_{20\to10} = 2p_0 p_1$$

$$P_{11\to11} = p_1 q_1 + p_2 q_2 \qquad P_{20\to11} = 2p_1 p2$$

$$P_{11\to20} = p_1 q_2 \qquad P_{20\to20} = p_1^2$$

$$P_{21\to 00} = p_0^2 q_0$$

$$P_{21\to 01} = 2p_0 p_2 q_0 + p_0^2 q_1$$

$$P_{21\to 02} = p_2^2 q_0 + 2p_0 p_2 q_1$$

$$P_{21\to 03} = p_2^2 q_1$$

$$P_{21\to 10} = 2p_0 p_1 q_0 + p_0^2 q_2$$

$$P_{21\to 11} = 2p_1 p_2 q_0 + 2p_0 p_1 q_1 + 2p_0 p_2 q_2$$

$$P_{21\to 12} = 2p_1 p_2 q_1 + p_2^2 q_2$$

$$P_{21\to 20} = p_1^2 q_0 + 2p_0 p_1 q_2$$

$$P_{21\to 21} = p_1^2 q_1 + 2p_1 p_2 q_2$$

$$P_{21\to 30} = p_1^2 q_2 \,.$$

To investigate under what conditions kaons are separable from the other particles in the topology, consider:

$$D_i^K = \sum_j D_{ij} \,.$$

The kaon vector elements equal:

$$\begin{aligned}
D_0^K &= G_{00} + (1-q_2)G_{01} \\
&\quad + (1-p_1)G_{10} + (1-q_2)(1-p_1)G_{11} \\
&\quad + (1-p_1)^2 G_{20} + (1-q_2)(1-p_1)^2 G_{21} \\
D_1^K &= q_2 G_{01} \\
&\quad + p_1 G_{10} + (p_1 + q_2(1-2p_1))G_{11} \\
&\quad + 2p_1(1-p_1)G_{20} + (2p_1(1-p_1) + q_2(1-p_1)(1-3p_1))G_{21} \\
D_2^K &= p_1 q_2 G_{11} \\
&\quad + p_1^2 G_{20} + \left(p_1^2 + p_1 q_2(2-3p_1)\right)G_{21} \\
D_3^K &= p_1^2 q_2 G_{21} \,.
\end{aligned}$$

From the above equations, it becomes apparent that the requirement $q_2 = 0$ will collapse the equations into a kaon-only form. Using:

$$G_i^K = \sum_j G_{ij}$$

the above expressions condense to:

$$D_0^K = G_0^K + (1-p_1)G_1^K + (1-p_1)^2 G_2^K$$
$$D_1^K = p_1 G_1^K + 2p_1(1-p_1)G_2^K$$
$$D_2^K = p_1^2 G_2^K \, .$$

One would obtain these same expressions from a fold matrix treatment of the problem.

This leaves only one requirement to separate a rank R topology into rank $R-1$ and rank 1 topologies: that no particle from the $R-1$ topology be misidentified as one from the rank 1 topology (i.e., the rank 1 topology event sample should be "pure").

Thus kaon ($K^{\pm}$, K^+, K^-, and K_S) and charged particle ($P^{\pm}$) classes of particles can be treated as single particle topologies, since the particle identification is sufficiently good to reject other classes. As well, π^-'s can be treated as single particle topologies, since K/π separation is very good and there are very few sources of negatively charged leptons to contaminate the sample.

Section 4.6 The [$\pi^{\pm}$, $X^{\pm}$] Topology Unfold

I now address the problem of unfolding the π^+ and $\pi^{\pm}$ classes of particles. For the $\pi^{\pm}$ class, the $[e^{\pm}, \mu^{\pm}, \pi^{\pm}, K^{\pm}]$ topology would be the ideal one to use. However, the large number of slots required in the various tensors presents formidable obstacles. The number of events filling each slot decreases as the number of slots increase, thus increasing statistical uncertainties. Also, the minimization program is limited in the number of unknown parameters that it can handle. To circumvent these problems, I use a [$\pi^{\pm}$, $X^{\pm}$] topology for the $\pi^{\pm}$ class, where $X^{\pm}$ now stands for any charged particle which is not a pion. This has the redeeming value that it requires only a pion accept /

reject signal. This problem cannot be reduced into a rank 1 tensor form, since the large number of muons and electrons produced in charmed meson decay cause significant contamination.

The π^+ class of particles uses a slight variation — the $[\pi^+, X^+]$ topology, where X^+ is any positively charged particle which is not a π^+.

Maximum Likelihood Unfold using Matrix Equivalent Form

Using a matrix equivalent form, the $[\pi^\pm, X^\pm]$ topology can be unfolded by the same maximum likelihood method described earlier. Although the parameters will have different meanings, there will be a 1–to–1 correspondence between the N_i and N_{ab}, G_j and G_{ij}, and F_{ij} and $P_{ij\to ab}$.

The final solutions, $G_i^{[\pi]}$, are related to the rank 2 form through $G_i^{[\pi]} = \sum_j G_{ij}^{[\pi,X]}$.

Section 4.7 Particle Class Definitions

Charged Particle Definition

A recoil charged particle is, by definition, a charged particle that does not comprise the tag. All tracks not comprising the tag are potential recoil particles. Extra requirements are set on the properties of these tracks in order to exclude secondary charged kaon and pion decays as well as spurious or noise-generated tracks. These requirements are:

1. The charged track must originate within 4 cm of the origin in radius ($R \leq 4$ cm) and 10 cm along the axis of the detector ($|z| \leq 10$ cm). This requirement rejects most secondary decays of charged kaons and pions.
2. The track must make a sufficiently large angle with the beam axis ($|\cos\theta| \leq 0.85$).
3. The track must be sufficiently well-defined to satisfy a helix fit. This rejects most spurious or noise generated tracks.
4. Since particle identification is not required, no dE/dx, TOF or shower counter information is used. This increases the acceptance of low momentum charged particles.

Charged Kaon Definition

Recoil charged kaons are defined as kaons which are not a part of the tag. Conditions over and above those required for a charged particle must be met for a particle to be classified as a kaon:

1. The kaon must originate within 8 cm of the origin in the z direction.
2. The kaon must have a transverse momentum of at least 65 MeV ($p_{xy} \geq 65$ MeV).
3. The Time-Of-Flight signal quality must be good.
4. The TOF identification must be within 3σ of the kaon hypothesis and the kaon hypothesis must be better than the pion hypothesis:

$$\frac{|t - t_K|}{\sigma_K} \leq 3 \qquad \text{and} \qquad \frac{|t - t_K|}{\sigma_K} \leq \frac{|t - t_\pi|}{\sigma_\pi}$$

where t is the measured time-of-flight, t_K and t_π are the predicted kaon and pion times, and σ_K and σ_π are the TOF hypothesis uncertainties.

Neutral Kaon Definition

Neutral kaons, specifically K_S, are detected via the decay $K_S \rightarrow \pi^+\pi^-$. All pairs of oppositely charged tracks are candidates to the K_S fitter, KLAMS, which is described in Reference 36. KLAMS uses the dE/dx corrected track parameters and calculates the crossing points of the track circles projected in the (x,y) plane. The best crossing point is chosen, the track parameters are "swum" to the point, and the $\pi^+\pi^-$ 4–momentum is calculated.

K_S candidates must:

1. have their momentum line up with the line from the crossing point to the interaction point with a $P(\chi^2) \geq 1\%$, and
2. have a decay length greater than 3 mm.

K_S candidates which share common tracks are weeded by performing a one constraint fit to the hypothesis, $K_S \rightarrow \pi^+\pi^-$. The K_S candidate with the better fit is selected.

Charged Pion Definition

In order for a track to be classified as a charged pion candidate it must first meet the criteria for a charged particle. The additional conditions in order for a track to be classified as a pion are:

1. The track must originate within 8 cm of the origin in the z direction.
2. The track must have a transverse momentum of at least 65 MeV ($p_{xy} \geq 65$ MeV).
3. The Time-Of-Flight signal quality must be good.
4. The TOF identification must be within 3σ of the pion hypothesis and the pion hypothesis must be better than the kaon hypothesis:

$$\frac{|t - t_\pi|}{\sigma_\pi} \leq 3 \qquad \text{and} \qquad \frac{|t - t_K|}{\sigma_K} \geq \frac{|t - t_\pi|}{\sigma_\pi}$$

where t is the measured time-of-flight, t_K and t_π are the predicted kaon and pion times, and σ_K and σ_π are the TOF hypothesis uncertainties.

Section 4.8 Determining the Initial Background

The initial estimate of the number of background events in the signal region is obtained by one of two methods. When there are a sufficient number of events, the tagged D mass spectrum is fit to a quartic polynomial function background. Events within the signal region (i.e., $\pm 3\sigma$ of the nominal D mass) are excluded from the fit. The resulting background curve is integrated under the signal region to yield the estimated background.

When there are insufficient numbers of events for a polynomial fit, an estimate of the number of events in the signal region is made by counting the number of events in sideband regions. This number is scaled by the ratio of signal region size to sideband region size to yield the background estimate.

Section 4.9 Estimating Systematic Errors

The sources of the systematic error arising from an unfolding procedure are:

1. Determination of background function shape. Quartic polynomials are used (when possible) to obtain the background shape. Other background shapes, ranging from first-order to eighth-order polynomials, are used to estimate the unfolded results' sensitivity to the background counts.
2. The choice of background probability distribution. A Gaussian distribution is used due to the additional information provided by having an independent standard deviation available. A Poisson distribution and a constant distribution are also examined to determine the systematic dependence.
3. Choice of tensor rank. The π^- class and all the kaon classes of particles can be analyzed using either a rank 1 topology or a rank 2 topology. Results agree within statistical error and differences are incorporated into the systematic error. The π^+ and $\pi^\pm$ classes of particles can only be analyzed with a rank 2 topology.
4. The statistical uncertainties of the fold matrix/tensor.* A number of Monte Carlo simulations are used to generate fold matrices/tensors. The statistical fluctuations among these matrices/tensors yield different unfold results, which are incorporated in the systematic error.
5. Dimension of the fold matrix/tensor. The upper limit cutoff can often be varied by ±1, affecting the dimension of the fold matrix/tensor. Even so, a ±1 shift rarely affects the results.
6. Particle definition. The exact placement of a cut level will change the number of recoiling particles as well as the fold tensor/matrix. Any resulting differences in the unfolded results are attributed to systematic uncertainty.

---

* The term "matrix/tensor" refers to matrix and/or tensor. "Matrix" alone refers to rank 1 topologies. "Tensor" alone refers to rank 2 topologies.

Section 4.10 Kaon Momentum Spectra

The center-of-mass momentum spectrum from a candidate class of recoiling particles is an inclusive property. In this thesis, the K^+, K^-, and K_S recoil momentum spectra are separately extracted from the data. All kaon candidates which do not comprise the tag are boosted back into the center-of-mass frame of the parent D meson. The resulting momentum spectra are then corrected for efficiency.

Three sources of inefficiency affect the momentum spectra:

1. Geometric losses. Incomplete angular coverage of the Mark III detector results in some particle loss. This inefficiency is expected to be constant across all momenta ranges.
2. Reconstruction losses. Tracks which physically enter the detector can be lost or mismeasured due to the limitations of the reconstruction algorithm. Tracks that are too short or overlap with other tracks are especially problematic.
3. The finite resolution of the detector. This causes an uncorrectable "smearing" of any features in the momentum spectra.
4. Particle identification losses. Cuts used to identify a particular class of particle will unavoidably reject some good candidates.

A Monte Carlo simulation can model the effect of these losses and an efficiency function can be obtained to correct for all losses except those due to resolution smearing.

Figure 4.1 shows a number of efficiency functions — the charged track detection efficiency (a combination of geometric loss and reconstruction loss), the charged kaon particle identification efficiency (for reconstructed tracks), the full charged kaon efficiency function which corrects for all of the above (except resolution), and the full neutral kaon efficiency function.

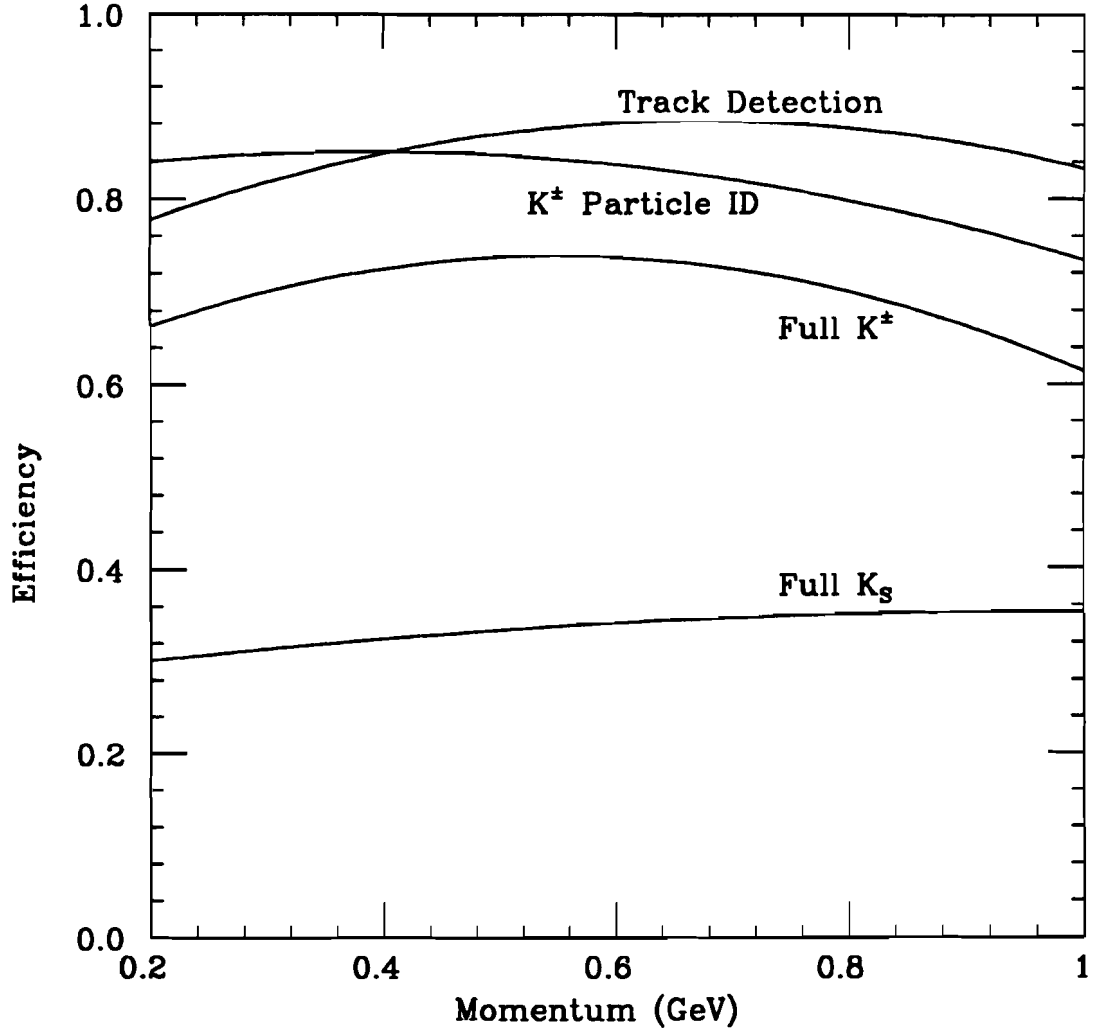

Figure 4.1 Kaon momenta efficiency correction functions

Chapter 5 Experimental Results

Section 5.1 D^+ Inclusive Multiplicity Distributions

Calculating the D^+ inclusive multiplicity distributions begins by determining the fold matrix/tensor* for every class of particle. The analysis continues with counting the number of signal and background i-candidates in the data. Performing the unfold concludes the process.

The D^+ Fold Matrices and Tensors

To determine the various D^+ fold matrices/tensors, a Monte Carlo generator simulated D^+D^- pair decays and 50,953 events were tagged. The produced tag matched the detected tag in 43,888 events.† I examined the recoil candidates in both the generated and reconstructed modes and constructed a fold matrix or tensor for each class of particle (see Tables 5.13–5.20 in Section 5.7). Table 5.1 summarizes the location of the relevant tables.

Table 5.1 Table identifiers for the D^+ results

D^+	Table numbers and page numbers for:					
	Fold Matrix/Tensor		Observed Events		Unfold Result	
Particle	Table	Page	Table	Page	Table	Page
$P^\pm$	5.13	85	5.37	96	5.2	63
K^+	5.14	85	5.38	97	5.3	65
K^-	5.15	85	5.39	97	5.3	65
$K^\pm$	5.16	86	5.40	97	5.3	65
K_S	5.17	86	5.41	97	5.3	65
π^+	5.19	87	5.42	98	5.4	67
π^-	5.18	86	5.43	98	5.4	67
$\pi^\pm$	5.20	88	5.44	99	5.4	67

* The term "matrix/tensor" refers to matrix and/or tensor. "Matrix" alone refers to rank 1 topologies. "Tensor" alone refers to rank 2 topologies.

† The remaining events are background due to mistagging.

Each fold matrix element, F_{ij},* of Tables 5.13–5.18 represents the probability that an i-candidate event is detected when a j-candidate event is produced by the Monte Carlo. Assuming Poisson statistics, the error associated with each element equals:

$$\sigma_{ij} = \left(\frac{F_{ij}(1 - F_{ij})}{(N_T)_j} \right)^{\frac{1}{2}}$$

where $(N_T)_j$ is the normalization used for column j. The normalizations, listed in the row marked "Normalization", indicate the total number of j-candidate events generated by the Monte Carlo.

Each fold tensor element, $P_{ij \to ab}$, (Tables 5.19—5.20) represents the probability that a generated (i, j) topology is detected as an (a, b) topology. The error associated with each element is not explicitly shown but can be calculated assuming Poisson statistics:

$$\sigma_{ij \to ab} = \left(\frac{P_{ij \to ab}(1 - P_{ij \to ab})}{(N_T)_{ij}} \right)^{\frac{1}{2}}$$

where $(N_T)_{ij}$ is the normalization used for "column" (i, j).

The unfold process does not directly use the statistical errors of the fold matrix/tensor. The errors are listed only to indicate the statistical accuracy of the fold matrix/tensor. The fluctuations in the fold matrix/tensor are taken into account, however, when calculating the systematic errors on the final results.

Elements of the fold tensor, $P_{ij \to ab}$, which have $a + b > i + j$ originate primarily from the electron tracks from photon conversions. These tracks are excluded from the generated recoil but are included in the observed, reconstructed data. The inclusion or exclusion of the tracks has no significant effect on the unfold for two reasons. First, the percentage of conversion events is very small. Second, it only affects the X component of the topology $[\pi, X]$ (i.e., $P_{ij \to ab} \to P_{i(j+2) \to ab}$) and not the pion component.

Determining Background in the Data

The signal region of the D^+ beam-constrained mass plot lies between 1.8621 GeV and 1.8763 GeV (i.e., $\pm 3\sigma$ from the nominal D^+ mass). To estimate the background

* (Row, column) order.

within the signal region for each of the i-candidate's mass plots, I perform a fit to a quartic polynomial using the histogram bins not considered part of the signal region. The total number of observed events and the estimated number of background events are tabulated in Tables 5.37–5.44.

Figure 5.1 shows the fitted background curves for the charged particle multiplicity distribution.

Unfold Results

Charged Particle Unfold The charged particle multiplicity distribution is unfolded as described in the previous chapter using the fold matrix from Table 5.13. The result is presented in Table 5.2. This unfold includes charged particles originating from K_S decays. See Chapter 11 for a comparison with previous experimental results.

The quoted statistical errors are returned by the minimization program used to perform the unfold. They correspond to a change in log likelihood function value of 0.5.

Table 5.2 D^+ unfolded charged particle multiplicity distribution and average

n	$B(D^+ \to nP^{\pm}X^0)$
1	$40.6 \pm 1.8 \pm 1.6$ %
3	$52.5 \pm 1.9 \pm 1.2$ %
5	$6.9 \pm 0.9 \pm 0.6$ %
7	$0.0 \pm 0.0 \pm 0.1$ %
$\langle n \rangle$	$2.33 \pm 0.04 \pm 0.04$

The average charge particle multiplicity is calculated from the distribution according to the formula $\langle n_{\rm ch} \rangle = \sum_{n=0} n \times B(D^+ \to nP^{\pm}X^0)$. The error matrix for the charged particle distribution is used to calculate the error on the average.

Figure 5.2 shows the log likelihood function as a function of the 1–prong and 5–prong percentages using a 6×3 fold matrix with constant background.* The likelihood function

* The 3–prong percentage is calculated so that the total sums to one.

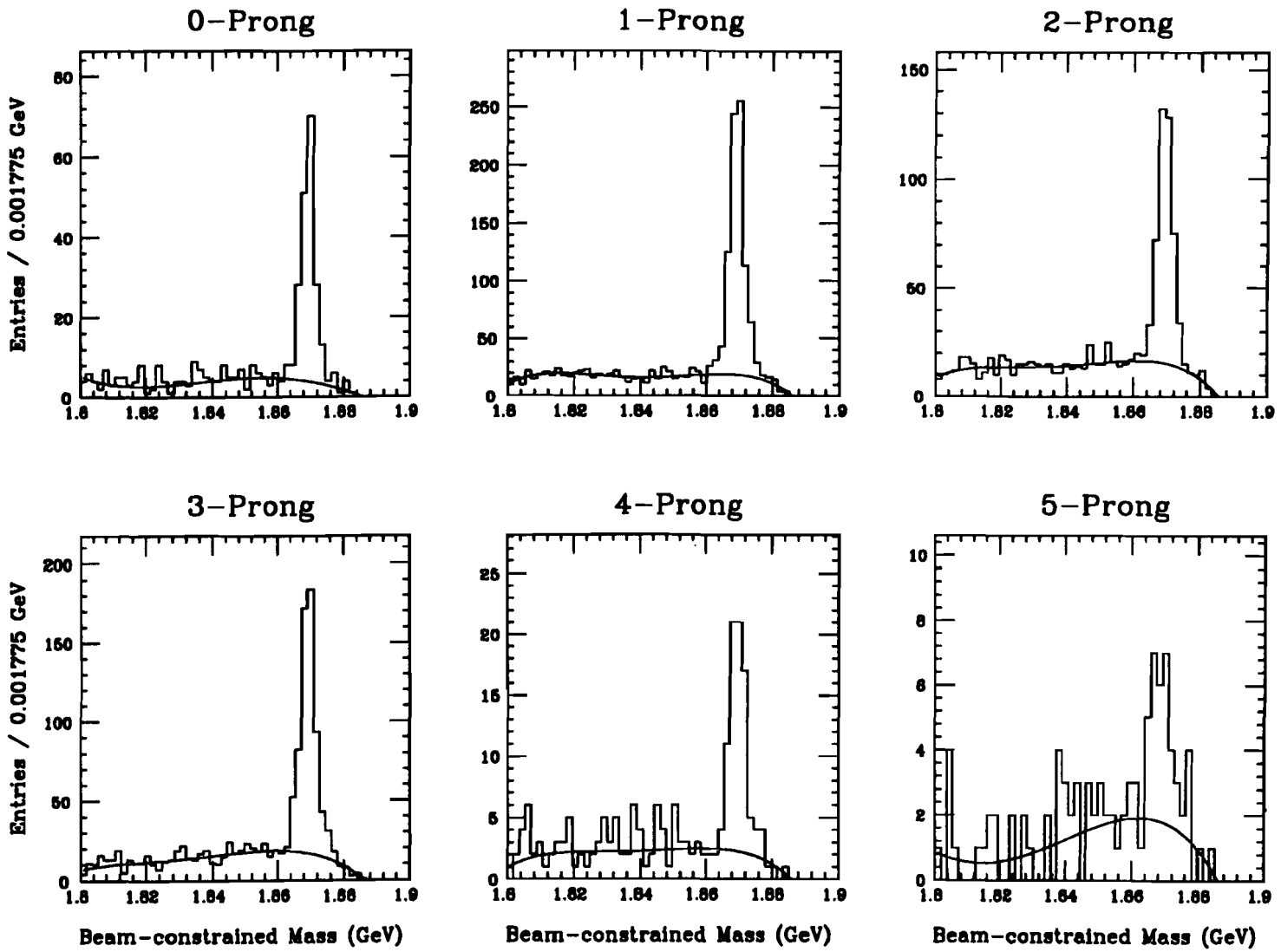

Figure 5.1 Background fits for various charged particle multiplicities for the D^+

is a smooth and well-behaved function with a clear maximum. The figure also shows the 1σ, 2σ, and 3σ contours of the log likelihood function. The location of the maximum and size of the error contours agree with the results returned by the minimization program.

The quoted systematic errors* in Table 5.2 arise from varying the degree of the polynomial used in background fits (1%), changing the choice of background probability distribution (0.3%), uncertainties in the fold matrix (0.6%), changing the dimension (6×3, 6×4, 7×4 and 8×4) of the fold matrix (0.3%) and changing the definition of a charged particle (1.2%) for a total quadrature-added error estimate of 1.7%.

Kaon Unfold The multiplicity distributions for the four classes of kaon (K^+, K^-, $K^\pm$, and K_S) are unfolded using rank 1 topology fold matrices as described in the previous chapter. The results are presented in Table 5.3.

Table 5.3 D^+ unfolded kaon multiplicity distribution and average

n	$B(D^+ \to nK^+X)$	$B(D^+ \to nK^-X)$	$B(D^+ \to nK^\pm X)$	$B(D^+ \to nK_SX)$
0	94.8 ± 1.0 ± 0.7 %	77.4 ± 1.9 ± 3.5 %	73.6 ± 2.7 ± 3.6 %	74.8 ± 2.5 ± 2.5 %
1	5.2 ± 1.0 ± 0.7 %	22.6 ± 1.9 ± 3.5 %	25.0 ± 2.8 ± 3.6 %	25.0 ± 2.7 ± 2.5 %
2			1.4 ± 0.8 ± 0.6 %	0.2 ± 0.4 ± 0.3 %
$n \geq 1$	5.2 ± 0.8 ± 0.7 %	22.6 ± 1.9 ± 3.5 %	26.4 ± 2.7 ± 3.6 %	25.2 ± 2.5 ± 2.5 %
$\langle n \rangle$	0.05 ± 0.01 ± 0.01	0.23 ± 0.02 ± 0.04	0.28 ± 0.03 ± 0.04	0.25 ± 0.03 ± 0.03

For each class of kaon, the kaon inclusive branching ratio $B(D^+ \to KX) \equiv 1 - B(D^+ \to {}_{(n=0)}KX)$ is derived from the unfolded distribution. See Chapter 11 for a comparison with previous experimental results.

Also for each class, the average number of kaons is calculated from the respective distribution according to the formula $\langle n_K \rangle = \sum_{n=0} n \times B(D^+ \to nKX)$. The error matrix returned by the minimization program is used to calculate the error on the average.

* The numerical values for the systematic error apply only to the average charged particle multiplicity. The systematic errors on the components of the multiplicity distribution are of different magnitudes, but have roughly the same ratios among the various sources of systematic contribution.

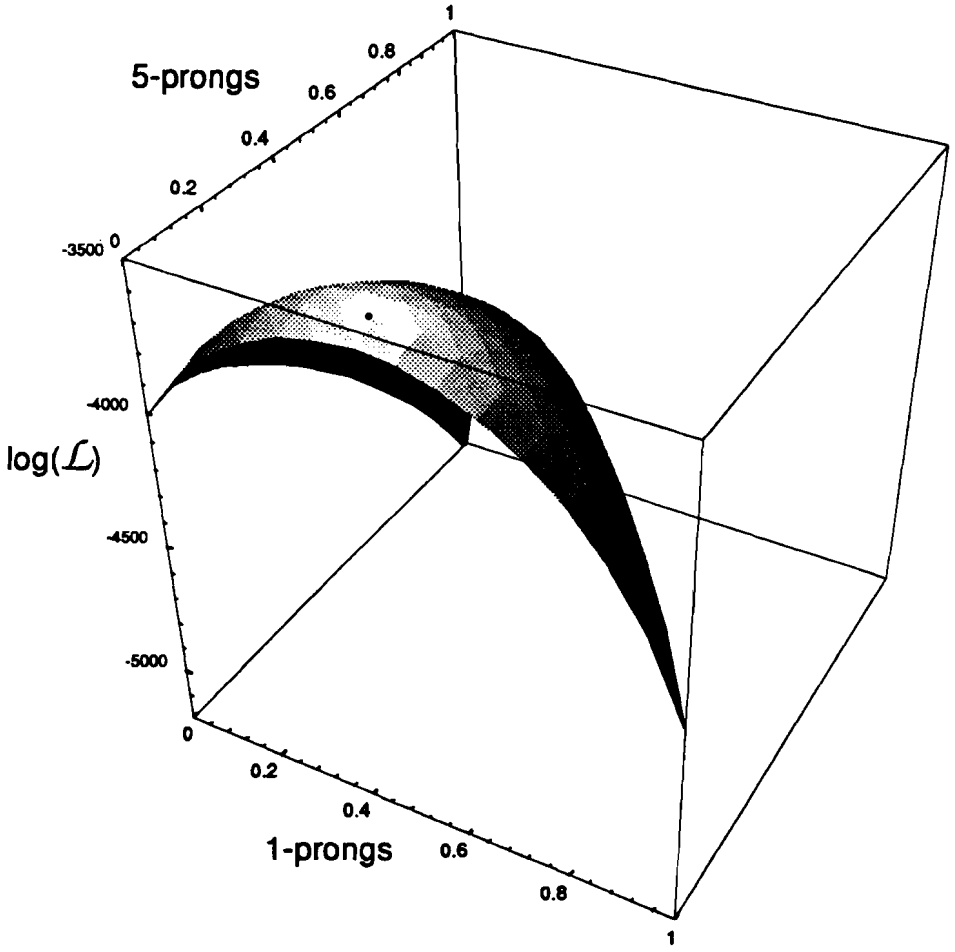

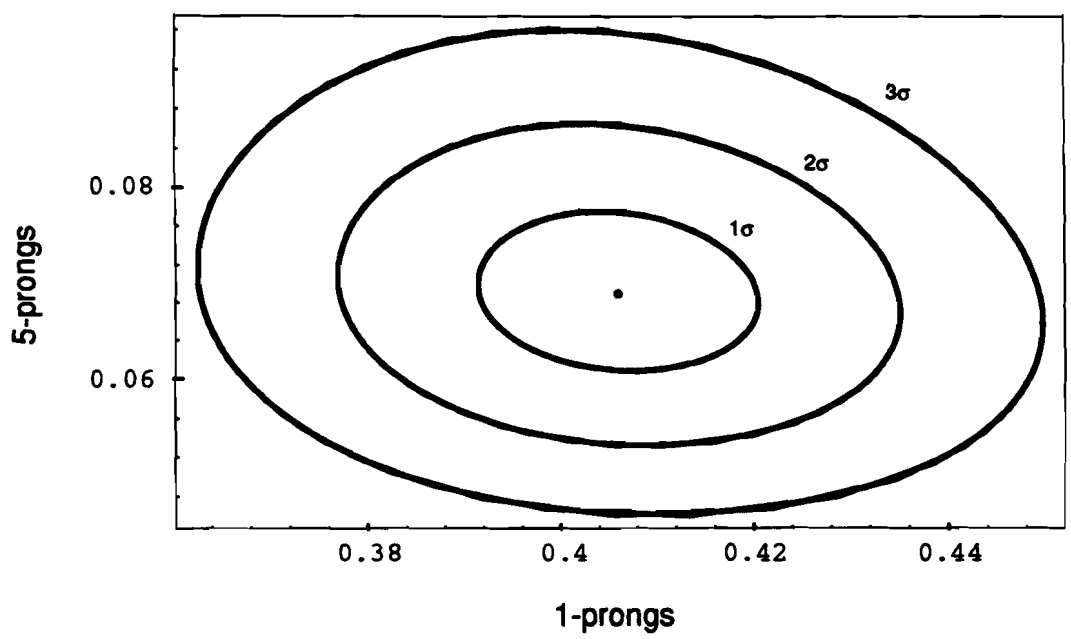

Figure 5.2 Log likelihood function for the charged multiplicity unfold of the D^+

The quoted systematic errors* in Table 5.3 arise from varying the degree of the polynomial used in background fits (1.2%), changing the choice of background probability distribution (0.3%), uncertainties in the fold matrix (0.5%), changing the dimension of the fold matrix (0%) and changing the definition of a kaon (0.8%) for a total quadrature-added error estimate of 1.6%.

The inclusive strange quark content from D^+ decays is calculated from $\langle n_s \rangle = \langle n_{K^\pm} \rangle + 2 \times \langle n_{K_S} \rangle$ and equals 0.78 ± 0.07.

Pion Unfold The π^- class of particles is unfolded using a rank 1 topology fold matrix (Table 5.18). The result of the unfold is presented in Table 5.4.

The π^+ and $\pi^\pm$ classes of pion are unfolded using rank 2 topology fold tensors as described in the previous chapter. The results are presented in Table 5.4.

Table 5.4 D^+ unfolded pion multiplicity distribution and average

n	$B(D^+ \to n\pi^+X)$	$B(D^+ \to n\pi^-X)$	$B(D^+ \to n\pi^\pm X)$
0	$16 \pm 8 \pm 5$ %	$66.8 \pm 2.0 \pm 1.6$ %	$17 \pm 8 \pm 8$ %
1	$41 \pm 9 \pm 8$ %	$29.2 \pm 2.2 \pm 1.3$ %	$39 \pm 8 \pm 9$ %
2	$39 \pm 16 \pm 3$ %	$4.0 \pm 1.0 \pm 0.3$ %	$22 \pm 3 \pm 1$ %
3	$4 \pm 2 \pm 1$ %	$0.0 \pm 0.0 \pm 0.0$ %	$17 \pm 1 \pm 1$ %
4	$0.3 \pm 0.2 \pm 0.1$ %		$5 \pm 4 \pm 2$ %
5			$0 \pm 0 \pm 2$ %
6			$0 \pm 0 \pm 0$ %
$n \geq 1$	$84 \pm 8 \pm 5$ %	$33.2 \pm 2.0 \pm 1.6$ %	$83 \pm 8 \pm 8$ %
$\langle n \rangle$	$1.3 \pm 0.3 \pm 0.1$	$0.37 \pm 0.03 \pm 0.02$	$1.6 \pm 0.1 \pm 0.1$

These multiplicity distributions include pions that have originated from K_S decays.

For each class of pion, the pion inclusive branching ratio $B(D^+ \to \pi X) \equiv 1 - B(D^+ \to {}_{(n=0)}\pi X)$ is derived from the unfolded distribution.

* The numbers refer to the systematic errors for the average $K^\pm$ multiplicity.

Also for each class, the average number of pions is calculated from the respective distribution according to the formula $\langle n_\pi \rangle = \sum_{n=0} n \times B(D^+ \to n\pi X)$. The like-sign to unlike-sign ratio $\langle n_{\pi^+} \rangle / \langle n_{\pi^-} \rangle = 3.5 \pm 0.8$.

Regrettably, but not surprising, the unfolded pion results are not internally consistent. The average charged pion multiplicity does not equal the sum of the like-sign and unlike-sign average multiplicities (i.e., $\langle n_{\pi^\pm} \rangle \neq \langle n_{\pi^+} \rangle + \langle n_{\pi^-} \rangle$). The combination of the background fitting and the unfold minimization combine to produce this inequality.

The quoted systematic errors* in Table 5.4 arise from varying the degree of the polynomial used in background fits (5%), changing the choice of background probability distribution (0.3%), uncertainties in the fold matrix (1.5%), changing the dimension of the fold matrix (0.1%), changing the rank of the tensor (1%) and changing the definition of a pion (1.2%) for a total quadrature-added error estimate of 5.4%. Systematic errors for the $\pi^\pm$ and π^+ unfold do not include contributions from changing either the rank or the dimension of the fold tensor.

Inclusive Lepton Multiplicity Although inclusive lepton properties are not directly measured in this analysis, it remains possible to estimate the average lepton multiplicity using information from the charged particle, charged kaon and charged pion unfolds. The average lepton multiplicity is related to the other three average multiplicities:

$$\langle n_{\rm ch} \rangle = \langle n_{K^\pm} \rangle + \langle n_{\pi^\pm} \rangle + \langle n_{\ell^\pm} \rangle .$$

Using the value of $\langle n_{\pi^\pm} \rangle$ above, the average lepton multiplicity equals 0.45 ± 0.1. This is comparable to the direct measurement of 0.34 ± 0.04 which I derive from the inclusive electron branching ratio[6] of $B(D^+ \to e^+ X) = (17.2 \pm 1.9)\%$ converted into an average multiplicity, assuming: a) lepton universality, b) a small inclusive branching ratio for $B(D^+ \to {}_{(n\geq 2)} e^+ X)$, and c) the unlike-sign electron branching ratio is small compared to the like-sign electron branching ratio (i.e., $B(D^+ \to e^- X) << B(D^+ \to e^+ X)$).

* The numbers refer to systematic error for the average π^- multiplicity.

Section 5.2 D^+ Inclusive Momenta Spectra

The momentum spectra of recoiling kaon candidates has the potential to be a very rich source of information. In particular, it is hoped that any two-body decay modes with a sufficiently large branching ratio can be observed in the center-of-mass spectra.

Recoiling kaons have their momenta boosted into their parent D^+ meson's center-of-mass reference frame using the momentum of the tagged D meson as a reference. The resulting spectra are then efficiency-corrected using the efficiency functions described in the previous chapter (see Figure 4.1).

Unfortunately, the inclusive momentum spectra of recoiling K^+, K^-, and K_S candidates (Figure 5.3) do not exhibit any readily identifiable structure. The isolated peak in the K^+ spectrum at 0.74 GeV does not correspond with any known process. No structure is expected in the K^- spectrum. In the K_S spectrum, there is a barely significant bump at 0.86 GeV, which could be a remnant of the decay mode $\overline{K}^0\pi^+$.

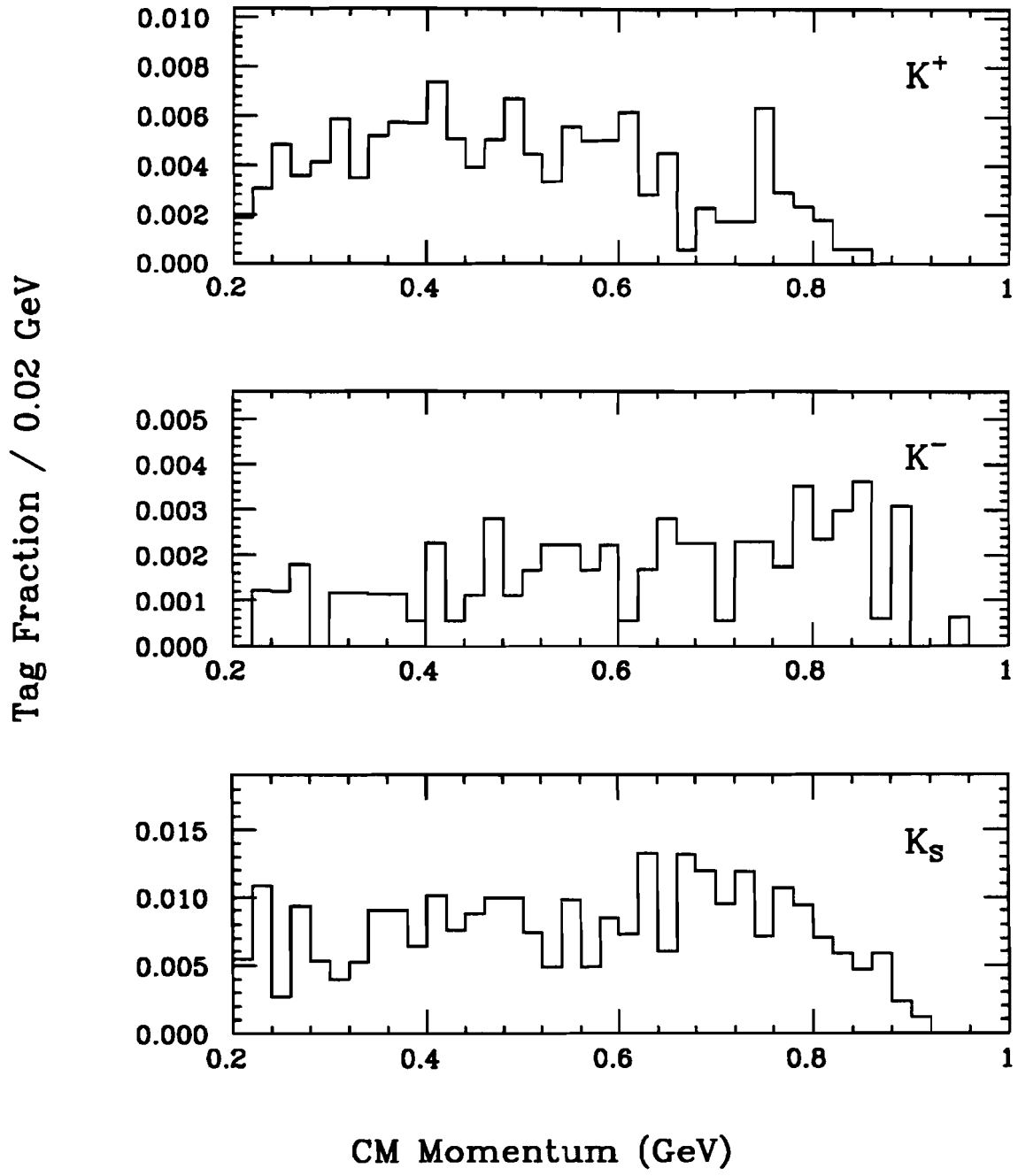

Figure 5.3 D^+ inclusive center-of-mass momentum spectra

Section 5.3 D^0 Inclusive Multiplicity Distributions

Calculating the D^0 inclusive multiplicity distributions proceeds in a manner similar to the D^+ unfolding procedure.

The D^0 Fold Matrices and Tensors

The various D^0 fold matrices/tensors were determined from a Monte Carlo simulation of $D^0\overline{D}^0$ pair decays. The produced tag was matched to the detected tag and recoil candidates were counted in both the generated and reconstructed modes. Using this information, a fold matrix was calculated for each class of particle as outlined in the previous chapter. The results are summarized in Tables 5.21–5.28. See Table 5.5 for a list of the relevant tables.

Table 5.5 Table identifiers for the D^0 results

D^0	Table numbers and page numbers for:					
	Fold Matrix/Tensor		Observed Events		Unfold Result	
Particle	Table	Page	Table	Page	Table	Page
prongs	5.21	89	5.45	100	5.6	73
K^+	5.22	89	5.46	100	5.7	74
K^-	5.23	89	5.47	100	5.7	74
$K^\pm$	5.24	90	5.48	100	5.7	74
K_S	5.25	90	5.49	100	5.7	74
π^+	5.27	91	5.51	101	5.8	75
π^-	5.26	90	5.50	101	5.8	75
$\pi^\pm$	5.28	92	5.52	102	5.8	75

Determining Background in the Data

The signal region of the D^0 beam-constrained mass plot lies between 1.8560 GeV and 1.8730 GeV (i.e., $\pm 3\sigma$ from the nominal D^0 mass). To estimate the background within the signal region for each the i-candidate's mass plots, I fit a quartic polynomial using only the histogram bins not considered part of the signal region. The total number

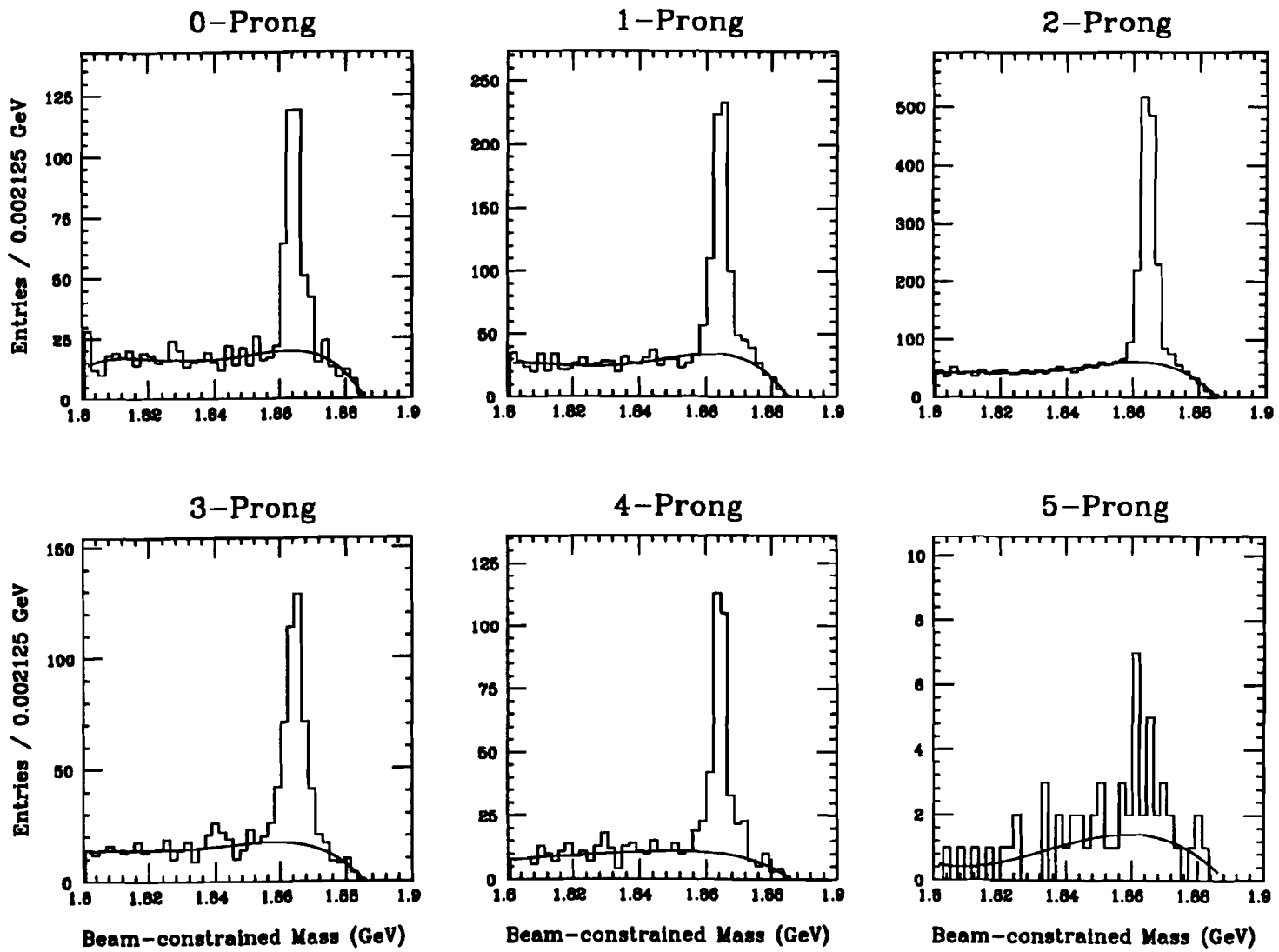

Figure 5.4 Background fits for various charged particle multiplicities for the D^0

of observed events and the estimated number of background events is listed in Tables 5.45–5.52. Figure 5.4 also shows the fitted background curves for the charged particle multiplicity distribution.

Unfold Results

Charged Particle Unfold The charged particle multiplicity distribution is unfolded using the fold matrix in Table 5.21. The average charge particle multiplicity is calculated from this distribution using $\langle n_{\rm ch}\rangle = \sum_{n=0} n \times B(D^0 \to nP^{\pm}X^0)$. These results are presented in Table 5.6 and include charged particles originating from K_S decays.

Table 5.6 D^0 unfolded charged particle multiplicity distribution and average

n	$B(D^0 \to nP^{\pm}X^0)$
0	$5.6 \pm 1.0 \pm 0.6$ %
2	$63.5 \pm 1.9 \pm 2.2$ %
4	$28.7 \pm 1.8 \pm 1.2$ %
6	$2.2 \pm 0.6 \pm 0.8$ %
$\langle n\rangle$	$2.55 \pm 0.04 \pm 0.05$

The quoted systematic error* in Table 5.6 arises from varying the degree of the polynomial used in background fits (1.6%), changing the choice of background probability distribution (0.3%), uncertainties in the fold matrix (0.5%), changing the definition of a charged particle (1.2%), and changing the dimension (6×4, 7×4 and 8×4) of the fold matrix (0%) for a total quadrature-added error estimate of 2.1%.

Kaon Unfold The multiplicity distributions for the four classes of kaon (K^+, K^-, $K^{\pm}$, and K_S) are unfolded using rank 1 topology fold matrices. For each class of kaon, the kaon inclusive branching ratio $B(D^0 \to KX) \equiv 1 - B(D^0 \to {}_{(n=0)}KX)$ is derived from the unfolded distribution. Also for each class, the average number of

* As with the D^+, the numerical breakdown of the systematic errors applies to the averaged charged particle multiplicity.

kaons is calculated from the respective distribution according to the formula $\langle n_K \rangle = \sum_{n=0} n \times B(D^0 \to nKX)$. All of these results are presented in Table 5.7.

Table 5.7 D^0 unfolded kaon multiplicity distribution and average

n	$B(D^0 \to nK^+X)$	$B(D^0 \to nK^-X)$	$B(D^0 \to nK^\pm X)$	$B(D^0 \to nK_SX)$
0	98.1 ± 0.8 ± 2.3 %	42.9 ± 2.5 ± 2.9 %	43.5 ± 2.8 ± 3.0 %	65.4 ± 4.9 ± 2.8 %
1	1.9 ± 0.8 ± 2.3 %	57.1 ± 2.5 ± 2.9 %	55.1 ± 3.1 ± 3.0 %	32.2 ± 6.2 ± 4.4 %
2			1.5 ± 1.0 ± 0.2 %	2.4 ± 2.7 ± 2.5 %
$n \geq 1$	1.9 ± 0.8 ± 2.3 %	57.1 ± 2.5 ± 2.9 %	56.5 ± 2.8 ± 3.0 %	34.6 ± 4.9 ± 2.8 %
$\langle n \rangle$	0.02 ± 0.01 ± 0.02	0.57 ± 0.03 ± 0.03	0.58 ± 0.03 ± 0.04	0.37 ± 0.05 ± 0.03

The quoted systematic error in Table 5.7 arises from varying the degree of the polynomial used in background fits (3%), changing the choice of background probability distribution (0.3%), uncertainties in the fold matrix (3%), changing the kaon particle identification cuts (0.8%) and changing the dimension of the fold matrix (0%) for a total quadrature-added error estimate of 4.3%.

The inclusive strange quark content from D^0 decays equals 1.3 ± 0.1.

Pion Unfold The π^- class of particles is unfolded using a rank 1 topology fold matrix (Table 5.26). The π^+ and $\pi^\pm$ classes of pion are unfolded using rank 2 topology fold tensors. For each class of pion, the pion inclusive branching ratio $B(D^0 \to \pi X) \equiv 1 - B(D^0 \to {}_{(n=0)}\pi X)$ is derived from the unfolded distribution. Also for each class, the average number of pions is calculated from the respective distribution according to the formula $\langle n_\pi \rangle = \sum_{n=0} n \times B(D^0 \to n\pi X)$. The result of these unfolds are presented in Table 5.8. These multiplicity distributions include pions that have originated from K_S decays.

Table 5.8 D^0 unfolded pion multiplicity distribution and average

n	$B(D^0 \to n\pi^+X)$	$B(D^0 \to n\pi^-X)$	$B(D^0 \to n\pi^\pm X)$
0	58.0 ± 1.4 ± 1.8 %	49.0 ± 2.0 ± 0.6 %	40.1 ± 3.4 ± 2.0 %
1	24.1 ± 3.0 ± 1.8 %	38.6 ± 2.6 ± 0.1 %	19.9 ± 1.0 ± 2.0 %
2	17.4 ± 1.0 ± 0.8 %	10.5 ± 2.0 ± 0.8 %	14.3 ± 3.7 ± 2.6 %
3	0.4 ± 0.1 ± 0.2 %	1.9 ± 0.6 ± 0.3 %	19.8 ± 4.0 ± 1.1 %
4			5.0 ± 1.3 ± 1.6 %
5			0.7 ± 0.2 ± 0.1 %
6			0.2 ± 0.1 ± 0.2 %
$n \geq 1$	42.0 ± 1.4 ± 1.8 %	51.0 ± 2.0 ± 0.6 %	59.9 ± 3.4 ± 2.0 %
$\langle n \rangle$	0.60 ± 0.04 ± 0.05	0.65 ± 0.03 ± 0.02	1.33 ± 0.15 ± 0.05

The quoted systematic errors* in Table 5.8 arise from varying the degree of the polynomial used in background fits (2%), changing the choice of background probability distribution (0.3%), uncertainties in the fold matrix (2%), changing the dimension of the fold matrix (0.1%), changing the rank of the tensor (1%) and changing the definition of a pion (1.2%) for a total quadrature-added error estimate of 3.1%. Systematic errors for the $\pi^\pm$ and π^+ unfold do not include contributions from changing either the rank or the dimension of the fold tensor.

The like-sign to unlike-sign ratio is $\langle n_{\pi^+} \rangle / \langle n_{\pi^-} \rangle = 0.92 \pm 0.07$.

Inclusive Lepton Multiplicity I estimate the average lepton multiplicity to be 0.64 ± 0.16 when using the values of $\langle n_{\rm ch} \rangle$, $\langle n_{K^\pm} \rangle$, and $\langle n_{\pi^\pm} \rangle$ from the above results. This conflicts with the direct measurement of 0.17 ± 0.03 which I derive from the inclusive electron branching ratio[6] of $B(D^0 \to e^+X) = (7.7 \pm 1.2)\%$ and the inclusive muon branching ratio[6] of $B(D^0 \to \mu^+X) = (8.8 \pm 2.5)\%$. The reason for this difference is not known. One possibility is that the unlike-sign lepton branching ratios are not insignificant compared to the like-sign lepton branching ratio. This would increase the

* The numbers refer to systematic error for the average π^- multiplicity.

direct measurement, although probably less than 50%. A direct measurement of the inclusive unlike-sign leptonic branching ratio could be of use in resolving this issue.

Section 5.4 D^0 Inclusive Momenta Spectra

The inclusive center-of-mass momentum spectra of recoiling K^+, K^-, and K_S candidates (Figure 5.5) do exhibit some identifiable structures. Kaon momenta for these spectra have been boosted into the D^0 center-of-mass reference frame. These spectra are efficiency-corrected using the efficiency functions described in the previous chapter (see Figure 4.1).

The K^+ spectrum appears to have a peak from 0.76 GeV – 0.80 GeV which is the momentum range expected for the decay K^-K^+. A parallel, but less significant peak is also seen in the K^- spectrum.

The K^- spectrum exhibits three possible structures. A fit of the data using three gaussian functions and a quartic polynomial background yields useful momentum and branching ratio information.

The peak marked (a) has a mean momentum value at 0.680 GeV (see Figure 5.6) with a width of 0.043 GeV. This peak corresponds to a branching ratio of 4.3 ± 1.3%. It may be due to the $K^-\rho^+$ decay mode which occurs at 0.679 GeV and has a measured branching ratio of 7.3 ± 1.1%.[6]

Peak (b) at 0.777 GeV has a width of 0.017 GeV and an associated branching ratio of 1.4 ± 0.7%. The K^-K^+ decay mode has an experimental branching ratio of 0.41 ± 0.04% and a monochromatic momentum of 0.791 GeV.[6]

Peak (c) is found at 0.855 GeV with a width of 0.017 GeV. This peak has a fitted branching ratio for $D^0 \rightarrow K^-\pi^+$ of 3.2 ± 0.6%. It's highly probably that it is the $K^-\pi^+$ decay mode, which has a monochromatic momentum of 0.861 GeV and a measured branching ratio of 3.65 ± 0.21%.[6]

No significant structure is seen in the K_S spectrum.

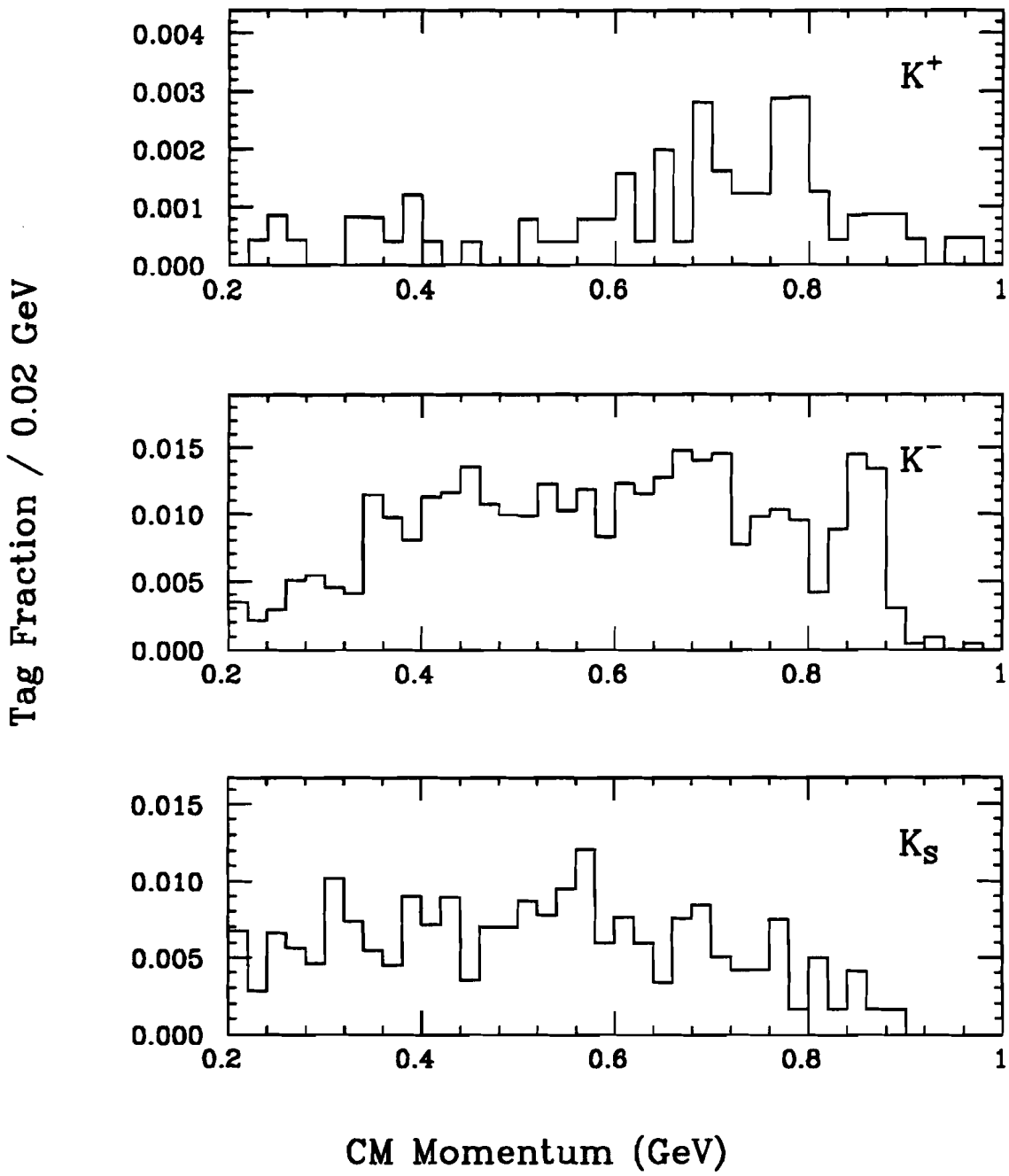

Figure 5.5 D^0 inclusive center-of-mass momentum spectra

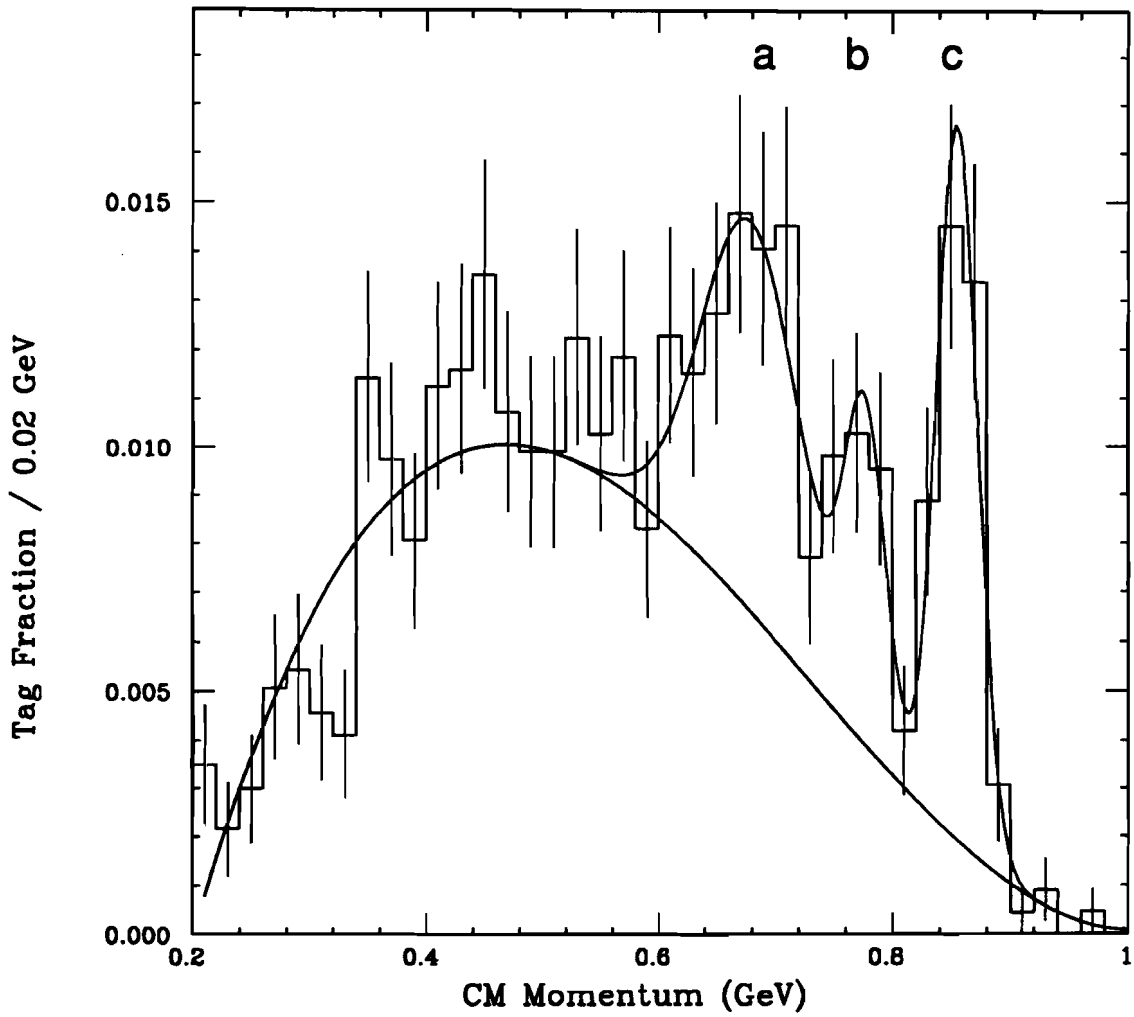

Figure 5.6 D^0 inclusive K^- center-of-mass momentum spectrum with fits

Section 5.5 D_s^+ Inclusive Multiplicity Distributions

Calculating the D_s^+ charge multiplicity distributions proceeds in a manner similar to the D^+ unfolding procedure. The smaller size of the D_s^+ data set means that the final unfolded results will have larger statistical uncertainties.

The D_s^+ Fold Matrices and Tensors

To calculate the D_s^+ fold matrices/tensors, a Monte Carlo generator simulated $D_s^\pm D_s^{*\mp}$ decays and 8,261 events were tagged. In 7,630 of these tags the produced tag and the detected tag could be matched. The recoil topology was examined in both cases and the fold matrices were calculated. The results are summarized in Tables 5.29–5.36. See Table 5.9 for a list of the relevant tables.

Table 5.9 Table identifiers for the D_s^+ results

D_s^+	Table numbers and page numbers for:					
	Fold Matrix/Tensor		Observed Events		Unfold Result	
Particle	Table	Page	Table	Page	Table	Page
prongs	5.29	93	5.53	102	5.10	80
K^+	5.30	93	5.54	103	5.11	82
K^-	5.31	93	5.55	103	5.11	82
$K^\pm$	5.32	94	5.56	103	5.11	82
K_S	5.33	94	5.57	103	5.11	82
π^+	5.35	95	5.59	104	5.12	83
π^-	5.34	94	5.58	103	5.12	83
$\pi^\pm$	5.36	96	5.60	104	5.12	83

Determining Background in the Data

The signal region of the D_s^+ invariant mass plot lies between 1.9416 GeV and 2.0016 GeV (i.e., $\pm 3\sigma$ from the nominal D_s^+ mass). To estimate the background within the signal region for each of the i-candidate's mass plot, a fit to a quartic polynomial is performed using the histogram bins not considered part of the signal region. The total

number of observed events and the estimated number of background events are tabulated in Tables 5.53–5.60.

Figure 5.7 shows the fitted background curves for the charged particle multiplicity distribution.

Unfold Results

Charged Particle Unfold The charged particle multiplicity distribution and the average charged particle multiplicity, which is calculated from the distribution according to the formula $\langle n_{\rm ch}\rangle = \sum_{n=0} n \times B(D_s^+ \to nP^{\pm}X^0)$, are presented in Table 5.29. This unfold includes charged particles originating from K_S decays. See Chapter 11 for a comparison with previous experimental results.

Table 5.10 D_s^+ unfolded charged particle multiplicity distribution and average

n	$B(D_s^+ \to nP^{\pm}X^0)$
1	$32 \pm 11 \pm 8$ %
3	$56 \pm 14 \pm 8$ %
5	$12 \pm 9 \pm 4$ %
7	$0 \pm 0 \pm 1$ %
$\langle n\rangle$	$2.6 \pm 0.3 \pm 0.1$

The systematic error on the average charged particle multiplicity arises from varying the degree of the polynomial used in background fits (3%), changing the choice of background probability distribution (0.3%), uncertainties in the fold matrix (3%), changing the charged particle definition (1.2%) and changing the dimension (6×3, 6×4, 7×4 and 8×4) of the fold matrix (0%) for a total quadrature-added error estimate of 4.4%.

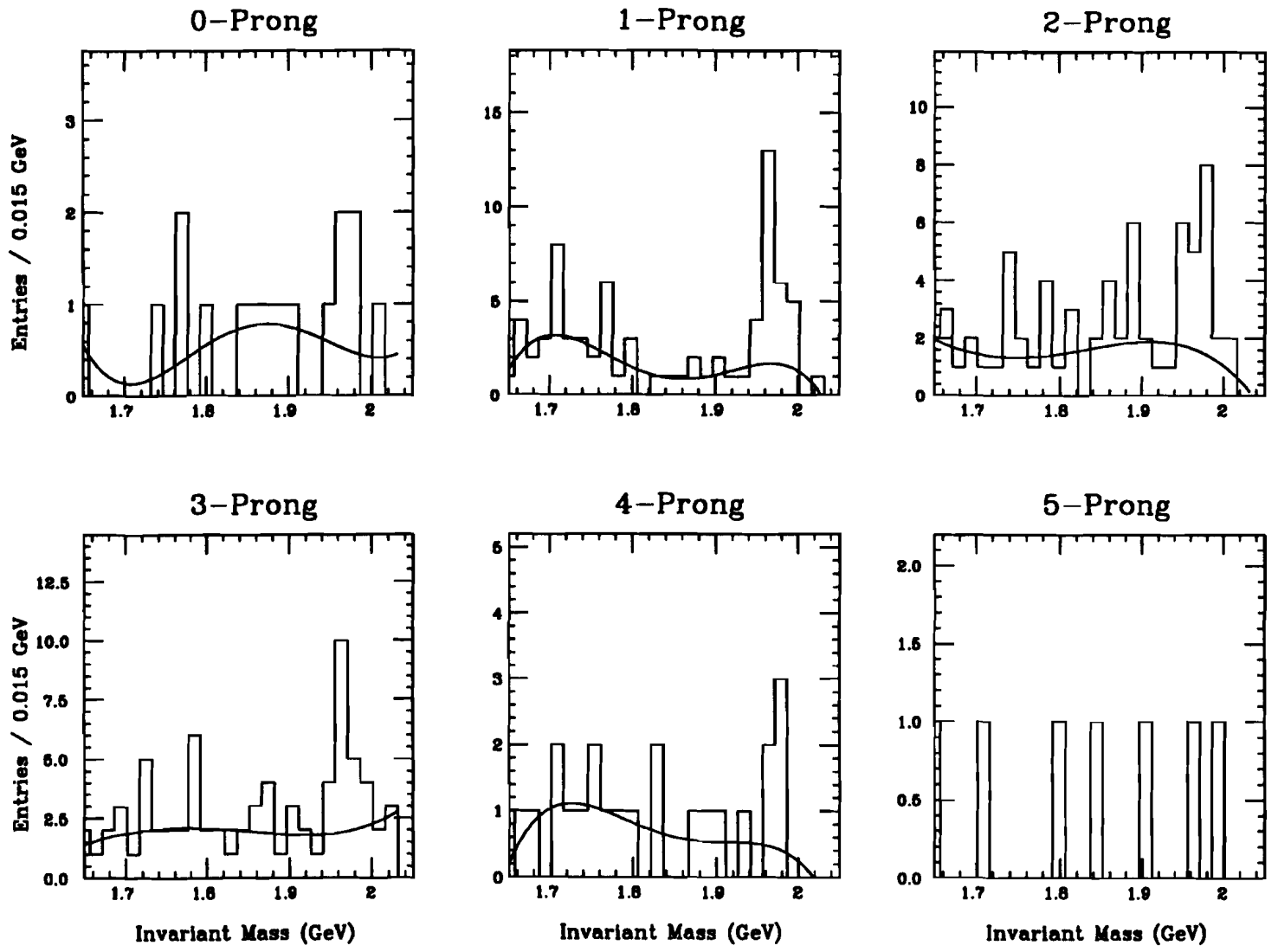

Figure 5.7 Background fits for various charged particle multiplicities for the D_s^+

Kaon Unfold The multiplicity distributions for the four classes of kaon (K^+, K^-, $K^\pm$, and K_S) are presented in Table 5.11.

For each class of kaon, the kaon inclusive branching ratio $B(D_s^+ \to KX) \equiv 1 - B(D_s^+ \to {}_{(n=0)}KX)$ is derived from the unfolded distribution. See Chapter 11 for a comparison with previous experimental results. Also for each class, the average number of kaons is calculated from the respective distribution according to the formula $\langle n_K \rangle = \sum_{n=0} n \times B(D_s^+ \to nKX)$.

Table 5.11 D_s^+ unfolded kaon multiplicity distribution and average

n	$B(D_s^+ \to nK^+X)$	$B(D_s^+ \to nK^-X)$	$B(D_s^+ \to nK^\pm X)$	$B(D_s^+ \to nK_SX)$
0	$68 \pm 18 \pm 6$ %	$95 \pm 8 \pm 3$ %	$68 \pm 14 \pm 4$ %	$65 \pm 20 \pm 9$ %
1	$32 \pm 18 \pm 6$ %	$5 \pm 8 \pm 3$ %	$32 \pm 14 \pm 4$ %	$35 \pm 20 \pm 9$ %
$n \geq 1$	$32 \pm 18 \pm 6$ %	$5 \pm 8 \pm 3$ %	$32 \pm 14 \pm 4$ %	$35 \pm 20 \pm 9$ %
$\langle n \rangle$	$.32 \pm .18 \pm .06$	$.05 \pm .08 \pm .03$	$.32 \pm .14 \pm .04$	$.35 \pm .20 \pm .10$

The inclusive strange quark content from D_s^+ decays equals 1.0 ± 0.4. In comparing this result with similar results for the D^+ and D^0, it is plain that the ratio of strange quark contents (D^+:D^0:D_s) is not 1:1:2 as one would naively expect in the spectator model, but is $1 : 1.7 \pm 0.2 : 1.3 \pm 0.5$. This would seem to indicate that weak annihilation processes are more important than previously thought.

Pion Unfold The π^- class of particles is unfolded using a rank 1 topology fold matrix (Table 5.34). The π^+ and $\pi^\pm$ classes of pion are unfolded using a rank 2 topology fold tensors. The results are presented in Table 5.12. These multiplicity distributions include pions that have originated from K_S decays.

For each class of pion, the pion inclusive branching ratio $B(D_s^+ \to \pi X) \equiv 1 - B(D_s^+ \to {}_{(n=0)}\pi X)$ is derived from the unfolded distribution.

Also for each class, the average number of pions is calculated from the respective distribution according to the formula $\langle n_\pi \rangle = \sum_{n=0} n \times B(D_s^+ \to n\pi X)$. The large

statistical error on the average like-sign pion multiplicity unfortunately renders the result almost meaningless. Nonetheless, it should be noted that the mean value of 1.3 rarely varies by much when calculating the systematic errors.

The like-sign to unlike-sign ratio is $\langle n_{\pi^+}\rangle/\langle n_{\pi^-}\rangle = 2.2 \pm 2.8$.

Table 5.12 D_s^+ unfolded pion multiplicity distribution and average

n	$B(D_s^+ \to n\pi^+X)$	$B(D_s^+ \to n\pi^-X)$	$B(D_s^+ \to n\pi^\pm X)$
0	$28 \pm 35 \pm 5$ %	$39 \pm 10 \pm 10$ %	$28 \pm 22 \pm 9$ %
1	$30 \pm 100 \pm 20$ %	$61 \pm 10 \pm 10$ %	$20 \pm 10 \pm 4$ %
2	$32 \pm 80 \pm 20$ %	$0 \pm 0 \pm 0$ %	$29 \pm 17 \pm 4$ %
3	$10 \pm 30 \pm 3$ %		$23 \pm 25 \pm 10$ %
$n \geq 1$	$72 \pm 35 \pm 5$ %	$61 \pm 10 \pm 10$ %	$72 \pm 10 \pm 9$ %
$\langle n\rangle$	$1.3 \pm 1.7 \pm 0.2$	$0.6 \pm 0.1 \pm 0.1$	$1.5 \pm 0.7 \pm 0.1$

Inclusive Lepton Multiplicity I estimate the average lepton multiplicity to be 0.8 ± 0.8 when using the values of $\langle n_{\rm ch}\rangle$, $\langle n_{K^\pm}\rangle$, and $\langle n_{\pi^\pm}\rangle$ from the above results. The direct measurement is an upper limit of 0.4 which I derive from an upper limit on the inclusive electron branching ratio[6] of $B(D_s^+ \to e^+X) < 20\%$. The two results are not in disagreement.

Section 5.6 D_s^+ Inclusive Momenta Spectra

Due to the paucity of kaons, the inclusive momentum spectra of recoiling K^+, K^-, and K_S candidates (Figure 5.8) do not exhibit any identifiable structure. These spectra are efficiency-corrected using the efficiency functions described in the previous chapter (see Figure 4.1).

Boosting the kaon momenta for these spectra into the D_s^+ center-of-mass reference frame has been attempted using the 4–momentum of the D_s^+ tag as a reference. Unlike the D^+ and D^0 decay process where the recoiling D's momentum is equal but opposite the tag D's momentum (thus making the boost 4–vector easy to calculate), the recoiling

D_s's momentum is not necessarily equal nor opposite the tag D_s's momentum, since there are $D_s^{\pm}D_s^{*\mp}$ events as well as $D_s^{\pm}D_s^{\mp}$ events. This introduces a smearing of any structure present due to incorrect boosting in all $D_s^{\pm}D_s^{*\mp}$ events. However, in this case the lack of structure is more likely due to a lack of kaons than any smearing effect.

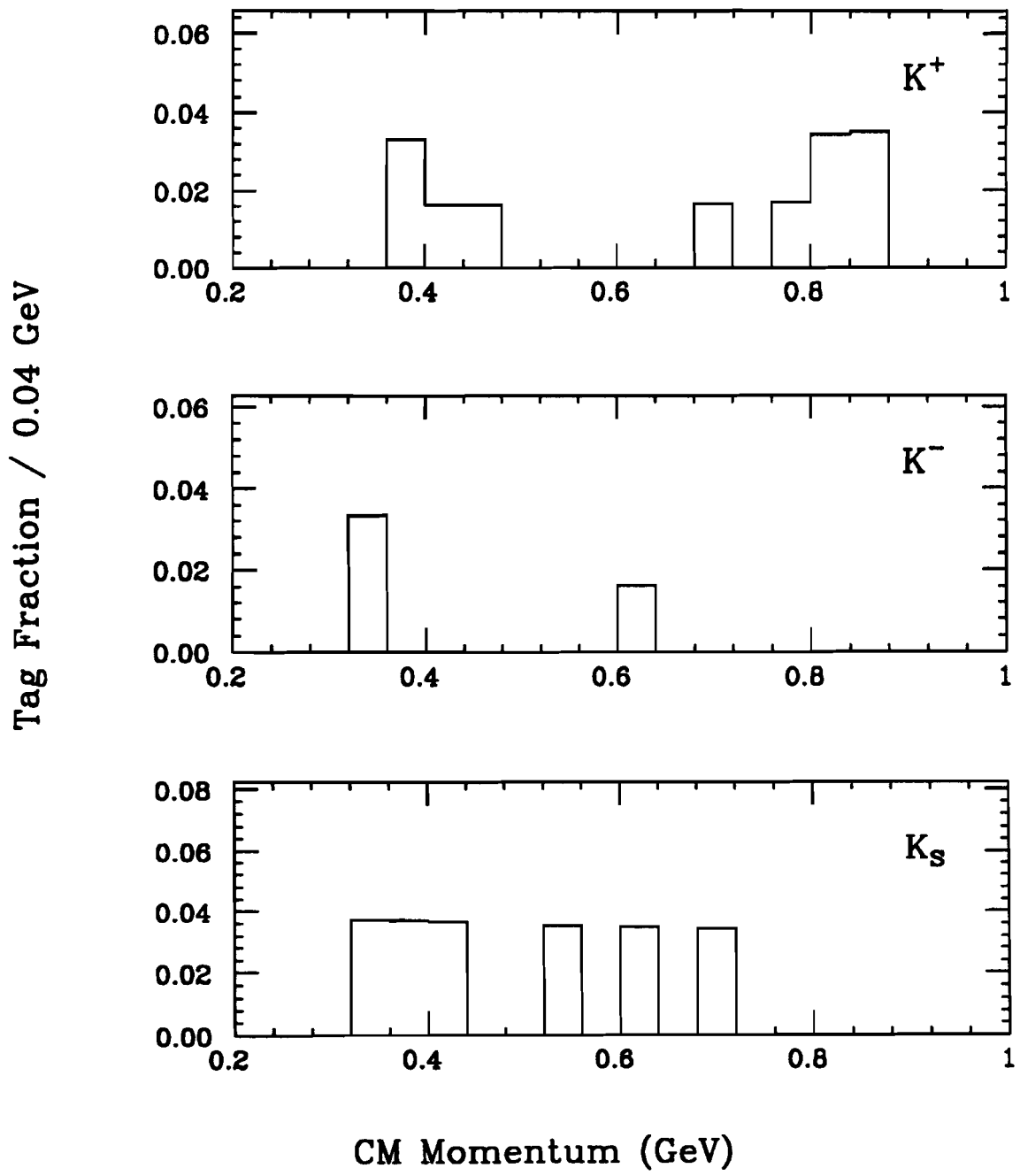

Figure 5.8 D_s^+ inclusive center-of-mass momentum spectra

Section 5.7 Tables of Fold Matrices/Tensors

Table 5.13 D^+ charged particle ($P^\pm$) fold matrix

D^+ Charged Particle Fold Matrix				
Observed	Generated			
	1-prongs	3-prongs	5-prongs	7-prongs
0-prongs	.178 ± .003	.017 ± .001	.001 ± .001	0 ± 0
1-prongs	.812 ± .003	.126 ± .002	.013 ± .002	.003 ± .002
2-prongs	.007 ± .001	.382 ± .003	.085 ± .005	.039 ± .007
3-prongs	.0033 ± .0005	.470 ± .003	.245 ± .008	.102 ± .011
4-prongs	$(6 \pm 6)\times10^{-5}$	.0034 ± .0004	.391 ± .009	.256 ± .015
5-prongs	$(6 \pm 6)\times10^{-5}$	.0012 ± .0002	.262 ± .008	.322 ± .017
6-prongs	0 ± 0	$(4 \pm 4)\times10^{-5}$	.002 ± .001	.217 ± .015
7-prongs	0 ± 0	0 ± 0	$(4 \pm 4)\times10^{-4}$	.062 ± .008
Normalization	15932	24473	2661	796

Table 5.14 D^+ like-sign kaon (K^+) fold matrix

D^+ K^+ Fold Matrix		
Observed	Generated	
	0-K^+	1-K^+
0-K^+	.988 ± .001	.458 ± .016
1-K^+	.012 ± .001	.539 ± .016
2-K^+	$(4.7 \pm 3.3)\times10^{-5}$	.003 ± .002
Normalization	42870	1018

Table 5.15 D^+ unlike-sign kaon (K^-) fold matrix

D^+ K^-Fold Matrix		
Observed	Generated	
	0-K^-	1-K^-
0-K^-	.997 ± .0003	.534 ± .004
1-K^-	.003 ± .0003	.466 ± .004
Normalization	29244	14644

Table 5.16 D^+ charged kaon fold ($K^\pm$) matrix

D^+ $K^\pm$ Fold Matrix			
Observed	Generated		
	0-$K^\pm$	1-$K^\pm$	2-$K^\pm$
0-$K^\pm$	.984 ± .001	.526 ± .004	.297 ± .022
1-$K^\pm$	.016 ± .001	.470 ± .004	.449 ± .024
2-$K^\pm$	$(2.1 \pm 0.9)\times10^{-4}$	.003 ± .0005	.254 ± .022
Normalization	28640	14834	414

Table 5.17 D^+ neutral kaon (K_S) fold matrix

D^+ K_S Fold Matrix			
Observed	Generated		
	0-K_S	1-K_S	2-K_S
0-K_S	.987 ± .001	.627 ± .004	.356 ± .071
1-K_S	.013 ± .001	.372 ± .004	.556 ± .074
2-K_S	$(3 \pm 3)\times10^{-5}$	.001 ± .0003	.089 ± .042
Normalization	29747	14096	45

Table 5.18 D^+ unlike-sign pion (π^-) fold matrix

D^+ π^- Fold Matrix				
Observed	Generated			
	0-π^-	1-π^-	2-π^-	3-π^-
0-π^-	.985 ± .001	.370 ± .004	.174 ± .009	.183 ± .035
1-π^-	.015 ± .001	.627 ± .004	.465 ± .011	.300 ± .042
2-π^-	0 ± 0	.003 ± .0005	.358 ± .011	.367 ± .044
3-π^-	0 ± 0	$(8 \pm 8)\times10^{-5}$	.004 ± .001	.150 ± .033
Normalization	28963	12791	1991	120

Table 5.19 D^+ like-sign pion (π^+) fold tensor

D^+ (π^+, X^+) Fold Tensor								
Observed	Generated							
	(0, 1)	(0, 2)	(1, 0)	(1, 1)	(2, 0)	(2, 1)	(3, 0)	(4, 0)
(0, 0)	.166	.118	.191	.049	.053	.022	.013	.004
(0, 1)	.200	.211	.123	.075	.051	.058	.020	.024
(0, 2)	.0007	.066	.001	.027	.016	.029	.015	.014
(0, 3)	0	0	0	.0003	.0002	.007	.006	.013
(1, 0)	.631	.276	.676	.240	.252	.144	.082	.059
(1, 1)	.003	.276	.008	.232	.153	.144	.121	.105
(1, 2)	0	0	.0001	.0009	.0002	.079	.036	.074
(2, 0)	0	.053	.0003	.374	.468	.259	.266	.171
(2, 1)	0	0	0	.001	.005	.245	.169	.155
(2, 2)	0	0	0	0	.0001	0	.002	.045
(3, 0)	0	0	0	.0004	.001	.014	.268	.160
(3, 1)	0	0	0	0	0	0	.0008	.083
(4, 0)	0	0	0	0	0	0	0	.065
N_T	7292	76	8629	7831	16494	139	2455	779

Table 5.20 D^+ charged pion ($\pi^\pm$) fold tensor

D^+ ($\pi^\pm$, $X^\pm$) Fold Tensor												
Observed	Generated											
	(0, 1)	(0, 3)	(1, 0)	(1, 2)	(2,1)	(2,3)	(3, 0)	(3, 2)	(4,1)	(5, 0)	(6, 1)	(7, 0)
(0, 0)	.165	.053	.188	.015	.018	.015	.016	0	.001	.001	0	0
(0, 1)	.201	.158	.124	.047	.034	0	.031	0	.009	.002	0	0
(0, 2)	.001	.145	.002	.058	.026	.044	.009	.026	.005	.008	.002	.009
(0, 3)	.001	.026	.0005	.018	.008	.029	.003	.013	.009	.002	0	0
(1, 0)	.630	.211	.673	.084	.086	.059	.101	0	.008	.005	.003	0
(1, 1)	.002	.197	.008	.231	.184	.118	.098	.077	.033	.020	.018	.009
(1, 2)	.001	.105	.004	.175	.086	.103	.034	.077	.031	.016	.020	.009
(1, 3)	0	0	0	.0002	.0004	.074	.001	0	.023	.007	.026	0
(1, 4)	0	0	0	0	0	.015	0	.026	.009	.002	.023	.009
(2, 0)	0	.026	.0001	.116	.176	.074	.255	.064	.045	.047	.020	.026
(2, 1)	0	.079	.0001	.241	.293	.147	.156	.244	.113	.084	.050	.034
(2, 2)	0	0	.0003	.0001	.0015	.147	.001	.115	.112	.052	.086	.043
(2, 3)	0	0	0	.0002	.0005	.044	.0004	.051	.036	.009	.047	.034
(3, 0)	0	0	0	.014	.083	.044	.290	.115	.086	.130	.033	.060
(3, 1)	0	0	0	.0007	.0006	.015	.002	.128	.200	.161	.091	.094
(3, 2)	0	0	0	0	.0003	.074	.001	.026	.100	.045	.106	.068
(3, 3)	0	0	0	0	0	0	0	0	0	.002	.068	.034
(4, 0)	0	0	0	0	0	0	0	0	.066	.177	.053	.111
(4, 1)	0	0	0	0	0	0	.0003	.026	.108	.121	.109	.077
(4, 2)	0	0	0	0	0	0	0	0	0	.001	.069	.094
(5, 0)	0	0	0	0	0	0	0	0	.006	.105	.045	.034
(5, 1)	0	0	0	0	0	0	0	0	0	.001	.042	.043
N_T	7292	76	8629	4083	12524	68	7717	78	1175	1280	662	117

Table 5.21 D^0 charged particle ($P^{\pm}$) fold matrix

D^0 Charged Particle Fold Matrix				
Observed	Generated			
	0-prongs	2-prongs	4-prongs	6-prongs
0-prongs	.984 ± .003	.072 ± .001	.003 ± .001	0 ± 0
1-prongs	.009 ± .002	.287 ± .003	.044 ± .002	.004 ± .002
2-prongs	.007 ± .002	.632 ± .003	.187 ± .004	.048 ± .008
3-prongs	0 ± 0	.0069 ± .0005	.409 ± .005	.173 ± .014
4-prongs	0 ± 0	.0024 ± .0003	.353 ± .005	.314 ± .017
5-prongs	0 ± 0	$(3 \pm 3)\times 10^{-5}$	.0023 ± .0005	.314 ± .017
6-prongs	0 ± 0	0 ± 0	.0007 ± .0003	.147 ± .013
Normalization	1538	32036	11172	770

Table 5.22 D^0 like-sign kaon (K^+) fold matrix

D^0 K^+ Fold Matrix		
Observed	Generated	
	0-K^+	1-K^+
0-K^+	.976 ± .001	.540 ± .016
1-K^+	.024 ± .001	.460 ± .016
2-K^+	$(4.5 \pm 3.2)\times 10^{-5}$	0 ± 0
Normalization	44526	990

Table 5.23 D^0 unlike-sign kaon (K^-) fold matrix

D^0 K^- Fold Matrix		
Observed	Generated	
	0-K^-	1-K^-
0-K^-	.996 ± .001	.503 ± .003
1-K^-	.004 ± .001	.496 ± .003
2-K^-	0 ± 0	$(1.6 \pm 0.7)\times 10^{-4}$
Normalization	14062	31454

Table 5.24 D^0 charged kaon fold ($K^{\pm}$) matrix

D^0 $K^{\pm}$ Fold Matrix			
Observed	Generated		
	0-$K^{\pm}$	1-$K^{\pm}$	2-$K^{\pm}$
0-$K^{\pm}$	.989 ± .001	.482 ± .003	.321 ± .017
1-$K^{\pm}$	.011 ± .001	.506 ± .003	.453 ± .018
2-$K^{\pm}$	$(7 \pm 7)\times 10^{-5}$	.011 ± .001	.226 ± .015
Normalization	13841	30906	769

Table 5.25 D^0 neutral kaon (K_S) fold matrix

D^0 K_S Fold Matrix			
Observed	Generated		
	0-K_S	1-K_S	2-K_S
0-K_S	.984 ± .001	.806 ± .004	.724 ± .036
1-K_S	.016 ± .001	.192 ± .004	.243 ± .035
2-K_S	$(12 \pm 6)\times 10^{-5}$	.0016 ± .0004	.033 ± .014
Normalization	32380	12932	152

Table 5.26 D^0 unlike-sign pion (π^-) fold matrix

D^0 π^- Fold Matrix				
Observed	Generated			
	0-π^-	1-π^-	2-π^-	2-π^-
0-π^-	.962 ± .001	.328 ± .004	.126 ± .005	.035 ± .020
1-π^-	.037 ± .001	.659 ± .004	.447 ± .007	.302 ± .050
2-π^-	.0004 ± .0001	.014 ± .001	.424 ± .007	.395 ± .053
3-π^-	0 ± 0	.0002 ± .0001	.002 ± .001	.267 ± .048
Normalization	25738	14858	4834	86

Table 5.27 D^0 like-sign pion (π^+) fold tensor

D^0 (π^+, X^+) Fold Tensor							
Observed	Generated						
	(0, 0)	(0, 1)	(1, 0)	(1, 1)	(2, 0)	(2, 1)	(3, 0)
(0, 0)	.984	.181	.184	.059	.051	.020	.021
(0, 1)	.013	.227	.119	.132	.052	.020	.028
(0, 2)	0	.003	.001	.037	.019	.040	.014
(1, 0)	.003	.584	.687	.285	.271	.200	.115
(1, 1)	0	.003	.008	.284	.158	.220	.145
(1, 2)	0	0	.0001	.004	.001	.040	.038
(2, 0)	0	.001	.002	.200	.444	.260	.245
(2, 1)	0	0	0	0	.003	.200	.168
(3, 0)	0	0	0	0	.0008	0	.218
N_T	1492	5650	25426	1032	9717	50	703

Table 5.28 D^0 charged pion ($\pi^{\pm}$) fold tensor

D^0 ($\pi^{\pm}$, $X^{\pm}$) Fold Tensor												
Observed	Generated											
	(0, 0)	(0, 2)	(1, 1)	(1, 3)	(2,0)	(2,2)	(3, 1)	(3, 3)	(4,0)	(4, 2)	(5, 1)	(6, 0)
(0, 0)	.980	.073	.079	.021	.046	0	.004	0	.002	0	.002	0
(0, 1)	.010	.165	.114	.093	.041	.028	.012	0	.006	0	0	0
(0, 2)	.007	.149	.077	.075	.017	.028	.011	0	.008	0	.003	0
(0, 3)	0	.0007	.001	.068	.0001	.018	.006	0	.003	0	.006	0
(0, 4)	0	.0005	.0002	.007	0	0	.002	0	.0008	0	.005	0
(1, 0)	.002	.133	.167	.054	.250	.078	.030	0	.028	0	.005	0
(1, 1)	.0006	.408	.444	.218	.155	.159	.085	.100	.042	0	.026	0
(1, 2)	0	.0005	.005	.189	.003	.148	.069	0	.023	.043	.014	.022
(1, 3)	0	.0002	.002	.111	.0007	.042	.020	.067	.005	.043	.011	.022
(2, 0)	.0006	.070	.108	.054	.482	.120	.095	.067	.118	0	.021	.044
(2, 1)	0	.0005	.001	.054	.003	.184	.212	.067	.128	.130	.084	.044
(2, 2)	0	0	.0002	.021	.002	.117	.096	.333	.040	.043	.087	.022
(2, 3)	0	0	0	0	0	.004	.0008	.033	.0008	.043	.046	.011
(3, 0)	0	.0002	.0008	.018	.0006	.035	.127	.033	.257	.130	.064	.044
(3, 1)	0	0	.0003	.004	0	.025	.190	.133	.140	.087	.121	.110
(3, 2)	0	0	0	0	0	0	.001	.033	.0005	.217	.097	.033
(3, 3)	0	0	0	0	0	0	0	.033	0	0	.031	0
(4, 0)	0	.0005	.0002	.004	0	.014	.038	.033	.197	.174	.071	.154
(4, 1)	0	0	0	0	0	0	.0004	.033	0	.087	.137	.143
(4, 2)	0	0	0	0	0	0	0	0	.0003	0	.051	.077
(5, 0)	0	0	0	0	0	0	.0003	0	0	0	.048	.165
(5, 1)	0	0	0	0	0	0	.0004	0	0	0	.049	.055
N_T	1587	4442	21638	280	6896	283	7124	30	3726	23	652	91

Table 5.29 D_s^+ charged particle ($P^{\pm}$) fold matrix

D_s^+ Charged Particle Fold Matrix				
Observed	Generated			
	1-prongs	3-prongs	5-prongs	7-prongs
0-prongs	.203 ± .008	.024 ± .002	.007 ± .003	0 ± 0
1-prongs	.770 ± .008	.149 ± .005	.037 ± .007	0 ± 0
2-prongs	.018 ± .003	.391 ± .007	.127 ± .012	.032 ± .032
3-prongs	.009 ± .002	.423 ± .007	.281 ± .016	.065 ± .044
4-prongs	0 ± 0	.010 ± .002	.333 ± .017	.258 ± .079
5-prongs	0 ± 0	.0022 ± .0002	.211 ± .015	.452 ± .089
6-prongs	0 ± 0	0 ± 0	.003 ± .002	.161 ± .066
7-prongs	0 ± 0	0 ± 0	.001 ± .001	.032 ± .032
Normalization	2370	4477	750	31

Table 5.30 D_s^+ like-sign kaon (K^+) fold matrix

D_s^+ K^+ Fold Matrix		
Observed	Generated	
	0-K^+	1-K^+
0-K^+	.985 ± .002	.564 ± .010
1-K^+	.015 ± .002	.434 ± .010
2-K^+	0 ± 0	.002 ± .001
Normalization	5205	2425

Table 5.31 D_s^+ unlike-sign kaon (K^-) fold matrix

D_s^+ K^- Fold Matrix		
Observed	Generated	
	0-K^-	1-K^-
0-K^-	.998 ± .001	.593 ± .013
1-K^-	.002 ± .001	.407 ± .013
Normalization	6106	1524

Table 5.32 D_s^+ charged kaon fold ($K^\pm$) matrix

D_s^+ K^+ Fold Matrix			
Observed	Generated		
	0-K^+	1-K^+	2-K^+
0-K^+	.983 ± .002	.529 ± .014	.371 ± .013
1-K^+	.017 ± .002	.469 ± .014	.447 ± .013
2-K^+	$(2 \pm 2)\times 10^{-4}$	.002 ± .001	.180 ± .001
3-K^+	0 ± 0	0 ± 0	.002 ± .001
Normalization	5043	1225	1362

Table 5.33 D_s^+ neutral kaon (K_S) fold matrix

D_s^+ K_S Fold Matrix			
Observed	Generated		
	0-K_S	1-K_S	2-K_S
0-K_S	.987 ± .002	.662 ± .013	.506 ± .057
1-K_S	.013 ± .002	.334 ± .013	.416 ± .056
2-K_S	0 ± 0	.004 ± .002	.078 ± .031
Normalization	6144	1409	77

Table 5.34 D_s^+ unlike-sign pion (π^-) fold matrix

D_s^+ π^- Fold Matrix				
Observed	Generated			
	0-π^-	1-π^-	2-π^-	3-π^-
0-π^-	.991 ± .002	.388 ± .009	.195 ± .017	.190 ± .086
1-π^-	.009 ± .002	.610 ± .009	.499 ± .021	.238 ± .093
2-π^-	0 ± 0	.002 ± .001	.306 ± .019	.429 ± .110
3-π^-	0 ± 0	0 ± 0	0 ± 0	.143 ± .076
Normalization	3794	3246	569	21

Table 5.35 D_s^+ like-sign pion (π^+) fold tensor

D_s^+ (π^+, X^+) Fold Tensor							
Observed	Generated						
	(0, 1)	(0, 2)	(1, 0)	(1, 1)	(2, 0)	(2, 1)	(3, 0)
(0, 0)	.245	.104	.187	.077	.056	.052	.027
(0, 1)	.408	.195	.122	.131	.055	.052	.027
(0, 2)	.006	.116	.003	.062	.018	.024	.021
(1, 0)	.336	.259	.670	.224	.274	.151	.107
(1, 1)	.005	.302	.017	.365	.168	.179	.107
(1, 2)	0	.006	0	.002	.003	.095	.035
(2, 0)	.001	.018	.002	.135	.418	.226	.268
(2, 1)	0	0	0	.003	.007	.167	.151
(3, 0)	0	0	0	0	0	.040	.249
N_T	861	328	1510	2130	2013	252	485

Table 5.36 D_s^+ charged pion ($\pi^\pm$) fold tensor

D_s^+ ($\pi^\pm$, $X^\pm$) Fold Tensor									
Observed	Generated								
	(0, 1)	(0, 3)	(1, 0)	(1, 2)	(2,1)	(3, 0)	(3, 2)	(4,1)	(5, 0)
(0, 0)	.235	.049	.185	.039	.019	.016	.008	.005	.005
(0, 1)	.414	.134	.120	.093	.037	.017	.016	0	.005
(0, 2)	.012	.137	.003	.115	.024	.013	.024	.005	.012
(0, 3)	0	.082	.001	.047	.007	.002	.008	.005	.005
(1, 0)	.329	.125	.664	.100	.104	.097	.057	.048	.014
(1, 1)	.006	.256	.015	.257	.184	.111	.049	.016	.035
(1, 2)	.003	.183	.009	.290	.085	.038	.065	.043	.021
(2, 0)	0	.006	.0007	.010	.174	.276	.114	.102	.059
(2, 1)	0	.018	.001	.040	.222	.153	.146	.112	.098
(2, 2)	0	.003	0	0	.003	.007	.130	.096	.061
(3, 0)	.001	0	0	.001	.135	.261	.089	.107	.152
(3, 1)	0	0	0	.001	.002	.006	.098	.150	.141
(3, 2)	0	0	0	0	.002	.0005	.057	.075	.054
(4, 0)	0	0	0	0	0	0	.008	.086	.138
(4, 1)	0	0	0	0	0	0	.008	.080	.077
(5, 0)	0	0	0	0	0	0	.008	.016	.094
N_T	865	328	1505	1002	1221	1926	123	187	427

Section 5.8 Tables of Observed Multiplicity Distributions

Table 5.37 D^+ observed charged particle ($P^\pm$) multiplicities

Observed	Total Events (N_i)	Background Events (B_i^0)
0-prongs	210	30.3 ± 11.1
1-prongs	904	142.4 ± 16.7
2-prongs	508	119.5 ± 16.8
3-prongs	678	131.3 ± 22.3
4-prongs	85	17.7 ± 3.0
5-prongs	35	13.9 ± 5.8
6-prongs	1	1.5 ± 0.7
7-prongs	0	0.4 ± 0.4

Table 5.38 D^+ observed like-sign kaon (K^+) multiplicities

Observed	Total Events (N_i)	Background Events (B_i^0)
0-K^+	2315	447.4 ± 30.5
1-K^+	105	29.3 ± 8.6
2-K^+	1	0.0 ± 1.0

Table 5.39 D^+ observed unlike-sign kaon (K^-) multiplicities

Observed	Total Events (N_i)	Background Events (B_i^0)
0-K^-	2184	445.6 ± 11.3
1-K^-	237	28.9 ± 10.3

Table 5.40 D^+ observed charged kaon ($K^\pm$) multiplicities

Observed	Total Events (N_i)	Background Events (B_i^0)
0-$K^\pm$	2089	417.4 ± 28.0
1-$K^\pm$	320	56.2 ± 19.6
2-$K^\pm$	12	3.2 ± 1.7

Table 5.41 D^+ observed neutral kaon (K_S) multiplicities

Observed	Total Events (N_i)	Background Events (B_i^0)
0-K_S	2184	441.0 ± 24.3
1-K_S	236	34.8 ± 10.6
2-K_S	1	0.0 ± 1.0

Table 5.42 D^+ observed like-sign pion (π^+) multiplicities

Observed (π^+, X^+)	Total Events (N_i)	Background Events (B_i^0)
(0, 0)	266	53.1 ± 7.3
(0, 1)	261	72.1 ± 8.5
(0, 2)	54	14.9 ± 3.9
(0, 3)	3	0.0 ± 0.0
(1, 0)	881	155.1 ± 12.5
(1, 1)	316	68.0 ± 8.3
(1, 2)	11	6.4 ± 2.5
(2, 0)	531	89.3 ± 9.5
(2, 1)	25	11.2 ± 3.4
(2, 2)	0	0.7 ± 0.8
(3, 0)	31	7.8 ± 2.8
(3, 1)	1	0.0 ± 0.0
(4, 0)	0	0.4 ± 0.6

Table 5.43 D^+ observed unlike-sign pion (π^-) multiplicities

Observed	Total Events (N_i)	Background Events (B_i^0)
0-π^-	1823	310.1 ± 16.0
1-π^-	555	140.7 ± 34.6
2-π^-	43	12.6 ± 7.1
3-π^-	0	0.1 ± 0.3

Table 5.44 D^+ observed charged pion ($\pi^\pm$) multiplicities

Observed ($\pi^\pm$, $X^\pm$)	Total Events (N_i)	Background Events (B_i^0)
(0, 0)	208	29.8 ± 5.7
(0, 1)	219	52.9 ± 13.1
(0, 2)	57	5.5 ± 2.2
(0, 3)	19	8.2 ± 2.4
(1, 0)	682	80.6 ± 20.9
(1, 1)	201	56.0 ± 12.1
(1, 2)	138	22.2 ± 2.2
(1, 3)	5	5.5 ± 1.3
(1, 4)	1	0.4 ± 0.6
(2, 0)	242	32.4 ± 6.1
(2, 1)	329	59.0 ± 5.3
(2, 2)	16	3.1 ± 4.3
(2, 3)	1	4.6 ± 4.2
(3, 0)	176	35.2 ± 5.0
(3, 1)	34	7.9 ± 3.3
(3, 2)	14	2.8 ± 0.8
(3, 3)	0	0.4 ± 0.6
(4, 0)	23	5.0 ± 2.7
(4, 1)	4	8.1 ± 2.0
(4, 2)	1	0.7 ± 2.0
(5, 0)	8	2.6 ± 1.6
(5, 1)	0	0.4 ± 0.6

Table 5.45 D^0 observed charged particle ($P^{\pm}$) multiplicities

Observed	Total Events (N_i)	Background Events (B_i^0)
0-prongs	449	155.0 ± 20.4
1-prongs	851	263.0 ± 37.1
2-prongs	1768	461.7 ± 21.2
3-prongs	515	132.6 ± 24.7
4-prongs	380	79.0 ± 20.9
5-prongs	26	10.7 ± 7.3
6-prongs	12	0.4 ± 3.4
7-prongs	3	0.2 ± 1.6

Table 5.46 D^0 observed like-sign kaon (K^+) multiplicities

Observed	Total Events (N_i)	Background Events (B_i^0)
0-K^+	3349	883.5 ± 53.2
1-K^+	82	19.0 ± 8.8

Table 5.47 D^0 observed unlike-sign kaon (K^-) multiplicities

Observed	Total Events (N_i)	Background Events (B_i^0)
0-K^-	2604	802.5 ± 62.6
1-K^-	827	107.0 ± 20.0

Table 5.48 D^0 observed charged kaon ($K^{\pm}$) multiplicities

Observed	Total Events (N_i)	Background Events (B_i^0)
0-$K^{\pm}$	3000	977.3 ± 65.4
1-$K^{\pm}$	981	142.2 ± 34.3
2-$K^{\pm}$	31	3.0 ± 3.0

Table 5.49 D^0 observed neutral kaon (K_S) multiplicities

Observed	Total Events (N_i)	Background Events (B_i^0)
0-K_S	3715	1067.9 ± 57.6
1-K_S	292	67.0 ± 18.9
2-K_S	5	1.0 ± 0.7

Table 5.50 D^0 observed unlike-sign pion (π^-) multiplicities

Observed	Total Events (N_i)	Background Events (B_i^0)
0-π^-	2047	497.5 ± 44.4
1-π^-	1166	341.7 ± 8.0
2-π^-	204	58.2 ± 14.4
3-π^-	14	1.5 ± 3.7

Table 5.51 D^0 observed like-sign pion (π^+) multiplicities

Observed (π^+, X^+)	Total Events (N_i)	Background Events (B_i^0)
(0, 0)	721	199.6 ± 14.13
(0, 1)	503	117.1 ± 10.82
(0, 2)	39	13.6 ± 3.69
(1, 0)	1491	323.5 ± 17.99
(1, 1)	199	53.9 ± 7.34
(1, 2)	11	2.4 ± 1.56
(2, 0)	325	76.7 ± 8.76
(2, 1)	9	4.4 ± 2.09
(3, 0)	5	2.4 ± 1.56

Table 5.52 D^0 observed charged pion ($\pi^{\pm}$) multiplicities

Observed ($\pi^{\pm}$, $X^{\pm}$)	Total Events (N_i)	Background Events ($B_i{}^0$)
(0, 0)	448	129.7 ± 11.39
(0, 1)	335	78.2 ± 8.84
(0, 2)	251	51.0 ± 7.14
(0, 3)	23	3.9 ± 1.97
(0, 4)	3	0.5 ± 0.70
(1, 0)	496	145.2 ± 12.05
(1, 1)	926	179.2 ± 13.39
(1, 2)	84	30.6 ± 5.53
(1, 3)	31	12.6 ± 3.55
(2, 0)	541	147.7 ± 12.15
(2, 1)	216	58.8 ± 7.67
(2, 2)	86	27.2 ± 5.22
(2, 3)	6	2.4 ± 1.56
(3, 0)	154	41.8 ± 6.46
(3, 1)	173	34.5 ± 5.87
(3, 2)	8	3.4 ± 1.84
(3, 3)	3	1.9 ± 1.39
(4, 0)	71	18.9 ± 4.35
(4, 1)	5	2.4 ± 1.56
(4, 2)	1	0.5 ± 0.70
(5, 0)	3	0 ± 0
(5, 1)	2	0 ± 0

Table 5.53 D_s^+ observed charged particle ($P^{\pm}$) multiplicities

Observed	Total Events (N_i)	Background Events ($B_i{}^0$)
0-prongs	5	2.0 ± 1.7
1-prongs	28	6.4 ± 3.0
2-prongs	21	6.0 ± 3.7
3-prongs	23	7.9 ± 3.4
4-prongs	5	1.7 ± 1.7
5-prongs	2	0.8 ± 0.5

Table 5.54 D_s^+ observed like-sign kaon (K^+) multiplicities

Observed	Total Events (N_i)	Background Events (B_i^0)
0-K^+	74	18.7 ± 6.1
1-K^+	10	4.4 ± 2.3

Table 5.55 D_s^+ observed unlike-sign kaon (K^-) multiplicities

Observed	Total Events (N_i)	Background Events (B_i^0)
0-K^-	81	25.4 ± 6.8
1-K^-	3	1.8 ± 0.7

Table 5.56 D_s^+ observed charged kaon ($K^\pm$) multiplicities

Observed	Total Events (N_i)	Background Events (B_i^0)
0-$K^\pm$	71	19.7 ± 5.9
1-$K^\pm$	13	3.2 ± 2.2
2-$K^\pm$	0	0.7 ± 1.0

Table 5.57 D_s^+ observed neutral kaon (K_S) multiplicities

Observed	Total Events (N_i)	Background Events (B_i^0)
0-K_S	78	24.9 ± 6.9
1-K_S	6	0.8 ± 0.5

Table 5.58 D_s^+ observed unlike-sign pion (π^-) multiplicities

Observed	Total Events (N_i)	Background Events (B_i^0)
0-π^-	55	15.4 ± 6.4
1-π^-	28	4.0 ± 3.3
2-π^-	1	1.8 ± 0.7

Table 5.59 D_s^+ observed like-sign pion (π^+) multiplicities

Observed (π^+, $X^\pm$)	Total Events (N_i)	Background Events ($B_i{}^0$)
(0, 0)	5	3.2 ± 2.57
(0, 1)	16	2.8 ± 3.21
(0, 2)	2	0.8 ± 0.89
(1, 0)	28	7.9 ± 3.85
(1, 1)	13	4.2 ± 2.42
(1, 2)	0	0.5 ± 0.73
(2, 0)	13	1.8 ± 3.47
(2, 1)	4	1.6 ± 1.46
(3, 0)	2	0.8 ± 0.89

Table 5.60 D_s^+ observed charged pion ($\pi^\pm$) multiplicities

Observed ($\pi^\pm$, $X^\pm$)	Total Events (N_i)	Background Events ($B_i{}^0$)
(0, 0)	5	2.0 ± 1.72
(0, 1)	10	2.8 ± 2.40
(0, 2)	4	0.1 ± 1.03
(0, 3)	2	0.1 ± 0.93
(1, 0)	18	2.7 ± 2.84
(1, 1)	10	3.8 ± 2.69
(1, 2)	1	2.4 ± 1.41
(2, 0)	7	1.2 ± 2.53
(2, 1)	10	1.3 ± 2.18
(2, 2)	3	1.8 ± 1.30
(3, 0)	10	4.9 ± 2.25
(3, 1)	0	1.6 ± 1.26
(3, 2)	2	0.3 ± 0.51
(4, 0)	2	0.8 ± 0.89
(4, 1)	0	0.3 ± 0.51
(5, 0)	0	0.3 ± 0.51

PART III
THEORETICAL PREDICTIONS

"Grau, teuer Freund, ist alle Theorie

Und grün des Lebens goldner Baum."

Johann Wolfgang Von Goethe

Faust I. Studierzimmer.

Chapter 6 Inclusive Predictions from Theoretical Models

Section 6.1 Introduction

One objective of this thesis is to use exclusive branching ratio predictions from theoretical models of weak decay to calculate predictions about inclusive properties. See Section 1.3 for a complete list of the inclusive properties calculated in this analysis.

I present three models in this thesis: the factorization model of Bauer, Stech, and Wirbel (BSW) in Chapter 7; the quark diagram scheme of Chau and Cheng (CC) in Chapter 8; and the QCD sum rules model of Blok and Shifman (BS) in Chapter 9. I also include a fourth "model" in Chapter 10, which consists of the known set of experimentally determined exclusive branching ratios, and which I call the Particle Data Group model.

In each model the authors make predictions for exclusive decay properties, namely the partial widths or the branching ratios of various two-body decay modes. Inclusive property predictions come out of their exclusive predictions by one of two methods.

The first method involves an analytic examination of the exclusive decay modes. For every decay mode, a complete listing of all possible final states with their associated branching ratios is compiled. This listing is processed to determine the inclusive properties.

The second method involves the use of a Monte Carlo simulation. The charmed meson in question (D^+, D^0 or D_s^+) is decayed into a single randomly selected exclusive mode with a probability proportional to the predicted branching ratio. This mode is decayed further into a final state. After repeating this process thousands of times for statistical accuracy, the final sample of simulated events is processed to determine the inclusive properties.

Section 6.2 Normalization Schemes

In order to convert a model's predicted partial widths to branching ratios, some form of normalization is needed. Three schemes are possible:

1. Normalize to the D lifetime by setting $\Gamma_{\text{tot}} = \hbar/\tau_D$, where τ_D is the lifetime of the D meson.
2. Normalize to 100% by setting $\Gamma_{\text{tot}} = \sum_i \Gamma_i$, where Γ_i is a partial width.
3. Normalize to a particular experimentally determined branching ratio (such as $D \to \overline{K}\pi$) by setting $\Gamma_{\text{tot}} = \Gamma(D \to K\pi)/B(D \to K\pi)$, where $B(D \to K\pi)$ is the experimentally determined branching ratio.

Of the three schemes, the first is the most physically correct, and is the one I will use throughout this analysis for all exclusive modes. Inclusive properties, however, must have a 100% normalization in order for the results to be meaningful. Thus, all inclusive calculations use the second method.

Section 6.3 Analytic Calculation of Inclusive Properties

Each inclusive property of a non–kinematic nature*, F, (e.g., the average pion multiplicity $\langle n_\pi \rangle$) can be calculated by summing the contributions (f_i) from each of the M decay modes multiplied by the branching ratio (B_i) of that decay mode:

$$F = \sum_i^M f_i B_i .$$

The f_i remain independent of the model, whereas the B_i depend solely on the model and are functions of the model's parameter space $\vec{x} = (x_1, x_2, ..., x_N)$.

For the value of F to be meaningful, the branching ratios must be normalized to unity (i.e., they add up to 100%). Redefining the branching ratios accomplishes this:

$$B_i = \frac{b_i}{b_T} \qquad \text{where} \qquad b_T = \sum_j^M b_j$$

* Inclusive properties of a kinematic nature, (e.g., the K^+ momentum spectrum, usually represented graphically) cannot easily be calculated with this method. For such properties, Monte Carlo methods will be used.

and the b_i are the unnormalized branching ratios.

The error on F is given by:

$$\sigma_F^2 = \sum_i^M \sum_j^M f_i f_j \sigma_{B_i B_j}^2$$

where $\sigma_{B_i B_j}^2$ is the (ij)th element of the *renormalized* branching ratio error matrix.

Parameterized Branching Ratios

When the branching ratios have parameterized functional forms, the elements of the branching ratio error matrix can be expressed in terms of the parameter space error matrix $\sigma_{x_k x_l}^2$:

$$\sigma_{B_i B_j}^2 = \sum_k^N \sum_l^N \left(\frac{\partial B_i}{\partial x_k}\right)\left(\frac{\partial B_j}{\partial x_l}\right)\sigma_{x_k x_l}^2 .$$

Since the branching ratios now sum to 100%, the normalization term of the branching ratios is also a function of the parameters:

$$B_i = \frac{b_i}{b_T} = \frac{\Gamma_i(\vec{x})}{\Gamma_T(\vec{x})} \qquad \text{where} \qquad \Gamma_T(\vec{x}) = \sum_j^M \Gamma_j(\vec{x}) .$$

Numerical Branching Ratios

When the branching ratios are simply numbers, the branching ratio error matrix must be calculated using the renormalized numbers. Assuming that the original errors are uncorrelated (i.e., $\sigma_{b_i b_j}^2 = \sigma_{b_i}^2 \delta_{ij}$), then the branching ratio error matrix becomes:

$$\sigma_{B_i B_j}^2 = \left(s_i^2 b_T^2 \delta_{ij} - b_T\left(s_i^2 b_j + s_j^2 b_i\right) + b_i b_j s_T^2\right)$$

where

$s_i = \sigma_{b_i}$ is the quoted error on the original unnormalized branching ratio, and

$s_T^2 = \sum_i s_i^2$ is the quadrature-added sum of the original errors.

Table 6.1 Branching ratios used to decay secondary particles ($\pi^{\pm}$, $K^{\pm}$, and K_L are considered "stable")

Particle	Decay Products	BR (%)
π^0	$\gamma\gamma$	98.8
	$e^+e^-\gamma$	1.2
η	$\gamma\gamma$	38.9
	$\pi^0\pi^0\pi^0$	31.9
	$\pi^+\pi^-\pi^0$	23.6
	$\pi^+\pi^-\gamma$	4.88
	$e^+e^-\gamma$	0.5
	$\mu^+\mu^-\gamma$	0.03
η'	$\eta\pi^+\pi^-$	44.2
	$\rho^0\gamma$	30.0
	$\eta\pi^0\pi^0$	20.5
	$\omega\gamma$	3.0
	$\gamma\gamma$	2.16
	$\pi^0\pi^0\pi^0$	0.153
$\rho^{\pm}$	$\pi^{\pm}\pi^0$	100.0
ρ^0	$\pi^+\pi^-$	98.89
	$\pi^+\pi^-\gamma$	1.11
ω	$\pi^+\pi^-\pi^0$	88.8
	$\rho^0\gamma$	8.5
	$\pi^+\pi^-$	2.21
ϕ	K^+K^-	49.5
	K_LK_S	34.4
	$\rho^+\pi^-$	4.3
	$\rho^-\pi^+$	4.3
	$\rho^0\pi^0$	4.3
	$\pi^+\pi^-\pi^0$	1.9
	$\eta\gamma$	1.28
	$\pi^0\gamma$	0.131

Particle	Decay Products	BR (%)
K_S	$\pi^+\pi^-$	68.6
	$\pi^0\pi^0$	31.4
K^0	K_S	50.0
	K_L	50.0
$\overline{K}^0$	K_S	50.0
	K_L	50.0
K^{*+}	$K^+\pi^0$	33.3
	$K^0\pi^+$	66.7
K^{*-}	$K^-\pi^0$	33.3
	$\overline{K}^0\pi^-$	66.7
K^{*0}	$K^0\pi^0$	33.3
	$K^+\pi^-$	66.7
$\overline{K}^{*0}$	$\overline{K}^0\pi^0$	33.3
	$K^-\pi^+$	66.7
$a_1{}^{\pm}$	$\rho^0\pi^{\pm}$	50.0
	$\rho^{\pm}\pi^0$	50.0
$a_1{}^0$	$\rho^+\pi^-$	50.0
	$\rho^-\pi^+$	50.0
$\tau^{\pm}$	$\rho^{\pm}\nu$	22.7
	$\mu^{\pm}\nu\nu$	17.8
	$e^{\pm}\nu\nu$	17.7
	$\pi^{\pm}\nu$	11.0
	$\pi^{\pm}\pi^0\pi^0\nu$	7.5
	$\pi^{\pm}\pi^0\pi^0\pi^0\nu$	3.0
	$\pi^{\pm}\rho^0\nu$	5.6
	$\pi^{\pm}\pi^+\pi^-\pi^0\nu$	4.4
	$\pi^{\pm}\pi^+\pi^-\nu$	1.7
	$K^{*\pm}\nu$	1.4
	$\pi^{\pm}\omega\nu$	1.6

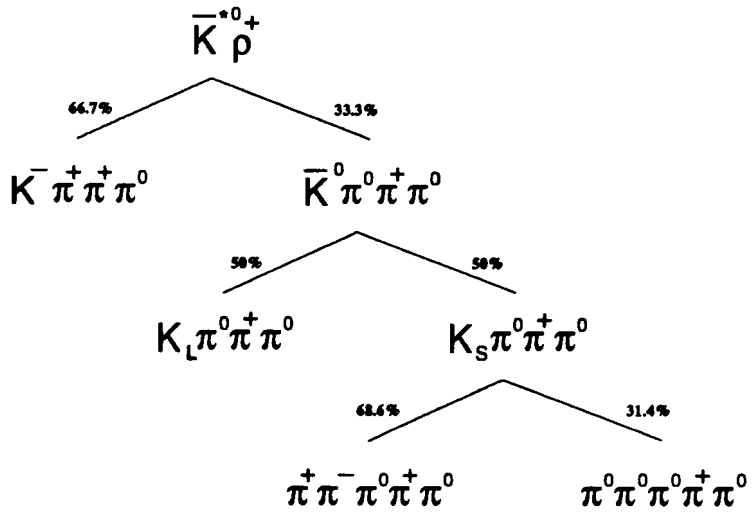

Figure 6.1 An example decay chain showing final states of $\overline{K}^{*0}\rho^+$

Example

The process of determining the multipliers f_i is demonstrated in Figure 6.1 for the mode $\overline{K}^{*0}\rho^+$. Each particle is decayed using a "dictionary" (Table 6.1).[6] The branching ratios used in the dictionary are assumed to be known exactly (i.e., with no experimental uncertainty). Note that for this example only, neutral pions are considered stable. There are four final states. Their branching ratios are:*

$$B(K^-\pi^+\pi^+\pi^0) = 0.667$$

$$B(K_L\pi^+\pi^0\pi^0) = 0.5 \times 0.333 = 0.1665$$

$$B(\pi^+4\pi^0) = 0.314 \times 0.5 \times 0.333 = 0.052281$$

$$B(\pi^+\pi^+\pi^-\pi^0\pi^0) = 0.686 \times 0.5 \times 0.333 = 0.114219\,.$$

The fraction of events from the mode $\overline{K}^{*0}\rho^+$ containing exactly one π^+ in the final state is:

$$f^{1\pi^+}_{\overline{K}^{*0}\rho^+} = 0.1665 + 0.052281 = 0.218781\,.$$

The fraction of events containing exactly zero π^+ is 0 ($f^{0\pi^+}_{\overline{K}^{*0}\rho^+} = 0$), since every final state has at least one π^+. The fraction of events containing exactly two π^+ is:

$$f^{2\pi^+}_{\overline{K}^{*0}\rho^+} = 0.667 + 0.114219 = 0.781219\,.$$

* High precision is carried throughout this example and in all stages of the calculation. Round off occurs only when tabulating the final value, F, of the inclusive property.

The average number of π^+'s from the mode $\overline{K}^{*0}\rho^+$ can be calculated two different ways — a) summing over the fractions of n π^+, or b) summing over the final states directly:

$$\text{a)}\quad f^{\langle N_{\pi^+}\rangle}_{\overline{K}^{*0}\rho^+} = 0 \times f^{0\pi^+}_{\overline{K}^{*0}\rho^+} + 1 \times f^{1\pi^+}_{\overline{K}^{*0}\rho^+} + 2 \times f^{2\pi^+}_{\overline{K}^{*0}\rho^+}$$
$$= 1.781219\,,$$
$$\text{b)}\quad f^{\langle N_{\pi^+}\rangle}_{\overline{K}^{*0}\rho^+} = 2 \times 0.667 + 1 \times 0.1665 + 1 \times 0.052281 + 2 \times 0.114219$$
$$= 1.781219\,.$$

Similarly, the average number of π^0's is:

$$f^{\langle N_{\pi^0}\rangle}_{\overline{K}^{*0}\rho^+} = 1 \times 0.667 + 2 \times 0.1665 + 4 \times 0.052281 + 2 \times 0.114219 = 1.437562\,.$$

Automated Calculation

Determining the multipliers f_i, evaluating the branching ratios $B_i(\vec{x})$, propagating errors and calculating error matrices, as well as calculating the inclusive properties has been computerized. I have written a program called PREDICT to do these analytic calculations. PREDICT is written in the interpretive computer language Rexx. Necessary symbolic computations (such as taking the derivatives of formulae for error propagation) are done via a MAPLE™ interface to PREDICT.

PREDICT currently runs under an IBM VM/CMS operating system that supports CMS Pipelines and MAPLE. However, it is modularized and should be straightforward to modify for use on other systems which support Rexx.

PREDICT reads in a file containing expressions for the partial widths of each decay mode. These expressions can either be numbers (with associated error if available) or functions of the parameters of the model. PREDICT also reads in the current values of the parameters and the error matrix of the parameters. It then computes the branching ratios of each mode and, via MAPLE, computes the error matrix of the branching ratios. A complete description of PREDICT is found in Appendix A.

Section 6.4 Monte Carlo Calculation of Inclusive Properties

The second method of calculating a model's inclusive properties is through the use of a Monte Carlo simulation. Monte Carlo simulations for predicting inclusive properties have, however, several limitations:

1. The branching ratios input into the Monte Carlo must be numeric, thus error propagation of model parameter errors cannot be done in a natural way.
2. A large number of events must be generated to reduce statistical fluctuations.
3. Undesired processes, such as photon conversions and charged pion or kaon decay, can be difficult to suppress in a Monte Carlo that was written to simulate "real" physics in a specific detector.

Comparison tests between the analytic predictions and the Monte Carlo predictions show that the results of the two methods always agree within statistical limits.* Thus the analytic approach, when applicable, is the method used throughout this analysis.

However, certain inclusive properties, namely those of a kinematic nature, cannot be easily obtained except through a Monte Carlo simulation. Therefore, all inclusive spectra predictions given in this analysis come from a Monte Carlo source.

* A benefit to having two different methods was the ability to spot programming errors when the results differed.

Chapter 7 The Factorization Model of Bauer, Stech, and Wirbel

Section 7.1 Introduction

Calculating hadronic weak decay rates in the Standard Model is quite difficult and many theoretical models have sprung forth in an attempt to simplify the calculations and gain additional insight into the weak decay process.

Recall from Chapter 1 that the weak decay Hamiltonian for Cabibbo-favored decays with hard gluon corrections is:

$$H_W = \frac{G_F}{\sqrt{2}} V_{cs} V_{ud} (c_+ O_+ + c_- O_-)$$

where $O_\pm = \frac{1}{2}[(\bar{s}c)(\bar{u}d) \pm (\bar{s}d)(\bar{u}c)]$. This can be rewritten in the form:

$$H_W = \frac{G_F}{\sqrt{2}} V_{cs} V_{ud} (c_1 (\bar{s}c)(\bar{u}d) + c_2 (\bar{s}d)(\bar{u}c))$$

with $c_1 = (c_+ + c_-)/2$ and $c_2 = (c_+ - c_-)/2$.

Bauer, Stech, and Wirbel[12] (BSW) use this form as a starting point in their model. However, they replace the quark currents with hadronic currents. The effective Hamiltonian becomes:

$$H_{\text{eff}} = \frac{G_F}{\sqrt{2}} V_{cs} V_{ud}^* \left[a_1 (\bar{u}d')_H (\bar{s}'c)_H + a_2 (\bar{s}'d')_H (\bar{u}c)_H \right]$$

where the subscript H indicates a hadronic field operator. The two parameters a_1 and a_2 relate to the coefficients c_1 and c_2 through a color factor $\xi = 1/N_c$: $a_1 = c_1 + \xi c_2$ and $a_2 = c_2 + \xi c_1$. The logical value of $\xi = 1/3$ is not assumed, however, and a_1 and a_2 are allowed to be free parameters.

The decay amplitude for $D \to XY$ is proportional to:

$$\begin{aligned} A &\propto \langle XY | H_{\text{eff}} | D \rangle \\ &\propto a_1 \langle XY | (\bar{s}c)_H (\bar{u}d)_H | D \rangle \\ &+ a_2 \langle XY | (\bar{u}c)_H (\bar{s}d)_H | D \rangle . \end{aligned}$$

BSW assume that the hadronic currents are factorizable:

$$\langle XY|(\bar{s}c)_H(\bar{u}d)_H|D\rangle = \langle Y|(\bar{u}d)_H|0\rangle\langle X|(\bar{s}c)_H|D\rangle$$
$$\langle XY|(\bar{u}c)_H(\bar{s}d)_H|D\rangle = \langle X|(\bar{s}d)_H|0\rangle\langle Y|(\bar{u}c)_H|D\rangle$$

and ignore weak-annihilation (WA) effects since these are inherently non-factorizable. Another non-factorizable contribution, final-state interactions, is put in by hand (see Section 7.7). Their model is also restricted to two-body decay modes and does not include any multi-body non-resonant modes.

There are three different types of decays: 1) decays solely dependent upon a_1, 2) decays solely dependent upon a_2, and 3) decays depending upon both a_1 and a_2. D^+ and D_s^+ decays can be of any type, whereas D^0 decays are only of types 1 or 2.

Section 7.2 Calculating Amplitudes — A General Description

The amplitude for a decay of the type $D \to XY$ is:

$$A(D \to XY) = \frac{G_F}{\sqrt{2}} V_1 V_2^* \Big(a_1 \langle Y|J_\mu|0\rangle\langle X|J^\mu|D\rangle + a_2 \langle X|J_\mu|0\rangle\langle Y|J^\mu|D\rangle \Big) .$$

The creation matrix elements for each type of particle are:[39]

$$\begin{aligned}
\langle X|J_\mu|0\rangle &= -if_X p_\mu && \text{Pseudoscalar } ({}^1S_0) \\
&= -if_X m_X \epsilon_\mu && \text{Vector } ({}^3S_1) \\
&= f_X p_\mu && \text{Scalar } ({}^3P_0) \\
&= F_X^V m_X \epsilon_\mu && \text{Axial-vector } ({}^3P_1) \\
&= F_X^A m_X \epsilon_\mu && \text{Axial-vector } ({}^1P_1)
\end{aligned}$$

where p_μ is the 4–momentum of the particle X, ϵ_μ is the polarization 4–vector of X, m_X is the mass of X, and f_X, F_X^V, F_X^A are the decay constants.

The hadronic matrix elements are:[39]

$$
\begin{aligned}
\langle X_P|J_\mu|D\rangle &= \left(p_D + p_X - \frac{m_D^2 - m_X^2}{q^2}q\right)_\mu F_1(q^2) + \frac{m_D^2 - m_X^2}{q^2}q_\mu F_0(q^2) \\
\langle X_V|J_\mu|D\rangle &= \epsilon_{\mu\nu\rho\sigma}\epsilon_X^\nu p_D^\rho p_X^\sigma \frac{2}{m_D + m_X}V(q^2) \\
&\quad + i\left(\epsilon_\mu^X(m_D + m_X)A_1(q^2) - \frac{\epsilon^X \cdot q}{m_D + m_X}(p_D + p_X)_\mu A_2(q^2)\right. \\
&\quad \left. - \frac{\epsilon^X \cdot q}{q^2}2m_X q_\mu A_3(q^2)\right) + i\frac{\epsilon^X \cdot q}{q^2}2m_X q_\mu A_0(q^2) \\
\langle X_S|J_\mu|D\rangle &= -\left((p_D + p_X)_\mu - \frac{m_D^2 - m_X^2}{q^2}q_\mu\right)A_1(q^2) - \frac{m_D^2 - m_X^2}{q^2}q_\mu A_0(q^2) \\
\left\langle X_{(^3P_1)}|J_\mu|D\right\rangle &= -i\left(\epsilon_\mu(m_D - m_X) - \frac{\epsilon^X \cdot q}{m_D + m_X}(p_D + p_X)_\mu\right)H_V(q^2) \\
&\quad - \epsilon_{\mu\nu\rho\sigma}\epsilon_X^\nu p_D^\rho p_X^\sigma \frac{2}{m_D - m_X}H_A(q^2) \\
\left\langle X_{(^1P_1)}|J_\mu|D\right\rangle &= i\left(\epsilon_\mu^X 2m_X H_{V_1}(q^2) - \frac{\epsilon^X \cdot q}{m_D^2 - m_X^2}2m_X(p_D + p_X)_\mu H_{V_2}(q^2)\right. \\
&\quad \left. + \frac{\epsilon^X \cdot q}{q^2}2m_X q_\mu H_{V_3}(q^2)\right) - i\frac{\epsilon^X \cdot q}{q^2}2m_X q_\mu H_{V_0}(q^2)
\end{aligned}
$$

where $F_i(q^2), V_i(q^2), A_i(q^2), H_V, H_A, H_{V_i}(q^2)$ are all form factors with a nearest pole dominance form:

$$F(q^2) = \frac{h}{1 - q^2/m^2}$$

where m is the pole mass and h is the wave function overlap factor (evaluated at $q^2 = 0$) calculated using relativistic bound states of quark-antiquark pairs in the infinite momentum frame.[40]

Section 7.3 The $\overline{K}\pi$ System

As an example of the factorization calculation, I will calculate the widths of the $\overline{K}\pi$ system. Considering explicitly only $D \to \overline{K}\pi$ decays, the amplitude for a general decay is:

$$
\begin{aligned}
A(D \to \overline{K}\pi) = \frac{G_F}{\sqrt{2}}V_{cs}V_{ud}\Big(&a_1\langle\pi|J_\mu|0\rangle\langle\overline{K}|J^\mu|D\rangle \\
&+ a_2\langle\overline{K}|J_\mu|0\rangle\langle\pi|J^\mu|D\rangle\Big).
\end{aligned}
$$

The creation matrix elements for pseudoscalar mesons are:

$$\langle \pi | J_\mu | 0 \rangle = -i f_\pi p_\mu^\pi$$

$$\langle K | J_\mu | 0 \rangle = -i f_K p_\mu^K$$

where p_μ^X is the 4–momentum of the particle and f_π and f_K are decay constants (Table 7.1). The other matrix element, governing the decay of the D into a K or π, is:

$$\langle X | J^\mu | D \rangle = \left(p_D + p_X - \frac{m_D^2 - m_X^2}{q^2} q \right)^\mu F_1(q^2) + \frac{m_D^2 - m_X^2}{q^2} q^\mu F_0(q^2)$$

where X stands for a kaon or pion as necessary. The transverse form factor $F_1(q^2)$ and the longitudinal form factor $F_0(q^2)$ assume nearest pole dominance and have the forms:

$$F_1(q^2) = \frac{h_1}{1 - q^2/m_{(1^-)}^2}$$

$$F_0(q^2) = \frac{h_0}{1 - q^2/m_{(0^+)}^2}.$$

The constants, h_1 and h_0, are wave function overlap factors (Table 7.2). $m(0^+)$ and $m(1^-)$ are the pole masses (Table 7.3).

Table 7.1 Values used in the calculations

Decay Constants[12]
f_π = 0.133 GeV
f_K = 0.162 GeV
$F_{a_1}^V$ = 0.221 GeV

Particle Masses (GeV)[41]					
D^0	1.8645	K^-	0.49365	π^+	0.13957
D^+	1.8693	$\overline{K}^0$	0.49767	π^0	0.13497
				a_1	1.26

Table 7.2 Overlap factors (form factors at $q^2 = 0$)[39]

Process	$h_0 = h_1$	h_A	h_V
$D \to K$	0.762		
$D \to \pi$	0.692		
$D \to a_1$		0.391	1.347

Before evaluating the amplitudes, it's helpful to first evaluate the product of the factorized currents. For a pion created from the vacuum, the momentum transfer is

$q^2 = m_\pi^2$. Using the 4–momentum relationship $p_\pi = p_D - p_K$, the first product, expressed as a 4–vector dot product, is:

$$
\begin{aligned}
&\langle \pi | J_\mu | 0 \rangle \langle \overline{K} | J^\mu | D \rangle \\
&= (-i f_\pi p_\pi) \cdot \left[\left(p_D + p_K - \frac{m_D^2 - m_K^2}{q^2} q \right) F_1 + \left(\frac{m_D^2 - m_K^2}{q^2} q \right) F_0 \right] \Bigg|_{q=p_\pi} \\
&= -i f_\pi \left[p_\pi \cdot (p_D + p_K) F_1 - \frac{m_D^2 - m_K^2}{m_\pi^2} (p_\pi \cdot p_\pi)(F_1 - F_0) \right] \\
&= -i f_\pi \left[(m_D^2 - m_K^2) F_1 - (m_D^2 - m_K^2)(F_1 - F_0) \right] \\
&= -i f_\pi (m_D^2 - m_K^2) F_0 \\
&= -i f_\pi (m_D^2 - m_K^2) \frac{h_0}{1 - m_\pi^2 / m_{c\bar{s}(0^+)}^2} .
\end{aligned}
$$

Similarly, when the kaon is created from the vacuum, the momentum transfer is $q^2 = m_K^2$ and the product becomes:

$$
\begin{aligned}
&\langle \overline{K} | J_\mu | 0 \rangle \langle \pi | J^\mu | D \rangle \\
&= (-i f_K p_K) \cdot \left[\left(p_D + p_\pi - \frac{m_D^2 - m_\pi^2}{q^2} q \right) F_1 + \left(\frac{m_D^2 - m_\pi^2}{q^2} q \right) F_0 \right] \Bigg|_{q=p_K} \\
&= -i f_K (m_D^2 - m_\pi^2) F_0 \\
&= -i f_K (m_D^2 - m_\pi^2) \frac{h_0}{1 - m_K^2 / m_{c\bar{u}(0^+)}^2} .
\end{aligned}
$$

Using the constants specified in Tables 7.1 through 7.4, the amplitude of the $D^0 \to K^- \pi^+$

Table 7.3 Pole masses used in the calculations[39]

Pole Masses (GeV)			
Current	$m(1^-)$	$m(0^+)$	$m(1^+)$
$c\bar{d}$	2.01	2.47	2.42
$c\bar{s}$	2.11	2.60	2.53

Table 7.4 Cabibbo-Kobayashi-Maskawa matrix elements

CKM Matrix Elements	
$V_{ud} = .975$	$V_{us} = .222$
$V_{cd} = .222$	$V_{cs} = .975$

mode evaluates to:

$$\begin{aligned}
A(D^0 \to K^-\pi^+) &= \frac{G_F}{\sqrt{2}} V_{cs} V_{ud}^* a_1 \langle \pi^+ | J_\mu | 0 \rangle \langle K^- | J^\mu | D^0 \rangle \\
&= \frac{G_F}{\sqrt{2}} V_{cs} V_{ud}^* a_1 \left(-i f_\pi (m_{D^0}^2 - m_{K^-}^2) \frac{h_0(D \to K)}{1 - m_{\pi^+}^2 / m_{c\bar{s}(0^+)}^2} \right) \\
&= (-i)\, 2.57 \times 10^{-6}\, a_1 \quad \text{GeV}.
\end{aligned}$$

The evaluation of the amplitude of the $D^0 \to K^0\pi^0$ mode (which has an extra factor of $1/\sqrt{2}$ to account for the quark mixing of $|u\bar{u}\rangle = \frac{|\pi^0\rangle}{\sqrt{2}} + \frac{|\eta_1\rangle}{\sqrt{3}} + \frac{|\eta_8\rangle}{\sqrt{6}}$) is:

$$\begin{aligned}
A\left(D^0 \to \overline{K}^0 \pi^0\right) &= \frac{G_F}{\sqrt{2}} V_{cs} V_{ud}^* a_2 \left\langle \overline{K}^0 | J_\mu | 0 \right\rangle \langle \pi^0 | J^\mu | D^0 \rangle \\
&= \frac{G_F}{2} V_{cs} V_{ud}^* a_2 \left(-i f_K (m_{D^0}^2 - m_{\pi^0}^2) \frac{h_0(D \to \pi)}{1 - m_{\overline{K}^0}^2 / m_{c\bar{u}(0^+)}^2} \right) \\
&= (-i)\, 2.24 \times 10^{-6}\, a_2 \quad \text{GeV}.
\end{aligned}$$

The evaluation for the amplitude of the $D^+ \to \overline{K}^0\pi^+$ mode is:

$$\begin{aligned}
A\left(D^+ \to \overline{K}^0 \pi^+\right) &= \frac{G_F}{\sqrt{2}} V_{cs} V_{ud}^* \Big(a_1 \langle \pi^+ | J_\mu | 0 \rangle \left\langle \overline{K}^0 | J^\mu | D^+ \right\rangle \\
&\qquad + a_2 \left\langle \overline{K}^0 | J_\mu | 0 \right\rangle \langle \pi^+ | J^\mu | D^+ \rangle \Big) \\
&= \frac{G_F}{\sqrt{2}} V_{cs} V_{ud}^* \left(-i a_1 f_\pi \left(m_{D^+}^2 - m_{\overline{K}^0}^2 \right) \frac{h_0(D \to K)}{1 - m_{\pi^+}^2 / m_{c\bar{s}(0^+)}^2} \right. \\
&\qquad \left. + -i a_2 f_K (m_{D^+}^2 - m_{\pi^+}^2) \frac{h_0(D \to \pi)}{1 - m_{\overline{K}^0}^2 / m_{c\bar{u}(0^+)}^2} \right) \\
&= (-i) 2.59 (a_1 + 1.23 a_2) \times 10^{-6} \text{ GeV}.
\end{aligned}$$

I convert these amplitudes to partial widths by considering the two-body decay kinematics (assuming no dependence on θ or ϕ by $|A|^2$ or p, which is reasonable in a P→PP (P=pseudoscalar) decay):

$$\begin{aligned}
d\Gamma &= \frac{1}{32\pi^2} |A|^2 \frac{p}{M_D^2} d\Omega \\
\therefore \quad \Gamma &= \frac{1}{8\pi} |A|^2 \frac{p}{M_D^2}
\end{aligned}$$

where the masses of the D mesons are those listed in Table 7.1 and p is the momentum of the kaon (or pion) in the D rest frame:

$$p(D \to K\pi) = \left(M_D^2 - (M_K + M_\pi)^2 \right)^{1/2} \left(M_D^2 - (M_K - M_\pi)^2 \right)^{1/2} / (2M_D)$$

$$p(D^0 \to K^-\pi^+) = 0.86088 \text{ GeV}$$
$$p\left(D^0 \to \overline{K}^0\pi^0\right) = 0.86019 \text{ GeV}$$
$$p\left(D^+ \to \overline{K}^0\pi^+\right) = 0.86239 \text{ GeV}.$$

The small difference in the partial widths (Table 7.5) between my results and BSW in the $\overline{K}^0\pi^0$ system is probably due to round-off and has no effect on later calculations.

Table 7.5 Partial width predictions for $D \to \overline{K}\pi$

Mode	This Thesis		BSW[12]	
	Γ (10^{-14} GeV)	Γ (10^{10} s^{-1})	Γ (10^{-14} GeV)	Γ (10^{10} s^{-1})
$D^0 \to K^-\pi^+$	$6.53\ a_1^2$	$9.92\ a_1^2$	$6.53\ a_1^2$	$9.92\ a_1^2$
$D^0 \to K^0\pi^0$	$4.94\ a_2^2$	$7.50\ a_2^2$	$4.97\ a_2^2$	$7.55\ a_2^2$
$D^+ \to K^0\pi^+$	$6.57(a_1+1.23a_2)^2$	$9.98(a_1+1.23a_2)^2$	$6.57(a_1+1.23a_2)^2$	$9.98(a_1+1.23a_2)^2$

Section 7.4 The $\overline{K}a_1$ System

As another example of a factorization calculation, the partial widths of the $\overline{K}a_1$ system are calculated. This is an example of a pseudoscalar—axialvector (PA) system. The amplitude for a general decay of the type $D \to \overline{K}a_1$ is:*

$$A(D \to \overline{K}a_1) = \frac{G_F}{\sqrt{2}} V_{cs}V_{ud}\Big(a_1\langle a_1|J_\mu|0\rangle\langle\overline{K}|J^\mu|D\rangle + a_2\langle\overline{K}|J_\mu|0\rangle\langle a_1|J^\mu|D\rangle\Big).$$

The creation matrix elements are:

$$\langle a_1|J_\mu|0\rangle = -F^V_{a_1} m_{a_1}\epsilon_\mu$$
$$\langle\overline{K}|J_\mu|0\rangle = -if_K p^K_\mu$$

where p_μ is the 4–momentum of the particle, ϵ_μ is the polarization vector of the a_1 and $F^V_{a_1}$ and f_K are the decay constants (Table 7.1). The current for $D \to K$ is:

$$\langle\overline{K}|J^\mu|D\rangle = \left(p_D + p_K - \frac{m_D^2 - m_K^2}{q^2}q\right)^\mu F_1(q^2) + \frac{m_D^2 - m_K^2}{q^2}q^\mu F_0(q^2)$$

* Beware of possible confusion between the particle a_1 and the parameter a_1.

and the element for $D \to a_1$ (a $^3P_1$ axialvector) is split into separate vector and axialvector components:*

$$\langle a_1|V^\mu|D\rangle = -i\left(\epsilon^\mu(m_D - m_{a_1}) - \frac{\epsilon q}{m_D + m_{a_1}}(p_D + p_{a_1})^\mu\right)H_V(q^2)$$
$$\langle a_1|A^\mu|D\rangle = \epsilon^{\mu\nu\rho\sigma}\epsilon_\nu p^D_\rho p^{a_1}_\sigma \frac{2}{m_D - m_{a_1}} H_A(q^2)\,.$$

As before, we assume nearest pole dominance for the transverse form factor $F_1(q^2)$ and the longitudinal form factor $F_0(q^2)$ using the same form as on page 116. The axial form factor $H_A(q^2)$ and the vector form factor $H_V(q^2)$ also have similar forms:

$$H_A(q^2) = \frac{h_A}{1 - q^2/m^2_{(1^+)}}$$
$$H_V(q^2) = \frac{h_V}{1 - q^2/m^2_{(1^-)}}\,.$$

The constants, h_1, h_0, h_V, and h_A, are wave function overlap factors (Table 7.2) and $m(0^+)$, $m(1^+)$, and $m(1^-)$ are the pole masses (Table 7.3).

In evaluating the amplitudes, some polarization vector properties to keep in mind are:

$$\epsilon^{(\pm 1)} = \mp(0, 1, \pm i, 0)/\sqrt{2}$$
$$\epsilon^{(0)} = (|\vec{p}|, 0, 0, E)/m$$
$$p^\mu \epsilon_\mu = 0$$
$$\sum_\lambda \epsilon^{(\lambda)}_\mu \epsilon^{(\lambda)}_\nu = -g_{\mu\nu} + \frac{p_\mu p_\nu}{M^2}$$
$$\sum_\lambda \epsilon^{(\lambda)}_\mu p^\mu_D = \sum_\lambda \epsilon^{(\lambda)}_\mu p^\mu_K = \frac{|\vec{p}_{a_1}|m_D}{m_{a_1}}\,.$$

---

* It should be noted that the form of the $\langle a_1|J^\mu|D\rangle$ used by BSW differs from one given in Reference 42 which lists for a $^3P_1$ matrix element:

$$\langle X(^3P_1)|V_\mu|D\rangle = l(t)\epsilon^*_\mu + c_+(t)(\epsilon^* \cdot P_D)(P_D + P_X)_\mu + c_-(t)(\epsilon^* \cdot P_D)(P_D - P_X)_\mu$$
$$\langle X(^3P_1)|A_\mu|D\rangle = iq(t)\epsilon_{\mu\nu\rho\sigma}\epsilon^{*\nu}(P_D + P_X)^\rho(P_D - P_X)^\sigma$$

Comparing the two forms one can see that the axial vector part is the same. The BSW model however is missing the $(\epsilon^* \cdot P_D)(P_D - P_X)$ contribution to the vector part. However, Kamal and Verma[43] indicate that the form factor normalization is zero for this term (i.e., $c_-(0) = 0$) due to the orthogonality of the wave functions.

Kamal and Verma also include terms due to the annihilation diagram which enhances the two D^0 modes. This effect will not be included in this study.

We begin by evaluating the first product of the two matrix elements at $q^2 = m_{a_1}^2$. Summation over all polarization states is implicit in these calculations. The product, in vector dot product notation, is:

$$
\begin{aligned}
&\langle a_1|J_\mu|0\rangle\langle\overline{K}|J^\mu|D\rangle \\
&= \left(-F_{a_1}^V m_{a_1}\epsilon_\mu\right)\cdot\left[\left(p_D + p_K - \frac{m_D^2 - m_K^2}{q^2}q\right)F_1 + \left(\frac{m_D^2 - m_K^2}{q^2}q\right)F_0\right]\Bigg|_{q=p_{a_1}} \\
&= -F_{a_1}^V m_{a_1}\left[\epsilon\cdot(p_D + p_K)F_1 - \frac{m_D^2 - m_K^2}{q^2}(\epsilon\cdot p_{a_1})(F_1 - F_0)\right] \\
&= -F_{a_1}^V m_{a_1}[\epsilon\cdot(p_D + p_K)F_1] \\
&= -F_{a_1}^V m_{a_1}\left[2|\vec{p}_{a_1}|\frac{m_D}{m_{a_1}}F_1\right] \\
&= -2F_{a_1}^V|\vec{p}_{a_1}|m_D F_1(m_{a_1}^2) \\
&= -2F_{a_1}^V|\vec{p}_{a_1}|m_D\frac{h_1}{1 - m_{a_1}^2/m_{c\bar{s}(1^-)}^2}\,.
\end{aligned}
$$

Similarly the second product of the two matrix elements at $q^2 = m_K^2$:

$$
\begin{aligned}
&\langle\overline{K}|J_\mu|0\rangle\langle a_1|J^\mu|D\rangle \\
&= \left(-if_K p_\mu^K\right)\Bigg[(-i)\left(\epsilon^\mu(m_D - m_{a_1}) - \frac{\epsilon\cdot q}{m_D + m_{a_1}}(p_D + p_{a_1})^\mu\right)H_V \\
&\qquad - \epsilon^{\mu\nu\rho\sigma}\epsilon_\nu p_\rho^D p_\sigma^{a_1}\frac{2}{m_D - m_{a_1}}H_A(q^2)\Bigg]\Bigg|_{q=p_K} \\
&= -f_K\left[(p_K\cdot\epsilon)(m_D - m_{a_1}) - \frac{\epsilon\cdot p_K}{m_D + m_{a_1}}p_\mu^K(p_D + p_{a_1})^\mu - 0\right]H_V \\
&= -f_K\left[(\epsilon\cdot p_K)(m_D - m_{a_1}) - \frac{\epsilon\cdot p_K}{m_D + m_{a_1}}(m_D^2 - m_{a_1}^2)\right]H_V \\
&= 0\,.
\end{aligned}
$$

Using the constants specified in Tables 7.1 through 7.4, the evaluation for the amplitude of the $D^0 \to K^- a_1^+$ mode proceeds:

$$
\begin{aligned}
A(D^0 \to K^- a_1^+) &= \frac{G_F}{\sqrt{2}}V_{cs}V_{ud}a_1\langle a_1^+|J_\mu|0\rangle\langle K^-|J^\mu|D^0\rangle \\
&= \frac{G_F}{\sqrt{2}}V_{cs}V_{ud}a_1\left(-2F_{a_1}^V|\vec{p}_{a_1}|m_{D^0}\frac{h_1(D\to K)}{1 - m_{a_1^+}^2/m_{c\bar{s}(1^-)}^2}\right) \\
&= -2.21\times 10^{-6}\,a_1\ \ \text{GeV}\,.
\end{aligned}
$$

The evaluation for the amplitude of the $D^0 \to \overline{K}^0 a_1^0$ mode is:

$$A\left(D^0 \to \overline{K}^0 a_1^0\right) = \frac{G_F}{2} V_{cs} V_{ud} a_2 \left\langle \overline{K}^0 | J_\mu | 0 \right\rangle \left\langle a_1^0 | J^\mu | D^0 \right\rangle$$
$$= 0 .$$

The evaluation for the amplitude of the $D^+ \to \overline{K}^0 a_1^+$ mode is:

$$A\left(D^+ \to \overline{K}^0 a_1^+\right) = \frac{G_F}{\sqrt{2}} V_{cs} V_{ud} \Big(a_1 \langle a_1^+ | J_\mu | 0 \rangle \left\langle \overline{K}^0 | J^\mu | D^+ \right\rangle$$
$$+ a_2 \left\langle \overline{K}^0 | J_\mu | 0 \right\rangle \langle a_1^+ | J^\mu | D^+ \rangle \Big)$$
$$= -\frac{G_F}{\sqrt{2}} V_{cs} V_{ud} a_1 \left(2 F_{a_1}^V |\vec{p}_{a_1}| m_{D^+} \frac{h_1(D \to K)}{1 - m_{a_1^+}^2 / m_{c\bar{s}(1^-)}^2} \right)$$
$$= -2.23 a_1 \times 10^{-6} \text{ GeV} .$$

I convert these amplitudes to partial widths via:*

$$\Gamma = \frac{1}{8\pi} |A|^2 \frac{p_{a_1}}{m_D^2}$$

and list the results, along with the BSW results, in Table 7.6.

Table 7.6 Partial width predictions for $D \to \overline{K} a_1$

Mode	This Thesis	BSW
	Γ (10^{10} s^{-1})	Γ (10^{10} s^{-1})
$D^0 \to K^- a_1^+$	2.45 a_1^2	2.43 a_1^2
$D^0 \to \overline{K}^0 a_1^0$	0	0
$D^+ \to \overline{K}^0 a_1^+$	2.49 a_1^2	2.49 a_1^2

Section 7.5 Semileptonic Decays

BSW also calculate the partial widths of semileptonic decays (see Table 7.7).[44] The amplitude for a decay of the type $D \to \overline{K} \ell^+ \nu$ is:

$$A(D \to \overline{K} \ell^+ \nu) = \frac{G_F}{\sqrt{2}} L^\mu H_\mu$$

* This assumes a narrow width of the a_1 mass. Reference 43 indicates that including the width of the a_1 makes no appreciable difference.

where the leptonic current is:

$$L^{\mu} = \bar{u}(\nu)\gamma^{\mu}(1-\gamma^{5})v(\ell^{+})$$

and the hadronic part is:

$$H_{\mu} = \langle \overline{K}|J_{\mu}|D\rangle .$$

The details of this calculation are given in Appendix B with the results summarized in Table 7.8.

Table 7.7 BSW semileptonic partial widths[39]

	$\Gamma(D \to K\ell\nu)$	$\Gamma(D \to K^{*}\ell\nu)$	$\Gamma(D \to \pi\ell\nu)$	$\Gamma(D \to \rho\ell\nu)$
10^{10} s^{-1}	8.26	9.53	0.73	0.70
10^{-14} GeV	5.44	6.27	0.48	0.46

Table 7.8 Semileptonic partial widths for $D \to \overline{K}\ell^{+}\nu$ decays

Process	Partial Width (10^{-14} GeV)	BR (%)
$D^{0} \to K^{-}e^{+}\nu$	5.54584	3.547
$D^{+} \to \overline{K}^{0}e^{+}\nu$	5.58960	9.019
$D^{0} \to K^{-}\mu^{+}\nu$	5.48088	3.506
$D^{+} \to \overline{K}^{0}\mu^{+}\nu$	5.5244	8.914

Section 7.6 Isospin Decomposition

BSW calculate the parameters a_1 and a_2 of their factorization model[12] by examining $D \to \overline{K}\pi$. Since they give expressions for *bare* amplitudes, without any final-state interactions, one must remove these interactions from the experimental results before fitting to a_1 and a_2. The cleanest system with which to do this is the $D \to \overline{K}\pi$ system. The isospin decomposition of $D \to \overline{K}\pi$ gives:

$$A_{-+} \equiv A(D^{0} \to K^{-}\pi^{+}) = \frac{1}{\sqrt{3}}\left(\sqrt{2}A_{1/2} + A_{3/2}\right)$$

$$A_{00} \equiv A\left(D^{0} \to \overline{K}^{0}\pi^{0}\right) = \frac{1}{\sqrt{3}}\left(-A_{1/2} + \sqrt{2}A_{3/2}\right)$$

$$A_{0+} \equiv A\left(D^{+} \to \overline{K}^{0}\pi^{+}\right) = \sqrt{3}A_{3/2}$$

where the $A_I = |A_I| \exp(i\delta_I)$ are the final-state amplitudes for isospin I=1/2 or I=3/2. These equations do not stem solely from an isospin decomposition.* The Wigner-Eckart theorem must be applied to reduce the isospin matrix elements. See Appendix C for the details of this decomposition.

Squaring these amplitudes, one obtains:

$$|A_{-+}|^2 = \frac{1}{3}\Big(2|A_{1/2}|^2 + |A_{3/2}|^2 + 2\sqrt{2}|A_{1/2}||A_{3/2}|\cos(\delta_{1/2} - \delta_{3/2})\Big)$$
$$|A_{00}|^2 = \frac{1}{3}\Big(|A_{1/2}|^2 + 2|A_{3/2}|^2 - 2\sqrt{2}|A_{1/2}||A_{3/2}|\cos(\delta_{1/2} - \delta_{3/2})\Big)$$
$$|A_{0+}|^2 = 3|A_{3/2}|^2 .$$

The solution to these three equations is:†

$$|A_{1/2}| = \left(|A_{-+}|^2 + |A_{00}|^2 - \frac{|A_{0+}|^2}{3}\right)^{1/2}$$
$$|A_{3/2}| = \frac{|A_{0+}|}{\sqrt{3}}$$
$$\cos(\delta_{1/2} - \delta_{3/2}) = \frac{\sqrt{3}\Big(|A_{-+}|^2 - 2|A_{00}|^2 + \frac{|A_{0+}|^2}{3}\Big)}{2\sqrt{2}|A_{0+}|\Big(|A_{-+}|^2 + |A_{00}|^2 - \frac{|A_{0+}|^2}{3}\Big)^{1/2}} .$$

The squared amplitudes, $|A_{-+}|^2$, $|A_{00}|^2$ and $|A_{0+}|^2$ are related to their branching ratios by:

$$B = \left(\frac{\tau_D}{\hbar}\right)\left(\frac{1}{8\pi}|A|^2\frac{p}{M_D^2}\right)$$

where:[41]

$$\tau(D^0) = (4.21 \pm 0.21) \times 10^{-13} s$$
$$\tau(D^+) = (10.62 \pm 0.28) \times 10^{-13} s .$$

---

* An isospin decomposition alone would not give the $\sqrt{3}$ factor in the A_{0+} term.

† If this solution yields $|\cos(\delta_{1/2} - \delta_{3/2})| > 1$ then a fitting technique must be used for the answers to be physically meaningful. One choice is to do a chi-squared minimization using

$$\chi^2 = \frac{(B_{+-}^{\rm fit} - B_{+-}^{\rm exp})^2}{\sigma^2_{B_{+-}^{\rm exp}}} + \frac{(B_{00}^{\rm fit} - B_{00}^{\rm exp})^2}{\sigma^2_{B_{00}^{\rm exp}}} + \frac{(B_{+0}^{\rm fit} - B_{+0}^{\rm exp})^2}{\sigma^2_{B_{+0}^{\rm exp}}}$$

where the $B_i^{\rm fit} = \frac{\tau}{\hbar}\left(\frac{p}{8\pi m_D^2}\right)|A_i|^2$ and fitting for $|A_{1/2}|$ and $|A_{3/2}|$ and $\delta = \delta_{1/2} - \delta_{3/2}$.

The latest Mark III branching ratios are used.[45, 41] These are:

$$B_{-+} \equiv B(D^0 \to K^-\pi^+) = 4.2 \pm 0.4\%$$
$$B_{00} \equiv B\left(D^0 \to \overline{K}^0\pi^0\right) = 1.8 \pm 0.2\%$$
$$B_{0+} \equiv B\left(D^+ \to \overline{K}^0\pi^+\right) = 3.2 \pm 0.5\%\,.$$

The errors on the isospin amplitudes are determined using the standard error propagation formula for a function $y = y(x_1, ..., x_i, ..., x_n)$:

$$\sigma_y^2 = \sum_{i=1}^{n}\sum_{j=1}^{n}\sigma_{ij}^2\left(\frac{\partial y}{\partial x_i}\right)\left(\frac{\partial y}{\partial x_j}\right).$$

After some experimentation with Mathematica™, I determined that the errors on the isospin amplitudes are dominated by the branching ratio errors. The expressions for the errors on $|A_{1/2}|$ and $|A_{3/2}|$ and $\delta = \delta_{1/2} - \delta_{3/2}$ in terms of the branching ratio errors are given below. Although no stated correlation exists between the B_{+-} and B_{00} measurements, I have included the correlation term in the error expressions. The error expressions reduce to:

$$\begin{aligned}
\sigma_{1/2}^2 &= \frac{1}{4|A_{1/2}|^2}\left[\frac{\sigma_{B_{-+}}^2}{B_{-+}^2}|A_{-+}|^4 + \frac{\sigma_{B_{00}}^2}{B_{00}^2}|A_{00}|^4 + \frac{2\sigma_{B_{-+},B_{00}}^2}{B_{-+}B_{00}}|A_{-+}|^2|A_{00}|^2 + \frac{\sigma_{B_{0+}}^2}{9B_{0+}^2}|A_{0+}|^4\right] \\
&= \frac{16\pi^2\hbar^2}{|A_{1/2}|^2}\left[\left(\frac{\sigma_{B_{-+}}^2}{p_{-+}^2} + \frac{\sigma_{B_{00}}^2}{p_{00}^2} + \frac{2\sigma_{B_{-+},B_{00}}^2}{p_{-+}p_{00}}\right)\left(\frac{M_{D^0}^2}{\tau_{D^0}}\right)^2 + \frac{\sigma_{B_{0+}}^2}{9p_{0+}^2}\left(\frac{M_{D^+}^2}{\tau_{D^+}}\right)^2\right] \\
\sigma_{3/2}^2 &= \frac{\sigma_{B_{0+}}^2}{4B_{0+}^2}\,|A_{3/2}|^2 \\
\sigma_\delta^2 &= \frac{\sigma_{\cos\delta}^2}{1-\cos^2\delta}\,.
\end{aligned}$$

Here the error on the cosine of the phase difference is:

$$\begin{aligned}\frac{\sigma^2_{\cos\delta}}{\cos^2\delta} &= \frac{\sigma^2_{B_{-+}}}{B^2_{-+}}\left(\frac{|A_{-+}|^4}{T^4}\right)\left(\frac{T^2}{2|A_{1/2}|^2}-1\right)^2 \\ &+ \frac{\sigma^2_{B_{00}}}{B^2_{00}}\left(\frac{4|A_{00}|^4}{T^4}\right)\left(\frac{T^2}{4|A_{1/2}|^2}-1\right)^2 \\ &+ \frac{\sigma^2_{B_{0+}}}{B^2_{0+}}\left[\left(\frac{|A_{0+}|^4}{9T^4}\right)\left(\frac{T^2}{2|A_{1/2}|^2}+1\right)^2\right. \\ &\qquad \left. -\left(\frac{|A_{3/2}|^2}{2|A_{1/2}|^2}+\frac{|A_{3/2}|}{2\sqrt{2}|A_{1/2}|\cos\delta}-\frac{1}{4}\right)\right] \\ &+ \frac{\sigma^2_{B_{-+},B_{00}}}{B_{-+}B_{00}}\left(\frac{4|A_{-+}|^2|A_{00}|^2}{T^4}\right)\left(\frac{T^2}{2|A_{1/2}|^2}-1\right)\left(\frac{T^2}{4|A_{1/2}|^2}+1\right)\end{aligned}$$

where:

$$T^2 = |A_{-+}|^2 - 2|A_{00}|^2 + \frac{|A_{0+}|^2}{3}.$$

The complete solution for the isospin amplitudes is:

$$|A_{1/2}| = (2.97 \pm 0.12) \times 10^{-6}\ \text{GeV}$$

$$|A_{3/2}| = (0.82 \pm 0.06) \times 10^{-6}\ \text{GeV}$$

$$\delta_{1/2} - \delta_{3/2} = (76 \pm 8)^\circ$$

$$\therefore\ |A_{1/2}|/|A_{3/2}| = 3.63 \pm 0.34.$$

The correlation coefficients for these quantities are listed in Table 7.9.*

Differences in the results (Table 7.10) stem from the fact that the branching ratios (and errors) used in the calculation have changed somewhat.

Table 7.9 Correlation coefficients from the $\overline{K}\pi$ isospin decomposition

	$\lvert A_{1/2}\rvert$	$\lvert A_{3/2}\rvert$
$(\delta_1 - \delta_3)$	-24.7%	1.3%
$\lvert A_{1/2}\rvert$		-14.7%

* The correlation coefficient between two functions $u = u(x_i)$ and $v = v(x_i)$ is defined as $\rho_{uv} = \sigma^2_{uv}/\sigma_u\sigma_v$ where the covariance term σ^2_{uv} is calculated by the expression:

$$\sigma^2_{uv} = \sum_i\sum_j \sigma^2_{ij}\left(\frac{\partial u}{\partial x_i}\right)\left(\frac{\partial v}{\partial x_j}\right).$$

Table 7.10 Comparison of $D \to \overline{K}\pi$ isospin decompositions.

	This Thesis	Bauer[39]	BSW[12]	Mark III[46]
$\lvert A_{1/2}\rvert$ (GeV)	2.97 ± 0.12	3.0 ± 0.2	3.35 ± 0.19	
$\lvert A_{3/2}\rvert$ (GeV)	0.82 ± 0.06	0.8 ± 0.1	0.99 ± 0.38	
$\lvert A_{1/2}\rvert/\lvert A_{3/2}\rvert$	3.63 ± 0.34	3.75	3.38	3.67 ± 0.27
$\Delta\delta$	$(76 \pm 8)^\circ$	$(79 \pm 11)^\circ$	$(77 \pm 11)^\circ$	$(77 \pm 11)^\circ$

Section 7.7 Solving for the Parameters a_1 and a_2

Bauer, Stech, and Wirbel[12] make predictions for the partial widths of $D \to \overline{K}\pi$ in terms of two parameters — a_1 and a_2 (see Table 7.5). However, their predictions do not account for the effects of final-state interactions. Final-state interactions (FSI) introduce imaginary components in the isospin amplitudes. Before solving for a_1 and a_2, the effects of FSI must be removed. Fortunately, with the results of the isospin decomposition available, it is easy to convert from a complex isospin amplitude to a real amplitude.

To obtain the bare amplitudes, an isospin decomposition is performed as in the previous section, but the phase difference is set to zero: $(\delta_{1/2} - \delta_{3/2}) = 0^0$. This gives the result:

$$A(D^0 \to K^-\pi^+; \delta = 0^\circ) = (2.90 \pm 0.10) \times 10^{-6}\ \text{GeV}$$
$$A\left(D^0 \to \overline{K}^0\pi^0; \delta = 0^\circ\right) = (-1.05 \pm 0.09) \times 10^{-6}\ \text{GeV}$$
$$A\left(D^+ \to \overline{K}^0\pi^+; \delta = 0^\circ\right) = (1.42 \pm 0.11) \times 10^{-6}\ \text{GeV}.$$

Converting these amplitudes to partial widths, and equating to the BSW theoretical predictions yields three equations in two unknowns (factors of 10^{-14} GeV have been pre-cancelled):

$$6.53\, a_1^2 = 8.30 \pm 0.57$$
$$4.97\, a_2^2 = 1.08 \pm 0.19$$
$$6.57\, (a_1 + 1.23\, a_2)^2 = 1.98 \pm 0.31\,.$$

This is solved by minimizing a chi-squared function. The errors are computed using the formula for an error matrix of a multivariable chi-squared function $\chi^2 = \chi^2(x_i)$:

$$\|\sigma^2\|_{ij} = \left\| \frac{1}{2} \frac{\partial^2 \chi^2}{\partial x_i \partial x_j} \right\|^{-1} .$$

The result of the minimization and comparisons to previous results are shown in Table 7.11. The 1σ and 2σ contours of the chi-squared function are displayed in Figure 7.1.

Table 7.11 Solution to a_1 and a_2 from $D \to \overline{K}\pi$ isospin analysis.

	This Thesis	Bauer[39]	BSW[12]
a_1	1.13 ± 0.03	1.2 ± 0.1	1.3 ± 0.1
a_2	-0.47 ± 0.03	-0.50 ± 0.1	-0.55 ± 0.1
Correlation	-51%	N/A	N/A

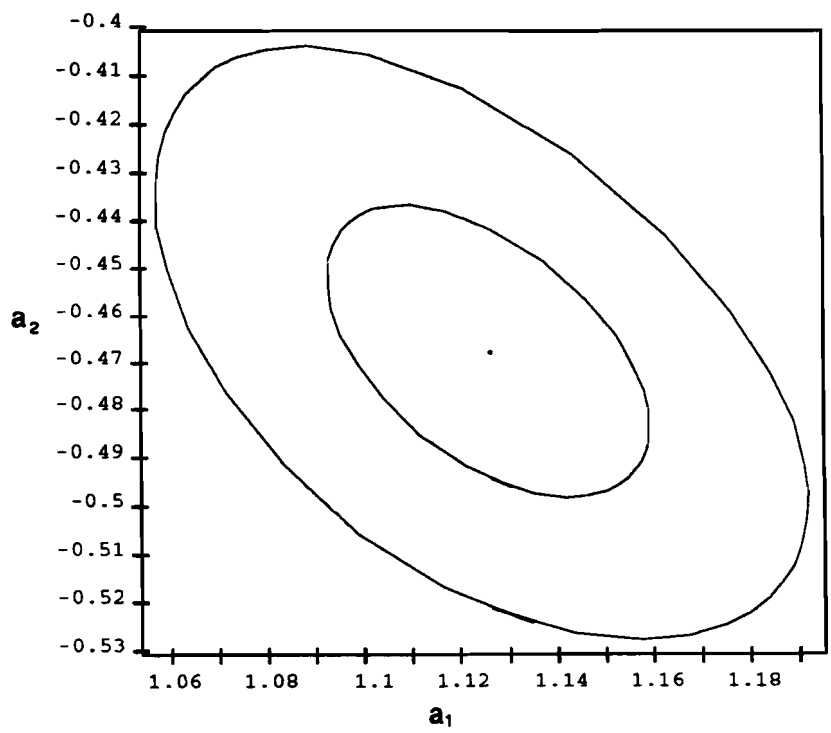

Figure 7.1 Contour plot of the χ^2 function showing 1σ and 2σ contours of a_1 and a_2

Section 7.8 Several Hadronic Predictions

Determination of a_1 and a_2 makes it a straightforward matter to evaluate the partial width predictions. However, these predictions do not include any FSI. Using a complex phase corrects for this. First, the widths must be converted to amplitudes. Then the isospin-decomposed equations (page 123) are solved for real values of $A_{1/2}$ and $A_{3/2}$. Using a chi-squared approach to solve these three equations in two unknowns yields solutions in terms of bare amplitudes:

$$A_{1/2} = \frac{1}{\sqrt{3}}\left(\sqrt{2}A^0_{-+} - A^0_{00}\right)$$
$$A_{3/2} = \frac{1}{4\sqrt{3}}\left(A^0_{-+} + \sqrt{2}A^0_{00} + 3A^0_{0+}\right)$$

with the constraint that $A_{-+} + \sqrt{2}A_{00} = A_{0+}$. The new branching ratios are then calculated using the value of the phase difference derived from the initial decomposition.

Using the values of a_1 and a_2 determined in the previous section, I have plotted the predicted branching ratios and experimentally measured branching ratios for the $\overline{K}\pi$, $\overline{K}\rho$, $\overline{K}^*\pi$, $\overline{K}^*\rho$ and $\overline{K}a_1$ systems. Figure 7.2 shows three things: a) the experimentally measured branching ratios, b) the predicted branching ratios *without* FSI, and c) the predicted branching ratios with FSI. This information is also tabulated in Table 7.12 along with the values of the mixing angles used.

Table 7.12 Comparison between BSW model predictions and

Mark III experimental results using a_1 = 1.13 and a_2 = –0.47.

Mode		Phase	Exp. BR	Ref	w/o FSI	with FSI
$\overline{K}\pi$	−+	76 ± 8	4.2 ± 0.4	45	5.3 ± 0.3	4.2 ± 0.3
	00		1.8 ± 0.2	47	0.7 ± 0.1	1.8 ± 0.2
	0+		3.2 ± 0.5	45	3.2 ± 0.4	3.2 ± 0.4
$\overline{K}\rho$	−+	0 ± 26	10.8 ± 0.4	46	9.4 ± 0.6	9.4 ± 0.6
	00		0.8 ± 0.1	46	0.3 ± .04	0.3 ± .04
	0+		6.9 ± 0.8	46	13.4 ± 0.9	13.4 ± 0.9
$\overline{K}^*\pi$	−+	84 ± 13	5.2 ± 0.3	46	2.8 ± 0.2	2.5 ± 0.2
	00		2.6 ± 0.3	46	0.9 ± 0.1	1.2 ± 0.1
	0+		2.0 ± 0.2	46	.25 ± .12	.25 ± .12
$\overline{K}^*\rho$	−+	61 ± 22	6.2 ± 2.3	48	18.3 ± 1.1	15.4 ± 2.1
	00		1.9 ± 0.3	48	1.7 ± 0.2	4.6 ± 1.9
	0+		4.8 ± 1.2	48	15.1 ± 1.5	15.1 ± 1.5
$\overline{K}a_1$	−+	0 ± 21	9.0 ± 0.9	48	1.3 ± 0.1	1.3 ± 0.1
	00		0.43 ± 0.40	48	0.0	0.0
	0+		7.1 ± 1.8	48	3.4 ± 0.2	3.4 ± 0.2

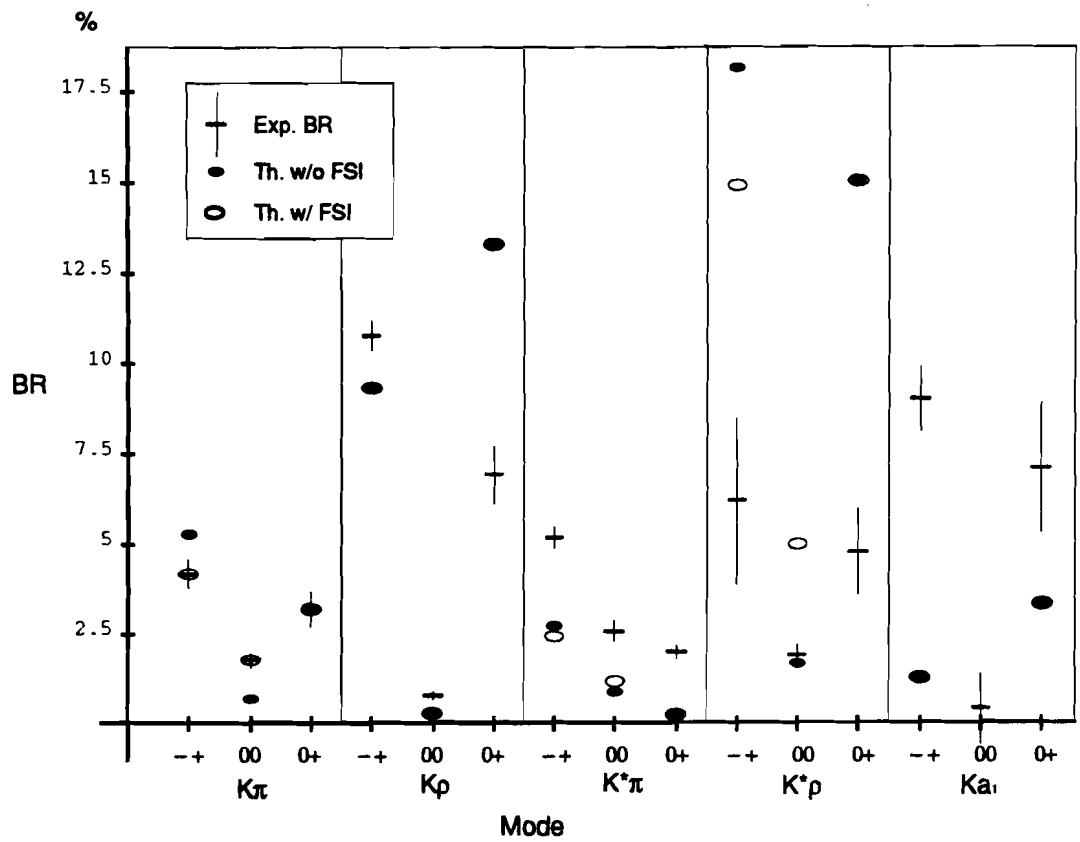

Figure 7.2 Comparison between BSW model predictions and Mark III experimental results

Section 7.9 Exclusive Mode Predictions

A complete list of predicted decay modes published by BSW is found in Tables 7.13, 7.14, and 7.15 for the D^+, D^0 and D_s^+ respectively.[12] The parameter values used were those calculated in this chapter for the $\overline{K}\pi$ system:

$$a_1 = +1.13 \pm 0.03$$

$$a_2 = -0.47 \pm 0.03$$

$$\rho_{a_1,a_2} = -51\% .$$

The errors on each branching ratio arise solely from the uncertainty in the parameters a_1 and a_2. The semileptonic decay mode branching ratios have no error listed since they have no dependence upon a_1 or a_2.

Table 7.13 BSW: D^+ exclusive decay modes

D^+ Decay Mode	Widths in 10^{10} s^{-1}	BR(%)
$\overline{K}^0 e^+ \nu$	8.49	9.02
$\overline{K}^0 \mu^+ \nu$	8.39	8.91
$\overline{K}^{*0} \ell^+ \nu$	9.53	10.12
$\pi^0 \ell^+ \nu$	0.73	0.78
$\rho^0 \ell^+ \nu$	0.70	0.74
$\overline{K}^0 \pi^+$	$9.98(a_1+1.23a_2)^2$	3.2 ± 0.4
$\eta \pi^+$	$0.10(a_1+2.73a_2)^2$	$(2.5 \pm 2.3)\times 10^{-3}$
$\eta' \pi^+$	$0.05(a_1-0.80a_2)^2$	0.120 ± 0.008
$\overline{K}^0 K^+$	$0.76{a_1}^2$	1.03 ± 0.06
$\pi^0 \pi^+$	$0.26(a_1+1.00a_2)^2$	0.12 ± 0.01
$\overline{K}^0 \rho^+$	$17.57(a_1+0.60a_2)^2$	13.4 ± 0.8
$\overline{K}^{*0} \pi^+$	$5.18(a_1+1.95a_2)^2$	0.25 ± 0.12
$\eta \rho^+$	$0.17(a_1+1.32a_2)^2$	0.047 ± 0.007
$\eta' \rho^+$	$0.02(a_1-0.34a_2)^2$	0.035 ± 0.002
$\overline{K}^0 K^{*+}$	$0.74{a_1}^2$	1.00 ± 0.05
$\overline{K}^{*0} K^+$	$0.29{a_1}^2$	0.39 ± 0.02
$\omega \pi^+$	$0.93(a_1+0.99a_2)^2$	0.44 ± 0.04
$\phi \pi^+$	$0.99{a_2}^2$	0.23 ± 0.03
$\pi^0 \rho^+$	$0.57(a_1+0.50a_2)^2$	0.49 ± 0.03
$\rho^0 \pi^+$	$0.14(a_1+2.00a_2)^2$	0.005 ± 0.003
$\pi^0 {a_1}^+$	$0.33{a_1}^2$	0.45 ± 0.02
$\overline{K}^0 {a_1}^+$	$2.49{a_1}^2$	3.4 ± 0.2
$\overline{K}^{*0} \rho^+$	$34.59(a_1+1.04a_2)^2$	15.1 ± 1.4
$\overline{K}^{*0} K^{*+}$	$1.50{a_1}^2$	2.0 ± 0.1
$\phi \rho^+$	$0.71{a_2}^2$	0.17 ± 0.02
$\rho^0 \rho^+$	$0.96(a_1+1.00a_2)^2$	0.44 ± 0.04
BR Sum (including leptonic modes)		83.7 ± 3.0

Table 7.14 BSW: D^0 exclusive decay modes

D^0 Decay Mode	Widths (10^{10} s^{-1})	BR(%)
$K^-\ell^+\nu$	8.26	3.48
$K^{*-}\ell^+\nu$	9.53	4.01
$\pi^-\ell^+\nu$	0.73	0.31
$\rho^-\ell^+\nu$	0.70	0.30
$K^-\pi^+$	$9.92a_1{}^2$	5.3 ± 0.3
K^-K^+	$0.75a_1{}^2$	0.40 ± 0.02
$\pi^-\pi^+$	$0.52a_1{}^2$	0.280 ± 0.015
$\overline{K}^0\eta$	$2.86a_2{}^2$	0.27 ± 0.03
$\overline{K}^0\eta'$	$1.15a_2{}^2$	0.11 ± 0.01
$\overline{K}^0\pi^0$	$7.55a_2{}^2$	0.70 ± 0.09
$\pi^0\eta$	$0.15a_2{}^2$	0.014 ± 0.002
$\pi^0\eta'$	$0.07a_2{}^2$	$(6.5 \pm 0.8)\times10^{-3}$
$\pi^0\pi^0$	$0.26a_2{}^2$	0.024 ± 0.003
$\eta\eta$	$0.29a_2{}^2$	0.027 ± 0.003
$\eta\eta'$	$0.03a_2{}^2$	$(2.8 \pm 0.4)\times10^{-3}$
$K^-\rho^+$	$17.43a_1{}^2$	9.4 ± 0.5
$K^{*-}\pi^+$	$5.12a_1{}^2$	2.75 ± 0.15
K^-K^{*+}	$0.74a_1{}^2$	0.40 ± 0.02
$K^{*-}K^+$	$0.28a_1{}^2$	0.151 ± 0.008
$\pi^-\rho^+$	$1.11a_1{}^2$	0.60 ± 0.03
$\rho^-\pi^+$	$0.28a_1{}^2$	0.151 ± 0.008
$\overline{K}^0\omega$	$3.04a_2{}^2$	0.28 ± 0.04
$\overline{K}^0\rho^0$	$3.14a_2{}^2$	0.29 ± 0.04
$\overline{K}^{*0}\eta$	$2.57a_2{}^2$	0.24 ± 0.03
$\overline{K}^{*0}\eta'$	$0.02a_2{}^2$	$(1.9 \pm (0.2)\times10^{-3}$
$\overline{K}^{*0}\pi^0$	$9.72a_2{}^2$	0.9 ± 0.1
$\pi^0\omega$	$0.06a_2{}^2$	$(5.6 \pm 0.7)\times10^{-3}$

Table 7.14 (Continued) BSW: D^0 exclusive decay modes

D^0 Decay Mode	Widths (10^{10} s^{-1})	BR(%)
$\pi^0\phi$	$0.49a_2{}^2$	0.046 ± 0.006
$\pi^0\rho^0$	$0.63a_2{}^2$	0.059 ± 0.007
$\rho^0\eta$	$0.01a_2{}^2$	$(9.3 \pm 1.2)\times10^{-4}$
$\rho^0\eta'$	$0.02a_2{}^2$	$(1.9 \pm 0.2)\times10^{-3}$
$\omega\eta$	$0.43a_2{}^2$	0.040 ± 0.005
$\eta\phi$	$0.11a_2{}^2$	0.010 ± 0.001
$K^-a_1{}^+$	$2.43a_1{}^2$	1.31 ± 0.07
$\pi^-a_1{}^+$	$0.65a_1{}^2$	0.35 ± 0.02
$\overline{K}^0a_1{}^0$	0	0
$\pi^0a_1{}^0$	$0.16a_2{}^2$	0.015 ± 0.002
$K^{*-}\rho^+$	$34.05a_1{}^2$	18.3 ± 1.0
$K^{*-}K^{*+}$	$1.45a_1{}^2$	0.78 ± 0.04
$\rho^-\rho^+$	$1.89a_1{}^2$	1.02 ± 0.05
$\overline{K}^{*0}\omega$	$17.64a_2{}^2$	1.6 ± 0.2
$\overline{K}^{*0}\rho^0$	$18.45a_2{}^2$	1.7 ± 0.2
$\rho^0\phi$	$0.82a_2{}^2$	0.08 ± 0.01
$\rho^0\rho^0$	$0.95a_2{}^2$	0.09 ± 0.01
$\omega\omega$	$0.87a_2{}^2$	0.08 ± 0.01
$\omega\phi$	$0.74a_2{}^2$	0.069 ± 0.009
BR Sum		64.1 ± 2.7

Table 7.15 BSW: D_s^+ exclusive decay modes

D_s^+ Decay Mode	Widths in 10^{10} s^{-1}	BR(%)
$\eta\ell^+\nu$	4.6	2.05
$\eta'\ell^+\nu$	1.3	0.58
$\phi\ell^+\nu$	7.8	3.47
$\overline{K}^0\ell^+\nu$	0.5	0.22
$\overline{K}^{*0}\ell^+\nu$	0.3	0.13
ηK^+	$0.38\ (a_1 + 1.31a_2)^2$	0.045 ± 0.006
$\eta' K^+$	$0.21\ (a_1 + 0.34a_2)^2$	0.088 ± 0.005
$\eta\pi^+$	$4.93\ a_1^2$	2.80 ± 0.15
$\eta'\pi^+$	$2.89\ a_1^2$	1.64 ± 0.09
$K^0\pi^+$	$0.44\ a_1^2$	0.25 ± 0.01
$\overline{K}^0 K^+$	$12.76\ a_2^2$	1.25 ± 0.02
$\pi^0 K^+$	$0.22\ a_2^2$	0.022 ± 0.003
ηK^{*+}	$0.41\ (a_1 + 0.82a_2)^2$	0.101 ± 0.007
$\eta' K^{*+}$	$0.06\ (a_1 + 0.19a_2)^2$	0.029 ± 0.002
$\eta\rho^+$	$9.27\ a_1^2$	5.3 ± 0.3
$\eta'\rho^+$	$2.62\ a_1^2$	1.49 ± 0.08
$K^0\rho^+$	$0.89\ a_1^2$	0.51 ± 0.03
$K^{*0}\pi^+$	$0.26\ a_1^2$	0.148 ± 0.008
$\overline{K}^0 K^{*+}$	$5.85\ a_2^2$	0.58 ± 0.07
$\overline{K}^{*0} K^+$	$15.04\ a_2^2$	1.5 ± 0.2
ωK^+	$0.41\ a_2^2$	0.040 ± 0.005
$\pi^0 K^{*+}$	$0.13\ a_2^2$	0.013 ± 0.002
$\phi\pi^+$	$4.72\ a_1^2$	2.7 ± 0.1
ϕK^+	$0.26\ (a_1 + 1.67a_2)^2$	0.014 ± 0.003
$a_1{}^0 K^+$	$0.16\ a_2^2$	0.016 ± 0.002
$\eta a_1{}^+$	$2.21\ a_1^2$	1.26 ± 0.07
$K^0 a_1{}^+$	$0.31\ a_1^2$	0.176 ± 0.009

Table 7.15 (Continued) BSW: D_s^+ exclusive decay modes

D_s^+ Decay Mode	Widths in 10^{10} s^{-1}	BR(%)
$K^{*0}\rho^+$	1.69 $a_1{}^2$	0.96 ± 0.05
$\overline{K}^{*0}K^{*+}$	32.54 $a_2{}^2$	3.2 ± 0.4
ωK^{*+}	0.80 $a_2{}^2$	0.08 ± 0.01
$\phi\rho^+$	29.74 $a_1{}^2$	16.90 ± 0.09
ϕK^{*+}	1.15 $(a_1 + 1.08a_2)^2$	0.20 ± 0.02
$\rho^0 K^{*+}$	0.85 $a_2{}^2$	0.08 ± 0.01
BR Sum (including leptonic decays)		57.3 ± 2.4

Section 7.10 Inclusive Predictions

Multiplicity Distributions

Following the procedure described in Chapter 6, the exclusive modes (Tables 7.13 – 7.15) are used to calculate inclusive properties (Tables 7.16–7.22). The quoted errors arise from the uncertainty in the values of the parameters a_1 and a_2.

In order to increase clarity and reduce data overload, 9–prong and higher multiplicities have not been listed in the charged particle multiplicity (Table 7.13). However, 16–prong events (with a branching ratio on the order of 10^{-22}) are possible with the D^0.

The π^+, π^-, and charged particle multiplicity distributions include pions arising from K_S decays.

The dependence of the D^+, D^0, and D_s^+ charged particle multiplicity averages on the parameters a_1 and a_2 is depicted in Figures 7.3-7.5.

Shading of these 3–D figures is height dependent — ranging from black at the minimum of $\langle n_{\rm ch}\rangle$, to white at the middle values, and back to black at the maximum value of $\langle n_{\rm ch}\rangle$. The grid lines of these figures represent equi-values of a_1 or a_2. The "cross" in each figure marks the position (with $\pm 1\sigma$ indicated) of $(a_1, a_2) = (1.13 \pm 0.03, -0.47 \pm 0.03)$ that was determined earlier in this chapter using the $\overline{K}\pi$ system.

Table 7.16 BSW: inclusive charged particle multiplicity distribution and average

n	$B(D^+ \to nP^\pm X^0)$	$B(D^0 \to nP^\pm X^0)$	$B(D_s^+ \to nP^\pm X^0)$
0		1.4 ± 0.1 %	
1	42.2 ± 0.1 %		32.4 ± 0.2 %
2		80.4 ± 0.5 %	
3	56.2 ± 0.1 %		64.4 ± 0.1 %
4		17.9 ± 0.4 %	
5	1.61 ± 0.05 %		3.24 ± 0.09 %
6		0.194 ± 0.004 %	
7	$(1.6 \pm 0.1)\times 10^{-3}$ %		$(2.3 \pm 0.02)\times 10^{-2}$ %
8		$(1.6 \pm 0.1)\times 10^{-4}$ %	
$\langle n \rangle$	2.188 ± 0.002	2.338 ± 0.004	2.419 ± 0.005

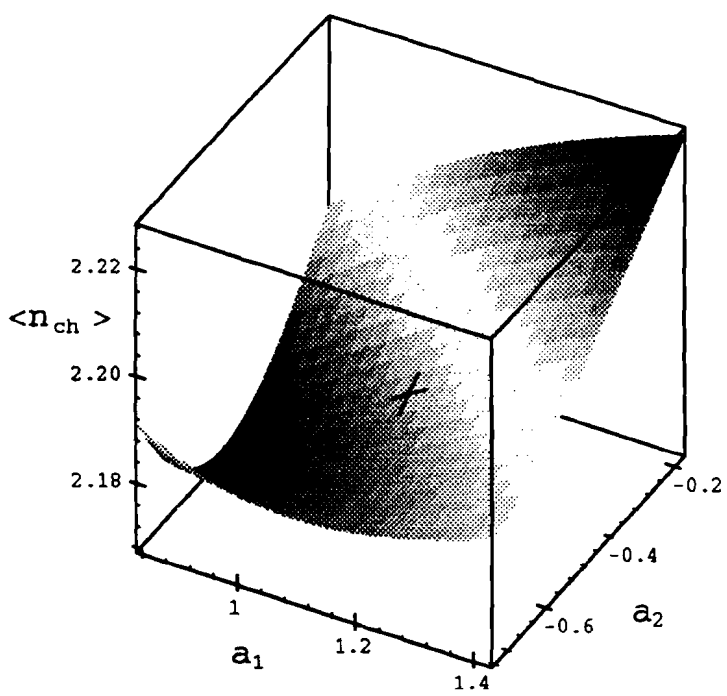

Figure 7.3 D^+ average charge multiplicity as a function of a_1 and a_2 in the BSW model

From these diagrams, it is evident that no value of a_1 and a_2 within 10σ of the fitted value will match the experimentally determined values. Attempts to solve for a_1 and a_2 by performing a least squares fit using the symbolic formula for the inclusive properties failed to provide a physically meaningful result.

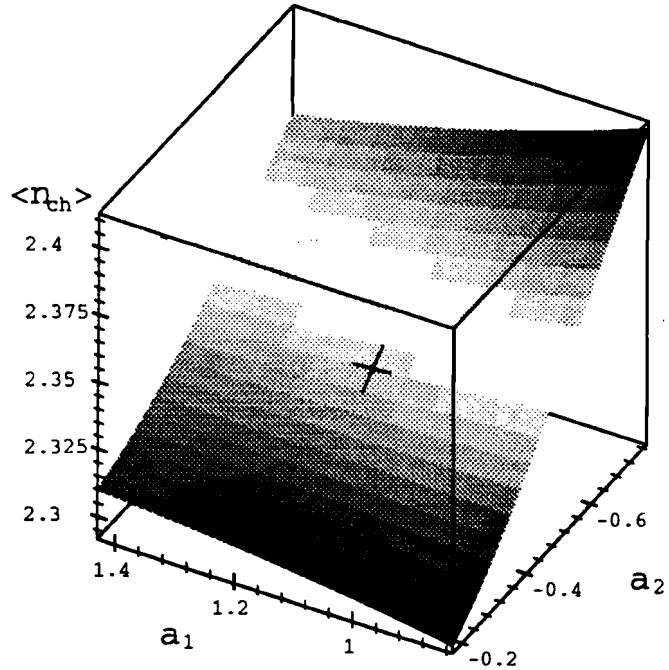

Figure 7.4 D^0 average charge multiplicity as a function of a_1 and a_2 in the BSW model

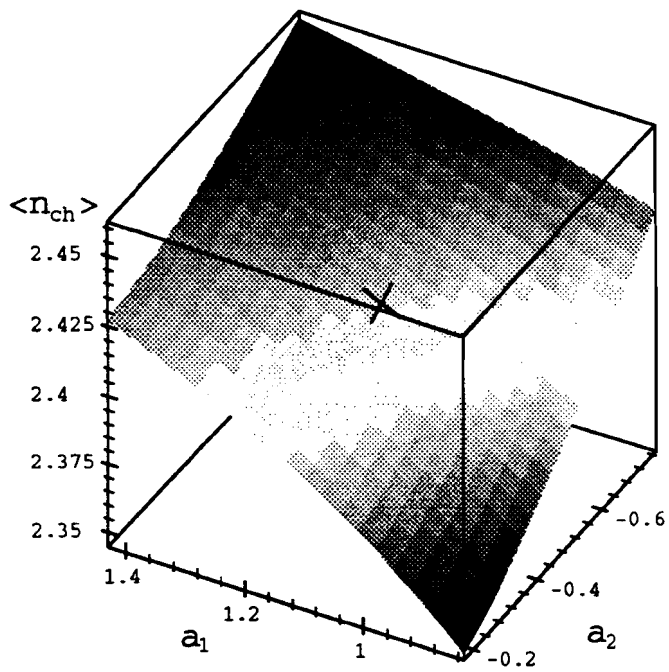

Figure 7.5 D_s^+ average charge multiplicity as a function of a_1 and a_2 in the BSW model

Table 7.17 BSW: D^+ inclusive kaon multiplicity distribution and average

n	$B(D^+ \to nK^+X)$	$B(D^+ \to nK^-X)$	$B(D^+ \to nK^\pm X)$
0	96.9 ± 0.1 %	69.5 ± 0.3 %	67.4 ± 0.2 %
1	3.1 ± 0.1 %	30.5 ± 0.3 %	31.5 ± 0.2 %
2			1.1 ± 0.1 %
$n \geq 1$	3.1 ± 0.1 %	30.5 ± 0.3 %	32.6 ± 0.2 %
$\langle n \rangle$	0.031 ± 0.001	0.305 ± 0.003	0.337 ± 0.001

n	$B(D^+ \to nK^0X)$	$B(D^+ \to n\overline{K}^0X)$	$B(D^+ \to n(K^0 \vee \overline{K}^0)X)$	$B(D^+ \to nK_SX)$
0	97.6 ± 0.1 %	37.1 ± 0.2 %	36.0 ± 0.2 %	67.5 ± 0.1 %
1	2.4 ± 0.1 %	62.9 ± 0.2 %	62.7 ± 0.2 %	32.2 ± 0.1 %
2			1.34 ± 0.05 %	0.34 ± 0.01 %
$n \geq 1$	2.4 ± 0.1 %	62.9 ± 0.2 %	64.0 ± 0.2 %	32.5 ± 0.1 %
$\langle n \rangle$	0.024 ± 0.001	0.629 ± 0.002	0.653 ± 0.003	0.328 ± 0.002

Table 7.18 BSW: D^+ inclusive pion multiplicity distribution and average

n	$B(D^+ \to n\pi^+X)$	$B(D^+ \to n\pi^-X)$	$B(D^+ \to n\pi^\pm X)$	$B(D^+ \to n\pi^0X)$
0	22.6 ± 0.8 %	73.0 ± 0.2 %	22.6 ± 0.8 %	44.3 ± 1.0 %
1	50.0 ± 0.4 %	26.1 ± 0.1 %	37.4 ± 0.1 %	37.4 ± 0.7 %
2	26.1 ± 1.1 %	0.87 ± 0.04 %	25.5 ± 0.4 %	12.5 ± 0.2 %
3	1.24 ± 0.05 %		13.2 ± 0.4 %	4.35 ± 0.06 %
4			0.37 ± 0.02 %	1.35 ± 0.05 %
5			0.87 ± 0.04 %	0.023 ± 0.001 %
6				0.0028 ± 0.0001 %
$n \geq 1$	77.4 ± 0.8 %	27.0 ± 0.2 %	77.4 ± 0.8 %	55.7 ± 1.0 %
$\langle n \rangle$	1.06 ± 0.02	0.279 ± 0.002	1.34 ± 0.02	0.81 ± 0.01

Table 7.19 BSW: D^0 inclusive kaon multiplicity distribution and average

n	$B(D^0 \to nK^+X)$	$B(D^0 \to nK^-X)$	$B(D^0 \to nK^\pm X)$
0	98.37 ± 0.02 %	42.5 ± 0.1 %	42.1 ± 0.1 %
1	1.63 ± 0.02 %	57.5 ± 0.1 %	56.7 ± 0.1 %
2			1.20 ± 0.02 %
$n \geq 1$	1.63 ± 0.02 %	57.5 ± 0.1 %	57.9 ± 0.1 %
$\langle n \rangle$	0.0163 ± 0.0002	0.575 ± 0.001	0.591 ± 0.001

n	$B(D^0 \to nK^0X)$	$B(D^0 \to n\overline{K}^0X)$	$B(D^0 \to n(K^0 \vee \overline{K}^0)X)$	$B(D^0 \to nK_SX)$
0	98.8 ± 0.02 %	63.9 ± 0.1 %	63.2 ± 0.1 %	81.3 ± 0.1 %
1	1.23 ± 0.02 %	36.1 ± 0.1 %	36.3 ± 0.1 %	18.5 ± 0.1 %
2			0.54 ± 0.01 %	0.135 ± 0.002 %
$n \geq 1$	1.23 ± 0.02 %	36.1 ± 0.1 %	36.8 ± 0.1 %	18.7 ± 0.1 %
$\langle n \rangle$	0.0123 ± 0.0002	0.361 ± 0.001	0.374 ± 0.001	0.188 ± 0.001

Table 7.20 BSW: D^0 inclusive pion multiplicity distribution and average

n	$B(D^0 \to n\pi^+X)$	$B(D^0 \to n\pi^-X)$	$B(D^0 \to n\pi^\pm X)$	$B(D^0 \to n\pi^0X)$
0	25.2 ± 0.9 %	54.2 ± 0.3 %	17.6 ± 0.6 %	35.6 ± 0.5 %
1	60.7 ± 0.7 %	33.4 ± 0.3 %	44.3 ± 0.4 %	44.3 ± 0.3 %
2	14.0 ± 0.4 %	12.37 ± 0.02 %	21.0 ± 0.3 %	16.0 ±0.1 %
3	0.072 ± 0.001 %	0.071 ± 0.001 %	7.7 ± 0.3 %	3.74 ± 0.06 %
4			9.4 ± 0.1 %	0.30 ± 0.03 %
5			$(2.4 \pm 0.2)\times10^{-4}$ %	0.036 ± 0.004 %
6			0.071 ± 0.001 %	0.012 ± 0.001 %
7				$(1.7 \pm 0.2)\times10^{-3}$ %
8				$(1.0 \pm 0.1)\times10^{-4}$ %
$n \geq 1$	74.8 ± 0.9 %	45.8 ± 0.3 %	82.4 ± 0.6 %	$64.4 \pm 0.5\times10^{-3}$ %
$\langle n \rangle$	0.890 ± 0.012	0.583 ± 0.003	1.473 ± 0.015	0.890 ± 0.008

Table 7.21 BSW: D_s^+ inclusive kaon multiplicity distribution and average

n	$B(D_s^+ \to nK^+X)$	$B(D_s^+ \to nK^-X)$	$B(D_s^+ \to nK^\pm X)$
0	68.0 ± 0.4 %	71.2 ± 0.3 %	65.3 ± 0.6 %
1	31.9 ± 0.4 %	28.8 ± 0.3 %	8.7 ± 0.6 %
2	0.07 ± 0.01 %		26.0 ± 0.1 %
3			0.07 ± 0.01 %
$n \geq 1$	32.0 ± 0.4 %	28.8 ± 0.3 %	34.7 ± 0.6 %
$\langle n \rangle$	0.320 ± 0.00	0.288 ± 0.003	0.608 ± 0.006

n	$B(D_s^+ \to nK^0X)$	$B(D_s^+ \to n\overline{K}^0X)$	$B(D_s^+ \to n(K^0 \vee \overline{K}^0)X)$	$B(D_s^+ \to nK_SX)$
0	92.7 ± 0.4 %	93.2 ± 0.6 %	87.8 ± 0.8 %	77.4 ± 0.2 %
1	7.3 ± 0.4 %	6.8 ± 0.6 %	10.3 ± 0.6 %	22.1 ± 0.2 %
2			1.9 ± 0.2 %	0.52 ± 0.04 %
$n \geq 1$	7.3 ± 0.4 %	6.8 ± 0.6 %	12.2 ± 0.8 %	22.6 ± 0.2 %
$\langle n \rangle$	0.073 ± 0.004	0.068 ± 0.006	0.141 ± 0.010	0.231 ± 0.003

Table 7.22 BSW: D_s^+ inclusive pion multiplicity distribution and average

n	$B(D_s^+ \to n\pi^+X)$	$B(D_s^+ \to n\pi^-X)$	$B(D_s^+ \to n\pi^\pm X)$	$B(D_s^+ \to n\pi^0X)$
0	18.8 ± 0.6 %	61.1 ± 0.1 %	18.8 ± 0.6 %	32.3 ± 0.5 %
1	52.2 ± 0.2 %	37.2 ± 0.1 %	40.7 ± 0.5 %	40.7 ± 0.3 %
2	26.8 ± 0.3 %	1.67 ± 0.01 %	13.2 ± 0.3 %	12.6 ± 0.1 %
3	2.2 ± 0.1 %	$(15 \pm 0.4)\times10^{-4}$ %	24.9 ± 0.4 %	9.9 ± 0.1 %
4	$(15 \pm 0.4)\times10^{-4}$ %		1.13 ± 0.08 %	3.81 ± 0.06 %
5			1.39 ± 0.02 %	0.720 ± 0.007 %
6			0 ± 0 %	0.171 ± 0.003 %
7			$(15 \pm 0.4)\times10^{-4}$ %	$(35 \pm 1)\times10^{-5}$ %
$n \geq 1$	81.2 ± 0.6 %	38.9 ± 0.1 %	81.2 ± 0.6 %	67.7 ± 0.5 %
$\langle n \rangle$	1.13 ± 0.01	0.406 ± 0.001	1.53 ± 0.01	1.152 ± 0.008

Momentum Spectra

I use the BSW exclusive decay modes (with their associated branching ratios) listed in Tables 7.13–7.15 to generate Monte Carlo simulations and obtain the center-of-mass momentum spectra for the D^+, D^0, and D_s^+. These exclusive modes are the only D decay modes present in the Monte Carlo. The spectra do not have any losses from geometric acceptance, reconstruction losses, resolution smearing, or particle identification cuts. I have normalized each spectrum to the total number of Monte Carlo tags, so that the heights of monochromatic peaks correspond directly to the branching ratios of the associated exclusive decay mode.

I have arranged the spectra so that related structures can be next to each other. For example, in the D^+ spectra, I have placed the K_S spectrum above the π^+ spectrum so that one can see the monochromatic peak from the decay $D^+ \rightarrow \overline{K}^0\pi^+$ at 0.862 GeV in both the K_S and π^+ spectra.

Structures noted in the D^+ momentum spectra (Figure 7.6) come from the following decay modes (stated values of the momenta derive from theoretical calculations and not from the figures):

a. $\overline{K}^0\pi^+$ — a monochromatic spike corresponding to a branching ratio of 3.96%,

b. $\overline{K}^0K^+$ — a monochromatic peak at 0.792 GeV visible in the K_S and K^+ spectra with an associated branching ratio of 1.22%,

c. $\overline{K}^0\rho^+$ — a peak in the K_S spectrum broadened due to the width of the ρ^+ and centered at 0.680 GeV,

d. $\overline{K}^0K^{*+}$ — a smaller broad peak in the K_S spectrum, appearing as a shoulder on structure (c) at 0.611 GeV,

e. $\overline{K}^{*0}K^+$ — a peak observable in the K^+ spectrum centered at 0.610 GeV and broadened due to the width of the $\overline{K}^{*0}$,

f. $\pi^0\pi^+$ — a monochromatic peak in the π^0 and π^+ spectra at 0.925 GeV,

g. $\pi^0\rho^+$ — a broad structure at 0.770 GeV in the π^0 spectrum,

h. $\phi\pi^+$ — a monochromatic structure in the π^+ spectrum with a momentum of 0.647 GeV,

i. $\eta'\pi^+$ — a small structure in the π^+ spectrum at 0.681 GeV,

j. $\overline{K}^{*0}\pi^+$ — centered at 0.712 GeV, a small structure in the π^+ spectrum,

k. $\omega\pi^+$ — a small structure at 0.764 GeV in the π^+ spectrum.

Any other apparent structures in the D^+ spectra are caused by statistical fluctuations in the Monte Carlo sample.

The following structures are notated in the D^0 momentum spectra (Figure 7.7):

a. $K^-\pi^+$ — a large, monochromatic peak at 0.861 GeV with an associated branching ratio of 8.3%,

b. K^-K^+ — a tall, monochromatic peak seen in both the K^- and K^+ spectra at 0.791 GeV and corresponding to a branching ratio of 0.59%,

c. $K^-\rho^+$ — a large peak broadened from the width of the ρ^+ and centered at 0.679 GeV,

d. K^-K^{*+} — a broad peak situated on the shoulder of structure (c) at 0.610 GeV in the K^- spectrum,

e. $\rho^-\pi^+$ — a peak seen in the π^+ spectrum at 0.767 GeV broadened by the width of the ρ^-,

f. $\pi^-\pi^+$ — a monochromatic peak visible in the π^- and π^+ spectra with a momentum of 0.922 GeV,

g. $K^{*-}\pi^+$ — a large, broad peak visible centered at 0.711 GeV in the π^+ spectrum,

h. $\overline{K}^0\pi^0$ — a monochromatic peak observable in the K_S and π^0 spectra at 0.860 GeV,

i. $\overline{K}^0\omega$ and $\overline{K}^0\rho^0$ — two narrow peaks at 0.670 GeV and 0.677 GeV visible in the K_S spectrum,

j. $\overline{K}^0\eta$ — a monochromatic peak at 0.771 GeV,

k. $\overline{K}^0\eta'$ — a narrow peak in the K_S spectrum at 0.565 GeV,

m. $\pi^0\pi^0$ — a small, monochromatic peak seen at 0.922 GeV in the π^0 spectrum,

n. $\overline{K}^{*0}\pi^0$ — a broadened peak due to the $\overline{K}^{*0}$ width seen in the π^0 spectrum and centered at 0.709 GeV,

p. $\pi^0\omega$ and $\pi^0\rho^0$ — two peaks clustered around 0.764 GeV seen in the π^0 spectrum,

s. $K^{*-}K^+$ — a short broad peak seen in the K^+ spectrum at 0.610 GeV.

Structures noted in the D_s^+ momentum spectra (Figure 7.8) come from the following decay modes:

a. $\overline{K}^0K^{*+}$ — a peak centered at 0.683 GeV and broadened by the width of the K^{*+},

b. $\overline{K}^0K^+$ — a large, monochromatic peak visible in both the K_S and K^+ spectra at 0.851 GeV,

c. $K^0\pi^+$ — a small, monochromatic peak see in both the K_S and π^+ spectra at 0.916 GeV,

d. $\eta'K^+$ — a short peak at 0.647 GeV in the K^+ spectrum,

e. $\overline{K}^{*0}K^+$ — a short broadened peak in the K^+ spectrum at 0.683 GeV,

f. π^0K^+ — a very small monochromatic peak seen in the π^0 and K^+ spectra with a momentum of 0.917 GeV,

g. $\phi\pi^+$ — a large, monochromatic peak in the π^+ spectrum at 0.712 GeV,

h. $\eta'\pi^+$ — a large, narrow peak at 0.744 GeV in the π^+ spectrum,

i. $\eta\pi^+$ — another large, monochromatic peak at 0.902 GeV in the π^+ spectrum,

k. ηK^+ — a short, monochromatic peak at 0.835 GeV seen in the K^+ spectrum.

All other apparent structures are a result of statistical fluctuations in the Monte Carlo data.

The generated momentum spectra in Figures 7.6—7.8 bear little resemblance to the experimentally determined spectra (Figures 5.3, 5.5 and 5.8). To see the effect of resolution smearing, I reconstructed, tagged, processed and efficiency-corrected the D^+ and D^0 Monte Carlo samples with the same techniques used on the real data. The resulting spectra (Figures 7.9 and 7.10) continue to exhibit structures corresponding to modes with large branching ratios. Using the same lettering scheme as before (i.e., the

same letters refer to the same structures), the following D^+ structures are observed:

a. $\overline{K}^0\pi^+$ — prominently seen as misidentified pions in the K^+ spectrum and also very prominent in the K_S spectrum,

b. $\overline{K}^0K^+$ — the most prominent peak in the K^+ spectrum, but not statistically significant in the K_S spectrum,

c. $\overline{K}^0\rho^+$ — still noticeable as a broad structure in the K_S spectrum,

e. $\overline{K}^{*0}K^+$ — a small broad rise in the K^+ spectrum.

In the D^0 spectra, the follow structures are seen:

a. $K^-\pi^+$ — the most prominent peaks in the K^+ and K^- spectra (appearing as misidentified pions in the K^+ spectrum),

b. K^-K^+ — still a detectable peak in the K^+ spectrum, but not statistically significant in the K^- spectrum,

c. $K^-\rho^+$ — seen as a broad rise in the K^- spectrum,

f. $\overline{K}^0\pi^0$ — possibly seen in the K_S spectrum,

j. $\overline{K}^0\eta$ — perhaps detectable in the K_S spectrum,

s. $K^{*-}K^+$ — a small, barely significant bump in the K^+ spectrum.

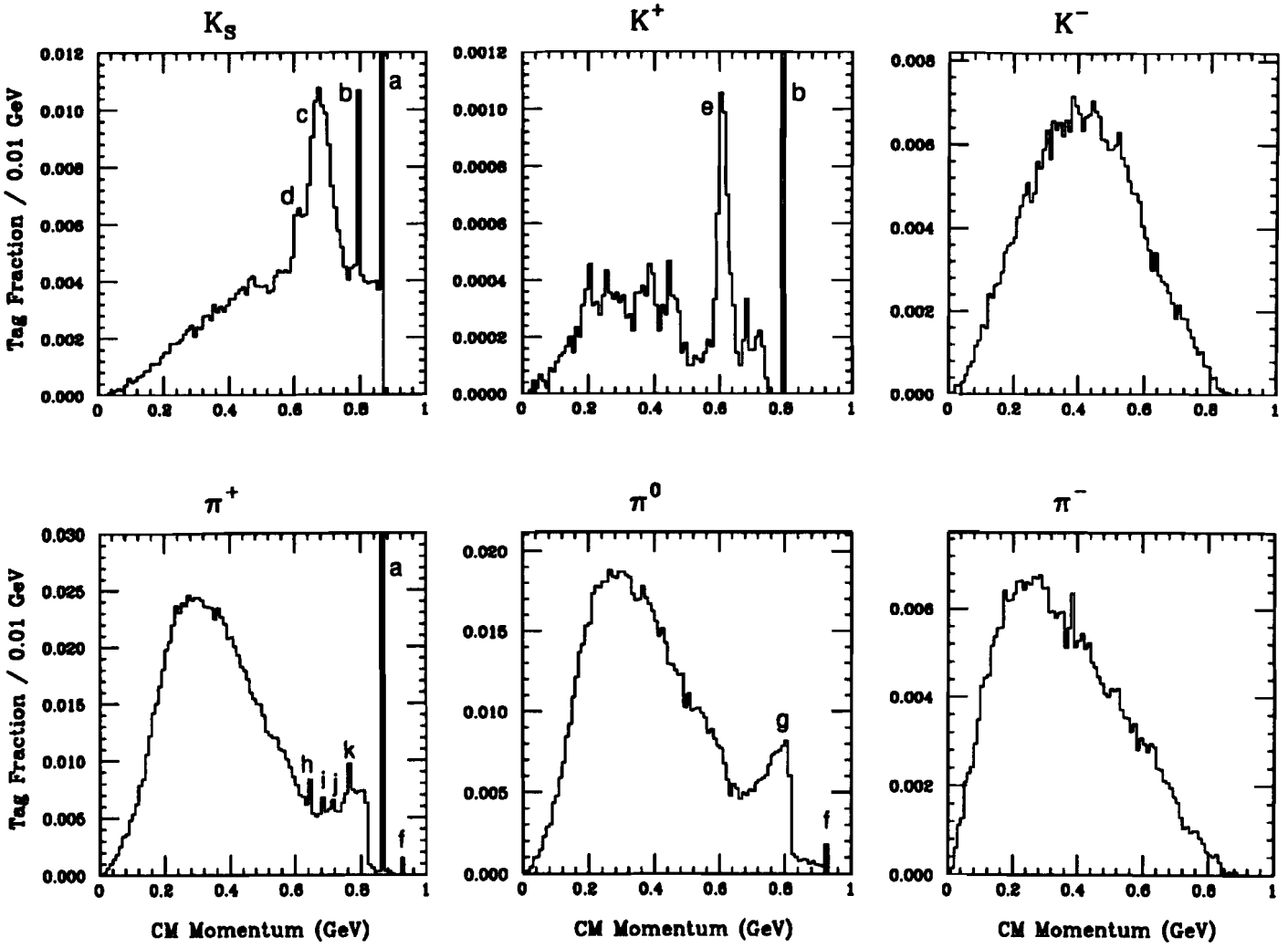

Figure 7.6 BSW: D^+ center-of-mass momentum spectra (letters indicating structure are explained in the text)

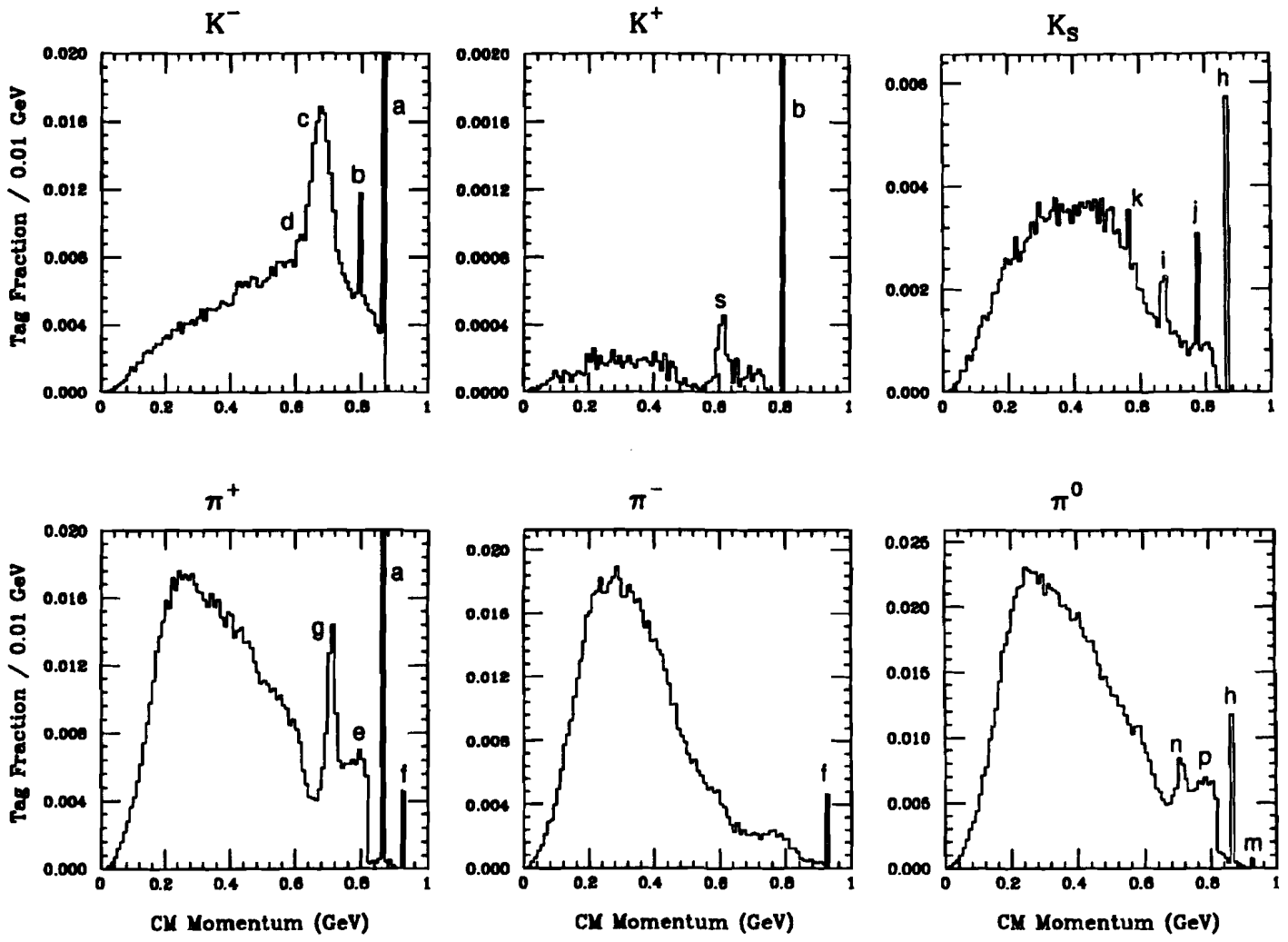

Figure 7.7 BSW: D^0 center-of-mass momentum spectra (letters indicating structure are explained in the text)

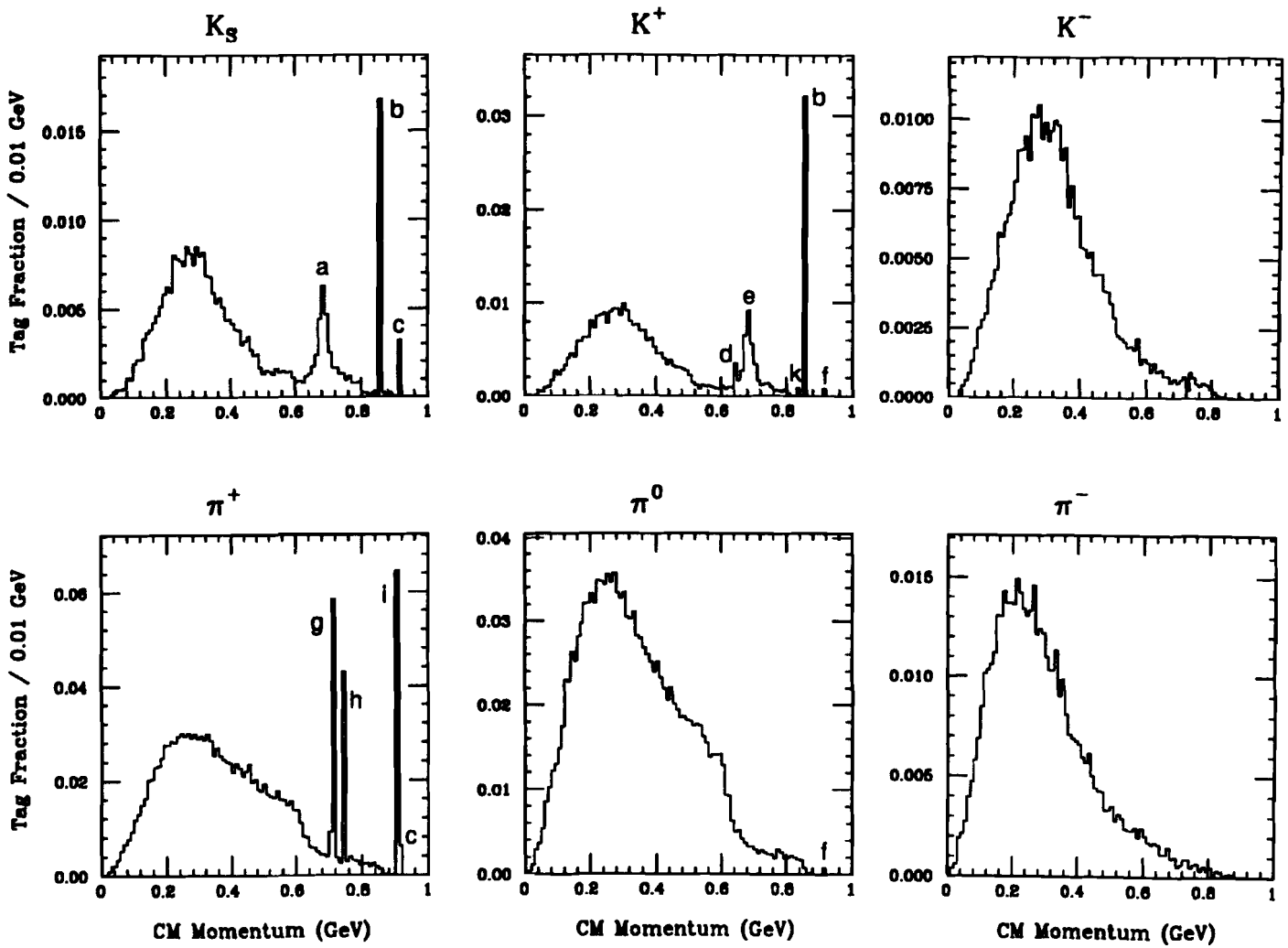

Figure 7.8 BSW: D_s^+ center-of-mass momentum spectra (letters indicating structure are explained in the text)

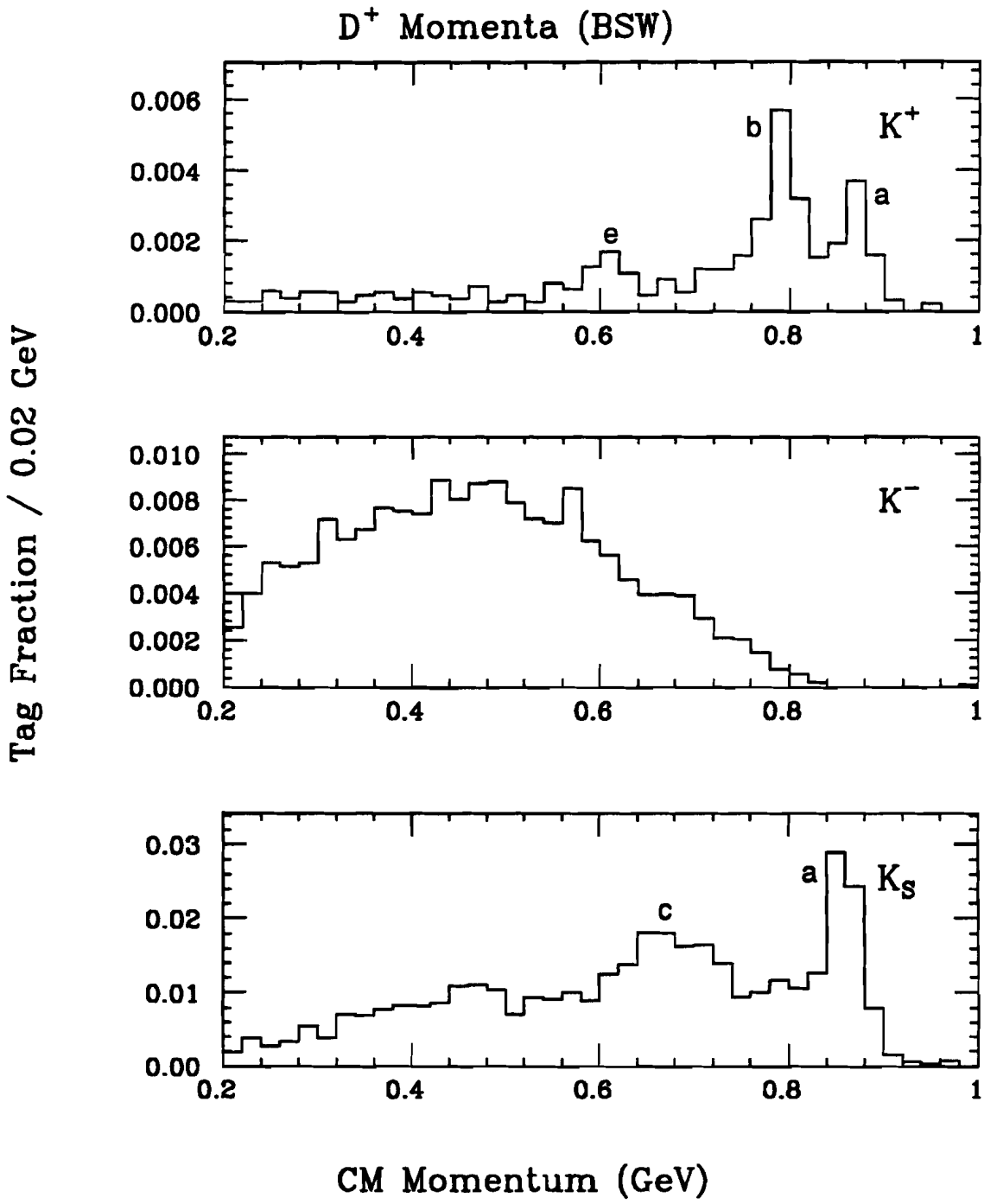

Figure 7.9 Efficiency-corrected BSW D^+ center-of-mass momentum spectra after reconstruction and processing

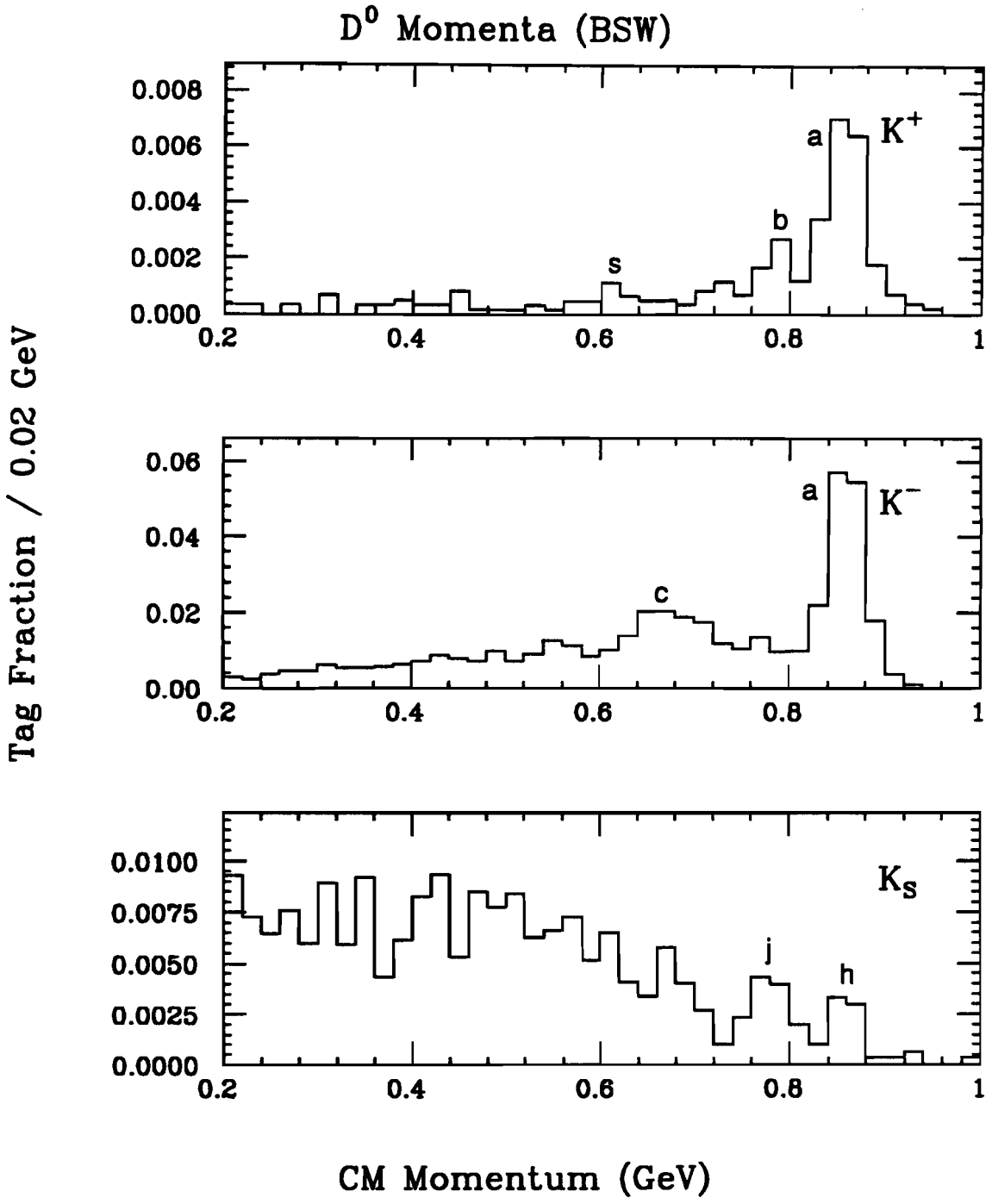

Figure 7.10 Efficiency-corrected BSW D^0 center-of-mass momentum spectra after reconstruction and processing

Section 7.11 Enhancements and Conclusions

Overall, the BSW model does a remarkable job in predicting both exclusive and inclusive properties of charmed meson decay. Comparing the BSW inclusive predictions with the experimentally determined results (see Table 7.23)* leads to the following observations and conclusions:

1. The average charged particle multiplicity is too low in the BSW model by about 7% which is 3.5σ, 5σ, and 0.5σ for the D^+, D^0, D_s^+ respectively. This is probably due to the lack of non-resonant multibody decay modes.
2. In D^+ decays, the average K^+ multiplicity is about right, but the K^- and K_S average multiplicities are too high by 3–4σ. The average pion multiplicities are 30% too low for the π^+ (equivalent to 1σ) and the π^- (equivalent to 3σ). Decay modes with high pion multiplicities are probably lacking in the model.
3. In D^0 decays, the average K^+ and K^- multiplicities are correctly predicted, but the K_S is only half the experimental value (about 3.5σ). The π^+ average is too large by 7σ, but the π^- average is too small by 2σ. Modes with neutral kaons and charged pions predominating are lacking from the model.
4. In D_s^+ decays, the average K^+ multiplicity is correctly predicted, but the K^- average is six times too large (3σ). The K_S average is low by less than 1σ. The experimental error on the π^+ average multiplicity is too large to make a meaningful comparison. The π^- average multiplicity is 2σ too low.

Based upon these observations, I created an "enhanced" model (called "BSW+") for the D^+ and D^0 consisting of the original BSW exclusive predictions with the addition of experimentally observed non-resonant multi-body decay modes. These additional modes (see Tables 7.24 and 7.25) are taken from the PDG model of Chapter 10.

* The uncertainty in the BSW predictions is much smaller than the experimental uncertainty and thus has not been listed in Table 7.23.

Table 7.23 Comparison between BSW predictions and experimental results

Average Multiplicity		BSW	BSW+	Experimental
$\langle n_{\rm ch} \rangle$	D^+	2.19	2.58	2.33 ± 0.04
	D^0	2.34	2.55	2.55 ± 0.04
	D_s^+	2.42		2.6 ± 0.3
$\langle n_{K^+} \rangle$	D^+	0.03	0.06	0.05 ± 0.01
	D^0	0.02	0.03	0.02 ± 0.01
	D_s^+	0.32		0.32 ± 0.18
$\langle n_{K^-} \rangle$	D^+	0.31	0.38	0.23 ± 0.02
	D^0	0.58	0.55	0.57 ± 0.03
	D_s^+	0.29		0.05 ± 0.08
$\langle n_{K_S} \rangle$	D^+	0.33	0.30	0.25 ± 0.03
	D^0	0.19	0.21	0.37 ± 0.05
	D_s^+	0.23		0.35 ± 0.20
$\langle n_{\pi^+} \rangle$	D^+	1.06	1.31	1.3 ± 0.3
	D^0	0.89	1.03	0.60 ± 0.04
	D_s^+	1.13		1.3 ± 1.7
$\langle n_{\pi^-} \rangle$	D^+	0.28	0.40	0.37 ± 0.03
	D^0	0.58	0.71	0.65 ± 0.03
	D_s^+	0.41		0.6 ± 0.1

The augmented D^+ model definitely improves the average pion multiplicities, but increases the average charged particle multiplicity and the average K^- multiplicity by too much.

The enhanced D^0 model now has the correct charged particle multiplicity, but has increased the average pion multiplicities too much and has not increased the K_S multiplicities enough.

Nonetheless, it seems clear that some combination of non-resonant decay modes will help complete the BSW model.

Table 7.24 BSW+: additional D^+ exclusive decay modes

D^+ Decay Mode	BR(%)
$\overline{K}^0\pi^+\pi^-\ell^+\nu$	2.2
$K^-\pi^+\pi^0\ell^+\nu$	4.4
$\overline{K}_1^0(1400)\pi^+$	4.4
$K^-\pi^+\pi^+$ (non-resonant)	6.7
$K^-\pi^+\pi^+\pi^0$ (non-resonant)	0.9
$K^-\pi^+\pi^+\pi^0\pi^0$	2.2
$K^-\pi^+\pi^+\pi^+\pi^-\pi^0$	0.19
$\overline{K}^0\pi^+\pi^0$ (non-resonant)	1.2
$\overline{K}^0\pi^+\pi^+\pi^-$ (non-resonant)	1.2
$\overline{K}^0\pi^+\pi^+\pi^-\pi^0$	8.7
$\overline{K}^0\pi^+\pi^+\pi^-\pi^+\pi^-$	0.1
$\overline{K}^0\overline{K}^0K^+$	2.7
$K^-K^+\pi^+$ (non-resonant)	0.40
$K^-K^+\pi^+\pi^0$ (non-ϕ)	1.5
$\pi^+\pi^+\pi^-$	0.28
$\pi^+\pi^+\pi^-\pi^0$	2.3
$\pi^+\pi^+\pi^-\pi^+\pi^-$	0.15
$\pi^+\pi^+\pi^-\pi^+\pi^-\pi^0$	0.28
$K^-\rho^+\pi^+$	0.8
$\overline{K}^{*0}\pi^+\pi^+\pi^-$	0.76
$\overline{K}^{*0}\rho^0\pi^+$	0.57
$\phi\pi^+\pi^0$	2.4
BR Sum	50.9

Table 7.25 BSW+: additional D^0 exclusive decay modes

D^0 Decay Mode	BR(%)
$K^-\pi^0\ell^+\nu$	1.6
$\overline{K}^0\pi^-\ell^+\nu$	2.8
$\overline{K}_1(1270)^-\pi^+$	1.09
$K^-\pi^+\pi^0$ (non-resonant)	1.1
$K^-\pi^+\pi^0\pi^0$	15.0
$K^-\pi^+\pi^+\pi^-$ (non-resonant)	1.8
$K^-\pi^+\rho^0$	6.4
$\pi^+\pi^-\pi^0$	1.5
$\pi^+\pi^-\pi^+\pi^-$	0.75
$\pi^+\pi^-\pi^+\pi^-\pi^0$	1.7
$\overline{K}^0\pi^+\pi^-$ (non-resonant)	1.8
$\overline{K}^0\pi^+\pi^-\pi^0$ (non-resonant)	2.2
$\overline{K}^0\pi^+\pi^-\pi^+\pi^-$	0.85
$\overline{K}^0K^+K^-$ (non-ϕ)	0.52
$K_SK_SK_S$	0.089
$K^+K^-\overline{K}^0\pi^0$	0.9
$K^0K^-\pi^+$ (non-resonant)	0.22
$\overline{K}^0K^+\pi^-$ (non-resonant)	0.37
$K^+K^-\pi^+\pi^-$	0.007
$K^+K^-\pi^+\pi^-\pi^0$	0.28
$\overline{K}^0\pi^+\pi^-\pi^0\pi^0$	12.7
$\overline{K}^{*0}\pi^+\pi^-\pi^0$	1.6
$\phi\pi^+\pi^-$	0.24
$\overline{K}^{*0}K^{*0}$	0.27
BR Sum	61.1

Chapter 8 The Quark Diagram Scheme of Chau and Cheng

Section 8.1 Diagrams and Parameters

Chau and Cheng[13, 49] use a quark-diagram scheme, designated herein as the CC model, which classifies all weak decays of mesons by six quark diagrams. These diagrams, which already include QCD corrections (Figure 8.1), are characterized by 6 parameters. The diagrams and associated parameters are: *a*) the external W-emission diagram, *b*) the internal W-emission diagram, *c*) the W-exchange diagram, *d*) the W-annihilation diagram, *e*) the horizontal W-loop diagram, and *f*) the vertical W-loop diagram. Four additional diagrams, called "hairpin" diagrams (see Figure 8.2), relate to diagrams c through f, but define four separate parameters c_h through f_h (the subscript "h" is used to distinguish these parameters).

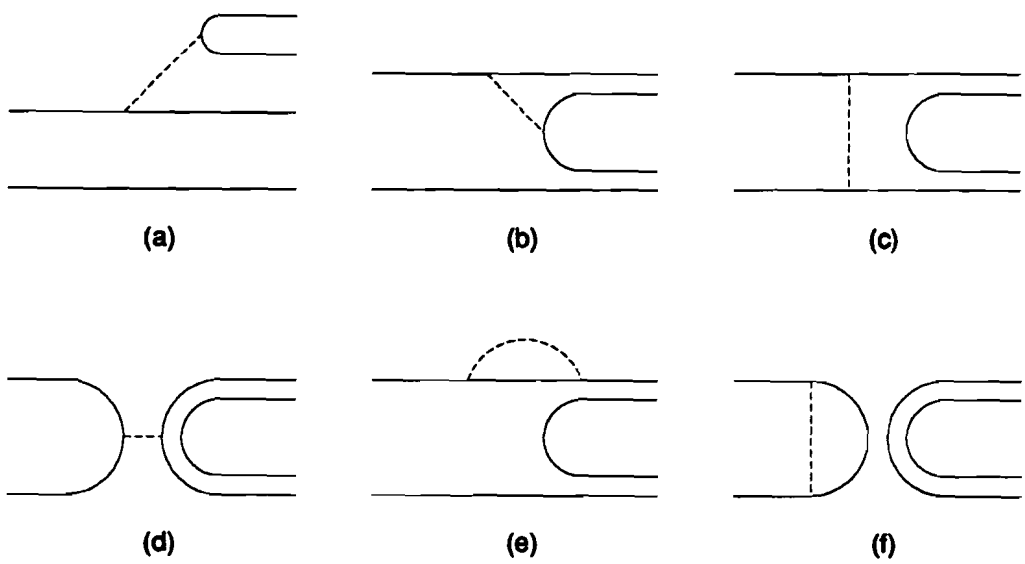

Figure 8.1 Chau and Cheng's quark diagrams and associated parameters

In the quark diagram formalism, each type of two-body decay (i.e., pseudoscalar-pseudoscalar (PP), vector-pseudoscalar (VP), etc.) has its own distinct set of parameters. Thus, parameter a in a PP decay does not equal parameter a in a VP decay. Appropriate subscripts (e.g., a_{PP}, a_{VP}) will be used in instances where confusion may arise.

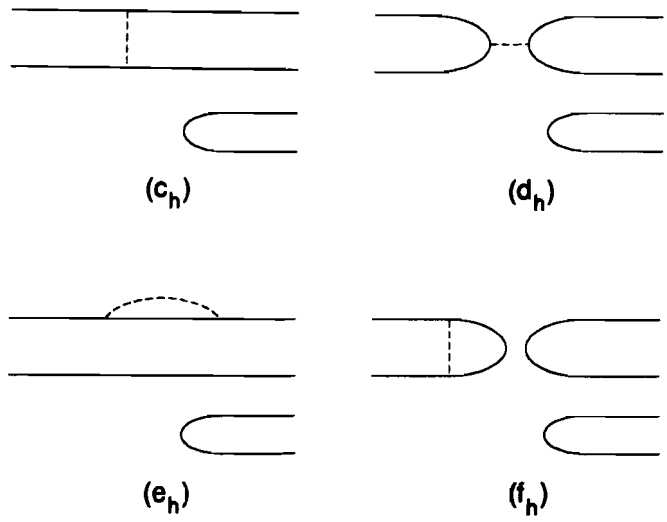

Figure 8.2 Hairpin diagrams

In the case of decays that have daughters of different spin-parity (e.g., a VP decay), the parameter set is doubled. For VP decays, unprimed parameters denote the case of the pseudoscalar meson coming from the decay of the c quark and primed parameters denote the case where the vector meson comes from the c quark. For diagram d, the parameter is unprimed when the pseudoscalar meson contains the primary q quark (arising from the decay of the W) and the vector meson contains the $\bar{q}$ quark. The parameter is primed if the vector meson contains the q and the pseudoscalar contains the $\bar{q}$.

In the case of broken SU(3) symmetry, whenever a $q\bar{q}$ pair is pulled from the vacuum, a distinction is made between $s\bar{s}$ coming from the vacuum and $u\bar{u}$ or $d\bar{d}$ coming from the vacuum. This splits parameters c through f (as well as c_h through f_h, c' through f', and c'_h through f'_h) into two sets. The set corresponding to $s\bar{s}$ pairs is designated with an underline (e.g., $\underline{c}$).

Thus the total parameter set includes: 18 parameters for PP decays — a, b, c, $\underline{c}$, c_h, $\underline{c}_h$, d, d_h, $\underline{d}$, $\underline{d}_h$, e, e_h, $\underline{e}$, $\underline{e}_h$, f, f_h, $\underline{f}$ and $\underline{f}_h$; 36 parameters for VP decays — a, a', b, b', c, c', $\underline{c}$, $\underline{c}'$, c_h, c'_h, $\underline{c}_h$, $\underline{c}'_h$, d, d', d_h, d'_h, $\underline{d}$, $\underline{d}'$, $\underline{d}_h$, $\underline{d}'_h$, e, e', e_h, e'_h, $\underline{e}$, $\underline{e}'$, $\underline{e}_h$, $\underline{e}'_h$, f, f', f_h, f'_h, $\underline{f}$, $\underline{f}'$, $\underline{f}_h$ and $\underline{f}'_h$; 18 parameters for VV decays — a, b, c, $\underline{c}$, c_h, $\underline{c}_h$, d, d_h, $\underline{d}$, $\underline{d}_h$, e, e_h, $\underline{e}$, $\underline{e}_h$, f, f_h, $\underline{f}$ and $\underline{f}_h$. Other spin-parity combinations have similar parameters.

One of the difficulties in obtaining inclusive predictions from the quark-diagram

scheme stems from the large number of parameters. A few shortcuts can help simplify the situation somewhat. According to Chau,[50] hairpin diagrams are expected to contribute negligibly in the case of VP decays, thus all the VP hairpin parameters will be set to zero. In the case of PP decays, insufficient experimental evidence does not allow separation of hairpin parameters from others. Thus the PP hairpin parameters will be set to zero as well.

Chau and Cheng list two amplitudes for each of their exclusive mode predictions. The first amplitude has SU(3) symmetry and no final-state interactions (FSI), while the second set accounts for SU(3) breaking and FSI. The FSI are imposed through the use of a complex isospin phase angle. Unfortunately, these phase angles are additional parameters which must be determined experimentally.

The current experimental situation is not complete enough to solve for all these parameters. Therefore, I calculate the inclusive properties using the first set of amplitudes (i.e., SU(3) symmetry and no FSI). This has two additional benefits: 1) the problem is handled in an manner analogous to the BSW model (i.e., no FSI corrections), and 2) none of the parameters belonging to the e and f families (e.g., e, e', e_h, e'_h, $\underline{e}$, $\underline{e'}$, $\underline{e}_h$, $\underline{e'}_h$, f, f', f_h, f'_h, $\underline{f}$, $\underline{f'}$, $\underline{f}_h$ and $\underline{f'}_h$) appear in the equations, thereby reducing the number of parameters.

Since Chau and Cheng only list exclusive decay mode predictions for PP and VP decays, I expect that the inclusive charged multiplicity will be underestimated, due to a lack of high multiplicity final-state decay contributions. Although one could formulate the expressions for the other decay modes, it would introduce many new parameters, and the current experimental situation is insufficient to solve for these new parameters.

Section 8.2 Octet-Singlet Mixing

The η and η' mesons are mass eigenstate mixtures of the singlet and octet quark states η_0 and η_8:

$$\eta = \eta_8 \cos\theta + \eta_0 \sin\theta$$

$$\eta' = -\eta_8 \sin\theta + \eta_0 \cos\theta$$

where θ is the weak mixing angle. Chau and Cheng use a value of 20°.

The η_0, η_8 and π^0 are mixtures of the $u\bar{u}$, $d\bar{d}$ and $s\bar{s}$ quark pairs:

$$\eta_0 = \frac{1}{\sqrt{3}}\left(u\bar{u} + d\bar{d} + s\bar{s}\right)$$
$$\eta_8 = \frac{1}{\sqrt{6}}\left(u\bar{u} + d\bar{d} - 2s\bar{s}\right)$$
$$\pi^0 = \frac{1}{\sqrt{2}}\left(u\bar{u} - d\bar{d}\right)$$

for which the inverse is:

$$u\bar{u} = \frac{1}{\sqrt{2}}\pi^0 + \frac{1}{\sqrt{3}}\eta_0 + \frac{1}{\sqrt{6}}\eta_8$$
$$d\bar{d} = \frac{-1}{\sqrt{2}}\pi^0 + \frac{1}{\sqrt{3}}\eta_0 + \frac{1}{\sqrt{6}}\eta_8$$
$$s\bar{s} = \qquad\qquad + \frac{1}{\sqrt{3}}\eta_0 - \frac{\sqrt{2}}{\sqrt{3}}\eta_8 \,.$$

Chau and Cheng list their predictions for the exclusive decay amplitudes in terms of η_0 and η_8. To convert to the mass eigenstates, the amplitudes are mixed as above:

$$A(\eta X) = A(\eta_8 X)\cos\theta + A(\eta_0 X)\sin\theta$$
$$A(\eta' X) = -A(\eta_8 X)\sin\theta + A(\eta_0 X)\cos\theta \,.$$

Two special cases are:

$$A(\eta\eta) = A(\eta_8\eta_8)\cos^2\theta + 2A(\eta_8\eta_0)\cos\theta\sin\theta + A(\eta_0\eta_0)\sin^2\theta$$
$$A(\eta\eta') = A(\eta_8\eta_0)\left(\cos^2\theta - \sin^2\theta\right) + \left(A(\eta_0\eta_0) - A(\eta_8\eta_8)\right)\cos\theta\sin\theta \,.$$

The decay mode $D^0 \to \eta'\eta'$ is not kinematically possible.

Section 8.3 Solving for the CC Model Parameters

Vector-Pseudoscalar Parameters

The decay amplitude for a VP decay is given by:

$$M = \epsilon^\mu p_\mu A$$
$$= p \times \frac{m_D}{m_V}$$

where ϵ^μ is the polarization vector of the V meson, p_μ is the four-momentum of the D meson, p is the magnitude of the three-momentum of the decay products, and A is the

amplitude of the decay as specified in the tables of Section 8.4. The partial width for a VP decay is then given by the expression:

$$\Gamma_{VP} = |A|^2 \frac{p^3}{8\pi m_V^2}$$
$$= |A|^2 \frac{\left\{\left[m_D^2 - (m_V + m_P)^2\right]\left[m_D^2 - (m_V - m_P)^2\right]\right\}^{3/2}}{64\pi m_D^3 m_V^2}.$$

I calculate the VP parameters by performing a least squares fit to the function:

$$S = \sum_{i=1}^{n} \frac{\left(B_i^{\text{pred}} - B_i^{\text{exp}}\right)^2}{\sigma^2_{B_i^{\text{exp}}}}$$

where:

B_i^{pred} is the predicted branching ratio and is a function of the parameters,

B_i^{exp} is the experimentally observed branching ratio,

$\sigma_{B_i^{\text{exp}}}$ is the error on the experimentally observed branching ratio.

The following experimental branching ratios are used in the fit:[46, 48, 41]

$$B(D_s^+ \to \phi\pi^+) = 0.027 \pm 0.007$$
$$B(D^+ \to \phi\pi^+) = 0.0057 \pm 0.0011$$
$$B\left(D^0 \to \phi\overline{K}^0\right) = 0.0080 \pm 0.0016$$
$$B\left(D^+ \to \overline{K}^{*0}\pi^+\right) = 0.020 \pm 0.002$$
$$B\left(D^0 \to \overline{K}^{*0}\pi^0\right) = 0.026 \pm 0.003$$
$$B(D^0 \to K^{*-}\pi^+) = 0.052 \pm 0.003$$
$$B\left(D^0 \to \omega\overline{K}^0\right) = 0.023 \pm 0.007$$
$$B\left(D^+ \to \rho^+\overline{K}^0\right) = 0.069 \pm 0.008$$
$$B\left(D^0 \to \rho^0\overline{K}^0\right) = 0.008 \pm 0.001$$
$$B(D^0 \to \rho^+K^-) = 0.108 \pm 0.004$$
$$B\left(D_s^+ \to K^{*+}\overline{K}^0\right) = 0.032 \pm 0.011$$
$$B\left(D_s^+ \to \overline{K}^{*0}K^+\right) = 0.026 \pm 0.007.$$

The functional forms for the predicted amplitudes are listed in the tables of Section 8.4. These amplitudes are converted into branching ratios using the above expression for Γ_{VP} and $B = \Gamma\tau/\hbar$. However, for four of these modes, the effect of final-state interactions are accounted for. The expressions for the isospin-mixed amplitudes are:

$$A(K^{*-}\pi^+) = \left[(a'+c') - \tfrac{1}{3}(a'+b')\left(1 - e^{i\Delta_{K^*\pi}}\right)\right]$$
$$A\left(\overline{K}^{*0}\pi^0\right) = \left[(b'-c') - \tfrac{2}{3}(a'+b')\left(1 - e^{i\Delta_{K^*\pi}}\right)\right]$$
$$A(K^-\rho^+) = \left[(a+c) - \tfrac{1}{3}(a+b)\left(1 - e^{i\Delta_{K\rho}}\right)\right]$$
$$A\left(\overline{K}^0\rho^0\right) = \left[(b-c) - \tfrac{2}{3}(a+b)\left(1 - e^{i\Delta_{K\rho}}\right)\right]$$

where:

$\Delta_{K^*\pi}$ is the isospin phase difference in the $\overline{K}^*\pi$ system, and

$\Delta_{K\rho}$ is the isospin phase difference in the $\overline{K}\rho$ system.

There are numerous equivalent solutions to this problem. The program, MINUIT, used to find the minimum of the least squares equation, is sensitive to the initial estimates of the parameters. The solution that most closely reflects the previous results of Chau and Cheng is:

$$a = +(3.29 \pm 0.16) \times 10^{-6} \qquad a' = +(1.77 \pm 0.17) \times 10^{-6}$$
$$b = -(1.64 \pm 0.16) \times 10^{-6} \qquad b' = -(2.65 \pm 0.17) \times 10^{-6}$$
$$c = -(0.38 \pm 0.16) \times 10^{-6} \qquad c' = -(4.28 \pm 0.18) \times 10^{-6}$$
$$\underline{c}' = -(1.61 \pm 0.16) \times 10^{-6}$$
$$\underline{d} = +(1.01 \pm 0.28) \times 10^{-6} \qquad \underline{d}' = -(0.18 \pm 0.35) \times 10^{-6}$$

$$\Delta_{K^*\pi} = (87 \pm 10)^\circ$$
$$\Delta_{K\rho} = (0 \pm 7)^\circ .$$

Following the example of Chau and Cheng, and motivated by the fact that $c' = 2.66\underline{c}'$, the missing parameters are estimated in a similar fashion, yielding:

$$\underline{c} = -(0.14 \pm 0.06) \times 10^{-6}$$
$$d = +(2.68 \pm 0.75) \times 10^{-6} \qquad d' = -(0.47 \pm 0.93) \times 10^{-6} .$$

Pseudoscalar-Pseudoscalar Parameters

The decay amplitude for PP decays is given by:[51]

$$M = m_D A$$

where m_D is the mass of the parent D meson. The partial width for PP decays is then:

$$\begin{aligned}\Gamma_{PP} &= |A|^2 \frac{p}{8\pi} \\ &= |A|^2 \frac{\left\{\left[m_D^2 - (m_V + m_P)^2\right]\left[m_D^2 - (m_V - m_P)^2\right]\right\}^{1/2}}{16\pi m_D}.\end{aligned}$$

Following a technique similar to that used for VP decays, a least squares fit is performed. The following experimentally determined branching ratios are used in the fit:[45, 52, 47, 6]

$$\begin{aligned}
B\left(D^+ \to \overline{K}^0 K^+\right) &= 0.0101 \pm 0.0032 \\
B\left(D_s^+ \to \overline{K}^0 K^+\right) &= 0.028 \pm 0.007 \\
B\left(D^+ \to \overline{K}^0 \pi^+\right) &= 0.032 \pm 0.005 \\
B\left(D^0 \to \overline{K}^0 \pi^0\right) &= 0.018 \pm 0.002 \\
B\left(D^0 \to K^- \pi^+\right) &= 0.042 \pm 0.004 \\
B\left(D^0 \to \overline{K}^0 \eta\right) &= 0.016 \pm 0.006 \\
B\left(D^0 \to \overline{K}^0 \eta'\right) &= 0.033 \pm 0.003 \\
B\left(D_s^+ \to \eta \pi^+\right) &= 0.015 \pm 0.004 \\
B\left(D_s^+ \to \eta' \pi^+\right) &= 0.037 \pm 0.012.
\end{aligned}$$

The functional forms for the predicted amplitudes are listed in the tables of Section 8.4. These amplitudes are converted into branching ratios using the above expression for Γ_{PP} and $B = \Gamma\tau/\hbar$. However, for two of these modes, the effect of final-state interactions are accounted for. These amplitudes include an isospin phase angle:

$$\begin{aligned}
A\left(K^- \pi^+\right) &= \left[(a + c) - \tfrac{1}{3}(a + b)\left(1 - e^{i\Delta_{K\pi}}\right)\right] \\
A\left(\overline{K}^0 \pi^0\right) &= \left[(b - c) - \tfrac{2}{3}(a + b)\left(1 - e^{i\Delta_{K\pi}}\right)\right]
\end{aligned}$$

where $\Delta_{\bar{K}\pi}$ is the isospin phase difference in the $\overline{K}\pi$ system.

The least-squares equation has numerous local minima. The solution that most closely reflects the previous results of Chau and Cheng is:

$$a = +(1.1 \pm 0.1) \times 10^{-6}$$

$$b = -(1.9 \pm 0.1) \times 10^{-6}$$

$$c = -(2.7 \pm 0.1) \times 10^{-6}$$

$$\underline{c} = -(6.1 \pm 0.4) \times 10^{-6}$$

$$d = +(0.8 \pm 0.1) \times 10^{-6}$$

$$\underline{d} = -(0.9 \pm 0.3) \times 10^{-6}$$

$$\Delta_{\bar{K}\pi} = (76 \pm 7)^{\circ} .$$

Section 8.4 Exclusive Mode Predictions

Tables 8.1—8.6 list the exclusive hadronic decay modes and amplitudes, with SU(3) symmetry and without final-state interactions, as predicted by Chau and Cheng. The branching ratios are calculated using the parameter values listed in the previous section. Normalizing the partial widths with the D meson lifetimes yields the branching ratios.

The errors quoted on these branching ratios derive solely from the uncertainty of the parameters.

The sum of the branching ratios for the D^+ is $(62.4 \pm 3.2)\%$; for the D^0 is $(79.6 \pm 3.9)\%$; and for the D_s^+ is $(96 \pm 21)\%$. These include the contributions from semileptonic and leptonic decays.

Table 8.1 CC: $D^+ \rightarrow$ PP exclusive decay modes

D^+ Decay Mode	Quark Mixing Factor	Amplitude with SU(3) symmetry	BR(%)
$\overline{K}^0\pi^+$	$(c_1)^2$	$(a+b)$	3.2 ± 1.4
$\eta_8\pi^+$	$-(1/\sqrt{6})(s_1c_1)$	$[(a+b)+2(b+d)]$	
$\eta_0\pi^+$	$-(1/\sqrt{3})(s_1c_1)$	$(a+2d)$	
$\eta\pi^+$			0.10 ± 0.07
$\eta'\pi^+$			0.76 ± 0.10
$\overline{K}^0K^+$	(s_1c_1)	$(a-d)$	1.0 ± 0.4
$\pi^0\pi^+$	$(1/\sqrt{2})(s_1c_1)$	$(a+b)$	0.09 ± 0.04
η_8K^+	$-(1/\sqrt{6})(s_1)^2$	$(a-d)$	
η_0K^+	$-(1/\sqrt{3})(s_1)^2$	$(a+2d)$	
ηK^+			0.006 ± 0.001
$\eta'K^+$			0.002 ± 0.001
$K^0\pi^+$	$-(s_1)^2$	$(b+d)$	0.018 ± 0.006
π^0K^+	$(1/\sqrt{2})(s_1)^2$	$(a-d)$	0.001 ± 0.001

Table 8.2 CC: $D^+ \rightarrow$ VP exclusive decay modes

D^+ Decay Mode	Quark Mixing Factor	Amplitude with SU(3) symmetry	BR(%)
$\overline{K}^0\rho^+$	$(c_1)^2$	$(a+b)$	8.4 ± 2.3
$\overline{K}^{*0}\pi^+$	$(c_1)^2$	$(a'+b')$	2.0 ± 1.1
$\eta_8\rho^+$	$-(1/\sqrt{6})(s_1c_1)$	$(a+3b+d+d')$	
$\eta_0\rho^+$	$-(1/\sqrt{3})(s_1c_1)$	$(a+d+d')$	
$\eta\rho^+$			2.5 ± 0.9
$\eta'\rho^+$			0.03 ± 0.03
$\overline{K}^0K^{*+}$	(s_1c_1)	$(a-\underline{d'})$	1.1 ± 0.2
$\overline{K}^{*0}K^+$	(s_1c_1)	$(a'-\underline{d})$	0.05 ± 0.05

Table 8.2 (Continued) CC: $D^+ \rightarrow$ VP exclusive decay modes

D^+ Decay Mode	Quark Mixing Factor	Amplitude with SU(3) symmetry	BR(%)
$\omega\pi^+$	$-(1/\sqrt{2})(s_1c_1)$	$(a'+b'+d+d')$	0.2 ± 0.4
$\pi^0\rho^+$	$(1/\sqrt{2})(s_1c_1)$	$(a+b-d+d')$	0.3 ± 0.4
$\phi\pi^+$	(s_1c_1)	b'	0.58 ± 0.08
ϕK^+	$-(s_1)^2$	$\underline{d}$	0.002 ± 0.001
$\rho^0\pi^+$	$(1/\sqrt{2})(s_1c_1)$	$(a'+b'+d-d')$	0.6 ± 0.7
η_8K^{*+}	$-(1/\sqrt{6})(s_1)^2$	$(a+d-2d')$	
η_0K^{*+}	$-(1/\sqrt{3})(s_1)^2$	$(a+d+d')$	
ηK^{*+}			0.06 ± 0.02
$\eta' K^{*+}$			$(1.9 \pm 1.6)\times 10^{-4}$
$K^0\rho^+$	$-(s_1)^2$	$(b+d')$	0.04 ± 0.04
$K^{*0}\pi^+$	$-(s_1)^2$	$(b'+d)$	$(1 \pm 4)\times 10^{-4}$
ρ^0K^+	$(1/\sqrt{2})(s_1)^2$	$(a'-d')$	0.02 ± 0.02
ωK^+	$-(1/\sqrt{2})(s_1)^2$	$(a'+d')$	0.007 ± 0.011
π^0K^{*+}	$(1/\sqrt{2})(s_1)^2$	$(a-d')$	0.001 ± 0.004

Table 8.3 CC: $D^0 \rightarrow$ PP exclusive decay modes

D^0 Decay Mode	Quark Mixing Factor	Amplitude with SU(3) symmetry	BR(%)
$K^-\pi^+$	$(c_1)^2$	$(a+c)$	1.3 ± 0.6
$\overline{K}^0\pi^0$	$(1/\sqrt{2})(c_1)^2$	$(b-c)$	0.6 ± 0.3
$\overline{K}^0\eta_8$	$(1/\sqrt{6})(c_1)^2$	$(b-c)$	
$\overline{K}^0\eta_0$	$(1/\sqrt{3})(c_1)^2$	$(b+2c)$	
$\overline{K}^0\eta$			2.3 ± 0.3
$\overline{K}^0\eta'$			21.4 ± 1.8
$K^0\overline{K}^0$	0		0 ± 0
K^-K^+	(s_1c_1)	$(a+c)$	0.25 ± 0.06

Table 8.3 (Continued) CC: $D^0 \rightarrow$ PP exclusive decay modes

D^0 Decay Mode	Quark Mixing Factor	Amplitude with SU(3) symmetry	BR(%)
$\pi^-\pi^+$	$-(s_1c_1)$	$(a+c)$	0.30 ± 0.07
$\pi^0\pi^0$	$(\sqrt{2})/2(s_1c_1)$	$(b-c)$	0.009 ± 0.004
$\pi^0\eta_8$	$-(1/\sqrt{3})(s_1c_1)$	$(b-c)$	
$\pi^0\eta_0$	$(1/\sqrt{6})(s_1c_1)$	$(b+2c)$	
$\pi^0\eta$			0.22 ± 0.04
$\pi^0\eta'$			0.59 ± 0.05
$\eta_8\eta_8$	$-(\sqrt{2})/2(s_1c_1)$	$(b-c)$	
$\eta_8\eta_0$	$(1/\sqrt{2})(s_1c_1)$	$(b+2c)$	
$\eta_0\eta_0$	$(\sqrt{2})0$		
$\eta\eta$			0.75 ± 0.08
$\eta\eta'$			1.1 ± 0.1
$\eta'\eta'$			0 ± 0
$K^+\pi^-$	$-(s_1)^2$	$(a+c)$	0.015 ± 0.003
$K^0\pi^0$	$-(1/\sqrt{2})(s_1)^2$	$(b-c)$	0.002 ± 0.001
$K^0\eta_8$	$-(1/\sqrt{6})(s_1)^2$	$(b-c)$	
$K^0\eta_0$	$-(1/\sqrt{3})(s_1)^2$	$(b+2c)$	
$K^0\eta$			0.007 ± 0.001
$K^0\eta'$			0.064 ± 0.005

Table 8.4 CC: $D^0 \rightarrow$ VP exclusive decay modes

D^0 Decay Mode	Quark Mixing Factor	Amplitude with SU(3) symmetry	BR(%)
K^-K^{*+}	(s_1c_1)	$(a+c)$	0.30 ± 0.05
$K^-\rho^+$	$(c_1)^2$	$(a+c)$	10.3 ± 1.6
$K^{*-}K^+$	(s_1c_1)	$(a'+c')$	0.23 ± 0.05
$K^{*-}\pi^+$	$(c_1)^2$	$(a'+c')$	6.5 ± 1.3
$\pi^-\rho^+$	(s_1c_1)	$(a+c)$	0.6 ± 0.1

Table 8.4 (Continued) CC: $D^0 \rightarrow$ VP exclusive decay modes

D^0 Decay Mode	Quark Mixing Factor	Amplitude with SU(3) symmetry	BR(%)
$\rho^-\pi^+$	(s_1c_1)	$(a'+c')$	0.8 ± 0.1
$\overline{K}^0\omega$	$(1/\sqrt{2})(c_1)^2$	$(b+c)$	2.3 ± 0.5
$\overline{K}^0\rho^0$	$(1/\sqrt{2})(c_1)^2$	$(b-c)$	1.0 ± 0.3
$\overline{K}^{*0}\eta_8$	$(1/\sqrt{6})(c_1)^2$	$(b'+c'-2c)$	
$\overline{K}^{*0}\eta_0$	$(1/\sqrt{3})(c_1)^2$	$(b'+c'+c)$	
$\overline{K}^{*0}\eta$			8.0 ± 0.7
$\overline{K}^{*0}\eta'$			0.028 ± 0.003
$\overline{K}^{*0}\pi^0$	$(1/\sqrt{2})(c_1)^2$	$(b'-c')$	1.3 ± 0.4
$\pi^0\omega$	$1/2(s_1c_1)$	$(b-b'+c+c')$	0.30 ± 0.06
$\pi^0\phi$	$(1/\sqrt{2})(s_1c_1)$	(b')	0.11 ± 0.02
$\pi^0\rho^0$	$1/2(s_1c_1)$	$(b+b'-c-c')$	0.003 ± 0.006
$\rho^0\eta_8$	$(1/\sqrt{12})(s_1c_1)$	$(-3b+b'+c+c')$	
$\rho^0\eta_0$	$(1/\sqrt{6})(s_1c_1)$	$(b'+c+c')$	
$\rho^0\eta$			0.17 ± 0.04
$\rho^0\eta'$			0.061 ± 0.004
$\omega\eta_8$	$(1/\sqrt{12})(s_1c_1)$	$(-3b-b'-c-c')$	
$\omega\eta_0$	$(1/\sqrt{6})(s_1c_1)$	$(b+c+c')$	
$\omega\eta$			0.33 ± 0.03
$\omega\eta'$			0.100 ± 0.009
$\phi\eta_8$	$(1/\sqrt{6})(s_1c_1)$	$(b'-2\underline{c'}-2\underline{c})$	
$\phi\eta_0$	$(1/\sqrt{3})(s_1c_1)$	$(b'+\underline{c'}+\underline{c})$	
$\phi\eta$			0.004 ± 0.002
$\phi\eta'$			0 ± 0
$\overline{K}^0\phi$	$(c_1)^2$	$(\underline{c'})$	0.8 ± 0.2
$\overline{K}^{*0}K^0$	$-(s_1c_1)$	$(c-c')$	0.53 ± 0.07
$\overline{K}^{*0}\overline{K}^0$	$-(s_1c_1)$	$(c'-c)$	0.53 ± 0.07
ϕK^0	$-(s_1)^2$	$(\underline{c})$	$(1.8 \pm 1.5) \times 10^{-5}$

Table 8.4 (Continued) CC: $D^0 \rightarrow$ VP exclusive decay modes

D^0 Decay Mode	Quark Mixing Factor	Amplitude with SU(3) symmetry	BR(%)
ωK^0	$-(1/\sqrt{2})(s_1)^2$	$(b+c')$	0.12 ± 0.01
$K^{*+}\pi^-$	$-(s_1)^2$	$(a+\underline{c})$	0.031 ± 0.003
$K^{*0}\pi^0$	$-(1/\sqrt{2})(s_1)^2$	$(b-\underline{c})$	0.007 ± 0.002
$K^{*0}\eta_8$	$-(1/\sqrt{6})(s_1)^2$	$(b'+c-2\underline{c'})$	
$K^{*0}\eta_0$	$-(1/\sqrt{3})(s_1)^2$	$(b'+c+\underline{c'})$	
$K^{*0}\eta$			$(1.2 \pm 0.5)\times 10^{-3}$
$K^{*0}\eta'$			$(5.6 \pm 0.7)\times 10^{-5}$
$\rho^- K^+$	$-(s_1)^2$	$(a'+c')$	0.023 ± 0.005
$\rho^0 K^0$	$-(1/\sqrt{2})(s_1)^2$	$(b-c')$	0.008 ± 0.002

Table 8.5 CC: $D_s^+ \rightarrow$ PP exclusive decay modes

D_s Decay Mode	Quark Mixing Factor	Amplitude with SU(3) symmetry	BR(%)
$\overline{K}^0 K^+$	$(c_1)^2$	$(b+d)$	2.5 ± 0.8
$\pi^0\pi^+$	0		0 ± 0
$\eta_8\pi^+$	$-(\sqrt{2}/\sqrt{3})(c_1)^2$	$(a-d)$	
$\eta_0\pi^+$	$(1/\sqrt{3})(c_1)^2$	$(a+2d)$	
$\eta\pi^+$			0.2 ± 0.2
$\eta'\pi^+$			4.3 ± 0.8
$K^0\pi^+$	$-(s_1c_1)$	$(a-d)$	0.01 ± 0.01
$K^+\pi^0$	$(1/\sqrt{2})(s_1c_1)$	$(b+d)$	0.07 ± 0.03
$K^+\eta_8$	$-(1/\sqrt{6})(s_1c_1)$	$[2(a+b+(b+d)]$	
$K^+\eta_0$	$(1/\sqrt{3})(s_1c_1)$	$(a+2d)$	
$K^+\eta$			8.0 ± 1.7
$K^+\eta'$			1.4 ± 0.6
K^0K^+	$-(s_1)^2$	$(a+b)$	0.004 ± 0.002

Table 8.6 CC: $D_s^+ \rightarrow$ VP exclusive decay modes

D_s^+ Decay Mode	Quark Mixing Factor	Amplitude with SU(3) symmetry	BR(%)
$\phi\pi^+$	$(c_1)^2$	a'	26.3 ± 5.1
$\omega\pi^+$	$(1/\sqrt{2})(c_1)^2$	$(d+d')$	5.4 ± 5.8
$K^{*+}\overline{K}^0$	$(c_1)^2$	$(b+d')$	4.3 ± 3.9
$K^+\overline{K}^{*0}$	$(c_1)^2$	$(b'+d)$	0.001 ± 0.044
$\rho^+\pi^0$	$(1/\sqrt{2})(c_1)^2$	$(d-d')$	11.5 ± 8.8
$\rho^0\pi^+$	$(1/\sqrt{2})(c_1)^2$	$(d'-d)$	11.5 ± 8.7
$\rho^+\eta_8$	$(1/\sqrt{6})(c_1)^2$	$(-2a+d+d')$	
$\rho^+\eta_0$	$(1/\sqrt{3})(c_1)^2$	$(a+d+d')$	
$\rho^+\eta$			0.5 ± 1.3
$\rho^+\eta'$			0.2 ± 0.4
ϕK^+	(s_1c_1)	$(a'+b'+\underline{d'})$	$(0.5 \pm 2.8)\times 10^{-3}$
ωK^+	$-(1/\sqrt{2})(s_1c_1)$	$(b'-d')$	0.4 ± 0.4
$K^{*0}\pi^+$	$-(s_1c_1)$	$(a'-d)$	0.06 ± 0.11
$K^{*+}\pi^0$	$-(1/\sqrt{2})(s_1c_1)$	$(b-d)$	0.7 ± 0.3
ρ^+K^0	$-(s_1c_1)$	$(a-d')$	1.3 ± 0.7
ρ^0K^+	$(1/\sqrt{2})(s_1c_1)$	$(b'-d')$	0.5 ± 0.3
$K^{*+}\eta_8$	$(1/\sqrt{6})(s_1c_1)$	$(-2a+3b+d-2\underline{d'})$	
$K^{*+}\eta_0$	$(1/\sqrt{3})(s_1c_1)$	$(a+d+\underline{d'})$	
$K^{*+}\eta$			0.2 ± 0.1
$K^{*+}\eta'$			0.12 ± 0.02
$K^{*+}K^0$	$-(s_1)^2$	$(a+b)$	0.008 ± 0.002
$K^{*0}K^+$	$-(s_1)^2$	$(a'+b')$	0.002 ± 0.001

Section 8.5 Inclusive Predictions

The inclusive decay properties for the CC model are listed in Tables 8.7 — 8.13. The exclusive hadronic branching ratios used are from Tables 8.1 — 8.6. Semileptonic

branching ratios, as calculated using the BSW model (see Tables 7.13 — 7.15) are added for completeness since Chau and Cheng do not have any explicit predictions for these modes.

Table 8.7 CC: inclusive charged particle multiplicity distribution and average

n	$B(D^+ \to nP^\pm X^0)$	$B(D^0 \to nP^\pm X^0)$	$B(D_s^+ \to nP^\pm X^0)$
0		8.1 ± 0.3	
1	46.9 ± 0.8		35.7 ± 4.5
2		71.2 ± 0.8	
3	52.6 ± 0.8		62.7 ± 4.6
4		19.3 ± 0.5	
5	0.46 ± 0.04		1.6 ± 0.3
6		1.4 ± 0.1	
7	$(2.0 \pm 0.3)\times 10^{-3}$		0.014 ± 0.003
8		0.014 ± 0.001	
$\langle n \rangle$	2.07 ± 0.02	2.28 ± 0.01	2.32 ± 0.09

The charged particle multiplicity (Table 8.7) is cut off at 8–prongs in order to increase clarity and reduce data overload. However, 15– and 16–prong events (with a branching ratio of $10^{-17}\%$) are possible in this model.

Table 8.8 CC: D^+ inclusive kaon multiplicity distribution and average

n	$B(D^+ \to nK^+X)$	$B(D^+ \to nK^-X)$	$B(D^+ \to nK^\pm X)$
0	97.2 ± 0.6 %	75.7 ± 1.5 %	73.4 ± 1.6 %
1	2.8 ± 0.6 %	24.3 ± 1.5 %	26.1 ± 1.6 %
2	0.002 ± 0.001 %		0.5 ± 0.1 %
3			0.002 ± 0.001 %
$n \geq 1$	2.8 ± 0.6 %	24.3 ± 1.5 %	26.6 ± 1.6 %
$\langle n \rangle$	0.03 ± 0.01	0.24 ± 0.02	0.27 ± 0.02

n	$B(D^+ \to nK^0X)$	$B(D^+ \to n\overline{K}^0X)$	$B(D^+ \to n(K^0 \vee \overline{K}^0)X)$	$B(D^+ \to nK_SX)$
0	98.7 ± 0.3 %	37.5 ± 2.3 %	37.3 ± 2.2 %	68.0 ± 1.1 %
1	1.3 ± 0.3 %	62.5 ± 2.3 %	61.5 ± 2.2 %	31.7 ± 1.1 %
2			1.2 ± 0.2 %	0.29 ± 0.06 %
$n \geq 1$	1.3 ± 0.3 %	62.5 ± 2.3 %	62.7 ± 2.2 %	32.0 ± 1.1 %
$\langle n \rangle$	0.013 ± 0.003	0.63 ± 0.02	0.64 ± 0.02	0.32 ± 0.01

Table 8.9 CC: D^+ inclusive pion multiplicity distribution and average

n	$B(D^+ \to n\pi^+X)$	$B(D^+ \to n\pi^-X)$	$B(D^+ \to n\pi^\pm X)$	$B(D^+ \to n\pi^0X)$
0	30.0 ± 1.6 %	71.8 ± 0.9 %	30.0 ± 1.6 %	59.5 ± 2.5 %
1	56.4 ± 0.7 %	27.9 ± 0.9 %	40.0 ± 1.2 %	27.1 ± 2.4 %
2	13.2 ± 1.6 %	0.30 ± 0.04 %	18.9 ± 1.3 %	7.5 ± 0.7 %
3	0.30 ± 0.04 %	$(9 \pm 7)\times10^{-6}$ %	11.1 ± 1.5 %	4.4 ± 0.4 %
4	$(9 \pm 7)\times10^{-6}$ %		$(5 \pm 1)\times10^{-4}$ %	1.3 ± 0.4 %
5			0.30 ± 0.04 %	0.08 ± 0.01 %
6			0 ± 0 %	0.003 ± 0.003 %
7			$(9 \pm 7)\times10^{-6}$ %	$(2 \pm 2)\times10^{-6}$ %
$n \geq 1$	70.0 ± 1.6 %	28.2 ± 0.9 %	70.0 ± 1.6 %	40.5 ± 2.5 %
$\langle n \rangle$	0.84 ± 0.03	0.29 ± 0.01	1.12 ± 0.04	0.61 ± 0.04

Table 9.2 (Continued) BS: D^0 exclusive decay modes

Mode	Amplitude (from Reference 16)	BR(%)
K^-K^{*+}	$(2(c_1+c_2/3)f_+^K f_\rho m_\rho - (c_1R_1+c_2R_3))(eq)$	0.23 ± 0.06
$K^{*-}K^+$	$((c_1+c_2/3)g_+ f_\pi m_D - (c_1R_1+c_2R_2))(eq)$	0.20 ± 0.05
Sum (including semi-leptonic modes)		44.0 ± 5.4

Table 9.3 BS: D_s^+ exclusive decay modes

Mode	Amplitude (from Reference 16)	BR(%)
$\omega\pi^+$	$-c_2R_2\sqrt{2}(eq)$	0.011 ± 0.014
$\rho\pi^+$	0	0 ± 0
$\phi\pi^+$	$f_\pi g_+(c_1+c_2/3)m_D - c_2R_2(eq)$	1.8 ± 0.6
$\eta\rho^+$	$(eq)\left(-\sqrt{\frac{2}{3}}\right)(2f_+^K f_\rho(c_1+c_2/3)m_\rho - c_2R_3 + c_2R_1)$	3.7 ± 1.1
$\overline{K}^0K^{*+}$	$(g_+f_\pi(c_2+c_1/3)m_D - (c_2R_1+c_1R_2))(eq)$	0.11 ± 0.05
$\overline{K}^{*0}K^+$	$(2f_+^K f_\rho m_\rho(c_2+c_1/3) + (c_1R_3 - c_2R_1))(eq)$	0.23 ± 0.16
$\pi^+\pi^0$	0	0 ± 0
$\overline{K}^0K^+$	$(c_2+c_1/3)f_\pi f_+^K m_D^2 - c_1M_2 - c_2M_1$	0.9 ± 0.4
$\pi^+\eta'$	$(f_\pi f_+^K(c_1+c_2/3)m_D^2 - c_2(M_2''+2M_1''))/\sqrt{3}$	0.3 ± 0.3
$\pi^+\eta$	$-(f_\pi f_+^K m_D^2(c_1+c_2/3) - (c_2M_2+c_2M_1))\sqrt{\frac{2}{3}}$	2.0 ± 0.8
Sum (including semi-leptonic modes)		25.1 ± 2.2

Section 9.3 Inclusive Predictions

The inclusive decay properties for the BS model are listed in Tables 9.4—9.10. In the charged particle multiplicity distribution 9–prong and higher multiplicities have been removed to improve clarity.

Table 9.2 BS: D^0 exclusive decay modes

Mode	Amplitude (from Reference 16)	BR(%)
$K^-\pi^+$	$m_D^2(c_1+c_2/3)f_+^K f_\pi-(c_1M_1+c_2M_2)$	6.0 ± 1.7
$\overline{K}^0\pi^0$	$((c_2+c_1/3)m_D^2 f_+^K f_\pi+c_1(M_1-M_3))/\sqrt{2}$	1.1 ± 0.4
$\overline{K}^0\eta$	$((c_2+c_1/3)f_+^K f_\pi m_D^2+c_1(M_1-M_2))/\sqrt{6}$	0.3 ± 0.1
$\overline{K}^0\eta'$	$((c_2+c_1/3)f_+^K f_\pi m_D^2-c_1(M_2''+2M_1''))/\sqrt{3}$	1.1 ± 1.1
$K^{*-}\pi^+$	$(m_D(c_1+c_2/3)g_+f_\pi-(c_1R_1+c_2R_2))(eq)$	5.8 ± 1.4
$K^-\rho^+$	$(2m_\rho(c_1+c_2/3)f_+^K f_\rho-(c_1R_1+c_2R_3))(eq)$	7.9 ± 2.0
$\overline{K}^0\rho^0$	$((c_2+c_1/3)f_\pi g_+m_D+c_1(R_1-R_2))(eq)/\sqrt{2}$	0.4 ± 0.2
$\overline{K}^{*0}\pi^0$	$((c_2+c_1/3)f_+^K f_\rho m_\rho+c_1(R_1-R_3))(eq)/\sqrt{2}$	1.6 ± 0.4
$\overline{K}^0\phi$	$-c_1R_1(eq)$	0.3 ± 0.1
$\overline{K}^0\omega$	$((c_2+c_1/3)f_\pi g_+m_D-c_1(R_1+R_2))(eq)/\sqrt{2}$	0.8 ± 0.3
$\overline{K}^{*0}\eta$	$(f_\pi g_+m_D(c_2+c_1/3)+c_1(R_1-R_2))(eq)/\sqrt{6}$	0.06 ± 0.03
K^-K^+	$m_D^2(c_1+c_2/3)f_+^K f_\pi-(c_1M_1+c_2M_2)$	0.30 ± 0.09
$\pi^-\pi^+$	$m_D^2(c_1+c_2/3)f_+^K f_\pi-(c_1M_1+c_2M_2)$	0.35 ± 0.10
$\pi^0\pi^0$	$(c_1/3+c_2)f_+^K f_\pi m_D^2+c_1(M_1-M_2)$	0.12 ± 0.05
$\overline{K}^0K^0$	0	0 ± 0
$\pi^0\eta'$	$3((c_2+c_1/3)f_+^K f_\pi m_D^2-2c_1M_2''/3-c_1M_1'')/\sqrt{6}$	0.03 ± 0.06
$\pi^0\eta$	$-((c_2+c_1/3)f_+^K m_D^2 f_\pi-c_1(M_2-M_1))/\sqrt{3}$	0.04 ± 0.01
$\rho^-\pi^+$	$(-(c_1+c_2/3)f_\pi g_+m_D+(c_1R_1+c_2R_2))(eq)$	0.5 ± 0.1
$\rho^+\pi^-$	$(-2(c_1+c_2/3)f_+^K f_\rho m_\rho+(c_1R_1+c_2R_3))(eq)$	0.6 ± 0.2
$\rho^0\pi^0$	$\Big((c_1/3+c_2)(2f_+^K f_\rho m_\rho+g_+f_\pi m_D)$ $+c_1(2R_1-R_2-R_3)\Big)(eq)/2$	0.16 ± 0.05
$\phi\pi^0$	$(2(c_2+c_1/3)m_\rho f_+^K f_\rho-c_1R_3/\sqrt{2})(eq)$	0.009 ± 0.004
$\omega\pi^0$	$\Big((c_2+c_1/3)(2f_+^K f_\rho m_\rho+g_+f_\pi m_D)$ $-c_1(R_2+R_3+2R_1)\Big)(eq)/2$	0.04 ± 0.03
$\eta\rho^0$	$\Big(-(c_2+c_1/3)f_\pi g_+m_D+m_\rho f_+^K f_\rho(c_2+c_1/3)2$ $+c_1(R_2-R_3-2R_1)\Big)(eq)/\sqrt{12}$	0.005 ± 0.004

Table 9.1 BS: D^+ exclusive decay modes

Mode	Amplitude (from Reference 16)	BR(%)
$\overline{K}^0\pi^+$	$\frac{4}{3}m_D^2(c_1+c_2)f_+^K f_\pi - (c_1M_3+c_2M_2)$	2.5 ± 2.0
$\overline{K}^{*0}\pi^+$	$\Big(2m_\rho(c_2+c_1/3)f_+^K f_\rho + (c_1+c_2/3)$ $\times f_\pi g_+ m_D - (c_1R_3+c_2R_2)\Big)(eq)$	1.0 ± 0.9
$\overline{K}^0\rho^+$	$\Big(m_D(c_2+c_1/3)f_\pi g_+ + 2(c_1+c_2/3)$ $\times f_+^K f_\rho m_\rho - (c_1R_2+c_2R_3)\Big)(eq)$	9.4 ± 3.1
$K^+\overline{K}^0$	$(c_1+c_2/3)m_D^2 f_+^K f_\pi - c_2(M_2-M_1)$	0.5 ± 0.2
$\pi^+\pi^0$	$4(c_1+c_2)f_+^K f_\pi m_D^2/(3\sqrt{2}) - (c_1M_3+c_2M_2)/\sqrt{2}$	0.07 ± 0.06
$\pi^+\eta'$	$\Big(2f_+^K f_\pi m_D^2(c_2+c_1/3) + (c_1+c_2/3)f_+^K f_\pi m_D^2 - 2c_1M_2''$ $-c_2(M_2''+2M_1'')\Big)/\sqrt{3}$	0.6 ± 0.3
$\pi^+\eta$	$\Big(-(m_D^2 f_+^K f_\pi(c_2+c_1/3) - c_1M_2) +$ $m_D^2 f_+^K f_\pi(c_1+c_2/3)$ $-c_2(M_2+2M_1)\Big)/\sqrt{6}$	0.11 ± 0.04
$K^+\overline{K}^{*0}$	$((c_1+c_2/3)g_+ f_\pi m_D - c_2(R_2-R_1))(eq)$	0.26 ± 0.07
$K^{*+}\overline{K}^0$	$(2(c_1+c_2/3)f_+^K f_\rho m_\rho - c_2(R_3-R_1))(eq)$	0.32 ± 0.09
$\pi^+\rho^0$	$\Big((c_1+c_2/3)f_\pi g_+ m_D + (c_2+c_1/3)2f_\rho f_+^K m_\rho$ $-(c_1R_3+c_2R_2)\Big) \times (eq)/\sqrt{2}$	0.05 ± 0.04
$\rho^+\pi^0$	$\Big((c_2+c_1/3)f_\pi g_+ m_D/\sqrt{2} + 2(c_1+c_2/3)f_+^K f_\rho m_\rho/\sqrt{2}$ $-(c_1R_2+c_2R_3)/\sqrt{2}\Big)(eq)$	0.4 ± 0.1
$\pi^+\phi$	$(2f_+^K f_\rho(c_2+c_1/3)m_\rho + c_1R_3)(eq)$	0.05 ± 0.02
$\pi^+\omega$	$\Big((c_1+c_2/3)g_+ f_\pi m_D/\sqrt{2} + \sqrt{2}(c_2+c_1/3)m_\rho f_+^K f_\rho$ $-(c_1R_3+c_2(R_2+2R_1))/\sqrt{2}\Big)(eq)$	$(0 \pm 2)\times 10^{-4}$
$\eta\rho^+$	$\Big(-g_+ f_\pi m_D(c_2+c_1/3)+(c_1+c_2/3)f_+^K f_\rho m_\rho + c_1R_2 - c_2$ $\times(R_3+2R_1)\Big)(eq)/\sqrt{6}$	$(.3 \pm 1.1)\times 10^{-3}$
Sum (including semi-leptonic modes)		56.6 ± 5.1

and Shifman set equal to 133 MeV. f_+^π and f_+^K are form factors for the matrix elements of the type:

$$\left\langle \overline{K}^0 \middle| (\bar{s}c)^{ij} \middle| D^+ \right\rangle = \frac{1}{3}\delta^{ij}\left(f_+^K \left(p^D + p^K\right)_\mu + f_-^K \left(p^D - p^K\right)_\mu \right)$$

with values determined by QCD sum rules to equal 0.5 ± 0.1.

Nonfactorizable Contribution

The dynamical parameters, M_i and R_i, for the nonfactorizable amplitudes are calculated by Block and Shifman using QCD sum rules.[16] The values of the parameters that they determine for PP decays are:

$$M_1 = -0.09 \pm 0.02 \text{ GeV}^3$$

$$M_2 = \quad 0.11 \pm 0.03 \text{ GeV}^3$$

$$M_3 = \quad 0.11 \pm 0.03 \text{ GeV}^3 .$$

For VP decays:

$$R_1 = -0.1 \pm 0.02 \text{ GeV}^2$$

$$R_2 = -0.016 \pm 0.01 \text{ GeV}^2$$

$$R_3 = +0.08 \pm 0.016 \text{ GeV}^2 .$$

For the class of decays $D \to P\eta'(P = \pi, K, \eta)$ there is another set of parameters:

$$M_1'' = -0.32 \pm 0.07 \text{ GeV}^3$$

$$M_2'' = \quad 0.34 \pm 0.07 \text{ GeV}^3$$

$$M_3'' = \quad 0.34 \pm 0.07 \text{ GeV}^3 .$$

Section 9.2 Exclusive Modes

Blok and Shifman's predictions for the exclusive hadronic decay modes and amplitudes are listed in Tables 9.1—9.3. I have calculated updated branching ratios for these modes. To calculate these branching ratios I used the same values for the parameters as mentioned in the previous section. Additionally, the following constants are defined: $f_\rho = .2$ GeV, $m_\rho = .75$ GeV, $c_1 = 1.19$, $c_2 = -0.38$, $g = 0.66 \pm 0.1$.

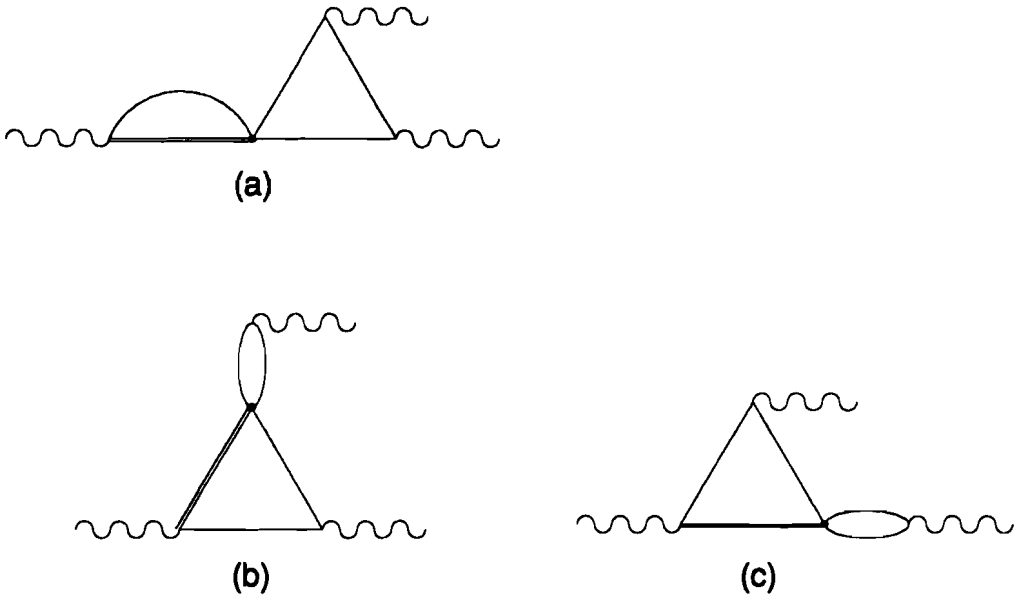

Figure 9.1 QCD sum rules: factorizable diagrams (a) annihilation (b,c) spectator; where a wavy line represents a meson current, a double line represents a charm quark, and a single line represents a light quark

Factorizable Contribution

The factorizable contribution to the decay amplitudes originates from the effective weak Hamiltonian (accounting for hard gluons) which was developed in Chapter 1.

$$H_W = \frac{G_F}{\sqrt{2}}\left(c_1(\bar{s}^i c)_L(\bar{u}d^i)_L + c_2(\bar{s}^i d^i)_L(\bar{u}c)_L\right)$$

The factorized decay amplitude for a decay, e.g., $D^+ \to K^0\pi^+$, is:[14]

$$\begin{aligned} M\left(D^+ \to \overline{K}^0\pi^+\right) = \frac{G_F}{\sqrt{2}}\cos^2\theta\Bigg(& c_1\left\langle \pi^+\middle|(\overline{u}d)^{jj}\middle|0\right\rangle\left\langle \overline{K}^0\middle|(\overline{s}c)^{ii}\middle|D^+\right\rangle \\ & + c_1\left\langle \overline{K}^0\middle|(\overline{s}d)^{ij}\middle|0\right\rangle\left\langle \pi^+\middle|(\overline{u}c)^{ji}\middle|D^+\right\rangle \\ & + c_2\left\langle \pi^+\middle|(\overline{u}d)^{ji}\middle|0\right\rangle\left\langle \overline{K}^0\middle|(\overline{s}c)^{ij}\middle|D^+\right\rangle \\ & + c_2\left\langle \overline{K}^0\middle|(\overline{s}d)^{jj}\middle|0\right\rangle\left\langle \pi^+\middle|(\overline{u}c)^{ii}\middle|D^+\right\rangle\Bigg) \\ = \frac{G_F}{\sqrt{2}}\cos^2\theta\left(\left(c_1+\frac{c_2}{3}\right)f_+^K f_\pi + \left(c_2+\frac{c_1}{3}\right)f_+^\pi f_K\right)(-im_D^2) \end{aligned}$$

where $(\overline{u}d)^{ij} \equiv \overline{u}^i\gamma_\mu(1-\gamma_5)d^j$ and summation over the color indices i and j is implied. f_π and f_K are decay constants (defined via $\left\langle \pi^+\middle|(\overline{u}d)^{ij}\middle|0\right\rangle = -\frac{1}{3}\delta^{ij}f_\pi p_\pi^\mu$), which Blok

Chapter 9 The QCD Sum Rules Model of Blok and Shifman

Section 9.1 Introduction

Blok and Shifman[14–17, 54] use QCD sum rules to calculate two-body decay widths. Regrettably, they limited their published calculations to non-leptonic PP and VP decays. This only accounts for about 60% of the total width after adding in estimates of the semileptonic decay modes and leads to an underestimate of the inclusive charged particle multiplicities. Although QCD sum rules can extend to other spin-parity decay types, such calculations lie beyond the scope of this thesis. Nonetheless, an analysis of the available information is presented here.

QCD sum rules are used to calculate the nonfactorizable part of the amplitudes for the two-body decays. In general the amplitudes are given by:

$$A = A_{fact} + T_n$$

$$T_n(D \to PP) = \sum_{i=1}^{3} \alpha_i M_i$$

$$T_n(D \to PV) = (eq) \sum_{i=1}^{3} \alpha_i R_i$$

where the T_n is the nonfactorizable part of the amplitude, α_i depend upon the quark content of the mesons, the M_i and R_i are the dynamical parameters of QCD sum rules, with e being the polarization vector of the vector meson and q being the momentum of the pseudoscalar meson. There are 3 parameters for PP decays and 3 parameters for VP decays. M_1 and R_1 correspond to the annihilation diagram (Figure 9.1a), M_2 and R_2 correspond to the external W-emission diagram (Figure 9.1b), while M_3 and R_3 correspond to the internal W-emission diagram (Figure 9.1c).

Table 8.14 Comparison between CC predictions and experimental results

Average Multiplicity		CC	Experimental
$\langle n_{\mathrm{ch}} \rangle$	D^+	2.07 ± 0.02	2.33 ± 0.04
	D^0	2.28 ± 0.01	2.55 ± 0.04
	D_s^+	2.32 ± 0.09	2.6 ± 0.3
$\langle n_{K^+} \rangle$	D^+	0.03 ± 0.01	0.05 ± 0.01
	D^0	0.014 ± 0.001	0.02 ± 0.01
	D_s^+	0.33 ± 0.06	0.32 ± 0.18
$\langle n_{K^-} \rangle$	D^+	0.24 ± 0.02	0.23 ± 0.02
	D^0	0.39 ± 0.02	0.57 ± 0.03
	D_s^+	0.17 ± 0.04	0.05 ± 0.08
$\langle n_{K_S} \rangle$	D^+	0.32 ± 0.01	0.25 ± 0.03
	D^0	0.28 ± 0.01	0.37 ± 0.05
	D_s^+	0.18 ± 0.03	0.35 ± 0.20
$\langle n_{\pi^+} \rangle$	D^+	0.84 ± 0.03	1.3 ± 0.3
	D^0	0.91 ± 0.01	0.60 ± 0.04
	D_s^+	1.17 ± 0.07	1.3 ± 1.7
$\langle n_{\pi^-} \rangle$	D^+	0.29 ± 0.01	0.37 ± 0.03
	D^0	0.73 ± 0.02	0.65 ± 0.03
	D_s^+	0.47 ± 0.03	0.6 ± 0.1

Section 8.6 Conclusions

Comparing the CC model's inclusive predictions with the experimentally determined results (see Table 8.14) leads to the following observations and conclusions:

1. The average charged particle multiplicity is too low in the CC model by about 11% (or 6σ) for both the D^+ and D^0 mesons, and 11% (or 1σ) for the D_s^+ meson. This is most certainly due to a lack of vector-vector (and other higher multiplicity) decay modes.
2. For the D^+, the average charged kaon multiplicities are about right, but the neutral K_S average is too high by 2σ. The average charged pion multiplicities are both too low by about 2σ. These facts support the argument that there are a lack of higher multiplicity decay modes, since these additional modes would tend to add pions.
3. For the D^0, the K^+ average are in close agreement, but the K^- average is too small (by 30% or 5σ), as is the K_S average (by 2σ). The average charged pion multiplicities are too high by 7σ for the π^+ and 3σ for the π^-.
4. For the D_s^+, the K^+ is about right. The K^- average is 2σ too high. The K_S average is less than 1σ (or 50%) too low. Both charged pion multiplicities are low, but are within 1σ of the experimental result.

Due to the potentially large number of missing decay modes, no attempt is made to "correct" or "patch" this model as is done in the BSW and PDG models. Further development of the quark diagram scheme, in particular predictions for vector-vector and other decay modes,[53] would allow a more detailed comparison with the data.

Table 8.12 CC: D_s^+ inclusive kaon multiplicity distribution and average

n	$B(D_s^+ \to nK^+X)$	$B(D_s^+ \to nK^-X)$	$B(D_s^+ \to nK^\pm X)$
0	67.5 ± 6.2 %	82.6 ± 4.1 %	67.3 ± 6.2 %
1	32.5 ± 6.2 %	17.4 ± 4.1 %	15.5 ± 3.2 %
2	0.002 ± 0.001 %		17.2 ± 4.0 %
3			$(0.2 \pm 1.4)\times 10^{-3}$ %
$n \geq 1$	32.5 ± 6.2 %	17.4 ± 4.1 %	32.7 ± 6.2 %
$\langle n \rangle$	0.33 ± 0.06	0.17 ± 0.04	0.5 ± 0.1

n	$B(D_s^+ \to nK^0X)$	$B(D_s^+ \to n\overline{K}^0X)$	$B(D_s^+ \to n(K^0 \vee \overline{K}^0)X)$	$B(D_s^+ \to nK_SX)$
0	94.8 ± 2.7 %	92.3 ± 3.2 %	90.1 ± 3.6 %	82.4 ± 2.7 %
1	5.2 ± 2.7 %	7.7 ± 3.2 %	6.9 ± 1.6 %	16.9 ± 2.6 %
2	0.006 ± 0.002 %		3.0 ± 2.3 %	0.8 ± 0.6 %
$n \geq 1$	5.2 ± 2.7 %	7.7 ± 3.2 %	9.9 ± 3.6 %	17.6 ± 2.7 %
$\langle n \rangle$	0.05 ± 0.03	0.08 ± 0.03	0.13 ± 0.06	0.18 ± 0.03

Table 8.13 CC: D_s^+ inclusive pion multiplicity distribution and average

n	$B(D_s^+ \to n\pi^+X)$	$B(D_s^+ \to n\pi^-X)$	$B(D_s^+ \to n\pi^\pm X)$	$B(D_s^+ \to n\pi^0X)$
0	18.9 ± 3.8 %	53.9 ± 2.9 %	18.9 ± 3.8 %	54.8 ± 2.4 %
1	45.9 ± 2.8 %	44.8 ± 3.1 %	35.0 ± 4.1 %	19.6 ± 5.7 %
2	34.2 ± 4.0 %	1.3 ± 0.3 %	10.9 ± 2.1 %	18.5 ± 6.0 %
3	1.0 ± 0.3 %	0.004 ± 0.001 %	33.9 ± 4.1 %	6.3 ± 1.2 %
4	0.004 ± 0.001 %		0.3 ± 0.1 %	0.3 ± 0.6 %
5			1.0 ± 0.3 %	0.5 ± 0.1 %
6			0 ± 0 %	0.01 ± 0.02 %
7			0.004 ± 0.001 %	$(8 \pm 2)\times 10^{-4}$ %
$n \geq 1$	81.1 ± 3.8 %	46.1 ± 2.9 %	81.1 ± 3.8 %	45.2 ± 2.4 %
$\langle n \rangle$	1.17 ± 0.07	0.47 ± 0.03	1.65 ± 0.09	0.79 ± 0.05

Table 8.10 CC: D^0 inclusive kaon multiplicity distribution and average

n	$B(D^0 \to nK^+X)$	$B(D^0 \to nK^-X)$	$B(D^0 \to nK^\pm X)$
0	98.6 ± 0.1 %	60.6 ± 1.8 %	60.3 ± 1.8 %
1	1.4 ± 0.1 %	39.4 ± 1.8 %	38.6 ± 1.8 %
2			1.1 ± 0.1 %
$n \geq 1$	1.4 ± 0.1 %	39.4 ± 1.8 %	39.7 ± 1.8 %
$\langle n \rangle$	0.014 ± 0.001	0.39 ± 0.02	0.41 ± 0.02

n	$B(D^0 \to nK^0X)$	$B(D^0 \to n\overline{K}^0X)$	$B(D^0 \to n(K^0 \vee \overline{K}^0)X)$	$B(D^0 \to nK_SX)$
0	98.8 ± 0.1 %	47.2 ± 1.6 %	46.2 ± 1.6 %	72.8 ± 0.8 %
1	1.2 ± 0.1 %	52.6 ± 1.6 %	53.4 ± 1.6 %	26.9 ± 0.8 %
2		0.22 ± 0.02 %	0.44 ± 0.04 %	0.28 ± 0.04 %
$n \geq 1$	1.2 ± 0.1 %	52.8 ± 1.6 %	53.8 ± 1.6 %	27.2 ± 0.8 %
$\langle n \rangle$	0.012 ± 0.001	0.53 ± 0.02	0.54 ± 0.02	0.28 ± 0.01

Table 8.11 CC: D^0 inclusive pion multiplicity distribution and average

n	$B(D^0 \to n\pi^+X)$	$B(D^0 \to n\pi^-X)$	$B(D^0 \to n\pi^\pm X)$	$B(D^0 \to n\pi^0X)$
0	27.5 ± 0.9 %	45.3 ± 1.4 %	21.4 ± 0.7 %	41.4 ± 0.9 %
1	55.2 ± 1.1 %	37.4 ± 0.9 %	30.0 ± 1.7 %	34.4 ± 1.4 %
2	16.0 ± 0.5 %	16.0 ± 0.5 %	29.0 ± 0.9 %	9.0 ± 0.3 %
3	1.2 ± 0.1 %	1.2 ± 0.1 %	4.7 ± 0.2 %	9.8 ± 0.4 %
4			13.7 ± 0.5 %	2.2 ± 0.1 %
5			$(3.0 \pm 0.4)\times 10^{-3}$ %	2.5 ± 0.2 %
6			1.2 ± 0.1 %	0.43 ± 0.02 %
7				0.28 ± 0.02 %
8				0.030 ± 0.002 %
$n \geq 1$	72.5 ± 0.9 %	54.7 ± 1.4 %	78.6 ± 0.7 %	58.6 ± 0.9 %
$\langle n \rangle$	0.91 ± 0.01	0.73 ± 0.02	1.64 ± 0.03	1.08 ± 0.02

Table 10.2 (Continued) PDG: D^0 exclusive decay modes

D^0 Decay Mode	BR(%)
$\overline{K}^0\pi^+\pi^-\pi^0\pi^0$	12.7 ± 3.0
$\overline{K}^{*0}\pi^+\pi^-\pi^0$	1.6 ± 0.8
$\phi\pi^+\pi^-$	0.24 ± 0.08
$\overline{K}^{*0}K^{*0}$	0.27 ± 0.14
BR Sum	112.8 ± 7.8

Table 10.3 PDG: D_s^+ exclusive decay modes

D_s^+ Decay Mode	BR(%)
$\phi e^+\nu$	1.6 ± 0.7
$\phi\mu^+\nu$	1.4 ± 0.5
$\eta\pi^+$	1.5 ± 0.4
$\eta'\pi^+$	3.7 ± 1.2
$\overline{K}^0K^+$	2.8 ± 0.7
$\eta\rho^+$	7.9 ± 2.1
$\eta'\rho^+$	9.5 ± 2.7
$\overline{K}^0K^{*+}$	3.3 ± 0.9
$\overline{K}^{*0}K^+$	2.6 ± 0.5
$\phi\pi^+$	2.8 ± 0.5
$\overline{K}^{*0}K^{*+}$	5.0 ± 1.7
$\phi\pi^+\pi^0$ (incl. $\phi\rho^+$)	6.7 ± 3.3
$\phi\pi^+\pi^+\pi^-$	1.2 ± 0.4
$K^+K^-\pi^+$ (non-resonant)	0.81 ± 0.30
$\pi^+\pi^+\pi^-$	1.2 ± 0.4
$K^0K^-\pi^+\pi^+$	3.3 ± 1.0
$K^+K^-\pi^+\pi^+\pi^-$ (non-ϕ)	0.19 ± 0.14
$\pi^+\pi^+\pi^+\pi^-\pi^-$	0.19 ± 0.20
$K^+\pi^+\pi^-$	0.14 ± 0.20
BR Sum	55.8 ± 5.6

Table 10.2 (Continued) PDG: D^0 exclusive decay modes

D^0 Decay Mode	BR(%)
$\overline{K}^0 K^0$	0.11 ± 0.04
$\overline{K}^0 \pi^0$	2.1 ± 0.5
$\overline{K}^0 \omega$	2.5 ± 0.5
$\overline{K}^0 \phi$	0.88 ± 0.12
$\overline{K}^0 \rho^0$	0.61 ± 0.30
$\overline{K}^{*0} \eta$	2.1 ± 1.2
$\overline{K}^{*0} \pi^0$	2.1 ± 1.0
$\overline{K}^{*0} \rho^0$	1.5 ± 0.6
$\rho^0 \phi$	0.18 ± 0.05
$\overline{K}_1(1270)^- \pi^+$	1.09 ± 0.33
$K^- \pi^+ \pi^0$ (non-resonant)	1.1 ± 0.7
$K^- \pi^+ \pi^0 \pi^0$	15.0 ± 5.0
$K^- \pi^+ \pi^+ \pi^-$ (non-resonant)	1.8 ± 0.5
$K^- \pi^+ \rho^0$	6.4 ± 0.5
$\pi^+ \pi^- \pi^0$	1.5 ± 1.0
$\pi^+ \pi^- \pi^+ \pi^-$	0.75 ± 0.09
$\pi^+ \pi^- \pi^+ \pi^- \pi^0$	1.7 ± 0.5
$\overline{K}^0 \pi^+ \pi^-$ (non-resonant)	1.8 ± 0.5
$\overline{K}^0 \pi^+ \pi^- \pi^0$ (non-resonant)	2.2 ± 2.2
$\overline{K}^0 \pi^+ \pi^- \pi^+ \pi^-$	0.85 ± 0.14
$\overline{K}^0 K^+ K^-$ (non-ϕ)	0.52 ± 0.09
$K_S K_S K_S$	0.089 ± 0.025
$K^+ K^- \overline{K}^0 \pi^0$	0.9 ± 0.5
$K^0 K^- \pi^+$ (non-resonant)	0.22 ± 0.22
$\overline{K}^0 K^+ \pi^-$ (non-resonant)	0.37 ± 0.2
$K^+ K^- \pi^+ \pi^-$	0.007 ± 0.007
$K^+ K^- \pi^+ \pi^- \pi^0$	0.28 ± 0.20

Table 10.1 (Continued) PDG: D^+ exclusive decay modes

D^+ Decay Mode	BR(%)
$K^-K^+\pi^+\pi^0$ (non-ϕ)	1.5 ± 0.6
$\pi^+\pi^+\pi^-$	0.28 ± 0.06
$\pi^+\pi^+\pi^-\pi^0$	2.3 ± 1.7
$\pi^+\pi^+\pi^-\pi^+\pi^-$	0.15 ± 0.11
$\pi^+\pi^+\pi^-\pi^+\pi^-\pi^0$	0.28 ± 0.29
$K^-\rho^+\pi^+$	0.8 ± 0.5
$\overline{K}^{*0}\pi^+\pi^+\pi^-$	0.76 ± 0.25
$\overline{K}^{*0}\rho^0\pi^+$	0.57 ± 0.27
$\phi\pi^+\pi^0$	2.4 ± 1.0
BR Sum	99.4 ± 9.1

Table 10.2 PDG: D^0 exclusive decay modes

D^0 Decay Mode	BR(%)
$K^-e^+\nu$	3.31 ± 0.29
$K^-\mu^+\nu$	2.9 ± 0.5
$\pi^-\ell^+\nu$	0.39 ± 0.17
$K^-\pi^0\ell^+\nu$	1.6 ± 0.9
$\overline{K}^0\pi^-\ell^+\nu$	2.8 ± 1.3
$K^{*-}\ell^+\nu$	1.7 ± 0.6
$K^-\pi^+$	3.65 ± 0.21
K^-K^+	0.401 ± 0.035
$\pi^-\pi^+$	0.163 ± 0.019
K^-K^{*+}	0.35 ± 0.08
$K^-\rho^+$	7.3 ± 1.1
$K^{*-}K^+$	0.2 ± 0.1
$K^{*-}\pi^+$	4.5 ± 0.6
$K^{*-}\rho^+$	6.2 ± 2.5
$K^-a_1{}^+$	7.4 ± 1.3

Table 10.1 PDG: D^+ exclusive decay modes

D^+ Decay Mode	BR(%)
$\overline{K}^0 e^+ \nu$	5.5 ± 1.2
$\overline{K}^0 \mu^+ \nu$	7.0 ± 2.5
$\overline{K}^{*0} \ell^+ \nu$	4.1 ± 0.6
$\overline{K}^0 \pi^+ \pi^- \ell^+ \nu$	2.2 ± 2.9
$K^- \pi^+ \pi^0 \ell^+ \nu$	4.4 ± 3.4
$\overline{K}^0 \pi^+$	2.6 ± 0.4
$\eta \pi^+$	0.66 ± 0.22
$\overline{K}^0 K^+$	0.73 ± 0.18
$\overline{K}^0 \rho^+$	6.6 ± 1.7
$\overline{K}^{*0} \pi^+$	1.9 ± 0.7
$\overline{K}^{*0} K^+$	0.47 ± 0.09
$\phi \pi^+$	0.60 ± 0.08
$\overline{K}^0 a_1{}^+$	7.5 ± 1.7
$\overline{K}_1^0(1400) \pi^+$	4.4 ± 1.2
$\overline{K}^{*0} \rho^+$	4.10 ± 1.4
$\overline{K}^{*0} K^{*+}$	2.6 ± 1.1
$K^- \pi^+ \pi^+$ (non-resonant)	6.7 ± 0.8
$K^- \pi^+ \pi^+ \pi^0$ (non-resonant)	0.9 ± 0.5
$K^- \pi^+ \pi^+ \pi^0 \pi^0$	2.2 ± 3.0
$K^- \pi^+ \pi^+ \pi^+ \pi^- \pi^0$	0.19 ± 0.20
$\overline{K}^0 \pi^+ \pi^0$ (non-resonant)	1.2 ± 0.9
$\overline{K}^0 \pi^+ \pi^+ \pi^-$ (non-resonant)	1.2 ± 0.8
$\overline{K}^0 \pi^+ \pi^+ \pi^- \pi^0$	8.7 ± 2.6
$\overline{K}^0 \pi^+ \pi^+ \pi^- \pi^+ \pi^-$	0.1 ± 0.1
$\overline{K}^0 \overline{K}^0 K^+$	2.7 ± 0.6
$K^- K^+ \pi^+$ (non-resonant)	0.40 ± 0.08

Chapter 10 The Particle Data Group Model

Section 10.1 Introduction

A good measure of the completeness of our understanding of exclusive D decay modes comes from performing an inclusive analysis on previously measured exclusive branching ratios.

If the high-energy physics community has completely and correctly measured the exclusive modes, then an inclusive analysis of the data should yield the same results as a direct experimental measurement of the inclusive properties. Any differences should indicate where our knowledge of exclusive modes is lacking.

Section 10.2 Exclusive Modes

The D^+, D^0 and D_s^+ exclusive modes and branching ratios (Tables 10.1—10.3) that I use in my inclusive analysis are based upon information taken from the "Review of Particle Properties,"[6] which is compiled and maintained by the Particle Data Group (PDG).* A few caveats are necessary:

1. For the semileptonic decays, universality is assumed to determine a semi-muonic branching ratio when only a semi-electronic branching ratio is given. I indicate this by listing a single semileptonic branching ratio in the tables.
2. Some of the decay modes listed in Reference 6 quote unequal positive and negative errors. The two errors are averaged for this calculation (e.g., $2.2^{+5.0}_{-0.9}$ becomes 2.2 ± 3.0) since PREDICT is unable to handle asymmetric errors.
3. The tables do not include final states for which only branching ratio upper limits are known.
4. Resonant modes are used when available.
5. The branching ratio errors are assumed to be uncorrelated.

* I call this model the "PDG model" although it is not an official product of the Particle Data Group, but instead is my summary of their published numbers.

missing modes, no attempt is made to patch or enhance this model. Further work on this model, especially in obtaining more exclusive decay modes, would permit a more detailed comparison with the data.

Table 9.11 Comparison between BS predictions and experimental results

Average Multiplicity		BS	Experimental
$\langle n_{\mathrm{ch}} \rangle$	D^+	2.06	2.33 ± 0.04
	D^0	2.14	2.55 ± 0.04
	D_s^+	2.08	2.6 ± 0.3
$\langle n_{K^+} \rangle$	D^+	0.02	0.05 ± 0.01
	D^0	0.02	0.02 ± 0.01
	D_s^+	0.22	0.32 ± 0.18
$\langle n_{K^-} \rangle$	D^+	0.25	0.23 ± 0.02
	D^0	0.62	0.57 ± 0.03
	D_s^+	0.19	0.05 ± 0.08
$\langle n_{K_S} \rangle$	D^+	0.34	0.25 ± 0.03
	D^0	0.16	0.37 ± 0.05
	D_s^+	0.16	0.35 ± 0.20
$\langle n_{\pi^+} \rangle$	D^+	0.78	1.3 ± 0.3
	D^0	0.68	0.60 ± 0.04
	D_s^+	0.74	1.3 ± 1.7
$\langle n_{\pi^-} \rangle$	D^+	0.27	0.37 ± 0.03
	D^0	0.44	0.65 ± 0.03
	D_s^+	0.34	0.6 ± 0.1

Table 9.9 BS: D_s^+ inclusive kaon multiplicity distribution and average

n	$B(D_S^+ \to nK^+X)$	$B(D_S^+ \to nK^-X)$	$B(D_S^+ \to nK^\pm X)$
0	77.9 ± 2.3 %	81.4 ± 1.7 %	77.2 ± 2.3 %
1	22.1 ± 2.3 %	18.6 ± 1.7 %	4.9 ± 1.6 %
2			17.8 ± 1.7 %
$n \geq 1$	22.1 ± 2.3 %	18.6 ± 1.7 %	22.8 ± 2.3 %
$\langle n \rangle$	0.22 ± 0.02	0.19 ± 0.02	0.41 ± 0.04

n	$B(D_S^+ \to nK^0x)$	$B(D_S^+ \to n\overline{K}^0x)$	$B(D_S^+ \to n(K^0 \vee \overline{K}^0)x)$	$B(D_S^+ \to nK_Sx)$
0	99.6 ± 0.1 %	93.4 ± 1.7 %	93.3 ± 1.7 %	84.6 ± 1.4 %
1	0.4 ± 0.1 %	6.6 ± 1.7 %	6.4 ± 1.7 %	15.3 ± 1.4 %
2			0.3 ± 0.1 %	0.07 ± 0.03 %
$n \geq 1$	0.4 ± 0.1 %	6.6 ± 1.7 %	6.7 ± 1.7 %	15.4 ± 1.4 %
$\langle n \rangle$	0.004 ± 0.001	0.07 ± 0.02	0.07 ± 0.02	0.16 ± 0.01

Table 9.10 BS: D_s^+ inclusive pion multiplicity distribution and average

n	$B(D_S^+ \to n\pi^+X)$	$B(D_S^+ \to n\pi^-X)$	$B(D_S^+ \to n\pi^\pm X)$	$B(D_S^+ \to n\pi^0X)$
0	39.0 ± 3.3 %	66.7 ± 0.4 %	39.0 ± 3.3 %	53.2 ± 2.7 %
1	48.4 ± 1.6 %	32.6 ± 0.4 %	27.7 ± 3.3 %	22.5 ± 1.0 %
2	12.4 ± 1.8 %	0.8 ± 0.1 %	20.8 ± 1.8 %	9.6 ± 0.3 %
3	0.17 ± 0.13 %		11.8 ± 1.8 %	9.5 ± 0.5 %
4			0.58 ± 0.05 %	4.7 ± 1.0 %
5			0.17 ± 0.13 %	0.37 ± 0.05 %
$n \geq 1$	61.0 ± 3.3 %	33.3 ± 0.4 %	61.0 ± 3.3 %	46.8 ± 2.7 %
$\langle n \rangle$	0.74 ± 0.05	0.341 ± 0.005	1.08 ± 0.06	0.91 ± 0.07

Section 9.4 Conclusions

Comparing the BS model's inclusive predictions with the experimentally determined results (see Table 9.11) reveals that the average charged particle multiplicity predictions are too low. This is expected since there are no predictions available for the high multiplicity decay modes (such as VV or PA decays). Due to the large number of

Table 9.7 BS: D^0 inclusive kaon multiplicity distribution and average

n	$B(D^0 \to nK^+X)$	$B(D^0 \to nK^-X)$	$B(D^0 \to nK^\pm X)$
0	98.3 ± 0.20 %	38.1 ± 3.2 %	37.8 ± 3.2 %
1	1.7 ± 0.2 %	62.0 ± 3.2 %	60.9 ± 3.1 %
2			1.4 ± 0.1 %
$n \geq 1$	1.7 ± 0.2 %	61.9 ± 3.2 %	62.2 ± 3.2 %
$\langle n \rangle$	0.017 ± 0.002	0.62 ± 0.03	0.64 ± 0.03

n	$B(D^0 \to nK^0X)$	$B(D^0 \to n\overline{K}^0X)$	$B(D^0 \to n(K^0 \vee \overline{K}^0)X)$	$B(D^0 \to nK_SX)$
0	99.65 ± 0.06 %	68.7 ± 3.2 %	68.3 ± 3.2 %	84.0 ± 1.6 %
1	0.35 ± 0.06 %	31.3 ± 3.2 %	31.7 ± 3.2 %	15.9 ± 1.6 %
2			0 ± 0 %	0.12 ± 0.04 %
$n \geq 1$	0.35 ± 0.06 %	31.3 ± 3.2 %	31.7 ± 3.2 %	16.0 ± 1.6 %
$\langle n \rangle$	0.004 ± 0.001	0.31 ± 0.03	0.32 ± 0.03	0.16 ± 0.02

Table 9.8 BS: D^0 inclusive pion multiplicity distribution and average

n	$B(D^0 \to n\pi^+X)$	$B(D^0 \to n\pi^-X)$	$B(D^0 \to n\pi^\pm X)$	$B(D^0 \to n\pi^0X)$
0	37.6 ± 4.0 %	65.2 ± 3.0 %	26.6 ± 2.7 %	53.1 ± 2.6 %
1	57.4 ± 3.8 %	25.6 ± 1.9 %	49.5 ± 3.6 %	39.4 ± 2.6 %
2	5.0 ± 1.0 %	9.1 ± 1.0 %	14.5 ± 2.0 %	5.5 ± 0.6 %
3	0.1 ± 0.1 %	0.1 ± 0.1 %	4.4 ± 0.5 %	1.4 ± 0.5 %
4			4.8 ± 1.0 %	0.29 ± 0.07 %
5			0 ± 0 %	0.2 ± 0.2 %
6			0.1 ± 0.1 %	0.007 ± 0.008 %
7				0.03 ± 0.03 %
$n \geq 1$	62.4 ± 4.0 %	34.8 ± 3.0 %	73.4 ± 2.7 %	46.9 ± 2.6 %
$\langle n \rangle$	0.68 ± 0.04	0.44 ± 0.04	1.12 ± 0.06	0.57 ± 0.04

Table 9.5 BS: D^+ inclusive kaon multiplicity distribution and average

n	$B(D^+ \to nK^+X)$	$B(D^+ \to nK^-X)$	$B(D^+ \to nK^\pm X)$
0	98.4 ± 0.2 %	74.6 ± 2.4 %	73.4 ± 2.2 %
1	1.6 ± 0.2 %	25.4 ± 2.4 %	26.3 ± 2.2 %
2			0.35 ± 0.09 %
$n \geq 1$	1.6 ± 0.2 %	25.4 ± 2.4 %	26.6 ± 2.2 %
$\langle n \rangle$	0.016 ± 0.002	0.25 ± 0.02	0.27 ± 0.22

n	$B(D^+ \to nK^0X)$	$B(D^+ \to n\overline{K}^0X)$	$B(D^+ \to n(K^0 \vee \overline{K}^0)X)$	$B(D^+ \to nK_SX)$
0	99.62 ± 0.08 %	33.1 ± 2.9 %	33.1 ± 2.9 %	66.4 ± 1.5 %
1	0.38 ± 0.08 %	66.9 ± 2.9 %	66.5 ± 2.8 %	33.5 ± 1.4 %
2			0.38 ± 0.08 %	0.09 ± 0.02 %
$n \geq 1$	0.38 ± 0.08 %	66.9 ± 2.9 %	66.9 ± 2.9 %	33.6 ± 1.5 %
$\langle n \rangle$	0.004 ± 0.001	0.67 ± 0.03	0.67 ± 0.03	0.34 ± 0.02

Table 9.6 BS: D^+ inclusive pion multiplicity distribution and average

n	$B(D^+ \to n\pi^+X)$	$B(D^+ \to n\pi^-X)$	$B(D^+ \to n\pi^\pm X)$	$B(D^+ \to n\pi^0X)$
0	32.3 ± 2.7 %	73.2 ± 0.6 %	32.3 ± 2.7 %	60.4 ± 2.9 %
1	57.8 ± 1.0 %	26.6 ± 0.6 %	39.8 ± 2.3 %	27.9 ± 2.4 %
2	9.7 ± 2.2 %	0.18 ± 0.07 %	19.2 ± 1.8 %	6.7 ± 0.3 %
3	0.18 ± 0.07 %		8.6 ± 2.1 %	4.9 ± 0.4 %
4			0 ± 0 %	0.009 ± 0.002 %
5			0.18 ± 0.07 %	0.07 ± 0.04 %
6				
7				
$n \geq 1$	67.7 ± 2.7 %	26.8 ± 0.6 %	67.7 ± 2.7 %	39.6 ± 2.9 %
$\langle n \rangle$	0.78 ± 0.05	0.269 ± 0.006	1.05 ± 0.05	0.56 ± 0.04

Table 9.4 BS: inclusive charged particle multiplicity distribution and average

n	$B(D^+ \to nP^\pm X^0)$	$B(D^0 \to nP^\pm X^0)$	$B(D_s^+ \to nP^\pm X^0)$
0		3.4 ± 0.7 %	
1	47.3 ± 1.8 %		47.1 ± 1.7 %
2		86.5 ± 1.5 %	
3	52.4 ± 1.8 %		51.9 ± 1.7 %
4		9.9 ± 1.1 %	
5	0.32 ± 0.07 %		1.0 ± 0.1 %
6		0.1 ± 0.1 %	
7	$(1.5 \pm 0.7) \times 10^{-3}$ %		0.008 ± 0.001 %
8		0.001 ± 0.001 %	
$\langle n \rangle$	2.06 ± 0.04	2.14 ± 0.03	2.08 ± 0.03

Section 10.3 Inclusive Predictions

Multiplicity Distributions

I calculate the inclusive predictions* (Tables 10.4—10.10) by employing the procedures described in Chapter 6 and by using the exclusive decay modes listed in Tables 10.1—10.3. Uncertainties listed for these inclusive properties emanate from the experimental uncertainties of the exclusive modes' branching ratios.

The next section presents a comparison of these inclusive predictions to the experimental results of Chapter 5. In Chapter 11 I tabulate the results of all the models and experimental results.

Table 10.4 PDG: inclusive charged particle multiplicity distribution and average†

n	$B(D^+ \to nP^\pm X^0)$	$B(D^0 \to nP^\pm X^0)$	$B(D_s^+ \to nP^\pm X^0)$
0		2.1 ± 0.4 %	
1	23.7 ± 2.4 %		26.8 ± 2.2 %
2		67.9 ± 1.6 %	
3	66.2 ± 2.3 %		62.8 ± 2.1 %
4		29.5 ± 1.6 %	
5	10.0 ± 1.5 %		10.3 ± 1.1 %
6		0.47 ± 0.05 %	
7	0.08 ± 0.04 %		0.07 ± 0.01 %
8		$(6.3 \pm 1.2)\times 10^{-4}$ %	
$\langle n \rangle$	2.73 ± 0.06	2.57 ± 0.03	2.67 ± 0.05

* See Section 1.3 for a description of these inclusive predictions.

† Charged particle multiplicities greater than eight have not been included in Table 10.4 in order that perspicuity be maintained.

Table 10.5 PDG: D^+ inclusive kaon multiplicity distribution and average

n	$B(D^+ \to nK^+X)$	$B(D^+ \to nK^-X)$	$B(D^+ \to nK^\pm X)$
0	91.8 ± 1.2 %	62.5 ± 4.4 %	58.6 ± 4.4 %
1	8.2 ± 1.2 %	37.5 ± 4.4 %	37.1 ± 4.5 %
2			4.3 ± 0.9 %
$n \geq 1$	8.2 ± 1.2 %	37.5 ± 4.4 %	41.4 ± 4.4 %
$\langle n \rangle$	0.08 ± 0.01	0.38 ± 0.04	0.46 ± 0.05

n	$B(D^+ \to nK^0X)$	$B(D^+ \to n\overline{K}^0X)$	$B(D^+ \to n(K^0 \vee \overline{K}^0)X)$	$B(D^+ \to nK_SX)$
0	98.2 ± 0.7 %	42.8 ± 4.5 %	41.6 ± 4.5 %	69.0 ± 2.3 %
1	1.8 ± 0.7 %	54.5 ± 4.4 %	55.1 ± 4.4 %	30.2 ± 2.2 %
2		2.7 ± 0.6 %	3.3 ± 0.7 %	0.8 ± 0.2 %
3			0.010 ± 0.003 %	0.0012 ± 0.0003 %
$n \geq 1$	1.8 ± 0.7 %	57.2 ± 4.5 %	58.4 ± 4.5 %	31.1 ± 2.3 %
$\langle n \rangle$	0.018 ± 0.007	0.60 ± 0.05	0.62 ± 0.05	0.32 ± 0.02

Table 10.6 PDG: D^+ inclusive pion multiplicity distribution and average

n	$B(D^+ \to n\pi^+X)$	$B(D^+ \to n\pi^-X)$	$B(D^+ \to n\pi^\pm X)$	$B(D^+ \to n\pi^0X)$
0	12.0 ± 1.8 %	60.2 ± 4.0 %	12.0 ± 1.8 %	42.3 ± 3.7 %
1	40.5 ± 3.7 %	31.9 ± 2.8 %	30.7 ± 4.1 %	40.0 ± 4.3 %
2	39.8 ± 3.3 %	8.0 ± 1.5 %	27.2 ± 3.4 %	12.8 ± 2.8 %
3	7.6 ± 1.1 %	0.04 ± 0.04 %	20.6 ± 2.5 %	3.9 ± 0.5 %
4	0.04 ± 0.04 %		3.3 ± 1.3 %	1.0 ± 0.2 %
5			6.1 ± 1.0 %	0.014 ± 0.006 %
6			0 ± 0 %	$(4 \pm 1)\times 10^{-5}$ %
7			0.04 ± 0.04 %	
$n \geq 1$	88.0 ± 1.8 %	39.8 ± 4.0 %	88.0 ± 1.8 %	57.7 ± 3.7 %
$\langle n \rangle$	1.43 ± 0.05	0.48 ± 0.05	1.91 ± 0.09	0.81 ± 0.05

Table 10.7 PDG: D^0 inclusive kaon multiplicity distribution and average

n	$B(D^0 \to nK^+X)$	$B(D^0 \to nK^-X)$	$B(D^0 \to nK^\pm X)$
0	96.7 ± 0.6 %	41.8 ± 3.1 %	41.2 ± 3.1 %
1	3.3 ± 0.6 %	58.2 ± 3.1 %	56.1 ± 3.1 %
2		003 ± 0.001%	2.7 ± 0.5 %
3			003 ± 0.001%
$n \geq 1$	3.3 ± 0.6 %	58.2 ± 3.1 %	58.8 ± 3.1 %
$\langle n \rangle$	0.033 ± 0.006	0.58 ± 0.03	0.62 ± 0.03

n	$B(D^0 \to nK^0X)$	$B(D^0 \to n\overline{K}^0X)$	$B(D^0 \to n(K^0 \vee \overline{K}^0)X)$	$B(D^0 \to nK_SX)$
0	99.4 ± 0.2 %	61.2 ± 3.1 %	60.8 ± 3.1 %	80.0 ± 1.6 %
1	0.6 ± 0.2 %	38.8 ± 3.1 %	39.1 ± 3.1 %	19.7 ± 1.6 %
2			0.13 ± 0.04 %	0.17 ± 0.02 %
3				0.08 ± 0.02 %
$n \geq 1$	0.6 ± 0.2 %	38.8 ± 3.1 %	39.2 ± 3.1 %	20.0 ± 1.6 %
$\langle n \rangle$	0.006 ± 0.002	0.39 ± 0.03	0.39 ± 0.03	0.20 ± 0.02

Table 10.8 PDG: D^0 inclusive pion multiplicity distribution and average

n	$B(D^0 \to n\pi^+X)$	$B(D^0 \to n\pi^-X)$	$B(D^0 \to n\pi^\pm X)$	$B(D^0 \to n\pi^0X)$
0	18.7 ± 1.8 %	46.0 ± 3.2 %	13.1 ± 1.4 %	35.6 ± 2.5 %
1	56.1 ± 2.4 %	39.5 ± 2.3 %	38.5 ± 3.3 %	28.5 ± 2.5 %
2	25.0 ± 1.6 %	14.2 ± 1.1 %	20.6 ± 2.1 %	31.5 ± 3.5 %
3	0.28 ± 0.05 %	0.28 ± 0.05 %	15.9 ± 1.3 %	2.3 ± 0.4 %
4			11.6 ± 1.1 %	2.2 ± 0.4 %
5			$(4 \pm 1) \times 10^{-4}$ %	$(5 \pm 1) \times 10^{-5}$ %
6			0.28 ± 0.05 %	0.03 ± 0.02 %
$n \geq 1$	81.3 ± 1.8 %	54.0 ± 3.2 %	86.9 ± 1.4 %	64.4 ± 2.5 %
$\langle n \rangle$	1.07 ± 0.03	0.69 ± 0.04	1.76 ± 0.06	1.07 ± 0.06

Table 10.9 PDG: D_s^+ inclusive kaon multiplicity distribution and average

n	$B(D_s^+ \to nK^+X)$	$B(D_s^+ \to nK^-X)$	$B(D_s^+ \to nK^\pm X)$
0	71.2 ± 2.6 %	71.1 ± 3.0 %	61.3 ± 3.3 %
1	28.8 ± 2.6 %	28.9 ± 3.0 %	19.7 ± 2.8 %
2			19.0 ± 2.4 %
$n \geq 1$	28.8 ± 2.6 %	28.9 ± 3.0 %	38.7 ± 3.3 %
$\langle n \rangle$	0.29 ± 0.03	0.29 ± 0.03	0.58 ± 0.05

n	$B(D_s^+ \to nK^0X)$	$B(D_s^+ \to n\overline{K}^0X)$	$B(D_s^+ \to n(K^0 \vee \overline{K}^0)X)$	$B(D_s^+ \to nK_SX)$
0	84.2 ± 2.7 %	84.5 ± 2.3 %	74.6 ± 3.5 %	77.4 ± 2.0 %
1	15.8 ± 2.7 %	15.5 ± 2.3 %	19.4 ± 2.7 %	21.1 ± 1.9 %
2			5.9 ± 1.2 %	1.5 ± 0.3 %
$n \geq 1$	15.8 ± 2.7 %	15.5 ± 2.3 %	25.4 ± 3.5 %	22.6 ± 2.0 %
$\langle n \rangle$	0.16 ± 0.03	0.16 ± 0.02	0.31 ± 0.04	0.24 ± 0.02

Table 10.10 PDG: D_s^+ inclusive pion multiplicity distribution and average

n	$B(D_s^+ \to n\pi^+X)$	$B(D_s^+ \to n\pi^-X)$	$B(D_s^+ \to n\pi^\pm X)$	$B(D_s^+ \to n\pi^0X)$
0	9.6 ± 1.420.0 %	51.7 ± 2.3 %	9.6 ± 1.4 %	36.9 ± 3.5 %
1	41.2 ± 2.3 %	43.5 ± 1.7 %	35.6 ± 2.5 %	33.7 ± 2.7 %
2	41.0 ± 2.0 %	4.9 ± 0.7 %	12.1 ± 1.7 %	13.6 ± 0.5 %
3	8.2 ± 0.9 %		34.5 ± 2.4	6.1 ± 0.5 %
4			3.4 ± 0.7 % %	8.1 ± 1.2 %
5			4.9 ± 0.7 %	0.5 ± 0.1 %
6				1.1 ± 0.3 %
$n \geq 1$	90.4 ± 1.4 %	48.3 ± 2.3 %	90.4 ± 1.4 %	63.1 ± 3.5 %
$\langle n \rangle$	1.48 ± 0.04	0.53 ± 0.03	2.01 ± 0.06	1.21 ± 0.07

Momentum Spectra

I derive the center-of-mass momentum spectra (Figures 10.1—10.3) using data generated by Monte Carlo simulations of the exclusive decay modes (Tables 10.1—10.3). Because the spectra use Monte Carlo generated data, they do not have any geometric,

reconstruction, resolution or particle identification losses. Each spectrum has been normalized to the total number of tags in the Monte Carlo. This assures that the height of a monochromatic peak directly indicates a mode's exclusive branching ratio. However, since the total branching ratio must equal 100%, the branching ratios derived from the momentum spectra will not equal the branching ratios put into the simulation, but will differ by a multiplicative constant equal to the sum of the branching ratios.

The following structure is noted in the D^+ spectra (Figure 10.1):

a. $\overline{K}^0\pi^+$ — a monochromatic peak equivalent to a branching ratio of about 2.7%, visible in the K_S and π^+ spectra,

b. $\overline{K}^0K^+$ — a monochromatic peak appearing in the K_S and K^+ spectra, corresponding to a branching ratio of 0.76%,

c. $\overline{K}^0\rho^+$ — a broadened peak due to the width of the ρ^+,

d. $\eta\pi^+$ — a monochromatic peak in the π^+ spectrum,

e. $\overline{K}^{*0}\pi^+$ — a wide structure due to the width of the $\overline{K}^{*0}$,

f. $\phi\pi^+$ — a monochromatic peak visible in the π^+ spectrum,

g. $\overline{K}^{*0}K^+$ — the width of the $\overline{K}^{*0}$ broadens this peak observable in the K^+ spectrum.

No other structures are identifiable or expected. Other apparent peaks, notably in the K^+ spectrum, result from statistical fluctuations in the Monte Carlo sample.

The D^0 spectra have the following structures notated (Figure 10.2):

a. $K^-\pi^+$ — visible as a monochromatic peak in both the K^- and π^+ spectra with peak height corresponding to a branching ratio of 3.4%,

b. K^-K^+ — a monochromatic peak equivalent to a branching ratio of approximately 0.36%,

c. $K^-\rho^+$ — a short peak, broadened by the width of the ρ^+,

d. $\pi^-\pi^+$ — a small, monochromatic peak visible in the π^+ and π^- spectra,

e. $K^{*-}\pi^+$ — broadened by the width of the K^{*-},

f. $K^{*-}K^{+}$ — a small peak, barely statistically significant, broadened by the width of the K^{*-}, observable in the K^{+} spectrum,

g. $\pi^{0}\overline{K}^{*0}$ — a small, broad peak in the π^{0} spectrum,

h. $\pi^{0}\overline{K}^{0}$ — a monochromatic peak visible in both the π^{0} and K_S spectra, corresponding to a branching ratio of about 1.9%,

i. $\overline{K}^{0}\omega$ — a narrow peak visible in the K_S spectrum,

j. $\overline{K}^{0}\phi$ — a narrow peak seen in the K_S spectrum.

Structures observed in the D_s^{+} spectra (Figure 10.3) are:

a. $\overline{K}^{0}K^{+}$ — a large monochromatic spike observed in both the K_S and K^{+} spectra, corresponding to a branching ratio of 4.8%,

b. $\overline{K}^{0}K^{*+}$ — a peak in the K_S spectrum broadened by the width of the K^{*+},

c. $\eta\pi^{+}$ — seen in the π^{+} spectrum as a monochromatic peak with a 2.5% branching ratio,

d. $\eta'\pi^{+}$ — a large monochromatic peak visible in the π^{+} spectrum,

e. $\phi\pi^{+}$ — a narrow peak observed in the π^{+} spectrum,

f. $\overline{K}^{*0}K^{+}$ — a broad peak, due to the width of the $\overline{K}^{*0}$, in the K^{+} spectrum.

Statistical fluctuations are responsible for all other apparent structures.

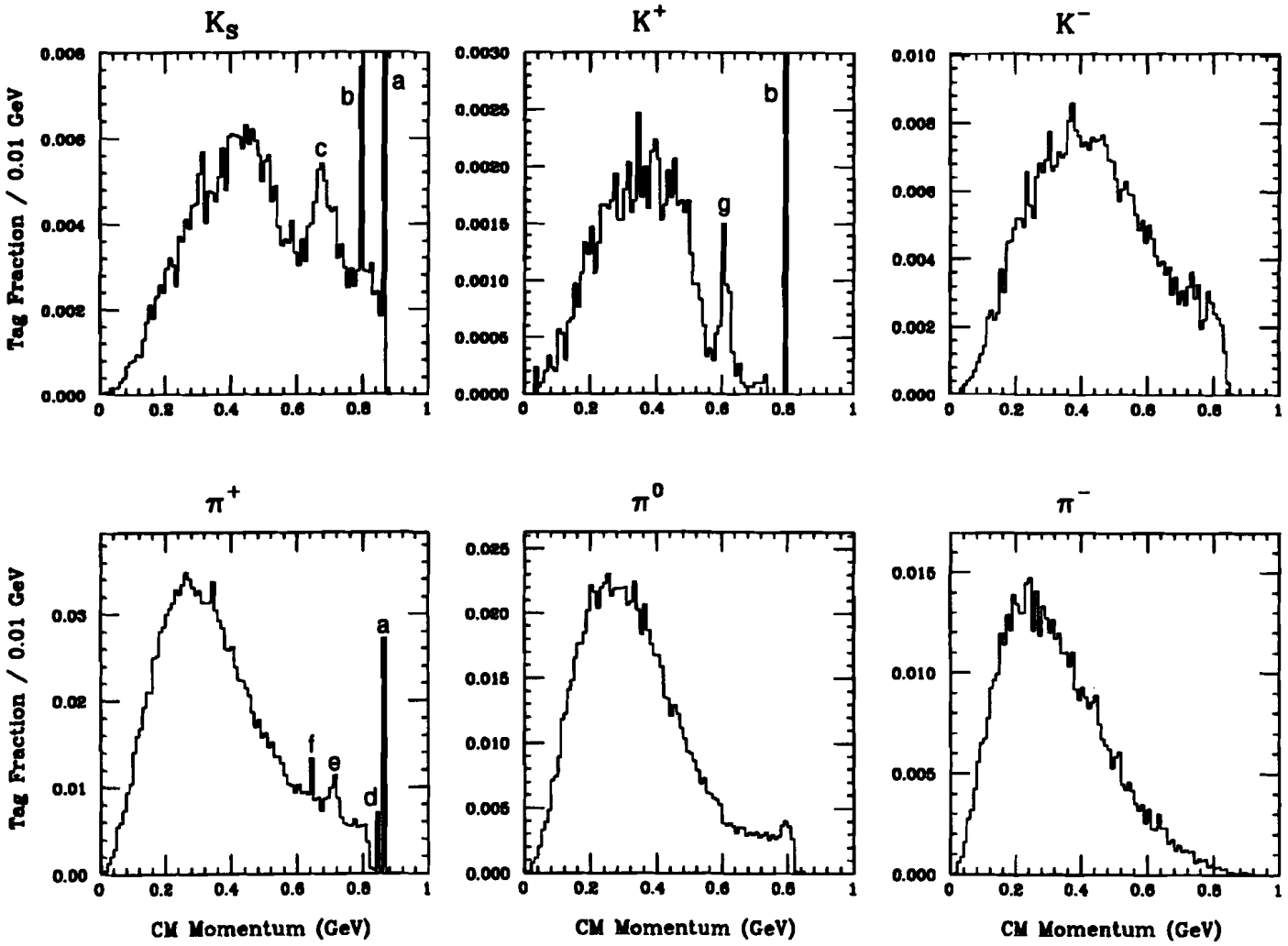

Figure 10.1 PDG: D^+ center-of-mass momentum spectra (letters indicating structure are explained in the text)

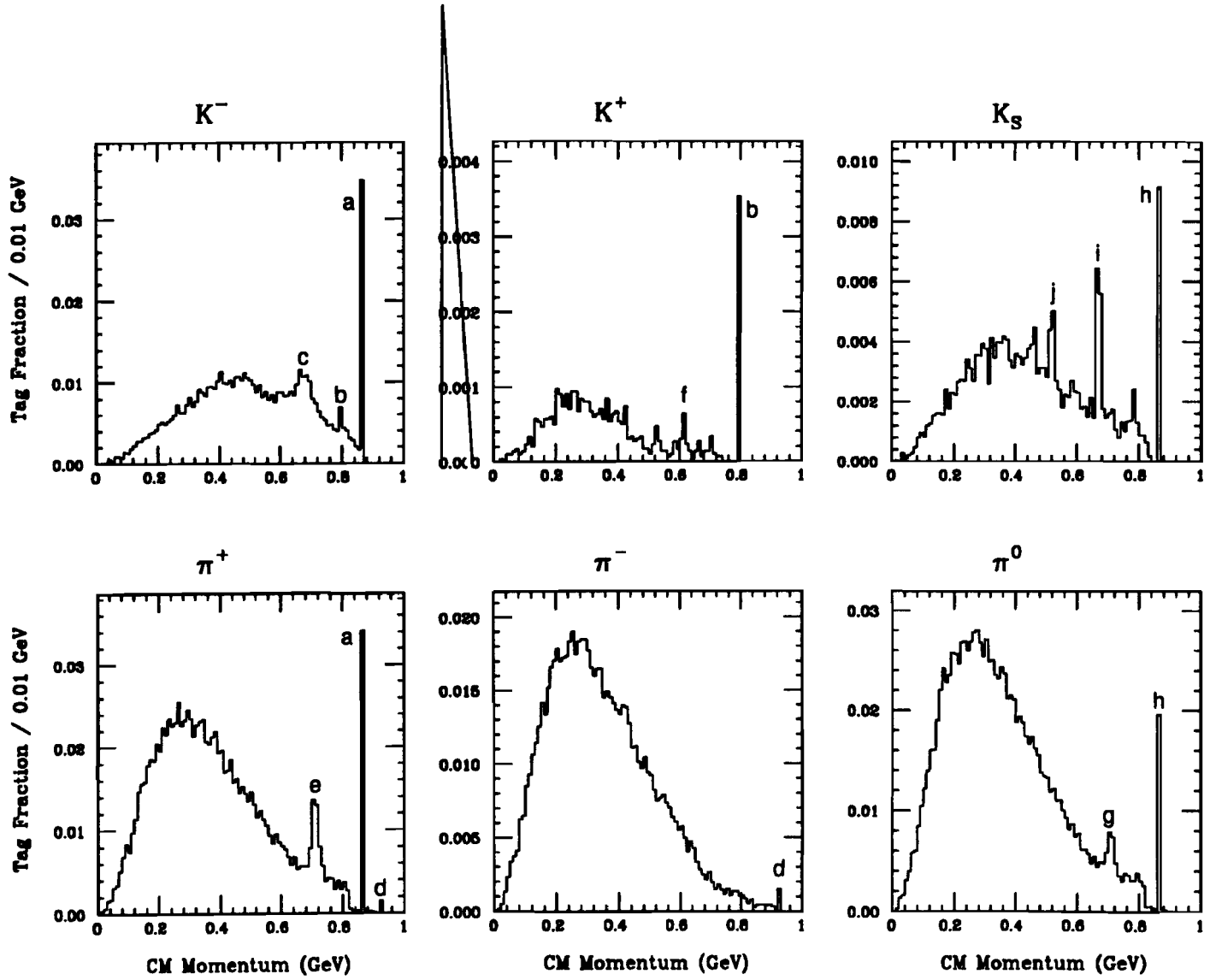

Figure 10.2 PDG: D^0 center-of-mass momentum spectra (letters indicating structure are explained in the text)

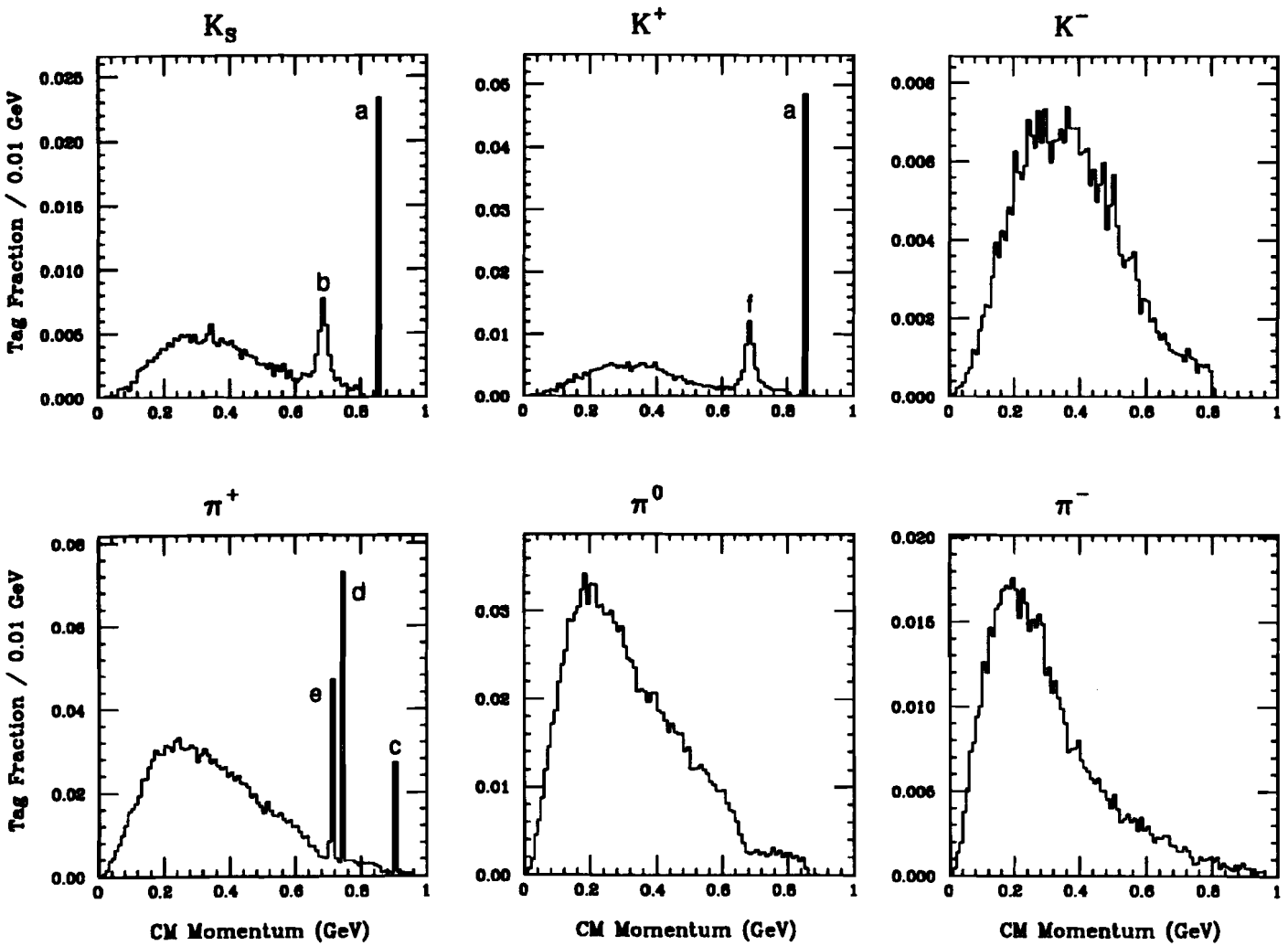

Figure 10.3 PDG: D_s^+ center-of-mass momentum spectra (letters indicating structure are explained in the text)

Section 10.4 Conclusions and Enhancements

A comparison between the predicted inclusive properties of the PDG model and my experimental results (see Table 10.11) reveals that the predicted average charged particle multiplicity for the D^+ is 6σ larger than the measured multiplicity (using a quadrature-added combination of theoretical and experimental errors). As well, the K^+, K^-, K_S, π^+, and π^- predicted average multiplicities are larger than their experimentally observed counterparts by varying degrees. This suggests that low charged particle multiplicity modes remain unaccounted for. One such source comes from modes with one kaon and many neutral pions. A comparison of the π^0 average multiplicity with a previous experimental result[35] strengthens this conviction.

In an attempt to test this hypothesis, I enhance the PDG model for the D^+ with additional modes (see Table 10.12). I use the branching ratios of the non-resonant decay modes of the D^+, which contain $\pi^+\pi^-$ pairs, to generate new modes with $\pi^0\pi^0$ pairs. This augmented model, called PDG+, results in a slight reduction in the average charged particle multiplicity as well as a reduction in the charged kaon average multiplicity (see Table 10.11 under the "PDG+" heading). A significant increase (38%) in neutral pions now makes the prediction less than 1σ from the observed result. Although the enhanced model does not match the experimental results, I believe that missing π^0 modes are the largest gap in our knowledge of D^+ exclusive decay modes.

D^0 predictions closely match experimental observations for charged particles, charged kaons and the π^-. However, a paucity of neutral kaons and neutral pions, combined with a surplus of π^+, leads to a hypothesis which is similar to that above — modes with neutral pions are missing. Augmentation of the D^0 model (see Table 10.13) results in a closer match for all three classes of pion, but lowers the overall charged particle multiplicity (Table 10.11).

Even with many exclusive decay modes almost certainly missing, the D_s^+ predictions do a remarkable job at matching the experimental results. The largest difference occurs

in the average K^- multiplicity. Enhancement of the D_s^+ model would be of limited value and is not performed.

Table 10.11 Comparison between PDG predictions and experimental results

Average Multiplicity		PDG	PDG+	Experimental
$\langle n_{\rm ch} \rangle$	D^+	2.73 ± 0.06	2.63 ± 0.09	2.33 ± 0.04
	D^0	2.57 ± 0.03	2.39 ± 0.05	2.55 ± 0.04
	D_s^+	2.67 ± 0.05		2.6 ± 0.3
$\langle n_{K^+} \rangle$	D^+	0.08 ± 0.01	0.07 ± 0.01	0.05 ± 0.01
	D^0	0.03 ± 0.01	0.03 ± 0.01	0.02 ± 0.01
	D_s^+	0.29 ± 0.03		0.32 ± 0.18
$\langle n_{K^-} \rangle$	D^+	0.38 ± 0.04	0.34 ± 0.04	0.23 ± 0.02
	D^0	0.58 ± 0.03	0.53 ± 0.03	0.57 ± 0.03
	D_s^+	0.29 ± 0.03		0.05 ± 0.08
$\langle n_{K_S} \rangle$	D^+	0.32 ± 0.02	0.32 ± 0.02	0.25 ± 0.03
	D^0	0.20 ± 0.02	0.20 ± 0.02	0.37 ± 0.05
	D_s^+	0.24 ± 0.02		0.35 ± 0.20
$\langle n_{\pi^+} \rangle$	D^+	1.43 ± 0.05	1.43 ± 0.07	1.3 ± 0.3
	D^0	1.07 ± 0.03	0.99 ± 0.03	0.60 ± 0.04
	D_s^+	1.48 ± 0.04		1.3 ± 1.7
$\langle n_{\pi^-} \rangle$	D^+	0.48 ± 0.05	0.46 ± 0.05	0.37 ± 0.03
	D^0	0.69 ± 0.04	0.65 ± 0.04	0.65 ± 0.03
	D_s^+	0.53 ± 0.03		0.6 ± 0.1
$\langle n_{\pi^0} \rangle$	D^+	0.81 ± 0.05	1.10 ± 0.08	1.2 ± 0.2[a]
	D^0	1.07 ± 0.06	1.31 ± 0.06	1.3 ± 0.2[a]
	D_s^+	1.21 ± 0.07		2.0 ± 1.1[a]

[a] result from Reference 35

Table 10.12 PDG+: postulated additional D^+ exclusive decay modes

D^+ Decay Mode	BR(%)
$\overline{K}^0 \pi^0 \pi^0 \ell^+ \nu$	2.2 ± 2.9
$K^- \pi^+ \pi^+ \pi^+ \pi^-$	2.2 ± 3.0

Table 10.12 (Continued) PDG+: postulated additional D^+ exclusive decay modes

D^+ Decay Mode	BR(%)
$K^-\pi^+\pi^+\pi^0\pi^0\pi^0$	0.19 ± 0.20
$\overline{K}^0\pi^+\pi^0\pi^0$	1.2 ± 0.8
$\overline{K}^0\pi^+\pi^0\pi^0\pi^0$	8.7 ± 2.6
$\overline{K}^0\pi^+\pi^+\pi^-\pi^0\pi^0$	0.1 ± 0.1
$\overline{K}^0\pi^+\pi^0\pi^0\pi^0\pi^0$	0.1 ± 0.1
$\pi^+\pi^0\pi^0$	0.28 ± 0.06
$\pi^+\pi^0\pi^0\pi^0$	2.3 ± 1.7
$\pi^+\pi^+\pi^-\pi^0\pi^0$	0.15 ± 0.11
$\pi^+\pi^0\pi^0\pi^0\pi^0$	0.15 ± 0.11
$\pi^+\pi^+\pi^-\pi^0\pi^0\pi^0$	0.28 ± 0.29
$\pi^+\pi^0\pi^0\pi^0\pi^0\pi^0$	0.28 ± 0.29
BR Sum	18.1

Table 10.13 PDG+: postulated additional D^0 exclusive decay modes

D^0 Decay Mode	BR(%)
$\pi^0\pi^0$	0.163 ± 0.019
$\pi^0\pi^0\pi^0$	1.5 ± 1.0
$\pi^+\pi^-\pi^0\pi^0$	0.75 ± 0.09
$\pi^0\pi^0\pi^0\pi^0$	0.75 ± 0.09
$\pi^+\pi^-\pi^0\pi^0\pi^0$	1.7 ± 0.5
$\pi^0\pi^0\pi^0\pi^0\pi^0$	1.7 ± 0.5
$\overline{K}^0\pi^0\pi^0$	1.8 ± 0.5
$\overline{K}^0\pi^0\pi^0\pi^0$	2.2 ± 2.2
$\overline{K}^0\pi^0\pi^0\pi^0\pi^0$	0.85 ± 0.14
$K^+K^-\pi^0\pi^0\pi^0$	0.28 ± 0.20
$\overline{K}^{*0}\pi^0\pi^0\pi^0$	1.6 ± 0.8
$\phi\pi^0\pi^0$	0.24 ± 0.08
BR Sum	13.5

PART IV
CONCLUSIONS

"This is not the end.

It is not even the beginning of the end.

But it is, perhaps, the end of the beginning."

Winston Churchill

(Nov. 10, 1942)

Chapter 11 Conclusions

Section 11.1 Comparisons

A comparison (see Table 11.1) of my unfolded inclusive charged particle distribution shows good agreement with three previous experimental results — a parallel Mark III analysis,[35] the Mark II collaboration's analysis,[37] and an early analysis by the Mark I (Lead Glass Wall) collaboration.[55] A summary of the theoretical models' results is also listed in Table 11.1, although the discussions of these results are presented in the relevant chapters describing each model. All of these analyses include the charged pions from K_S decays in their distributions. While the charged particle distribution without K_S pions is not accessible, the average charged particle multiplicity without K_S pions, $\langle n_{\rm ch}\rangle'$, is calculable through the formula:

$$\langle n_{\rm ch}\rangle' = \langle n_{\rm ch}\rangle - 2 \times \langle n_{K_S}\rangle \times (0.686 + 0.314 \times 0.012 \times 2)$$

which subtracts the contributions from $K_S \rightarrow \pi^+\pi^-$ (68.6%) and from $K_S \rightarrow \pi^0\pi^0$ (31.4%), where one of the neutral pions decays via $\pi^0 \rightarrow \gamma e^+e^-$ (1.2%).

A comparison of kaon inclusive branching ratios (see Table 11.2) reveals generally good agreement except in the case of $B\left(D^0 \rightarrow \left(K^0 \vee \overline{K}^0\right)X\right)$, which shows a 4σ disparity, the origin of which is unknown.

I convert my K_S results to a $K^0 \vee \overline{K}^0$ form assuming that K_S's only arise from K^0 or $\overline{K}^0$ decays. If k_i is the fraction of i-($K^0 \vee \overline{K}^0$) and s_i is the percentage of i-K_S events with $\sum k_i = \sum s_i = 1$, then it is easy to convert between the two distributions via:

$$s_0 = k_0 + \frac{k_1}{2} + \frac{k_2}{4}$$
$$s_1 = \frac{k_1}{2} + \frac{k_2}{2}$$
$$s_2 = \frac{k_2}{4}$$
$$B(D \to K_S X) = 1 - s_0$$

$$k_0 = s_0 - s_1 + s_2$$
$$k_1 = 2s_1 - 4s_2$$
$$k_2 = 4s_2$$
$$B\left(D \to \left(K^0 \vee \overline{K}^0\right)X\right) = 1 - k_0 .$$

There are no previous experimental results with which to compare my average charged pion multiplicity. I have, however, included the measurement[35] of the average neutral pion multiplicity in Table 11.3 for comparison with the theoretical models.

All of the experimental and theoretical inclusive pion properties include pions from the decay of K_S. To calculate the average pion multiplicity without this source of pions, $\langle n_\pi \rangle'$, use the following formulae:

$$\langle n_{\pi^\pm} \rangle' = \langle n_{\pi^\pm} \rangle - \langle n_{K_S} \rangle \times 0.686 \times 2$$
$$\langle n_{\pi^+} \rangle' = \langle n_{\pi^+} \rangle - \langle n_{K_S} \rangle \times 0.686$$
$$\langle n_{\pi^-} \rangle' = \langle n_{\pi^-} \rangle - \langle n_{K_S} \rangle \times 0.686$$
$$\langle n_{\pi^0} \rangle' = \langle n_{\pi^0} \rangle - \langle n_{K_S} \rangle \times 0.314 \times 2 .$$

Section 11.2 Conclusions

Inclusive analyses provide new insight into our understanding of weak decay physics. Both experimental and theoretical realms benefit from the new techniques developed and presented in this thesis.

On the experimental side, the use of a new analysis tool, the fold tensor, has enabled the first inclusive charged pion results to be obtained, albeit without any surprises. In the kaon sector, however, the ratio of strangeness content for the D^+, D^0, and D_s^+ decays is about $1 : 1.7 \pm 0.2 : 1.3 \pm 0.5$ and not the 1:1:2 as one would naively suspect in the spectator model — suggesting that weak annihilation processes play a larger role than first thought.

These pion and kaon results, coupled with the average charged particle multiplicity permits a "back-door" method of obtaining the inclusive lepton multiplicities. From the relation $\langle n_{\rm ch} \rangle = \langle n_{K^\pm} \rangle + \langle n_{\pi^\pm} \rangle + \langle n_{\ell^\pm} \rangle$ one can obtain the average lepton multiplicity. There are no surprises in the D^+ and D_s^+ results, but my D^0 lepton multiplicity was four times (or 3σ) greater than previous results. This invites future research.

On the theoretical side, a new program, PREDICT, provides the first inclusive look at theoretical models and reveals major shortcomings, namely an insufficient number of exclusive modes. Both two-body resonant and multi-body non-resonant modes must be added to all the models before a better examination of the models can be accomplished. It is hoped that the models' authors will accept the challenge and provide predictions for the missing modes.

Table 11.1 Comparison of inclusive charged particle properties

		Charged Particle Properties							
		$B(D \to nP^{\pm}X^0)$ (%)							$\langle n_{ch} \rangle$
Experimental		0	1	2	3	4	5	6	
This Thesis	D^+		40.6 ± 1.8		52.5 ± 1.9		6.9 ± 0.9		2.33 ± .04
	D^0	5.6 ± 1.0		63.5 ± 1.9		28.7 ± 1.8		2.2 ± 0.6	2.55 ± .04
	D_s^+		32 ± 11		56 ± 14		12 ± 9		2.6 ± .3
Ref. 35	D^+		38.4 ± 1.8		54.1 ± 2.2		7.5 ± 1.3		2.38 ± .04
	D^0	5.4 ± 0.9		63.4 ± 1.5		29.3 ± 1.8		1.9 ± 0.2	2.56 ± .04
	D_s^+		37 ± 10		42 ± 15		21 ± 11		2.69 ± .31
Ref. 37	D^+		47 ± 5		47 ± 5		6 ± 2		2.16 ± .11
	D^0	9 ± 3		63 ± 5		22 ± 5		5 ± 3	2.47 ± .10
Ref. 55	D^+		37 ± 10		59 ± 13		4 ± 4		2.3 ± .3
	D^0	8 ± 5		73 ± 10		15 ± 5		4 ± 3	2.3 ± .3
Theoretical		0	1	2	3	4	5	6	$\langle n_{ch} \rangle$
BSW	D^+		42.2		56.2		1.6		2.19
	D^0	1.4		80.4		17.9		0.2	2.34
	D_s^+		32.4		64.4		3.2		2.42
CC	D^+		46.9		52.6		0.5		2.07
	D^0	8.1		71.2		20.3		1.4	2.28
	D_s^+		35.7		62.7		1.6		2.32
BS	D^+		47.3		52.4		0.3		2.06
	D^0	3.4		86.5		9.9		0.1	2.14
	D_s^+		47.1		51.9		1.0		2.08
PDG	D^+		23.7		66.2		10.0		2.73
	D^0	2.1		67.8		29.6		0.5	2.57
	D_s^+		26.8		62.8		10.3		2.67

Table 11.2 Comparison of inclusive kaon properties

		Kaon Inclusive Branching Ratio (%)			
Experimental		K^+	K^-	K_S	$K^0 \vee \overline{K}^0$
This Thesis	D^+	5.2 ± 0.8	22.6 ± 1.4	25.2 ± 1.8	50
	D^0	1.9 ± 0.8	57.1 ± 2.5	34.6 ± 4.9	64.4
	D_s^+	32 ± 18	5 ± 8	35 ± 20	70
Ref. 35	D^+	5.5 ± 1.3	27.1 ± 2.3		61.2 ± 6.5
	D^0	2.8 ± 0.9	60.9 ± 3.2		45.5 ± 5.0
	D_s^+	$20\,^{+18}_{-13}$	$13\,^{+14}_{-12}$		$39\,^{+28}_{-27}$
Ref. 37	D^+	6 ± 4	19 ± 5		52 ± 18
	D^0	8 ± 3	55 ± 11		29 ± 11
Ref. 55	D^+	6 ± 6	10 ± 7		39 ± 29
	D^0	$B(D^0 \to K^{\pm}X) = 35 \pm 10$			57 ± 26
Theoretical		K^+	K^-	K_S	$K^0 \vee \overline{K}^0$
BSW	D^+	3.1	69.5	67.5	36.0
	D^0	1.6	57.5	18.7	36.8
	D_s^+	32.0	28.8	22.6	12.2
CC	D^+	2.8	24.3	32.0	62.7
	D^0	1.4	39.4	27.2	53.8
	D_s^+	32.5	17.4	17.6	9.9
BS	D^+	1.6	25.4	33.5	66.9
	D^0	1.7	61.9	16.0	31.7
	D_s^+	22.1	18.6	15.4	6.7
PDG	D^+	8.2	37.5	31.1	58.4
	D^0	0.03	58.4	20.0	39.3
	D_s^+	28.8	28.9	22.6	25.4

Table 11.3 Comparison of inclusive pion properties

		Average Pion Multiplicity		
Experimental		$\langle n_{\pi^+} \rangle$	$\langle n_{\pi^-} \rangle$	$\langle n_{\pi^0} \rangle$
This Thesis	D^+	1.3 ± 0.3	0.37 ± 0.03	
	D^0	0.6 ± 0.04	0.65 ± 0.03	
	D_s^+	1.3 ± 1.7	0.6 ± 0.1	
Ref. 35	D^+			1.18 ± 0.21
	D^0			1.31 ± 0.17
	D_s^+			2.0 ± 1.1
Theoretical		$\langle n_{\pi^+} \rangle$	$\langle n_{\pi^-} \rangle$	$\langle n_{\pi^0} \rangle$
BSW	D^+	1.06	0.28	0.81
	D^0	0.89	0.58	0.89
	D_s^+	1.13	0.41	1.15
CC	D^+	0.84	0.29	0.61
	D^0	0.91	0.73	1.08
	D_s^+	1.17	0.47	0.79
BS	D^+	0.78	0.27	0.56
	D^0	0.68	0.44	0.57
	D_s^+	0.74	0.34	0.91
PDG	D^+	1.43	0.48	0.81
	D^0	1.07	0.69	1.07
	D_s^+	1.48	0.53	1.21

PART V
APPENDICES

Appendix A PREDICT User's Guide

The following is adapted from the online help file PREDICT DOC.

Section A.1 Inclusive Analysis with PREDICT

PREDICT is a multipurpose analysis tool that can calculate the inclusive decay properties of a theoretical model by using the model's predicted exclusive decay rates, i.e., the partial widths or branching ratios of its decay modes.

PREDICT can:

1. calculate the inclusive multiplicity distribution for any class of particle, i.e., $B(D \rightarrow nYX)$, where D is the parent particle, Y is the class of particle under study (e.g., K^+, K^-, $K^\pm$, K_S, γ, η, π^0, $P^\pm$ [charged particle]), $n = 0, 1, 2, \ldots$ is the number of particles Y in the final state, and X represents all remaining particles which are not members of class Y;
2. calculate the inclusive branching ratio for any class of particle, i.e., $B(D \rightarrow YX) \equiv B(D \rightarrow {}_{(n\geq 1)}YX)$ the branching ratio of events with at least one member of the class present;
3. calculate the average number of any class of particle, $\langle n \rangle = \sum_{n=0}^{\infty} n \times B(D \rightarrow nYX)$;
4. input partial widths as symbolic formulae;
5. define any variable in a symbolic formula as a non-changing parameter ("constant"), or as a changing parameter ("variable");
6. output results symbolically as a function of a model's variables;
7. calculate errors on the inclusive properties when given the error matrix for a model's variables or branching ratios;
8. generate N-dimensional arrays of the inclusive properties as functions of a model's variables. These arrays can then be used for plotting purposes.

Section A.2 Syntax

PREDICT *models_file* (*options*

models_file..... the *fn ft fm* of the decay model file
default is "PREDICT MODELS *"

options ..... a list of keywords which change the default
behavior of PREDICT

Note: There are a variety of ways of specifying option syntax:

1.	*name* = "*value*"	Delimiters can be single quotes, double quotes or
2.	*name* "*value*"	parenthesis. The "=" sign is optional. Zero or
3.	*name* = (*value*)	more spaces can be used to separate *name* from
4.	*name* (*value*)	the delimited *value*.
5.	*name* = *value*	Delimiters are optional if *value* is a single word.

Method 1 is the method used to describe the options below. When a value contains a single quote, it is necessary to use the other type of quote character as the delimiter.

Options

MODELS="[+] *model_list*"

model_list..... space separated list of model identifiers (e.g., BSW PDG)
Values for the parameters can be specified via:
id1(p1 = v1; p2 = v2; ...) id2(...) ...
id..... model identifier (single word alphanumeric)
p..... name of parameter (case insensitive)
v..... either a single-valued expression or
VARY(*start, end, # steps*) if used with PLOT
+..... If first character, append *model_list* to lower hierarchy
list, otherwise override lower hierarchy list.

GLOBAL="*global_file*"

global_file..... the *fn ft fm* of the global parameters file
default is "PREDICT GLOBAL *"
(Set to " " to use no global file.)

RPP="*rpp_file* , [NO]NORM [NO]PRINT"

rpp_file	the *fn ft fm* of the RPP particle dictionary
NORM	Normalize each RPP decay mode BR to 100%.
NONORM	Use the RPP BR's as typed. (Default)
PRINT	Print the processed dictionary in "RPP OUT A".
NOPRINT	Don't print the dictionary. (Default)

OUT="*output_file*"

output_file.....	the *fn ft fm* of the output file Default is "PREDICT OUTPUT A"

PARTICLES="[+] *particles*"

particles	string of particle names to analyze which can be listed singly or grouped e.g., pi0 <pi+ pi->
<pi+ pi->	Analyze π^+, π^- and the union of π^+ and π^- (i.e., $\pi^\pm$).
+	If first character, add list to default list, otherwise string replaces the default list.

NORM="0 | 1 | 2 | 3 | ? | LIFE(*time*) | 100 | MODE(*mode*) BR(*br*)"

0.....	Don't normalize. Use when model consists of BR's.
1.....	Use 1/lifetime normalization. Needs LIFE suboption. (Model consists of partial widths.)
2.....	Normalize BR sum to 100%.
3.....	Use special mode normalization. Needs MODE and BR.
?.....	Prompt for input.
100	Normalize BR's to 100%. (identical to option 2)
LIFE(*time*)	Use 1/lifetime normalization.
time	lifetime of particle in seconds
MODE(*mode*)	Use special mode normalization. Needs BR.
mode	the special mode to use
BR(*br*)	Use special mode normalization. Needs MODE.
br.....	the branching ratio to be used, expressed as a percentage

ERRORS	Calculate inclusive errors if possible. (Default)
NOERRORS	Don't calculate any errors.

SYMBOLIC	Express results symbolically.
NOSYMBOLIC.....	Express results numerically. (Default)

PLOT	Produce an N-dimensional array of coordinate points.
NOPLOT	Evaluate variables at a single point. (Default)
BATCH(*batch_opts*) .	Submit the job as a batch job.
batch_opts.	batch submittal options
NOBATCH	Run the job interactively. (Default)
DICTIONARY.	Create a Monte Carlo dictionary using exclusive BR's.
NODICTIONARY	Don't create a dictionary. (Default)
DEFAULT	Use variable parameters as given. Don't prompt.
NODEFAULT	Prompt for updated values. (Default)
KEEP	Keep all temporary files.
NOKEEP	Delete all temporary files. (Default)

Examples

```
PREDICT D+ ( MODEL="1(a1 = 1.1; a2 = -.5)" NORM="1" DEF
```

Use "D+ MODELS *" and a 1/lifetime normalization with model 1.
Set model 1 variable a1 = 1.1 and a2 = –.5 (overriding defaults).
Do not prompt for updated values of any variable.

```
PREDICT Ds (NORM=(BR(2.3)) MODEL=(3 CC4) PART(+ pi0) DEF RPP=(,NORM)
```

Process file "Ds MODELS *". Use models 3 and CC4.
Set default mode BR to 2.3%. Include the π^0 in the inclusive analysis.
Don't prompt for updated values of any variable parameters.
Normalize the RPP dictionary BR's to 100%.

```
PREDICT D0 ( MOD="BSW(A1=Vary(.9,1.3,10); A2=Vary(-.6,-.3,10))" PLOT
```

Using file "D0 MODELS *" and the BSW model, vary parameters A1 and A2 (any others will be prompted) so as to produce a 2–D array of coordinate points that can later be plotted.

```
PREDICT TAU MODEL2 B (GLOBAL="TAU PARMS" MODEL=2 NORM=0 PART="+ eta eta'"
```

Use "TAU MODEL2 B" models file and "TAU PARMS *" global file.

Use model number 2 and don't normalize the BR's.
Include the η and η' in the list of particles to analyze.

```
PREDICT B+ ( MOD(BSW) DEF ERR BATCH(TIME 4 CPU A)
```

Use "B+ MODELS *" model file and default global file.
Submit as a batch job with 4 minute cpu. Run on CPU A.
Use default parameters (DEF is the default with BATCH).
Calculate errors if possible.

System Support Required

PREDICT uses the following system tools on SLACVM:

PIPE	– CMS Pipeline technology
MAPLE	– symbolic algebra processor
GLOBALV	– retrieve global options
RIPPLE	– maintains set of backup files
XEDIT	– editor used to display help

Files

The package consists of several files:

PREDICT	EXEC	– the main program (written in Rexx)
PREDICT	REXX	– a PIPE filter to handle the needed arithmetic
fn	MODELS	– the list of decay modes and partial widths for the particle in question (*fn* = D+, D0, Ds, TAU, ...)
PREDICT	GLOBAL	– a list of global parameters used by the models
RPP	DAT	– "Review of Particle Properties" file listing all the secondary decays and BR's
PREDICT	DOC	– the online help file

Section A.3 Hierarchy of Options and Parameters

Options and parameters can be specified on the command line, in the Global file or in the Models file. For the Global file or the Models file, options are defined within the ".options" section and parameters are defined within the ".parms" section.

The order of precedence in the determination of options and parameters is the: 1) command line, 2) Models file, 3) Global file, 4) GLOBALV, 5) built-in defaults.

When an option is specified more than once within a hierarchy level (e.g., twice on the command line, or twice in the Global file), the last invocation of the option completely supersedes previous uses within the level.

When an option at a higher hierarchy level is similar to one at a lower level, what occurs depends upon the option. For options with substructure, a concatenation of all the hierarchies is done and for repeated suboptions, the highest hierarchy level takes precedence. For nonrepeated suboptions, the sole specification is used. For options without substructure, the highest hierarchy takes precedence.

Models File

The Models file is primarily used to define the decay modes and branching ratios (or partial widths) for all models corresponding to the particle being analyzed. Additionally, one may specify options or model parameters that are unique to this file (e.g., the lifetime of the particle).

The models file consists of 3 parts:

a) the options section

b) the parameters section

c) the model section

a) The options section is used to set any options specific to the model. These options and their syntax are the same as the command line options (with the exception of the GLOBAL option, which has no effect since it has already been read by this time).

- The first line of the options section is `".options"`.
- The last line of the options section is `".end"`.
- Any option from the command line can be specified here.
- Option syntax is identical to the command line syntax described above.
- If an option is repeated with the Models file, the last use completely supersedes previous uses (no concatenation).
- See the Options section above for the syntax of the options.

b) The parameters section is used to specify all model independent constants and model dependent constants and variables. Parameters can be either of the "constant" or "variable" type. PREDICT prompts for new values for variable parameters unless the DEFAULT option is set.

- The first line of the parameters section is ".parms".
- The last line of this section is ".end".
- All model independent constants (e.g., the constant $\hbar$) are listed following the ".parms" line and before any ".id" lines. PREDICT will not prompt for updated values for these constants.
- For parameters which are model dependent, begin each model subsection with:

  .id model_identifier model_title
- Specify the value of constant parameters with:

  parm == value (double "=")

  PREDICT will not prompt for updated values for these parameters, nor will they be considered part of the error matrix.
- Specify the value of variable parameters with:

  parm = value (single "=")

  PREDICT will prompt for updated values for these variables unless the DEFAULT option is enabled. Additionally these variables, in the order specified, are considered to be part of the error matrix.
- Specify the error matrix for variable parameters as a MAPLE matrix, i.e., a list of lists using the "[" and "]" characters as delimiters, or a list of ordered pairs, (e.g., [(1,1) = 0.02, (2,2) = 0.03]).

c) The model section describes the formulae for the different models.

- The first line of the models section is ".models".
- The last line is ".end".
- Begin each decay mode by typing the names of the particles.

– Input the model-dependent formulae for this mode as "*id = formula*" where *id* is a model identifier.

Example Models File

```
.options
  norm  "MODE(K0-bar pi+) BR(2.8) LIFE(10.62 * 10**-13)"
  default = 1
  particles  "+ eta'"
.end
.parms
  hbar == 6.582 * 10**-25       ! Global constants
  C12 == 0.975 * 0.975               ! Cosine(Cabibbo angle) ^ 2
  S12 == 0.223 * 0.223               ! Sine(Cabibbo angle) squared
  S1C1 == 0.975 * 0.223              ! Cos * Sin
  .id 1 "Bauer, Stech and Wirbel" ! Model "1" parameters
    A1 = 1.13                             ! variable
    A2 = -0.47                            ! variable
    [[ .0009, -.000457],                  ! Error matrix (MAPLE format)
     [ -.000457, .0009]]
  .id CC "Chau and Cheng"          ! Model "CC" parameters
    a = .98                               ! variable
    b = -.23                              ! variable
    d = 1.0                               ! variable
    dbarp == 1.0                          ! constant
.end
.models
K0-bar  pi+
     1= 9.98*(A1 + 1.23*A2)**2  * 10**10
    CC= (c12 * (a+b))**2
     3= 18.1
  TEST= 2.8
K0-bar  K+
     1=  0.76 * A1**2           * 10**10
    CC= ( s1c1 *(a-d))**2
     3= 3.8
  TEST= 0.84
K0-bar  K*+
     1= 0.74*A1**2              * 10**10
    CC= ( s1c1 * (a - dbarp) )**2
     3= 6
.end
```

Global File

The Global file contains information which is common to many different models file. For example, one may have D+ MODELS, D0 MODELS and Ds MODELS files, and be testing the Bauer, Stech, Wirbel model in all three. The default value for the parameters a1 and a2 is the same for all three models. This value can be specified in the Global file instead of repeating it 3 times.

The Global file has the same structure as the Models file. However, it's likely that only the parameters section will be of interest since the other sections tend to be more Models file dependent. Even so, one may put any or all of the three sections into the Global file.

The Global file is not a required file.

RPP File

The RPP file, whose name is specified via the RPP option and defaults to "RPP DAT *", is a summary of "Review of Particle Properties" by the Particle Data Group. It can be modified to the characteristics of a detector by modifying, for instance, the percentage of charged pions or charged kaons decaying in the detector (or by turning off charged kaon and pion decays altogether if one's analysis requires).

The format of the file is:

```
particle_name  charge  mcid
   Decay_Mode_1_BR  Decay_Mode_1_List
         :                 :
         :                 :
   Decay_Mode_n_BR  Decay_Mode_n_List
```

where:

- `particle_name` is the name of the particle (e.g., `pi+, eta', K-, pi0`);
- `charge` is the charge of the particle (e.g., `0, 1, -1`);

- mcid is the monte carlo id of the particle (This feature is used only when the DICTIONARY option has been specified.);
- Decay_Mode_n_BR is the branching ratio of one of the daughters, given as a percentage (e.g., 23.2);
- Decay_Mode_n_List is the list of daughters for this decay mode.

Example:

```
eta 0 11
 38.9 gamma gamma
 31.9 pi0 pi0 pi0
 23.6 pi+ pi- pi0
 4.88 pi+ pi- gamma
 0.5  e+ e- gamma
 0.03 mu+ mu- gamma
```

It is not required that the branching ratios add to 100% nor does PREDICT normalize them to 100% unless the NORM suboption of the RPP option has been specified.

Section A.4 Defining Defaults via GLOBALV

Default values for many of the options can be specified in one's LASTING GLOBALV file via the GLOBALV facility. (For more info about GLOBALV, type HELP GLOBALV.) The GLOBALV group is called PREDICT. There is only one variable, called DEFAULTS.

The names and values allowed are the same as described in the options section above.

To see default values type:

```
GLOBALV SELECT PREDICT LIST
```

To setup default values type:

GLOBALV SELECT PREDICT SETLP DEFAULTS *string*

where three examples of *string* follow:

```
NORM="3 MODE(K- pi+) BR(2.8)" RPP=",PRINT"
NORM(1 LIFE(7.2 * 10**-13) PARTICLES="<pi+ pi-> pi0"
NORM=0 GLOBAL(MY GLOBAL B) RPP="MY RPP B"
```

PREDICT cannot set the GLOBALV defaults yet. It must be done via the GLOBALV command. Perhaps one day setting these GLOBALV options will be handled within PREDICT itself. I suggest using GLOBALV technology only to reset the GLOBAL option. All other options should be set in the Global file for clarity.

Section A.5 Output

The following is an example of the screen output and the file output using the following command:

```
PREDICT DOC (MOD="1 CC 3 TEST" NORM=2 PART=(<pi+ pi-> pi0) GLOBAL=""
```

The file DOC MODELS was set up to look exactly like the example above in the "Models File" section.

Screen Output

```
Reading in the options and parameters...
RIPPLE059I Backup copy 'PREDICT 1@OUTPUT A' ERASEd.
OUT file   = PREDICT OUTPUT A
KEEP       = 0
DEFAULT    = 1
PLOT       = 0
ERRORS     = 1
BATCH      = 0
DICTIONARY = 0
SYMBOLIC   = 0
Calling RPP...
RIPPLE059I Backup copy 'RPP 1@OUT A' ERASEd.
Reading in the models...
Starting multiplicity counts (3 modes)...
...processing mode 1 (K0-bar  pi+)...
...processing mode 2 (K0-bar  K+)...
...processing mode 3 (K0-bar  K*+)...
Using MODEL 1: "Bauer, Stech and Wirbel"
Computing error matrix...
                        ...for model 1...
Using MODEL CC: "Chau and Cheng"
Using MODEL 3: Model 3
Using MODEL TEST: Model 4
Formatting output...
PREDICT EXEC B1 done.  Output in PREDICT OUTPUT A
```

Output File

```
Predictions 92/10/02 15:18:17 from PREDICT EXEC B1 V# 2.4-090
Command: PREDICT DOC (MOD="1 CC 3 TEST" NORM=2 PART=(<pi+ pi-> pi0) GLOBAL=""
Using model  file: DOC MODELS B1 (CSM191)
No global file specified
Using RPP    file: RPPDOC DAT B1 (CSM191)

Using MODEL 1: "Bauer, Stech and Wirbel"

Constants used in model 1
HBAR = 6.582E-25
Parameters for model 1
A1 = 1.13
A2 = -0.47
Error Matrix =
[[ .0009, -.000457],
[ -.000457, .0009]]

Using MODEL CC: "Chau and Cheng"

Constants used in model CC
HBAR = 6.582E-25
DBARP = 1.0
S1C1 = 0.217425
S12 = 0.049729
C12 = 0.950625
Parameters for model CC
A = .98
B = -0.23
D = 1.0
Error Matrix =
0

Using MODEL 3: Model 3

Constants used in model 3
HBAR = 6.582E-25
Parameters for model 3
Error Matrix =
0

Using MODEL TEST: Model 4

Constants used in model TEST
HBAR = 6.582E-25
Parameters for model TEST
Error Matrix =
0
```

Decay Mode	1 BR%	Error	CC BR%	3 BR%	TEST BR%
K0-bar pi+	61.347	2.747	99.995	64.875	76.923
K0-bar K+	19.584	1.392	3.418-3	13.620	23.077
K0-bar K*+	19.069	1.355	1.238-3	21.505	
BR Sum	10.000+1	0.000	10.000+1	1.000+2	1.000+2
Fudge Factor	1.000		1.000	1.000	1.000

Num 0 pi+	17.039	1.211	2.516-3	13.653	15.162
Num 1 pi+	54.690	0.782	65.699	55.942	58.454
Num 2 pi+	26.774	0.535	34.299	28.717	26.385
Num 3 pi+	1.496	0.106	9.715-5	1.688	0.000
Avg # of pi+	1.127	0.015	1.343	1.184	1.112
BR pi+ X %	82.961	1.211	99.997	86.347	84.838
Num 0 pi-	62.834	0.204	65.700	62.468	65.700
Num 1 pi-	35.670	0.097	34.300	35.845	34.300
Num 2 pi-	1.496	0.106	9.715-5	1.688	0.000
Avg # of pi-	0.387	3.101-3	0.343	0.392	0.343
BR pi- X %	37.166	0.204	34.300	37.532	34.300
Num 0 pi+ pi-	17.039	1.211	2.516-3	13.653	15.162
Num 1 pi+ pi-	45.795	1.415	65.697	48.814	50.538
Num 2 pi+ pi-	8.895	0.632	1.314-3	7.128	7.915
Num 3 pi+ pi-	26.774	0.535	34.299	28.717	26.385
Num 4 pi+ pi-	0.000	0.000	0.000	0.000	0.000
Num 5 pi+ pi-	1.496	0.106	9.715-5	1.688	0.000
Avg # of pi+ pi-	1.514	0.012	1.686	1.577	1.455
BR pi+ pi- X %	82.961	1.211	99.997	86.347	84.838
Num 0 pi0	77.264	0.500	84.300	76.365	84.300
Num 1 pi0	5.353	0.380	3.475-4	6.037	0.000
Num 2 pi0	16.073	0.027	15.700	16.121	15.700
Num 3 pi0	0.997	0.071	6.472-5	1.124	0.000
Num 4 pi0	0.314	0.022	2.035-5	0.354	0.000
Avg # of pi0	0.417	7.351-3	0.314	0.431	0.314
BR pi0 X %	22.736	0.500	15.700	23.635	15.700
Num of 1 Prongs	62.395	0.208	65.325	62.020	65.325
Num of 3 Prongs	36.047	0.098	34.672	36.223	34.672
Num of 5 Prongs	1.558	0.111	2.362-3	1.757	2.261-3
Num of 7 Prongs	2.011-4	1.429-5	1.306-8	2.268-4	0.000
Num of 9 Prongs	6.501-9	4.620-10	4.221-13	7.332-9	0.000
Avg charge mult	1.783	6.378-3	1.694	1.795	1.694

Note: numbers of the form "3.418-3" are a short-form notation for 3.418×10^{-3}. Also, the notation "Num 2 pi+ pi-" means the percentage of events with exactly two charged pions ($\pi^{\pm}$).

Section A.6 Questions?

The PREDICT package was developed by Chris Matthews at Caltech in Pasadena, California. Any questions, bug reports or suggestions should be forwarded to MATTHEWS @ SLACVM.BITNET or MATTHEWS @ VM.SLAC.STANFORD.EDU.

Appendix B Calculation of the Semileptonic Decay Width $D \to \overline{K}\ell^+\nu$ using the BSW Model

The amplitude for a decay of the type $D \to M\ell^+\nu$ is:

$$A(D \to M\ell^+\nu) = \frac{G_F}{\sqrt{2}} L^\mu H_\mu$$

where the leptonic current is:

$$L^\mu = \bar{u}(\nu)\gamma^\mu(1-\gamma^5)v(\ell^+)$$

and the hadronic current has the same form as used in the Bauer, Stech and Wirbel model (see Chapter 7):

$$H_\mu = \langle M|J_\mu|D\rangle .$$

The amplitude for this decay $D \to \overline{K}\ell^+\nu$ is:

$$\begin{aligned} A(D \to K\ell^+\nu) = {} & \frac{G_F}{\sqrt{2}} V_{cs}\bar{u}(\nu; p_\nu, s_\nu)\gamma^\mu(1-\gamma^5)v(\ell; p_\ell, s_\ell) \\ & \times \left((p_D + p_K)_\mu F_1(q^2) - \frac{m_D^2 - m_K^2}{q^2} q_\mu (F_1(q^2) - F_0(q^2)) \right) . \end{aligned}$$

Considering only the term with the momentum sum $p_\mu \equiv (p_D + p_K)_\mu$, define:

$$A_+ = \bar{u}\gamma^\mu(1-\gamma^5)vp_\mu .$$

Squaring and summing over spin states, we get:

$$\begin{aligned} \Sigma A_+^2 &= \sum_{s_\ell, s_\nu} \left[\bar{u}\gamma^\mu(1-\gamma^5)vp_\mu\right]^* \left[\bar{u}\gamma^\sigma(1-\gamma^5)vp_\sigma\right] \\ &= \sum_{s_\ell, s_\nu} \left[p_\mu \bar{v}(1+\gamma^5)\gamma^\mu u\right] \left[\bar{u}\gamma^\sigma(1-\gamma^5)vp_\sigma\right] \\ &= \sum_{s_\ell} \left[p_\mu \bar{v}(1+\gamma^5)\gamma^\mu(\not{p}_\nu + m_\nu)\gamma^\sigma(1-\gamma^5)vp_\sigma\right] \\ &= \mathrm{Tr}\left[p_\mu(1+\gamma^5)\gamma^\mu(\not{p}_\nu)\gamma^\sigma(1-\gamma^5)p_\sigma(\not{p}_\ell - m_\ell)\right] \\ &= \mathrm{Tr}\left[(1+\gamma^5)\not{p}(\not{p}_\nu)\not{p}(1-\gamma^5)(\not{p}_\ell - m_\ell)\right] \\ &= 8[2(p\cdot p_\ell)(p\cdot p_\nu) - (p\cdot p)(p_\ell \cdot p_\nu)] \end{aligned}$$

using the normalization $\bar{u}u = 2m$ and $\bar{v}v = -2m$, so that:

$$\sum_s u_\alpha(p,s)\bar{u}_\beta(p,s) = (\not{p} + m)_{\alpha\beta}$$
$$\sum_s v_\alpha(p,s)\bar{v}_\beta(p,s) = (\not{p} - m)_{\alpha\beta}\,.$$

Now consider the term with $q_\mu = (p_D - p_K)_\mu = (p_\ell + p_\nu)_\mu$ and recall the fact that the spinors u and v satisfy the Dirac equation:

$$(\not{p} - m)u = 0$$
$$(\not{p} + m)v = 0$$
$$\bar{u}(\not{p} - m) = 0$$
$$\bar{v}(\not{p} + m) = 0\,.$$

This term, called A_-, thus reduces to:

$$\begin{aligned}
A_- &= \bar{u}(p_\nu)\gamma^\mu(1-\gamma^5)v(p_\ell)q_\mu \\
&= \bar{u}(p_\nu)\gamma^\mu(1-\gamma^5)v(p_\ell)(p_\ell + p_\nu)_\mu \\
&= \bar{u}(p_\nu)(1+\gamma^5)\,\not{p}_\ell\, v(p_\ell) + \bar{u}(p_\nu)\,\not{p}_\nu\,(1-\gamma^5)v(p_\ell) \\
&= -m_\ell\bar{u}(p_\nu)(1+\gamma^5)v(p_\ell) + m_\nu\bar{u}(p_\nu)(1-\gamma^5)v(p_\ell) \\
&= -m_\ell\bar{u}(p_\nu)(1+\gamma^5)v(p_\ell)\,.
\end{aligned}$$

The square of this term is:

$$\begin{aligned}
\Sigma A_-^2 &= \Sigma m_\ell^2\left[\bar{v}(p_\ell)(1-\gamma^5)u(p_\nu)\right]\left[\bar{u}(p_\nu)(1+\gamma^5)v(p_\ell)\right] \\
&= m_\ell^2\mathrm{Tr}\left[(1-\gamma^5)(\not{p}_\nu + m_\nu)(1+\gamma^5)(\not{p}_\ell - m_e)\right] \\
&= m_\ell^2(8p_\ell\cdot p_\nu)\,.
\end{aligned}$$

The cross term between the A_- and A_+ is:

$$\begin{aligned}
\Sigma\left|A_+^* A_-\right| &= -\Sigma m_\ell\left[\bar{v}(p_\ell)(1+\gamma^5)\,\not{p}\,u(p_\nu)\right]\left[\bar{u}(p_\nu)(1+\gamma^5)v(p_\ell)\right] \\
&= -m_\ell\mathrm{Tr}\left[(1+\gamma^5)\,\not{p}\,(\not{p}_\nu)(1+\gamma^5)(\not{p}_\ell - m_\ell)\right] \\
&= m_\ell^2(8p\cdot p_\nu) \\
&= \Sigma\left|A_-^* A_+\right|\,.
\end{aligned}$$

The terms involving the q_μ contain factors of m_ℓ^2, which is small compared to the A_+^2 term and can thus be neglected.* Thus, the amplitude squared for $D \to \overline{K}\ell^+\nu$ is:

$$\begin{aligned} A^2 &= \frac{G_F^2}{2} V_{cs}^2 F_1^2(q^2) A_+^2 \\ &= 4G_F^2 V_{cs}^2 F_1^2(q^2)[2(p\cdot p_\ell)(p\cdot p_\nu) - (p\cdot p)(p_\ell\cdot p_\nu)]\,. \end{aligned}$$

In considering the functional dependence of the amplitude squared, A^2, it is worth noting that in the rest frame of the D meson $q^2 = (p_D - p_K)^2 = m_D^2 + m_K^2 - 2m_D E_K$, thus q^2 is a function only of E_K. Hence the form factor, $F_1(q^2)$, is a function only of E_K. The remainder of the amplitude squared is a function of the energies and momenta of the kaon, lepton and neutrino, as well as a function of $\cos(\theta)$, where θ is the angle between the kaon and the lepton. This functional dependence can be rewritten in terms of only E_K and E_ℓ as will be shown.

The decay width, in the rest frame of the D meson, is:

$$\Gamma = \frac{1}{2m_D(2\pi)^5}\int A^2(p_K, p_\ell, p_\nu)\delta^4(p_D - p_K - p_\ell - p_\nu)\frac{d^3p_K}{2E_K}\frac{d^3p_\ell}{2E_\ell}\frac{d^3p_\nu}{2E_\nu}\,.$$

This three–body form, which is an integral over nine variables, can be reduced to an integral in two variables, E_K and E_ℓ, through some simple techniques. First, the delta function is split into separate energy and momentum components:

$$\delta^4(p_D - p_K - p_\ell - p_\nu) = \delta(m_D - E_K - E_\ell - E_\nu)\delta^3(-\vec{p}_K - \vec{p}_\ell - \vec{p}_\nu)\,.$$

We now perform the integral over $\vec{p}_\nu$ and obtain:

$$\Gamma = \frac{1}{2m_D(2\pi)^5}\int A^2(p_K, p_\ell, E_\nu, \cos\theta)\delta(m_D - E_K - E_\ell - E_\nu)\frac{d^3p_K}{2E_K}\frac{d^3p_\ell}{2E_\ell}\frac{1}{2E_\nu}\,.$$

We have thus eliminated three of the variables of integration. Second, having defined θ to be the angle between the kaon and the lepton, we rewrite the differentials in spherical coordinates. We integrate over the solid angle of the kaon, and the axial angle, ϕ, of the lepton. This eliminates three more integration variables.

$$\begin{aligned} (d^3p_K)(d^3p_\ell) &= \left(|\vec{p}_K|^2 d|\vec{p}_K| d\Omega_K\right)\left(|\vec{p}_\ell|^2 d|\vec{p}_\ell| d\Omega_e\right) \\ &\to \left(4\pi|\vec{p}_K|^2 d|\vec{p}_K|\right)\left(2\pi|\vec{p}_\ell|^2 d|\vec{p}_\ell| d(\cos\theta)\right)\,. \end{aligned}$$

* Assuming $F_0(q^2)$ is of similar magnitude as $F_1(q^2)$.

The integral over $\cos(\theta)$ is performed next in conjunction with the energy delta function integral by using the following property of the Dirac delta function:

$$\int f(x)\delta[g(x)]dx = \frac{f(x_0)}{|g'(x_0)|} \qquad \text{where} \quad g(x_0) = 0\,.$$

Here, $g(\theta) = m_D - E_K - E_\ell - E_\nu(\theta)$ where we have rewritten E_ν as a function of θ:

$$E_\nu^2 = |\vec{p}_\nu|^2 = -(\vec{p}_K + \vec{p}_\ell)^2 = |\vec{p}_K|^2 + |\vec{p}_\ell|^2 + 2|\vec{p}_K||\vec{p}_\ell|\cos\theta$$

and:

$$\frac{dg(\theta)}{d\cos\theta} = -\frac{|\vec{p}_K||\vec{p}_\ell|}{E_\nu}\,.$$

All terms involving E_ν are replaced by $m_D - E_K - E_\ell$ and instances of $\cos(\theta)$, which arise only in the expression $\vec{p}_K \cdot \vec{p}_\ell$, are replaced as follows:

$$\begin{aligned} |\vec{p}_K||\vec{p}_\ell|\cos\theta &\rightarrow \frac{(m_D - E_K - E_\ell)^2 - |\vec{p}_K|^2 - |\vec{p}_\ell|^2}{2} \\ &\rightarrow \frac{m_D^2 + m_K^2 + m_\ell^2 - 2m_D E_K - 2m_D E_\ell + 2E_K E_\ell}{2} \end{aligned}$$

which depends only upon E_K and E_ℓ. Performing the integral, the decay width now becomes:

$$\begin{aligned} \Gamma &= \frac{1}{2m_D(2\pi)^5}\int\int A^2(E_K, E_\ell)\frac{8\pi^2|\vec{p}_K|^2 d|\vec{p}_K|}{2E_K}\frac{|\vec{p}_\ell|^2 d|\vec{p}_\ell|}{2E_\ell}\frac{1}{2E_\nu}\left(\frac{E_\nu}{|\vec{p}_K||\vec{p}_\ell|}\right) \\ &= \frac{1}{8m_D(2\pi)^3}\int\int A^2(E_K, E_\ell)\frac{|\vec{p}_K|d|\vec{p}_K|}{E_K}\frac{|\vec{p}_\ell|d|\vec{p}_\ell|}{E_\ell} \\ &= \frac{1}{8m_D(2\pi)^3}\int\int A^2(E_K, E_\ell)dE_K dE_\ell \end{aligned}$$

where the relation $EdE = |\vec{p}|d|\vec{p}|$ is used in obtaining the last line. Thus the integral reduces to one in only two variables.

The simplification of the amplitude squared is a three step process. Starting with the previously obtained expression:

$$A^2 = 4G_F^2 V_{cs}^2 F_1^2(q^2)[2(p\cdot p_\ell)(p\cdot p_\nu) - (p\cdot p)(p_\ell\cdot p_\nu)]$$

the three steps are:

1. Perform the 3–momenta delta function integral: $\vec{p}_\nu \rightarrow -\vec{p}_K - \vec{p}_\ell$.

2. Replace $|\vec{p}|^2 \to E^2 - m^2$ for the kaon and electron momenta.
3. Do the energy delta function integral: $E_\nu \to m_D - E_K - E_\ell$ and $\vec{p}_K \cdot \vec{p}_\ell = \left(m_D^2 + m_K^2 + m_\ell^2 - 2(m_D E_K + m_D E_\ell - E_K E_\ell)\right)/2$.

The result of these three steps is an integral in E_K and E_ℓ:

$$\Gamma = \frac{(G_F V_{cs})^2}{4m_D(2\pi)^3} \int\int F_1^2(q^2)\Big[-4m_D^4 + 8m_D^3(E_K + 2E_\ell) - m_D^2\big(16E_\ell(E_K + E_\ell) + 4m_K^2 + 3m_\ell^2\big) + 2m_D m_\ell^2(3E_K + 4E_\ell) + m_e^2\big(m_K^2 - m_\ell^2\big)\Big] dE_K dE_\ell$$

where the functional form of the form factor is:

$$F_1(q^2) = F_1\big(m_D^2 + m_K^2 - 2E_K m_D\big) = \frac{h_1(D \to K)}{1 - \big(m_D^2 + m_K^2 - 2E_K m_D\big)/m_{c\bar{s}(1^-)}^2}.$$

The integration may be done in one of two ways, either integrating over the kaon energy first or the lepton energy first. Due to the complexity of the integrand, Mathematica™ is used to perform the integrations. The first integration is performed symbolically, but the second is performed numerically.

The limits of the second integration are from the minimum to the maximum allowed energies. The minimum energy is simply the mass of the particle. The maximum energy of a particle in a three-body decay is given by the expression:

$$W_e \equiv E_\ell^{\max} = \frac{m_D^2 + m_\ell^2 - (m_K^2 + m_\nu^2)}{2m_D} = \frac{m_D^2 + m_\ell^2 - m_K^2}{2m_D}$$

$$W_K \equiv E_K^{\max} = \frac{m_D^2 + m_K^2 - m_\ell^2}{2m_D}.$$

For the specific decay $D \to \overline{K} e^+ \nu$:

$$W_e \equiv E_e^{\max} = 0.8669\,\text{GeV for the } D^0$$
$$= 0.8684\,\text{GeV for the } D^+$$
$$W_K \equiv E_K^{\max} = 0.9976\,\text{GeV for the } D^0$$
$$= 1.0009\,\text{GeV for the } D^+.$$

The limits of integration for the first integral, however, will depend upon the energy and momentum of the second integral. For a given first integral energy and momentum, the maximum and minimum energies ($E_2^{\pm}$) of the second integral (i.e., its limits of integration) are derived as follows:

$$\vec{p}_2 = -(\vec{p}_1 + \vec{p}_\nu)$$

$$|\vec{p}_2|^2 = |\vec{p}_1|^2 + |\vec{p}_\nu|^2 + 2|\vec{p}_1||\vec{p}_\nu|\cos\theta$$

$$\therefore \left(|\vec{p}_2|^2\right)^{\pm} = (|\vec{p}_\nu| \pm |\vec{p}_1|)^2 = (E_\nu \pm |\vec{p}_1|)^2$$

$$E_2^{\pm 2} - m_2^2 = \left(m_D - E_2^{\pm} - E_1 \pm |\vec{p}_1|\right)^2$$

$$= (m_D - E_1 \pm |\vec{p}_1|)^2 + E_2^{\pm 2} - 2E_2^{\pm}(m_D - E_1 \pm |\vec{p}_1|)$$

$$\therefore E_2^{\pm} = \frac{(m_D - E_1 \pm |\vec{p}_1|)^2 + m_2^2}{(m_D - E_1 \pm |\vec{p}_1|)}.$$

The final form of the integral is just:

$$\Gamma = \frac{(G_F V_{cs})^2}{4m_D(2\pi)^3} \int_{m_\ell}^{W_\ell} dE_\ell \int_{E_K^-}^{E_K^+} [\ldots] dE_K$$

$$= \frac{(G_F V_{cs})^2}{4m_D(2\pi)^3} \int_{m_K}^{W_K} dE_K \int_{E_\ell^-}^{E_\ell^+} [\ldots] dE_\ell .$$

Table B.1 lists the calculated partial widths for the processes $D \to \overline{K}\ell^+\nu$. It includes the results of the integral containing only the A_+^2 (labeled "1 Term") as well as the integral using the complete amplitude squared including the A_-^2 and A_+A_- cross terms (labeled "3 Terms").

Table B.1 Semileptonic partial widths for $D \to \overline{K}\ell^+\nu$ decays

Process	Partial Width (10^{-14} GeV)		BR (%)
	1 Term	3 Terms	
$D^0 \to K^- e^+ \nu$	5.54584	5.54584	3.547
$D^+ \to \overline{K}^0 e^+ \nu$	5.58960	5.58960	9.019
$D^0 \to K^- \mu^+ \nu$	5.44716	5.48088	3.506
$D^+ \to \overline{K}^0 \mu^+ \nu$	5.49041	5.5244	8.914

Appendix C Decomposition with the Wigner-Eckart Theorem

Using a $\langle j_1 j_2 m_1 m_2 | T | JM \rangle$ notation, we write the isospin amplitudes from page 123 in terms of an isospin changing tensor operator, $T_q^{(k)} = T_1^{(1)}$, which changes I by $k = 1$ and I_3 by $q = 1$.

$$A(D^0 \to K^-\pi^+) = \left\langle \pi^+ K^- \middle| T_1^{(1)} \middle| D^0 \right\rangle \tag{1a}$$

$$= \left\langle 1\tfrac{1}{2}1\tfrac{-1}{2} \middle| T_1^{(1)} \middle| \tfrac{1}{2}\tfrac{-1}{2} \right\rangle \tag{1b}$$

$$= \sqrt{\frac{2}{3}} \left\langle \tfrac{1}{2}\tfrac{1}{2} \middle| T_1^{(1)} \middle| \tfrac{1}{2}\tfrac{-1}{2} \right\rangle + \frac{1}{\sqrt{3}} \left\langle \tfrac{3}{2}\tfrac{1}{2} \middle| T_1^{(1)} \middle| \tfrac{1}{2}\tfrac{-1}{2} \right\rangle \tag{1c}$$

Equation 1c is the isospin part of the decomposition. The Wigner-Eckart theorem is (see, for example, Reference 56):

$$\left\langle \alpha j m \middle| T_q^{(k)} \middle| \alpha' j' m' \right\rangle = \frac{1}{\sqrt{2j+1}} \langle j' k m' q | j m \rangle \left\langle \alpha j \middle\| \mathbf{T}^{(k)} \middle\| \alpha' j' \right\rangle$$

where $\left\langle \alpha j \middle\| \mathbf{T}^{(k)} \middle\| \alpha' j' \right\rangle$ is the reduced matrix element.

We apply the Wigner-Eckart Theorem to obtain the irreducible tensor forms:

$$\begin{aligned} A(D^0 \to K^-\pi^+) &= \sqrt{\frac{2}{3}} \frac{1}{\sqrt{2}} \langle \tfrac{1}{2}\, 1\, \tfrac{-1}{2}\, 1 \mid \tfrac{1}{2}\, \tfrac{1}{2} \rangle \left\langle \tfrac{1}{2} \middle\| \mathbf{T}^{(1)} \middle\| \tfrac{1}{2} \right\rangle \\ &\quad + \frac{1}{\sqrt{3}} \frac{1}{2} \langle \tfrac{1}{2}\, 1\, \tfrac{-1}{2}\, 1 \mid \tfrac{3}{2}\, \tfrac{1}{2} \rangle \left\langle \tfrac{1}{2} \middle\| \mathbf{T}^{(1)} \middle\| \tfrac{3}{2} \right\rangle \\ &= \sqrt{\frac{2}{3}} \frac{1}{\sqrt{2}} \left(-\sqrt{\frac{2}{3}} \right) A_1 + \frac{1}{\sqrt{3}} \frac{1}{2} \frac{1}{\sqrt{3}} A_3 \\ &= \sqrt{\frac{2}{3}} A_{1/2} + \frac{1}{\sqrt{3}} A_{3/2} \end{aligned}$$

where I have defined the following:

$$\begin{aligned} A_x &= \left\langle \frac{1}{2} \middle\| \mathbf{T}^{(1)} \middle\| \frac{x}{2} \right\rangle \\ A_{1/2} &= \frac{-1}{\sqrt{3}} A_1 \\ A_{3/2} &= \frac{1}{2\sqrt{3}} A_3 . \end{aligned}$$

Continuing with the other 2 modes in a similar and consistent manner:

$$\begin{aligned}
A\left(D^0 \to \overline{K}^0\pi^0\right) &= \left\langle \pi^0\overline{K}^0 \middle| T_1^{(1)} \middle| D^0 \right\rangle \\
&= \left\langle 1\tfrac{1}{2}\,0\,\tfrac{1}{2} \middle| T_1^{(1)} \middle| \tfrac{1}{2}\,\tfrac{-1}{2} \right\rangle \\
&= \frac{-1}{\sqrt{3}}\left\langle \tfrac{1}{2}\,\tfrac{1}{2} \middle| T_1^{(1)} \middle| \tfrac{1}{2}\,\tfrac{-1}{2} \right\rangle + \sqrt{\frac{2}{3}}\left\langle \tfrac{3}{2}\,\tfrac{1}{2} \middle| T_1^{(1)} \middle| \tfrac{1}{2}\,\tfrac{-1}{2} \right\rangle .
\end{aligned}$$

Applying the Wigner-Eckart theorem:

$$\begin{aligned}
A\left(D^0 \to \overline{K}^0\pi^0\right) &= \frac{-1}{\sqrt{3}}\frac{1}{\sqrt{2}}\left\langle \tfrac{1}{2}\,1\,\tfrac{-1}{2}\,1 \;\middle|\; \tfrac{1}{2}\,\tfrac{1}{2} \right\rangle \left\langle \tfrac{1}{2} \middle\| \mathbf{T}^{(1)} \middle\| \tfrac{1}{2} \right\rangle \\
&\quad + \sqrt{\frac{2}{3}}\frac{1}{2}\left\langle \tfrac{1}{2}\,1\,\tfrac{-1}{2}\,1 \;\middle|\; \tfrac{3}{2}\,\tfrac{1}{2} \right\rangle \left\langle \tfrac{1}{2} \middle\| \mathbf{T}^{(1)} \middle\| \tfrac{3}{2} \right\rangle \\
&= \frac{-1}{\sqrt{3}}\frac{1}{\sqrt{2}}\left(-\sqrt{\frac{2}{3}}\right)A_1 + \sqrt{\frac{2}{3}}\frac{1}{2}\frac{1}{\sqrt{3}}A_3 \\
&= \frac{-1}{\sqrt{3}}A_{1/2} + \sqrt{\frac{2}{3}}A_{3/2}.
\end{aligned}$$

Finally,

$$\begin{aligned}
A\left(D^+ \to \overline{K}^0\pi^+\right) &= \left\langle \pi^+\overline{K}^0 \middle| T_1^{(1)} \middle| D^+ \right\rangle \\
&= \left\langle 1\frac{1}{2}1\frac{1}{2} \middle| T_1^{(1)} \middle| \frac{1}{2}\frac{1}{2} \right\rangle \\
&= \left\langle \frac{3}{2}\frac{3}{2} \middle| T_1^{(1)} \middle| \frac{1}{2}\frac{1}{2} \right\rangle .
\end{aligned}$$

Applying the Wigner-Eckart Theorem:

$$\begin{aligned}
A\left(D^+ \to \overline{K}^0\pi^+\right) &= \frac{1}{2}\left\langle \tfrac{1}{2}\,1\,\tfrac{1}{2}\,1 \;\middle|\; \tfrac{3}{2}\,\tfrac{3}{2} \right\rangle \left\langle \tfrac{1}{2} \middle\| \mathbf{T}^{(1)} \middle\| \tfrac{3}{2} \right\rangle \\
&= \frac{1}{2}A_3 \\
&= \sqrt{3}A_{3/2}.
\end{aligned}$$

Bibliography

1. S.L. Glashow, J. Iliopoulos, and L. Maiani. Weak interactions with lepton-hadron symmetry. *Phys. Rev.*, **D2**:1285–1292, 1970.

2. J.J. Aubert et al. Experimental observation of a heavy particle *J. Phys. Rev. Lett.*, **33**:1404, 1974.

3. J.E. Augustin et al. Discovery of a narrow resonance in e^+e^- annihilation. *Phys. Rev. Lett.*, **33**:1406, 1974.

4. G. Goldhaber et al. Observation in e^+e^- annihilation of a narrow state at 1865 MeV/c^2 decaying to $K\pi$ and $K\pi\pi\pi$. *Phys. Rev. Lett.*, **37**:255, 1976.

5. I. Peruzzi et al. Observation of a narrow charged state at 1876 MeV/c^2 decaying to an exotic combination of $K\pi\pi$. *Phys. Rev. Lett.*, **37**:569, 1976.

6. Particle Data Group. Review of particle properties. *Phys. Rev.*, **D45**(11):1, 1992.

7. M. Kobayashi and T. Maskawa. CP-violation in the renormalizable theory of weak interaction. *Prog. Theor. Phys.*, **49**(2):652–657, 1973.

8. Luciano Maiani. Lattice calculations of f_D and f_B. *Helv. Phys. Acta.*, **64**:853–870, 1991.

9. J. Adler et al. Search for the decay $D^+ \rightarrow \mu^+\nu_\mu$ and an upper limit on the pseudoscalar decay constant. *Phys. Rev. Lett.*, **60**:1375–1378, 1988.

10. Frederick J. Gilman. An introduction to charm and heavy quark physics. In Ming-Han Ye and Tao Huang, editors, *Charm Physics*, CCAST (World Laboratory) Symposium/Workshop Proceedings, pages 1–87, 1988.

11. R. Rückl. Weak decays of heavy flavours. Habilitationsschrift University of Munich, 1983.

12. M. Bauer, B. Stech, and M. Wirbel. Exclusive non-leptonic decays of D-, D_s-, and B-mesons. *Z. Phys.*, **C34**:103–115, 1987.

13. Ling-Lie Chau and Hai-Yang Cheng. Quark-diagram analysis of two-body charm decays. *Phys. Rev. Lett.*, **56**(16):1655–1658, 1986.

14. B.Yu. Blok and M.A. Shifman. Toward a theory of weak hadronic decays of charmed mesons. *Sov. J. Nucl. Phys.*, **45**(1):135–142, 1987.

15. B.Yu. Blok and M.A. Shifman. Weak nonleptonic decays of charmed mesons in QCD sum rules. *Sov. J. Nucl. Phys.*, **45**(2):301–311, 1987.

16. B.Yu. Blok and M.A. Shifman. Weak nonleptonic decays of charmed mesons. Comparing theory with experiment. *Sov. J. Nucl. Phys.*, **45**(3):522–531, 1987.

17. B.Yu. Blok and M.A. Shifman. Weak nonleptonic decays of charmed mesons (addendum). *Sov. J. Nucl. Phys.*, **46**(4):767, 1987.

18. I.I. Bigi. Strong interactions in charm decays. *Nucl. Phys. B (Proc. Suppl.)*, **7A**:318–336, 1989.

19. I.I. Bigi. Inclusive decays of beauty (and charm): QCD vs. phenomenological models. Technical report, University of Notre Dame, 1992. Preprint UND-HEP-92-BIG06.

20. A.J. Buras. The 1/N approach to non-leptonic weak decays. In C. Jarlskag, editor, *CP Violations*, pages 575–645. World Scientific, 1988.

21. K. Lane and E. Eichten. Charm threshold in electron-positron annihilation. *Phys. Rev. Lett.*, **37**:477, 1976.

22. David Hitlin. A third generation detector for SPEAR. *Physica Scripta*, **23**:634–641, 1981.

23. D. Bernstein et al. The Mark III spectrometer. *Nucl. Instr. Meth.*, **226**:301, 1984.

24. Jay Hauser. *A Systematic Study of the Decays of Charmed D Mesons*. Ph.D. thesis, California Institute of Technology, 1985.

25. Daniel Mark Coffman. *The Properties of Semileptonic Decays of Charmed D Mesons.* Ph.D. thesis, California Institute of Technology, 1987.

26. Gregory P. Dubois. *Upper Limits on Inclusive Branching Fractions to Narrow States in Radiative J/ψ Decays.* Ph.D. thesis, California Institute of Technology, 1992.

27. J. Adler et al. The Mark III vertex chamber. *Nucl. Inst. Meth.*, **A276**:42, 1989.

28. J. Roehrig et al. The central drift chamber for the Mark III detector at SPEAR. *Nucl. Inst. Meth.*, **226**:319–329, 1984.

29. J. S. Brown et al. The Mark III time-of-flight system. *Nucl. Inst. Meth.*, **221**:503–522, 1984.

30. Walter Toki et al. The barrel shower counter for the Mark III detector at SPEAR. *Nucl. Inst. Meth.*, **219**:479–486, 1984.

31. R. Fabrizio et al. The endcap shower counters for the Mark III detector. *Nucl. Inst. Meth.*, **227**:220–226, 1984.

32. A. L. Spadafora. *Phi Meson Production in J/Psi Decays and Determination of the Spin and Parity of the eta-c(2980).* Ph.D. thesis, University of Illinois at Urbana-Champaign, 1984.

33. R. M. Baltrusaitis et al. Direct measurements of charmed D meson hadronic branching fractions. *Phys. Rev. Lett.*, **56**:2140–2143, 1986.

34. Steven R. Wasserbaech. *Hadronic Decays of the D_S Meson.* Ph.D. thesis, Stanford University, 1989. Preprint SLAC-345.

35. D. Coffman et al. Measurement of the inclusive decay properties of charmed mesons. *Phys. Lett.*, **B263**:135–140, 1991.

36. Steven R. Wasserbaech. K^0 and lambda finder / track swimmer. KLAMS program documentation, 1988.

37. R. H. Schindler et al. Measurements of the properties of D-meson decays. *Phys. Rev.*, **D60**:78–97, 1981.

38. F. James and M. Roos. 'MINUIT' a system for function minimization and analysis of the parameter errors and correlations. *Computer Physics Commun.*, **10**:343–367, 1975.

39. Manfred Bauer. *Exklusive Zerfälle der schweren Mesonen.* Ph.D. thesis, Ruprecht-Karls-Universität, 1987.

40. M. Bauer and M. Wirbel. Formfactor effects in exclusive D and B decays. *Z. Phys. C*, **42**:671–678, 1989.

41. Particle Data Group. Review of particle properties. *Phys. Lett. B*, **239**:1, 1990.

42. B. Grinstein, M.B. Wise, and N. Isgur. DOE research and development report. Technical report, California Institute of Technology, 1985. CALT-68-1311.

43. A.N. Kamal and R.C. Verma. The effect of a_1 width on $D \to \overline{K}a_1$ decays. *Phys. Rev.*, **D45**:982–985, 1991.

44. M. Wirbel, B. Stech, and M. Bauer. Exclusive semileptonic decays of heavy mesons. *Z. Phys.*, **C29**:637–642, 1985.

45. J. Adler et al. A reanalysis of charmed D meson branching fractions. *Phys. Rev. Lett.*, **60**:89, 1988.

46. J. Adler et al. Resonant substructure in $K\pi\pi$ decays of charmed D mesons. *Phys. Lett.*, **196B**:107, 1987.

47. P. Kim. $\overline{K}^0\pi^0$ results. Mark III Internal Memo, 1991.

48. D. Coffman et al. Resonant substructure in $\overline{K}\pi\pi\pi$ decays of D mesons. *Phys. Rev.*, **D45**:2196–2211, 1992.

49. Ling-Lie Chau and Hai-Yang Cheng. Analysis of two-body decays of charm mesons using the quark-diagram scheme. *Physical Review*, **D36**(1):137–153, 1987.

50. Ling-Lie Chau and Hai-Yang Cheng. Analysis of two-body decays of charm mesons using the quark-diagram scheme: Addendum on hairpin diagrams. *Physical Review*, **D39**(9):2788–2791, 1989.

51. Ling-Lie Chau. Private communication.

52. J. F. Labs. Recent results in charm decays from Mark III. Technical report, Stanford Linear Accelerator Center, 1990. Preprint SLAC-PUB-5372.

53. Ling-Lie Chau and Hai-Yang Cheng. Nonresonant three-body decays of charmed mesons. *Phys. Rev.*, **D41**(5):1510–1516, 1990.

54. M.A. Shifman. Theoretical status of weak decays. *Nuclear Physics B (Proc. Suppl.)*, **3**:289–340, 1988.

55. V. Vuillemin et al. Inclusive studies of D meson decays at the $\psi(3772)$. *Phys. Rev. Lett.*, **41**:1149–1152, 1978.

56. Mitchel Weissbluth. *Atoms and Molecules (Student Edition)*. Academic Press, New York, 1978.